The Use of Novel Mechanical Devices for Enhancing the Performance of Railway Vehicle Systems

by

Alejandra Zamary Matamoros Sanchez

Thesis submitted in partial fulfillment of the requirements for the award of
Doctor of Philosophy of Loughborough University

May 2013

Abstract

Following successful implementation of inerters for passive mechanical control in racing cars, this research studies potential innovative solutions for railway vehicle suspensions by bringing the inerter concept to the design of mechatronic systems. The inerter is a kinetic energy storage device which reacts to relative accelerations; together with springs and dampers, it can implement a range of mechanical networks distinguished by their frequency characteristics. This thesis investigates advantages of inerter-based *novel* devices to simplify the design of active solutions. Most of the research work is devoted to the enhancement of vertical ride quality; integrated *active-plus-novel-passive* solutions are proposed for the secondary suspensions. These are defined by different active control strategies and passive configurations including inerters. By optimisation of the suspension parameters, a synergy between passive and active configurations is demonstrated for a range of ride quality conditions. The evidence of cooperative work is found in the reduction of the required active forces and suspension travelling. This reveals a potential for reducing the actuator size. Benefits on power requirements and actuator dynamic compensation were also identified. One of the strategies features a nonlinear control law proposed here to compensate for 'sky-hook' damping effects on suspension deflection; this, together with inerter-based devices attains up to 50% in active force reduction for a setting providing 30% of ride quality enhancement. The study is developed from both, an analytical and an engineering perspective. Validation of the results with a more sophisticated model is performed. The lateral stability problem was briefly considered towards the end of the investigation. A potential use of inerter-based devices to replace the static yaw stiffness by dynamic characteristics was identified. This leads to a synergy with 'absolute stiffness', an active stability solution for controlling the wheelset 'hunting' problem, for reducing the creep forces developed during curve negotiation.

Keywords: Inerter, passive suspension, active suspension, railway vehicle, mechanical control, kinetic energy.

To my parents...

Acknowledgements

I want to express my most sincere thanks to my supervisors, Professor Roger Goodall and Dr Argyrios Zolotas for giving me this opportunity to pursue my PhD within the Control Systems Group in Loughborough University. Thanks for trusting on me for the conduction and development of this research work. I owe my deepest gratitude to Professor Goodall for his guidance on the exciting field of railway vehicle dynamics, his patience, his confidence and his incredible support in all respects... "keep it simple...!" an unforgettable advice from an indisputably successful and acknowledged academic and sensible person. Many thanks also to Dr Zolotas for his friendly and valuable support and advising even with his tight agenda.

Special thanks go also to Professor Malcolm Smith, the inerter inventor, and to Dr Jason Jiang, from the Control Group of the Engineering Department of the University of Cambridge, for the collaborative work on the research of passive suspensions for railway vehicles and for sharing their expertise in the field.

I had also the great honour of being accepted for a two-month research visit at CINVESTAV-Mexico at an early stage of my studies. Profound thanks for the warm welcome and support I received. Infinite thanks to Professor Hebertt Sira Ramírez, a bright Latin American icon of the Control Systems area and approachable person. Many thanks for your orientation on Passivity-Based Control and introducing me to the GPI observers on which we had pleasant and intense academic discussions.

My appreciation also to my examiners, Prof. T. X. Mei and Dr. Roger Dixon for their valuable suggestions and corrections required to enhance the final quality of this work.

Many thanks to my employer, Universidad de Los Andes —Venezuela, for the secondment and studentship scheme which has enabled me to pursue my PhD studies in the UK. My gratitude expressions to my colleagues from the Control Systems Department and the Office of Professorial Affairs for their diligence and support.

I would like to acknowledge also the studentship awarded by the School of Electronic, Electrical and Systems Engineering of Loughborough University, which have covered my PhD registration fees.

I acknowledge SIMPACK UK Ltd, for providing me with a short-term free license of Simpack/Rail and Simpack/Control modules to perform multibody simulation to validate my results.

Many thanks to all the financial institutions which have made possible my attendance to professional meetings: Control Systems Group, Systems Division, School of Electronic, Electrical and Systems Engineering, and the Research Office from Loughborough University. Also to Santander Bank and the Royal Academy of Engineering.

Thank you so much also to my friendly and supportive colleagues from the CSG, specially to Dr Chris Ward who was there, always willing to help, since I just started this journey.

Many thanks to the '*Parkroaders*' (present and past) for their presence and kindness, including dogs :)

I owe my warm gratitude to my friends in Loughborough in special to Lina (MDBF), Vianney, Gloria, Rose, Norman, Mariale, Richard, Carolina, Ksenija, Ricardo, Sultan&Diana, you have made of this experience simply great and memorable! Friendship lasts forever...

Thanks to all my family and friends from Venezuela who encouraged me with their shows of trust, love, and support. I am lucky for having you all even in the far distance.

Last but not least, an unmeasurable thanks to my parents to whom there are no words to describe what having them means to my achievements and my entire life. I simply love you and owe what I am today to you both...

Thanks God for all Your blessings!!

Alejandra

Contents

List of Figures

List of Tables

Nomenclature

$(*)_b$, $(*)_\rho$ Denote, respectively, bounce and pitch component of the variable in parentheses $(*)$. For instance, $(z_v)_b$ ($(z_v)_\rho$) denotes bounce (pitch) component of the vehicle body displacement.

$\bar{U}_1$, $\bar{U}_b$ Respectively, normalised kinetic energy function stored by the passive subsystem Σ_1 (vehicle body), and normalised kinetic energy stored by the inerter

β_m Bodies mass ratio: $\beta_m = {}^{m_b}/_{m_q v}$

$\beta_{b,\,i}$ Pitching motion of the front ($i = 1$)/rear ($i = 2$) bogie

β_v Pitching motion of the vehicle body

$\boldsymbol{\mathcal{A}}$, $\boldsymbol{\mathcal{B}}_{\hat{\delta}}$, $\boldsymbol{\mathcal{C}}$ State-space realisation of the closed-loop system

ΔJ_1 Changes in the ride quality J_1, expressed in percentage of J_1^* (nominal ride quality)

$\delta(t)$ Normal Dirac delta function

$\delta_z(t)$ Track profile/wheels and track irregularities model

ϵ Reciprocal of the cut-off frequency of the low-pass filter applied to the stochastic track inputs; $\epsilon = 0.008\,[\text{Hz}]$ gives $20\,[\text{Hz}]$ of filter cut-off frequency (typical value)

$\hat{F}_{cL}^{J_1}$, $\hat{F}_{cT}^{J_1}$ Leading/Trailing active force designed to control ride quality

$\hat{F}_{cL}^{J_2}$, $\hat{F}_{cT}^{J_2}$ Leading/Trailing active force designed to regulate suspension deflection

$\hat{}$ Symbol denoting Laplace Transform

κ Coefficient of the 'adaptive stiffness' control strategy

λ Wheel conicity

$\mathbf{A}$ System matrix

$\mathbf{A}_{af}$, $\mathbf{B}_{af}$, $\mathbf{C}_{af}$, $\mathbf{D}_{af}$ State-space realisation of an active sub-system

$\mathbf{A}_{pf}$, $\mathbf{B}_{pf}$, $\mathbf{C}_{pf}$, $\mathbf{D}_{pf}$ State-space realisation of a novel passive network

$\mathbf{B}_{\delta}$ Excitation input matrix

$\mathbf{B}_{u}$ Control input matrix

$\mathbf{C}$ Damping matrix

$\mathbf{K}$ Stiffness matrix

$\mathbf{K}_{ciD}$ Time-domain integral of the relative displacement of the leading (1)/trailing(2) suspension

$\mathbf{M}$ Inertia matrix

$\mathbf{Q}_m$, $\dot{\mathbf{Q}}_m$ Excitation matrices

$\mathcal{P}$ Measure of power

$\mathcal{P}_p$ Power dissipated in the primary suspensions, [W]

$\mathcal{P}_s$ Power dissipated in the passive secondary suspensions, [W]

$\mathbf{C}_{\mathrm{y}}$ Open-loop system output matrix

$\mathbf{C}_m$ Open-loop system measurements vector

$\mathcal{L}$ Lagrangian function

ω_s Spatial circular frequency

ω_t Temporal circular frequency

Ω_z Vertical roughness coefficient of the track

ρ Real-positive value weighting the cost of the active force in an LQR optimal control design

S0 Label for the conventional airspring.

Σ_1, Σ_2 Passive subsystems

τ_u Control torque in the yaw direction

τ_i Time delay for the i-th wheelset to be excited by $\delta(t)$

θ_m Motor rotation in the electromechanical actuator model

θ_b Bogie yaw motion

$\theta_{c,i}$	Cant angle of the curved track
$\theta_{w,\,i}$	Wheelset i yaw motion
$\underline{\delta_m}(t)$	Excitation vector
$\underline{\sigma_{zacc}}$	Root-mean-square vector of vehicle body acceleration assessed at the leading, trailing and middle position
$\underline{F}$	Generalised forces vector
$\underline{H_1}(s)$	Transfer function matrix for the vehicle body acceleration in response to track input velocity
$\underline{J_1}$	Ride quality vector index
$\underline{J_1}^{sup}$	Least ride quality index
$\underline{q}$	Generalised coordinates vector
$\underline{w}$	Wheelsets generalised coordinates vector
$\underline{x_{cl}}$	Closed-loop state vector
$\underline{x}(t)$	State vector
$\underline{y_m}$	Open-loop system measurements vector
$\underline{y_o}$	Open-loop system output vector
ζ_c	Least damping ratio of the system
$_{L}$, $_{T}$	Denote, respectively, Leading and Trailing; these are often used to refer to ride quality, suspension deflection, and active forces at these positions
b	Inertance
b_g	Airspring inertance
c_g	Pipework losses coefficient for the airspring system
c_m	Motor friction coefficient in the electromechanical actuator model
c_p	Primary suspension damping
c_r	Airspring damping
c_{b1}	Mechanical inerter internal friction
c_{py}	Primary lateral damping per axle box

c_{sc} Lead screw friction in the electromechanical actuator model

c_{sky} Skyhook damping coefficient

c_{sy} Secondary lateral damping per axle box

d_i Horizontal distance from the i -th wheelset to the reference frame

F Force symbol

f and f_t Linear temporal frequency, [Hz]

$f(t)$ Time-function modelling a railway gradient

f_c Corner frequency, [Hz]

F_x, F_{x1}, F_{x2} Longitudinal creep forces

F_y, F_{y1}, F_{y2} Lateral creep forces

f_{11} Longitudinal creepage coefficient

f_{22} Lateral creepage coefficient

$F_{a,\,i}$ Front ($i = 1$)/rear ($i = 2$) airspring force

F_i i-th entry of the vector $\underline{F}$

$F_{u,\,i}$ Linear control and/or compensation force at the front (i=1) / rear (i=2) secondary suspension

$F_{\mathrm{act},\,i}$ Front ($i = 1$)/rear ($i = 2$) actuator force

F_{act} Actuator force

g Gravity, $9.81[\mathrm{ms}^{-2}]$

$G_{\mathrm{PI}}(s)$ Transfer function of the actuator PI control

$G_{\mathrm{HPF}}(s)$ High-pass filter transfer function

$G_{\mathrm{HPF}}^{f_{cb}}(s)$, $G_{\mathrm{HPF}}^{f_{c\rho}}(s)$ High-pass filters with respective cut-off frequency f_c and f_ρ for modal implementation of skyhook damping

$G_{\mathrm{LPF}}(s)$ Low-pass filter transfer function

$H_{J_1}(s)$ Transfer function for ride quality assessment

$H_{J_2}(s)$ Transfer function for suspension deflection assessment

i_m Motor induced current in the electromechanical actuator model

I_{by} Bogie pitch inertia

I_{gz} Bogie frame yaw inertia

I_{vy} Vehicle body pitch inertia

I_{wz} Wheelset yaw inertia

J_1^* Nominal ride quality of the vehicle

J_2, $\bar{J}_2$, $\hat{J}_2$ Suspension deflection index actual value, average value calculated for a range of available data, and normalised value, all respectively.

J_3 Active force assessment index

J_3, $\bar{J}_3$, $\hat{J}_3$ Active force index actual value, average value calculated for a range of available data, and normalised value, all respectively.

J_4 Assessment index for the power extracted by the active suspensions

J_m Rotor inertia in the electromechanical actuator model

J_P Rayleigh energy dissipation function by the primary suspension

J_P Rayleigh energy dissipation function by the secondary suspension

J_{1L} Ride quality assessed at the leading end of the vehicle body

J_{1M} Ride quality assessed at the middle postion of the vehicle

J_{1T} Ride quality assessed at the trailing end of the vehicle body

J_ζ Stability assessment index, equivalent to the system's least damping ratio ζ_c

J_{LQR} LQR expected value

K_*, $\bar{K_*}$, $\hat{K_*}$ The star subindex '$_*$' denotes generic. In the same order, the symbols refer to: actual value, average value calculated for a range of available data, and normalised value with respect to $\bar{K_*}$, all respectively. This applies, equivalently, for other passive or active control parameter.

K_ρ Feedback gain of the pitch feedback loop in the implementation of modal skyhook damping

k_a Airspring change of area stiffness

K_b Feedback gain of the bounce feedback loop in the implementation of modal skyhook damping

k_c	Rotational stiffness of the coupling between the motor and the screw in the electromechanical actuator model
K_e	Back-emf gain in the electromechanical actuator model
K_l	Feedback gain of the feedback loop in the implementation of skyhook damping
k_p	Primary suspension stiffness
k_r	Airspring reservoir stiffness
k_s	Airspring stiffness
K_T	Motor torque constant in the electromechanical actuator model
K_u	Absolute yaw stiffness feedback gain
k_x	Yaw/longitudinal stiffness
k_{b1}	Mechanical inerter stiffness
k_e	End-stiffness of a mechanical device; here, $k_e = 3.5 \times 10^6\,[\mathrm{Nm}^{-1}]$
k_{pc}	Proportional gain of the actuator PI control
k_{px}	Primary longitudinal stiffness per axle box
k_{py}	Primary lateral stiffness per axle box
k_{sc}	Lead screw stiffness in the electromechanical actuator model
k_{sy}	Secondary lateral stiffness per axle box
l_b	Semi-longitudinal spacing of wheelsets
l_v	Semi-longitudinal spacing of secondary suspension
l_{wx}	Semi-longitudinal spacing of wheelsets
l_{wy}	Half gauge of wheelset
l_x	Semi-lateral spacing of steering linkages and primary longitudinal suspension
m_p	Auxiliar midpoint mass
m_v	Vehicle body mass
m_b	Bogie mass
m_g	Bogie frame mass

m_{qv}	Half-vehicle mass
m_{sc}	Concentrated screw mass in the electromechanical actuator model
m_w	Wheelset mass
n_{sc}	Lead screw pitch in the electromechanical actuator model
p	Factor of the mean spectral density function autocorrelation
R	Radius of the curved track
r_0	Wheel radius
$R_{\omega}^{\dot{\delta}_z}(0)$	Autocorrelation of the mean spectral density function
R_{arm}	Armature winding inductance in the electromechanical actuator model
R_{arm}	Armature winding resistance in the electromechanical actuator model
s	Laplace variable
$S_s^{\delta z}(\omega_s)$	Mean spectral density of the spatial elevation of the track in $\left[\mathrm{m}^2\,(^{rad}/_{\mathrm{m}})^{-1}\right]$
$S_t^{\delta z}(\omega_t)$	Mean spectral density of the spatial elevation of the track in $\left[\mathrm{m}^2\,(^{rad}/_{\mathrm{s}})^{-1}\right]$
T	Potential energy symbol
t	Time
T_P	Potential energy stored in the primary suspension
T_S	Potential energy stored in the secondary suspension
T_T	Total potential energy
T_{pc}	Integration time constant of the actuator PI control
U	Kinetic energy symbol
U_1, $\dot{U}_1$	Kinetic energy and kinetic energy rate functions of the passive subsystem Σ_1
U_b	Kinetic energy stored by an inerter
U_P	Kinetic energy stored in the primary suspension
U_S	Kinetic energy stored in the secondary suspension
U_T	Total kinetic energy
U_T^*	Co-content of total kinetic energy

$U_{b,\,i}$ Kinetic energy stored by the front ($i = 1$)/rear ($i = 2$) bogie

U_v Kinetic energy stored by the vehicle body

V Vehicle speed

v Vehicle speed

v_c Voltage applied to the motor in the electromechanical actuator model

$x_{af,\,i}$ State vector of the i-th active sub-system (i=1: front, i=2: rear suspension)

$x_{pf,\,i}$ State vector of the i-th novel passive network (i=1: front, i=2: rear suspension)

y_b Bogie lateral motion

y_v Vehicle body lateral motion

$y_{w,\,i}$ Wheelset i lateral motion

z Vertical displacement measurement symbol

$z_{b,\,i}$ Bouncing motion of the front ($i = 1$)/rear ($i = 2$) bogie

$z_D(t)$ Leading and trailing secondary suspension deflection vector

z_m Lead screw travel in the electromechanical actuator model

$z_{p1,\,i}$ Dynamic of the front (i=1)/rear (i=2) airspring midpoint between k_s and the pipework and reservoir mechanical model

$z_{p2,\,i}$ Dynamic of the front (i=1)/rear (i=2) airspring midpoint between c_g and b_g

z_v Bouncing motion of the vehicle body

$z_{w,\,i}$ i-th wheel/track contact point, with i =1, 2, 3, 4

z_{act} Actuator displacement

$\mathrm{F}_{p,\,i,\,j}(s)$ Primary suspension forces, with $j = 1, 2$ for $i = 1$ (front bogie), and $j = 3, 4$ for $i = 2$ (rear bogie)

Y' Receptance

$\mathrm{Y}_a(s)$ Airspring mechanical admittance

$\mathrm{Y}_{pn}(s)$ Passive network mechanical admittance

$\mathrm{Y}_p(s)$ Primary suspension mechanical admittance

F&Si Label employed in Chapters 5–7 for an integrated suspension *active-plus-novel-passive* with passive structure S0 − −S6 from Figure 5.12, and active control strategy specified in the context

Li Mechanical network from Figure 8.4

Si Label employed in Chapters 5–7 for an inerter-based device in parallel to a conventional airspring, with $i = 0, 2, ..., 6$, identifying the structure from Figure 5.12.

Si' Label employed in Chapters 5–7 for an inerter-based device, with $i = 1, 2, ..., 6$, identifying the structure from Figure 5.12

(Local SHD-AS) Abbr. for Local Skyhook Damping with Absolute Stiffness

(Local SHD-CF) Abbr. for Local Skyhook Damping with Complementary Filtering

(LQG Reg.) Abbr. for LQG-HPF Output Regulator

(Modal HPF-SHD) Abbr. for Modal Skyhook Damping with High-Pass Filtering

τ_u&Li Active stability control combined with a mechanical network Li from Figure 8.4

Y Mechanical admittance

Z Mechanical impedance

1

Introduction

The growing demand for high quality railway transportation services has forced the raikinl industry to search for better solutions in order to remain in the competition with other forms of transport, e.g. automotive and aircraft. For the rail industry, research has played an important and backing role in the study of a range of different aspects in railway systems as well as in the technology development towards the systems enhancement. In particular, the need for gaining fundamental understanding and to generate outstanding answers to the dynamic problems of the vehicles, including ride and stability for example, dates to several decades ago.

Railway is a very complex system comprising a variety of interacting elements and subsystems, including vehicles, infrastructure, machinery, management, logistics, personnel and passengers. As in any large-scale system, those elements and subsystems involve multidisciplinary areas and hence are commonly separated. Thus, individual properties and behaviours of a subsystem, considering its connection with its environment, allow comprehension of the problems and the provision of specific solutions. That has enabled the definition of key research areas such as technology, vehicle dynamics and structures, power systems, track, roadbed and fixed structures, and control and signalling, as distinguished in the earlier times by the Joint Transport Research Committee from the United Kingdom in 1967 [2].

In this context, this research is focused on dynamic-related problems arising in the individual vehicles of a passenger high-speed train. Dynamic performance encompasses problems associated to ride quality, stability and response to track features (e.g. curved sections of the rail track). These together impose a range of challenges to the design of modern railway vehicles. As trending solutions, active suspensions have shown to facilitate higher speed and reduced track interaction, for example.

By the introduction of controlled actuators, the use of active suspensions offers enhanced performance and some flexibility in the way the suspensions dynamic evolves. However, this approach introduces the issue of energy consumption of the controlled element.

Notwithstanding that active technologies can offer a wide range of solutions for vehicle systems in general, on the other hand, passive suspensions technology have been also in constant development, which due to safety and reliability reasons still have major acceptance in vehicle dynamics. For instance, the design of passive suspensions (e.g. mechanical, hydraulic) supported on passive linear control and mechanical networks theory has progressed with the introduction of a novel concept to the synthesis of novel mechanical devices: the *inerter* [3]. Since then, a range of applications based on this type of passive suspensions has been investigated, with successful implementation in racing cars.

The invention of the inerter for passive suspensions exalted the interest on exploring innovative possibilities for improved mechatronic solutions as principal objective of this thesis. By exploiting engineering, mathematical and computational skills, this work addresses the analysis and design of suspension systems around a synergy between active solutions and inerter-based devices. For this, theoretical modelling of the vehicle is considered, as well as assumptions on the infrastructure characteristics and travelling conditions. Well stablished control strategies for active suspensions, together with the examination and formulation of more complex validation strategies are integrated with inerter-based suspensions as novel devices, designed by formulation of mechanical networks. Analytical and numerical assessment methods, together with computing-based optimisation are employed to derive the outcomes of the research.

1.1 Research Overview

This section introduces the most relevant aspects involved with this research. Further aspects are presented with the literature survey and the subsequent chapters, where appropriate.

1.1.1 Railway Vehicles

In the study of certain dynamical characteristics, engineering abstractions are normally accepted and are common in the study of railway vehicles. This derives in an also common simplification of the models towards extracting the main features of the vehicle dynamic performance. One of the basis of these abstractions is the weak

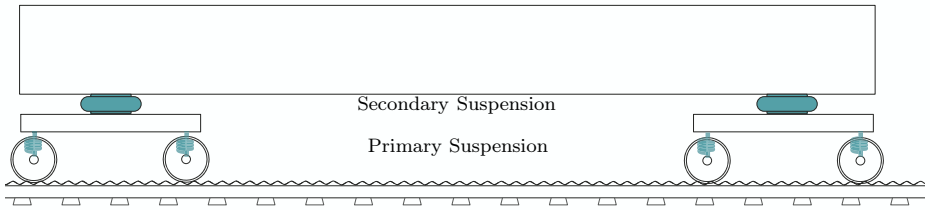

Figure 1.1: Vehicle bodies and suspension layers involved in the vertical dynamics of a railway vehicle.

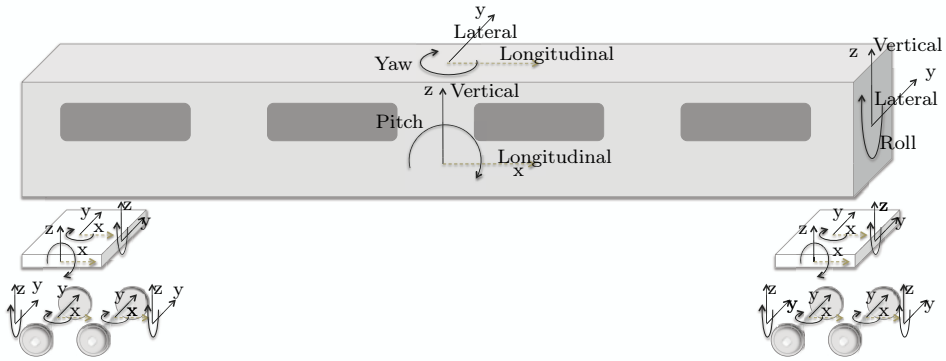

Figure 1.2: Degrees-of-freedom of a modern railway vehicle from different spatial views.

coupling between motions described by different plans of the vehicle, e.g. between vertical and lateral motions [4].

This thesis distinguishes between two types of vehicle: the two solid-axle wheelsets vehicle provided with only one stage of suspension, and the bogied vehicle which comprises four solid-axle wheelsets and with two stages of suspension, primary and secondary. The latter models a high-speed vehicle [5], on which this thesis concentrates. Figure 1.1 is an illustration of a bogied vehicle in side-view comprising: a carbody and two bogies with two solid-axle wheelsets each, interconnected by primary and secondary suspension elements. Figure 1.2 depicts the degrees-of-freedom (DoF) of the vehicle bodies in the 3D space, distinguishing: lateral (y), longitudinal (x) and vertical (z) translations, and rotation in the yaw (θ), roll (γ) and pitch (β) directions. Constraints on some of the DoF normally apply, e.g. the longitudinal translation for assessments based on constant travelling speeds.

In particular, track features and travelling speeds are very determinant factors of a railway vehicle dynamics. Railway dynamicists normally distinguish between track irregularities (stochastic excitations) and low frequency track features (deterministic excitations). Service speeds of 200 [km/h] and above are considered high-speed trains. Nowadays, the fastest commercial wheeled train in operation travels at a nominal

speed of 280 [km/h] and the last record testing speed is of 574.8 [km/h] for the TVG POS trains.

There is a wide range of research opportunities around railway vehicles dynamics. Aspects including ride comfort (tilting and vibration), wheelset stability, and reduction of track wear and noise, have been principal concerns in the field during many years. A railway vehicle is a multibody system and thus, providing the vehicle with appropriate interconnection between bodies is fundamental in regard to the mentioned problems. In fact, the suspension systems in a railway vehicle are the core for guaranteeing adequate linkages between the vehicle bodies, so that individual dynamics are either adequately isolated or conveniently compensated.

1.1.2 Conventional Suspensions

Railway vehicles are conventionally equipped with passive suspensions. Together with the vehicle geometry, these define important characteristics of the vehicle dynamics. The suspension systems are reasonably subject to operational constraints and performance limitations mainly due to the mechanical setup (e.g. combinations of springs and dampers, pneumatic suspensions, and mechanical linkages). The secondary suspension of a high-speed vehicle typically comprises airsprings to guarantee acceptable levels of ride comfort and constant height [6, 7, 5, 8, 9]. Airsprings provide the vehicle with multidirectional impact and vibrations attenuation in a mechanical manner, through the dynamics of an elastic chamber filled with compressed gas (usually with a self-levelling mechanism, i.e. mechanical control). The secondary suspensions should transmit only low-frequency intended movements so that the vehicle follows the track and isolates irregularities. On the other hand, primary vertical suspensions normally comprise a parallel arrangement of a spring and a viscous damper; those are fairly stiff suspensions that conveniently cause the bogies to follow all the track vertical changes. Conversely, primary lateral and longitudinal suspensions are important in the control of the wheelset dynamics and thus in the kinematic stability problem. Normal arrangements of conventional mechanical suspensions for the lateral dynamics are shown in the plan-view schematic of the high-speed vehicle in Figure 1.3, which also depicts the application of active stability control. Note that this diagram represents a half-vehicle model which is a common simplification, discussed later.

1.1.3 Active Suspensions

Over the past thirty years, the use of sensors, electronic controllers, and actuation technology, has enabled important changes in modern trains to deal with some of the

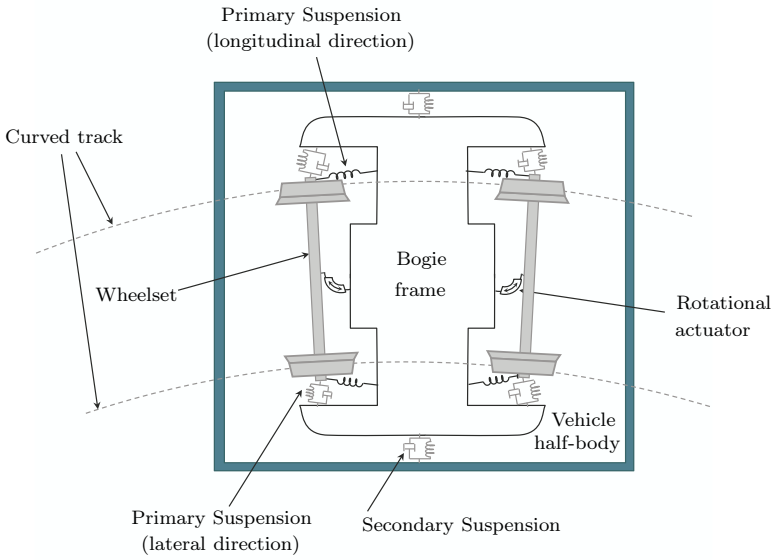

Figure 1.3: Plan-view schematic of a high-speed railway half-vehicle with passive and active suspension, running onto a curve.

issues arising from the dynamics of a railway vehicle, hence enhancing the vehicle system performance and capabilities. In this context, active solutions have played a significant role in complementing conventional passive suspensions [4].

Active suspensions expand the existing mechanical suspensions by convenient feedback of the measurement of some physical variables (or states, more generally) defining the vehicle dynamical behaviours. This may include also estimation of the states when certain measurements are not feasible. An active suspension for enhancing the vehicle vertical dynamic consists of an actuator (e.g. electromechanical, electrohydraulic, or electromagnetic) driven by an electronically implemented control law, u, which can be placed in parallel to the conventional suspensions, for example (see Figure 1.4 –right, contrasted with the pure passive suspensions of the system at the left). Figure 1.5 shows a generalised schematic of the system with active suspensions.

The state-of-the-art of research in railway suspensions [10] reports that mechatronic solutions are emerging as one of the most remarkable sources of innovation in the future generations of railway vehicles. They provide the modern railway vehicles with very advanced features. For mechatronic suspensions, the fact of "closing the loop" by including sensing and electronically-controlled actuators leads to dynamics that vehicles with only mechanical suspensions cannot achieve. However, some difficulties arise in the design of the control systems and some of the most relevant are treated in the development of this thesis.

As a worldwide operational example, tilting trains is an already well established and mature active suspension technology. There has been also a growing consensus

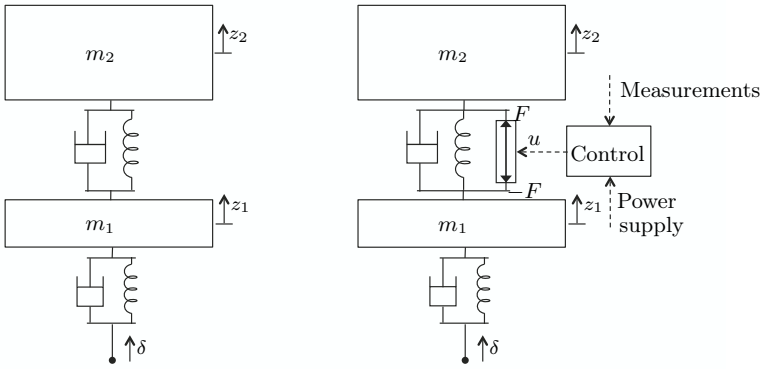

Figure 1.4: Left: Two-mass system with passive suspensions. Right: Two-mass system with secondary active suspension.

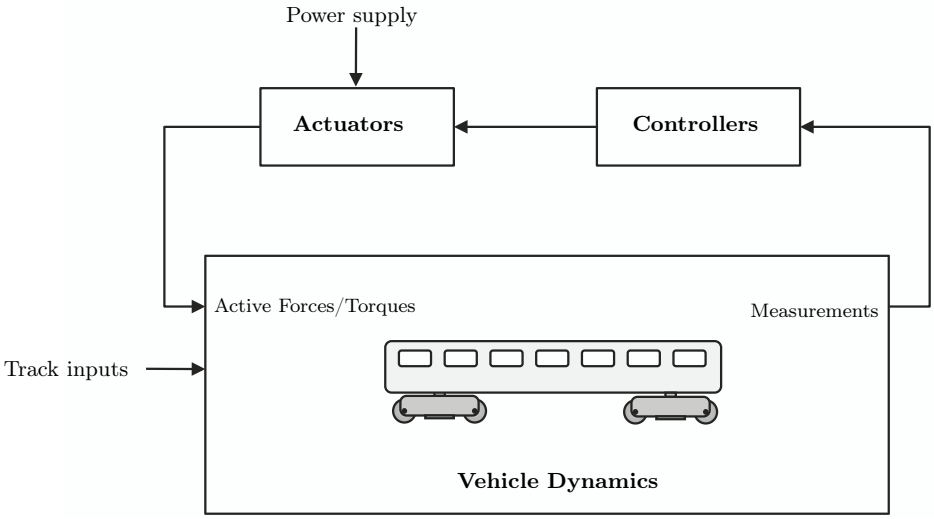

Figure 1.5: General scheme of a railway vehicle with active solutions.

about the future use of active control to improve railway vehicles' running behaviour through new technologies in the primary suspensions, although different proposed technologies are still in the experimental stage. Progress on concepts for mechatronic based technologies for active secondary suspensions is likewise well advanced, but the business case of enhancing the current secondary suspensions has not been proved yet. The latter is because the benefits attained with the currently proposed technologies are still unclear.

In spite of that, there is continuing research interest on the vertical secondary suspensions. Hence, this work claims a contribution to the railway vehicle control area. Enhancement of the vertical ride characteristic is attained here via control of the bouncing and pitching modes of the railway vehicle, by a synergy between active and passive technologies. For this, the inerter, as a concept and as a novel device, is integrated. Also, control of the lateral stability problem is explored as a matter of particular importance; interesting outcomes from integrated solutions *active-plus-novel-passive* are obtained for the rail-wheel interface after a stability control design.

1.1.4 A novel device called *inerter*

In 2003, a novel concept called "the *inerter*" was introduced for the synthesis of mechanical networks. Professor Malcolm Smith, from University of Cambridge, concerned with the safety of the electronic active suspension systems for racing cars — banned by the Formula One™ rules in the early 1990s— invented the aforementioned novel mechanical concept. The concept covered the need for having a two-terminal mechanical device whose applied force was proportional to the relative acceleration between its end-points, providing fundamental analogies with electrical components. That is, following the force-current analogy: spring↔inductor, damper↔resistor, mass↔grounded capacitor, and inerter↔capacitor (either grounded or ungrounded) [3]. From the energy viewpoint [11], this would be classed as a kinetic energy storage device. Several prototypes of the device have been successfully created at Cambridge University to comply with the concept (e.g. the ball-screw inerter in the photo in Figure 1.6). Some of the inerter-based current inventions are introduced in the next chapter.

The invention of the inerter was based on the fact that conventional suspensions, using springs and dampers only, did not provide the car with the required passive mechanical control; ride height control in that particular application. The set of high-performance mechanical admittances for car suspensions realisable using simple elements, including low weight masses, was then constrained. Hence, the inerter was the 'missing element' in the synthesis of passive mechanical networks in contrast to electrical networks comprising inductors, resistors and capacitors only. Thus, if

novel passive suspensions using inerters could safely compensate the car dynamics as required, then some of the capabilities of the electronic active suspensions could be recovered. It is worth noting that nowadays, several Formula One™ teams have adopted passive technology employing inerters. Still, the issue of active suspensions is not forgotten for the racing cars business; other means of —non electronic dependent— active suspensions concepts are in progress.

As introduced in [3], the action/reaction force that the inerter develops is proportional to the relative acceleration between its nodes through the *inertance* characteristic, b, defined in kilograms: $F = -b\,(\ddot{x}_1 - \ddot{x}_2)$. The inertance of an ideal inerter is therefore a proportionality constant which can be accepted in the same sense that real springs and dampers are approximated as linear relations of relative displacements and velocities through their stiffness and damping coefficients, respectively, for a certain range of operation. The symbol used for the inerter in mechanical networks representation is illustrated in Figure 1.7(a). The concept of the inerter for the deployment of mechanical networks, as it is performed in electrical networks, has enabled another vision in the design of passive suspension systems. An example for a mechanical network using inerters is shown in Figure 1.7(b). Although the leading application of this novel device is in racing cars suspensions, its properties have been shown to be promising for other systems. For instance, as it is discussed later in Chapter 2, some research have been conducted already for railway vehicles equipped with passive suspensions only.

From here, novel mechanical devices refer to a passive control element that can be modelled as a mechanical network comprising springs, dampers, and inerters. The implementation of a mechanical network is feasible by either using conventional springs, dampers and *mechanical* inerters, under physical considerations on the elements, or by other technologies (e.g. hydraulics-based). Mechanical networks are characterised by complex admittance functions which establish relations of the type velocity–force. Thus, inerter-based devices, in general, are conceived here as devices (mechanical, hydraulic) whose translational dynamic resembles that of an inerter-based mechanical network (or vice versa). Hence, the mechanical inerter itself is a novel mechanical device, and an inerter-based device according to the terminology adopted here.

1.1.5 The synergy: integration of active solutions with novel devices

It is well known that the force exerted by a passive suspension system is a reaction to the relative dynamic between the suspension terminals. However, a wide range of vibrating systems are better controlled by feeding-back measurements that may be different to these relative behaviours. Hence, active suspensions retain their im-

Figure 1.6: Photo of a ball-screw inerter.

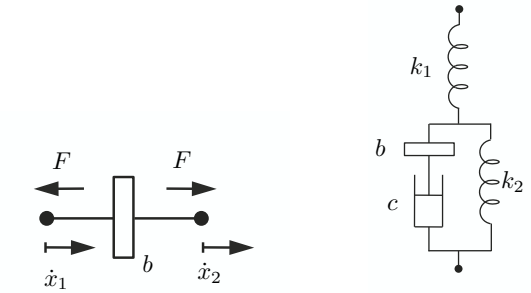

(a) Inerter symbol

(b) Example of a mechanical network

Figure 1.7: Inerter symbol and example of a mechanical network comprising springs, a damper, and an inerter.

portance with the introduction of the inerter concept. Indeed, one could also think that the compensation given by an inerter-based device can be implemented by active means, provided the relevant relative motions are measured. Nevertheless, there are some issues around active suspensions design and implementation, such as: reliability of the mechatronic systems, the actuators bandwidth, their size due to the maximum control forces required, and the need of external power supply.

After the demonstrated success of the inerter in racing cars and previous research on its application in railway vehicles revealing some potential benefits, there is a possibility of inerter-based suspensions and active suspensions complementing each other to ease some of the design and implementation issues. The approach proposed in this research work integrates different active secondary suspension configurations and novel passive networks in order to investigate the potential of the new concept in the simplification of the normal conflicts arising in the controller design. Figure 1.8 contains a block diagram for a general integration, and Figure 1.9 illustrates a secondary suspension augmented by the components of the synergy in a two-mass system. In a railway vehicle, the structure would be replicated for each suspension. In order to produce a synergy among the elements of the suspension, this work pays special attention to the design of the passive network (PN) and the controller from Figure 1.9. In addition, a form of active stabilisation of the lateral dynamic of a bogie wheelsets, which has been a problem of a more practical interest from the cost-benefit

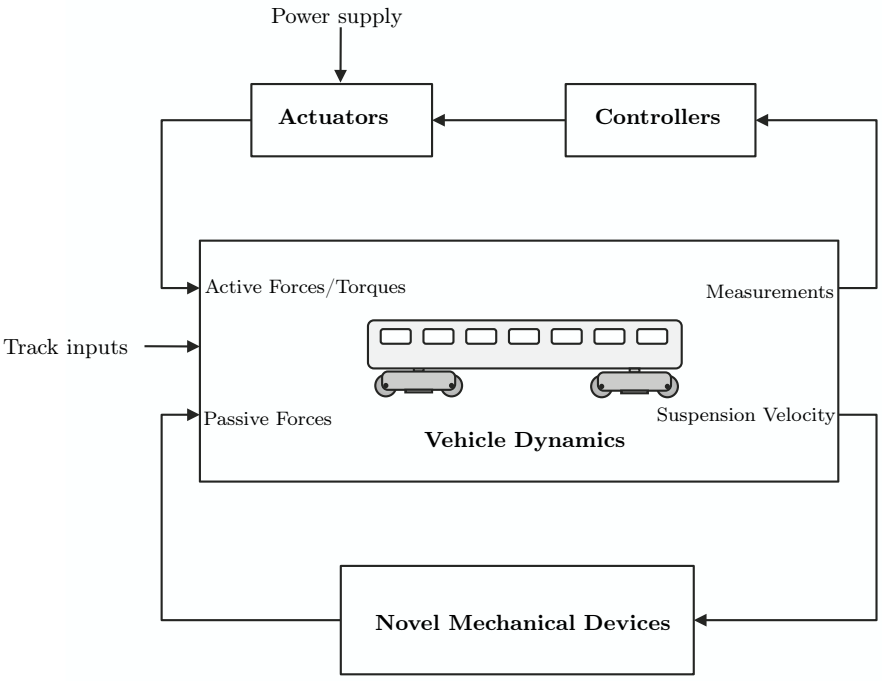

Figure 1.8: General scheme of the integration *active-plus-novel-passive*.

viewpoint, is combined with a fairly simple inerter-based passive structure. This is a continued assessment of the approach. Hence, this research focuses essentially on the following two design objectives: 1) maximum improvement of the vertical ride quality, and 2) maximum stability of the vehicle's kinematic modes, i.e. wheelset lateral stability.

1.2 Motivation and Problem Statement

Advantages of the inerter use have been already demonstrated for racing car suspensions [12], motorcycle steering [13, 14], and it is being investigated for buildings anti-seismic applications [15]; its implementation possibilities in railway vehicle systems are wider and some of them have been previously researched [16, 17, 18, 19, 20, 21, 22]. The synergy between the inerter-based devices with active solutions had not been reported before.

Even though active secondary suspensions are now well developed, the following facts, derived from the novelty of the inerter concept, motivated this research:

1. It is still necessary to find a solution whose benefits justify the investments in the involved technology,

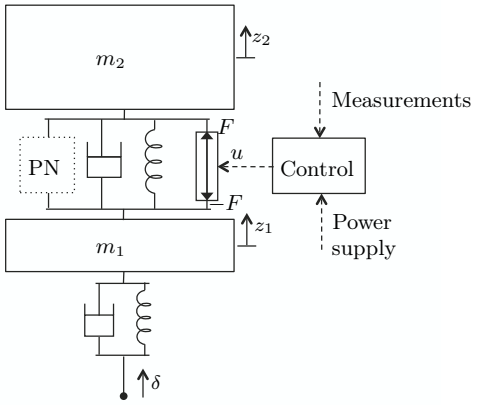

Figure 1.9: Two-mass system with conventional secondary suspension in parallel to a passive network (PN) and an electronically controlled actuator.

2. The vertical dynamic is a relatively simple case of study in railway vehicles for a first investigation on the potential of the inerter in the integrated technology.

Moreover, an interest on also offering to the body of knowledge an insight into the application of the synergy to a more complex dynamic of a railway vehicle, motivated a revision of the synergy for the solution of the wheelset lateral stability problem.

This research concerned: the dynamical problem in a high-speed railway vehicle, and the design of integrated *active-plus-novel-passive* solutions.

1.2.1 The dynamical problem

For passenger comfort in the vertical dynamics, the design of the secondary suspensions is concerned with the isolation of the vehicle body from the transmitted vibrations caused by the track irregularities, with suspension deflections within sensible limits in the transition of the vehicle to deterministic track profiles (e.g. gradients). This defines a design conflict characterised by the vehicle body accelerations to stochastic inputs (i.e. track irregularities) and an estimation of the maximum deflection of the suspension to both stochastic and deterministic inputs.

On the other hand, conventional passive stabilising suspensions allocated in the yaw direction define a trade-off between the vehicle's kinematic mode stability — wheelset oscillations— and curving (i.e. wheelset effects on curved track wear and noise). Therefore, for the wheelset lateral stability problem, the need for actuation and suspension improvements is justified by these undesirable effects that otherwise arise at curving due to the rigid coupling between the wheelsets and the bogie frame in conventional passive bogies.

1.2.2 The design problem

The introduction of new possibilities for mechanical suspensions using the inerter concept is translated into new possibilities of passive mechanical control. However, because of some practicalities, the set of mechanical controllers available would be still limited and therefore required adequate design considerations.

Active solutions are commonly designed by accordingly choosing from an extensive range of appropriate control strategies. These rely upon the system's input and output ports as well as on inherent constraints, e.g. the available measurements, the location of the actuators, and the action/reaction condition for the application of the controlled forces. In order to be able to evaluate the quality of the innovative synergy proposed in this research, the control strategies required meticulous selection and formulation.

In this research, the designed active solutions were individually combined with the conventional suspensions and those newly realisable passive mechanical controllers. For most of the configurations, a multiobjective optimisation problem was numerically solved in order to obtain the best setting of the design parameters.

Altogether, those individual problems constituted a general matter for this research: to investigate if the possible benefits —and/or disadvantages otherwise— of the *inerter* concept in the proposed synergy could be generalised or are only applicable for a particular control strategy or dynamical arrangement.

1.3 Research Hypothesis

The structural modification of the total energy of the mechanical system through the addition of new forms of kinetic energy storage, leads to the simplification of the active suspensions design.

1.4 Research Objectives

The objectives of the research work are as follows:

- to formulate distinct passive networks using the inerter concept,
- to evaluate and propose control solutions for the secondary active suspensions,
- to investigate the potential of inerter-based devices in the simplification of active secondary suspensions design,

- to explore other potentials of inerter-based devices in the implementation of active secondary suspensions,
- to assess the integration on a more sophisticated railway vehicle model,
- to initiate the investigation on the potential of the inerter with active solutions for the stability versus track wear problem.

1.5 Thesis Structure

The remainder of the thesis is organised into eight chapters with its structure and contents summarised as follows:

Chapter 2 *Literature Review, Theoretical Aspects and Thesis Contribution*, reviews relevant aspects of high-speed railway vehicles dynamics, the inerter in the synthesis of novel mechanical devices, current trends on railway vehicle active suspensions and on the use of the inerter, and some pertinent facts for analysis and design. A description of the thesis contribution and the list of publications is provided at the end of the chapter.

Chapter 3 *Mathematical Modelling of the Side-View and Numerical Assessment Methods*, contains the mathematical modelling of a railway vehicle. It is focused on the vertical and pitch dynamics of the bodies. It develops an inerter-based model for the conventional secondary suspensions and analyses its effects on the vehicle dynamics. Intuitive validation of the models is provided through analysis of the vibration modes of the system and step responses. In addition, the chapter includes the model of an electromechanical actuator which is analysed according to the interests of this thesis and a simple actuator force control scheme is presented. Further, it describes the track features considered for assessment of the vertical dynamics, as well as the methods for assessing the relevant performance indices.

Chapter 4 *Analytical Assessment on Railway Vehicle Dynamics Aspects and the Inerter Potential*, contains analytical assessments on the effects of the inerter and other parameters of the passive suspensions for the vehicle body accelerations, the vehicle body kinetic energy function and its first-time derivative, and for the power dissipated in the passive suspensions of the vehicle.

Chapter 5 *Design of Passive and Active Suspensions*, proposes candidate layouts for the mechanical networks describing the novel devices, and presents the

configurations and control strategies of the integrated secondary suspensions studied later in Chapter 6. It introduces a novel nonlinear control strategy for active suspension deflection regulation.

Chapter 6 *Integration of Inerter-based Devices with Active Suspensions*, starts with the definition of a methodology of analysis for the study and comparison of the attained numerical results. It presents and discusses on achievements from the integration for secondary suspensions and optimal tuning of the design parameters.

Chapter 7 *Integration Test in Advanced Simulation*, is a report on results attained by integrating an example case of the integrated secondary suspensions to a more sophisticated model of a railway vehicle using SIMPACK®.

Chapter 8 *Potential of the Inerter for Lateral Stability with Active Solutions*, is a short chapter with an application on the use of inerter-based suspensions in the longitudinal primary suspensions, integrated with active stability control. It describes the lateral dynamics of a half-vehicle system. This aims to open the path for continuing the research in this direction for the enhancement of railway vehicle dynamics employing new concepts.

Chapter 9 *Conclusions and Future Work*, discusses the overall thesis results on the basis of the hypothesis formulated to conclude this research work. It makes suggestions for future work.

1.5.1 Collaborative research work

It was a first collaborative activity between the Control Groups from Loughborough University and University of Cambridge, in which the aforementioned Professor Malcolm Smith and his collaborator Dr. Jason Jiang shared their expertise in the formulation of inerter-based passive networks that later could become in more complex novel mechanical devices. Join investigation on passive suspensions for bogied and two-axle vehicles, for both vertical and lateral dynamic problems, was carried in parallel to the development of this research on the synergy active-plus-novel-passive suspensions. Also, a collaboration with Professor Hebert Sira-Ramirez from CINVESTAV-Mexico took place for a review on some advanced control techniques, including concepts on passivity based control (PBC), dissipativity, and robust techniques for estimation and feedback of the system flat output.

2

Literature Review, Theoretical Aspects and Thesis Contribution

This chapter alludes to research published in the literature related to railway vehicle suspension systems and the use of the inerter concept, setting the background of this research. The taxonomy of this survey reviews concepts from three key and common areas of the design of control systems identified in Figure 2.1, namely: modelling and simulation, analysis, and design. Moreover, special attention is given to the body of knowledge available on vertical ride quality and lateral stability.

The modelling and simulation section reviews: considerations of modelling, solution challenges, and available computational resources for the study of railway vehicle dynamics. The analysis section is focused on two possibly divergent topics: an engineering review on assessment of solutions for railway vehicle dynamics, and a re-

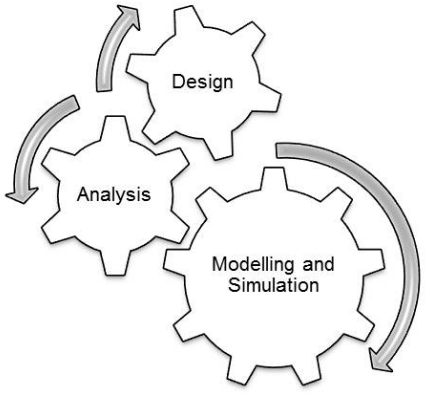

Figure 2.1: Key research aspects.

view relevant to energy and power-based analyses presented later in this thesis. For the latter in particular, optimisation methods based on energy storage and power absorption were examined. Because there is no literature reported yet in this direction for suspension devices based on the inerter concept, this part of the review is on the vibration absorber invented more than a century ago, which finds similarity with inerter-based devices due to their capabilities to store kinetic energy. The design section is dedicated to different types of suspension systems for vehicles dynamics. Much of the review follows topics on suspension systems for conventional high speed railway vehicles [7]. Particular attention is given to suspensions for vertical and lateral dynamics with the inherent pitch and yaw modes. Novel mechanical devices together with the inerter concept are discussed naturally as part of the classification. Techniques previously investigated for railway active suspensions and the inerter concept, as well as the formulation and synthesis of mechanical networks, are summarised. This review makes particular emphasis on railway vehicles although applications for other forms of ground transportation may be also noticed. As a final section, a description on the contribution of this thesis to the field of railway suspensions is provided, together with the list of publications derived from the investigation which is expected to increase in the near future.

2.1 Modelling and Simulation

The study of new concepts feasibility for railway vehicle dynamics is commonly supported by the performance of virtual simulations [23]. These should prove if specifications and possible improvements, within limit values, can be achieved. Mathematical models of the railway vehicle dynamics are normally as complex as the objectives of the model require. Nowadays, with the easier access to fast computing and numerical algorithms, the order of magnitude of the models is far from being a limitation for numerical simulation. However, in the design of control systems for the vehicle dynamics, certain levels of simplicity are required to identify and analyse dominant behaviours.

For the particular case of the description of railway vehicle dynamics, the reader is invited to refer to [24, 23] where the authors discuss on the fundamentals to be considered for the production of models for a typical railway vehicle. The challenging task of modelling railway vehicle suspension components and rail-wheel interaction has been considerably addressed, see for example [6, 25, 26]. Work for the definition of benchmarks for a typical railway vehicle simulation was conducted by Iwnicki [27, 28], presenting vehicle and track models for software and models validation, and the initiation to the analysis and research in the field. Practically possible simplifications are normally included in benchmark models and further simplifications are accepted

if desired.

In multi-body (MBS) systems modelling, an elemental distinction between the vehicle components is made into body components and suspension components. For railway vehicle modelling, Polach et al. [23], point out the need of considering aspects such as the structural flexibility of the passengers cabin, justified by the contribution of the prominent structural modes (normally around 10 [Hz]) to the vertical accelerations at frequencies at which the human body is more sensitive (below 20 [Hz] [29]), specially at the centre of the cabin for fairly high running speeds or relatively poor track conditions. Nevertheless, the models considered in this thesis are focused on rigid bodies only which is a well accepted practice for initial assessment of new technologies. A careful modelling of the suspensions components [25], the wheel-rail interaction [30, 31, 32], and the track characteristics (flexibility, geometry and irregularities) [33] is essential. Evans in [34] discusses about the requirements for multi-body simulation. Adequate assumptions enable simpler modelling suitable for certain studies, e.g. those derived from linear analysis. The work in [35] is a review on existing models for suspension components and track models for railway vehicle dynamics simulation, and methods for model validation. The authors in [23] highlight the strong frequency dependence of the airsprings related to the airbag dynamics itself and the inertial effects of the air mass and losses in the pipe connecting the airsprings with their air supply reservoir (if so). Research on the frequency characteristic of airsprings vertical dynamic, in particular, is reported in [36, 37, 38, 39]. In [40, 8], the authors give special attention to modelling requirements for the design of active suspensions.

For representing the disturbed dynamics of the vehicle, Pratt [5] used simplified linear systems of ODEs (Ordinary Differential Equations) to research active suspensions and actuator technologies applied to single vehicles and trains on the basis of planar models. In brief, the equations of motion of a general mechanical system, such as a railway vehicle, described by ODEs are presented in the form of a second order ODE: $\mathbf{M}(q)\underline{\ddot{q}}(t) = \underline{f}(q, \dot{q}, t)$ with $\mathbf{M}(q)$ the positive definite inertia matrix of the system. Zheng [41] employed also linear ODEs for the description of the rigid bodies motions and the description of the first two flexible motions of the passengers cabin for the analysis and design of active suspensions via smart structures. Md Yusof [42] developed control strategies for control of the forces applied by actuators in the vertical direction of the secondary suspension of a railway vehicle modelled using also linear ODEs.

Arnold et al. in [43] discussed the complexity of the models described in ODEs or DAEs (Differential Algebraic Equations) to characterise and simulate the constrained dynamic of a vehicle in general, together with a review on the state-of-the-art of numerical methods for solving this type of problems. In the study of vehicle dynamics

it is fundamental to count with solution methods enabling to perform analyses such as: quasi-static analysis, linear stability, eigenmode, and stochastic analyses, among others. Also, time-stepping integration for the solution of linear and nonlinear equations of motion for which a wide range of numerical methods are available constitutes a very relevant method. For a complete list on the typical dynamic analyses and calculation methods applied in railway vehicle engineering, see [23].

As for virtual simulation, among the major MBS computational packages available for railway dynamics, feature: ADAMS/Rail-MEDYNA©, SIMPACK/Rail®, NUCARS®, GENSYS® and VAMPIRE®. Software systems provided with suitable solvers as MATLAB/Simulink®, Mathematica® and Maple®, are on the other hand available for implementation of analytical and simplified models, as well as for the control systems design. For the development of this thesis, MATLAB/Simulink® and *Mathematica*® dedicated solvers were employed; Chapter 8 presents results obtained for advanced simulations performed in SIMPACK/Rail®.

2.2 Analysis

Core techniques and concepts of analysis are discussed here and extended later with specific details in the appropriate chapters. It is important to remember at this point that the main body of this research is dedicated to analysis and design of the synergy applied on the secondary suspensions for vertical ride quality. This justifies the content of this sub-section.

2.2.1 Ride characteristics

Ride characteristics are important aspects of the vehicle dynamic behaviour and can be assessed through the computation of the vehicle body accelerations. For this, considerations of a straight track and constant running speed are normally made [5, 44, 41, 45]. Ride comfort, in particular, indicates the influence of the vehicle behaviour on the human body and is typically calculated through frequency-weighted functions applied to the vehicle body accelerations power spectral density (PSD) function (e.g. ISO 2631 [46], the Sperling's method [47], or ENV 12299 [48]). Orvnäs [49] presents a categorisation of ride comfort according to the most common norms. However, recent research has demonstrated that these commonly known standard norms to determine ride comfort indices underestimate the effects of vibrations on the passengers' normally sedentary activity (e.g. writing, reading, sketching, working with laptops) [50, 51, 52]. Unweighted accelerations are used along this thesis for the assessment of 'ride quality', instead of focusing on particular comfort characteristics. Standards and specifications associated to ride characteristics of a railway vehicle

are normally given for the most unfavourable location on the vehicle body (among front and rear positions above the bogies and at the centre of the vehicle body in the longitudinal direction, and centre, left and right in the transverse direction) [23]. Thus, designs attempting the enhancement of comfort levels should target to improve the measurement at such position without deteriorating the measurement at the other locations. According to [23], the main sources of ride comfort deterioration are: low damping or instability of the vehicle body mode, resonance from the eigenmode of the vehicle components, and the vehicle speed influence in the excitation of 'critical wavelengths'.

2.2.2 Lateral stability

For the study of the lateral stability, analysis of the eigenmodes of the lateral dynamics of the vehicle bodies is typically performed [53, 54, 1, 23]. In that sense, the normal objectives for the control system design (applied either in the lateral, longitudinal and/or yaw direction) and assessment of the results are either to improve the most critical damping coefficient of the system modes for a nominal speed or to increase the value of the critical speed. Besides stability, the forces emerging from the wheel-rail interface when wheelsets negotiate curved tracks impose additional requirements to the design, albeit the control solutions for this aim are normally separated from the stability solutions. Steering control is dedicated to *perfect curving*, targeting: a) equal lateral creep forces on all the wheelsets to minimise track shifting forces, and b) zero steady-state longitudinal creep forces on all wheelsets. Some lateral creep is required in order to provide the necessary force to counterbalance the centrifugal force on curves, while longitudinal creep forces are associated to wear and noise and thus the design requirement is to significantly reduce them [10, 55, 56, 1].

2.2.3 Energy and power dissipation

Furthermore, an analytical study based on the system energy functions and the suspensions power dissipation was found of importance in this thesis to understand the inerter effects, as a kinetic energy store.

Although outside the inerters theme, Efatpenah et al. [57], for example, investigated energy requirements of passive and active suspension systems implemented by means of electromechanical actuators. By using bond graph theory, they related longitudinal and transverse energy paths, found savings of the overall energy of the system with the implementation of active suspensions, and realised that supplementing actuators by passive springs reduces the amount of energy required to drive the electromechanical actuator as compared with the energy dissipated by conventional shock absorbers. Corriga et al. [58] and Giua et al. [59], on the other hand,

developed optimal approaches for the design of active suspensions with minimised power consumption by employing passive together with the active suspensions. As for power dissipation of passive suspensions, Smith and Swift [60] investigated, for an automotive application, the effects of the parameters of the suspensions (springs and dampers) and the tyres on the total power dissipated, finding that the suspensions parameters practically have no influence on the total mean dissipated power. Continuing with energy matters, topics such as regenerative suspensions and energy harvesting suspensions have been the focus of many researchers [61, 62, 63, 64]. In particular, Ichchou et al. [65] proposed a 'global semi-active (or regenerative) control' strategy with an efficient energy management protocol of the optimal control process through the use of accumulators so that it performs equivalently to an active control strategy, by considering dissipative and energy-demanding phases (unlike semi-active suspensions).

Moreover, for a first understanding on the effects of inertance in the vehicle suspensions for the ride characteristic and on the active suspensions design and performance, it is of interest to recall the classical concept of *dynamic vibration absorbers* (DVA) patented in 1911 by Frahm as a device to absorb bodies vibrations [66, 67]. If a damper is included to a DVA, it becomes in a so-called tuned mass damper (TMD), and attenuation for a range of frequencies is provided to the primary system. For the TMD, the optimisation problem results less obvious than setting the natural frequency of the device at the frequency of the harmonic to cancel, as in the DVA. Hence, tuning the TMD for an optimal performance will always depend on the chosen optimisation criterion. Defining the optimisation criterion has been a classical problem for analytical optimisation as a body of knowledge. For this, it is normally considered that the primary system consists of (or can be approximated to) a single-mode spring-mass structure for the vibrational mode of interest, more often without damping. Zilletti et al. present in [68] a brief review on different optimisation criteria used to tune the dynamic absorber parameters. Among these, it is worth to extract the main idea of the work of Warburton in 1982 (referenced in [68]) consisting of a tuning method to optimise the kinetic energy of the primary system by averaging its frequency function. Zilletti et al. further studied this optimisation problem and found that the device parameters resulting from the maximisation of the power absorbed by the damper of a TMD corresponds to the minimisation of the kinetic energy of the primary system, which is exposed to random force-type excitations at the base with flat power spectral density. Furthermore, they found that the area under the PSD curve for the velocity of the primary system mass in response to the excitation with flat spectrum is minimised for the method of 'minimised kinetic energy' (and, thus, for the maximised power absorbed by the damper), as compared with other optimisation criteria including $\mathcal{H}_2$ and $\mathcal{H}_\infty$ methods applied

for the primary mass displacement. Even if these findings are not formally translated to the current problem in this research, they will be useful to follow the analyses and results on the potential of the inerter presented later, starting from Chapter 4.

2.3 Suspension Design

In the following, a survey on suspension design for vehicle dynamics is presented. Challenges for railway vehicle dynamics are particularly discussed with reference to previous research reported in the literature. A classification according to power requirements is provided, with a more general review on applications and techniques developed in both automotive and railway dynamics.

2.3.1 Challenges

The analysis and design of suspension systems and other forms of vehicle dynamics compensators find particular and rich applications in railway, automotive, bicycling, motorcycling, aircraft landing, among other forms of transportation vehicles. Suspension and compensation objectives range among ride comfort, stability, handling, grip, steering, and safety, to mention a few.

In railway vehicles, challenges are differentiated from other forms of wheeled transport because of the guidance of the wheels provided by the track in the lateral direction. Track irregularities and deterministic profiles (such as curves) cause dynamic forces and produced accelerations that are transmitted to the passengers cabin causing discomfort and motion sickness. In addition, contact forces generated in the wheel-rail interface are responsible for self-excited lateral oscillations that cause stability problems at high speeds. Moreover, solutions for stability normally conflict with the provision of effective and efficient guidance around curves, which includes reduction of track wear [69]. Solutions for ride enhancement, on the other hand, conflict with stiffness requirements to guarantee effective load support [8]. Therefore, opportunities for different forms of suspension systems are evident. Either selective or frequency dependent behaviours in the dissipative systems for ride comfort, for example, contribute to the provision of alternatives to the simplification of the dynamical problems. Stability, ride quality, safety factors, wear levels, and critical speed are factors determined by the vehicle suspensions and linkages, and by other elements of the running gear. Orlova and Boroenko in [70] presented a complete description of the running gear elements with appropriate description on the type, role and selection of the mechanical components.

For the matter that concerns this research, it is important to distinguish between primary and secondary suspensions for bogied vehicles (Figure 1.1), for which im-

portant definitions and detailed descriptions appear in [7]. Given the type of interconnection these provide, it is also necessary to differentiate between vertical, lateral and longitudinal suspensions. Compensation schemes implemented at the secondary suspension layer in the vertical (Figure 1.1) and/or lateral (Figure 1.3) direction allow for performance improvements for ride quality in the correspondent direction, whilst the primary suspensions in the lateral and longitudinal direction (Figure 1.3) determine stability and guidance quality ([10] for a distinction on the suspensions degrees-of-freedom, although already with particular attention to active solutions).

2.3.2 Classification

The classification of vehicle dynamic suspensions —and vehicle dynamics control in the same context— involve different criteria. In the light of this research this follows the power supply requirements criterion only: those without external power supply requirements, such as passive and semi-active (the former having fixed characteristics as opposed to the latter for which the characteristic can be rapidly varied by electronic controllers), and those with external power supply, known as active or *full-active* (see [4]). Therefore, according to the control law designed for the active suspensions, energy can flow in or out of the active suspension. Suspension systems in the primary and secondary layers are discussed with particular focus on control for vertical and lateral ride quality and bogie stability; technology and control methods for tilting trains are not included.

2.3.2.1 Passive suspensions

Passive suspensions cover the range of mechanical, pneumatic and hydraulic suspensions, without electronics-based actuation. Conventional vehicle suspensions with fixed characteristics enter this group, together with the novel mechanical devices —inerter-based— investigated in this thesis.

2.3.2.1.1 Conventional suspensions Conventional suspensions comprise complex elements characterised by either linear (quasilinear) or strictly nonlinear behaviours, and mechanical networks employing simpler elements (e.g. linear coil springs, dampers, masses, and levers). The simplest form of conventional suspensions comprise a parallel configuration of spring and damper (e.g. primary suspensions in railway vehicles, tyre modelling in most forms of vehicle systems, and also coincides with the linear model of the bushes of mechanical appliances and simple forms of buffer networks). For the case of secondary suspensions in railway vehicles, conventional passive suspensions typically comprise air suspensions —airsprings— normally

with a damping valve controlling the air flow (automatic regulation of the valve turns the suspension into a semi-active mechanism). Airsprings show frequency dependent stiffness characteristics [37, 36, 71], providing the vehicle with —*pneumatic*— support and dynamic compensation for ride comfort. In a railway vehicle, as mentioned before, lateral and longitudinal conventional stiffnesses distinguished in the plan-view of the vehicle must provide the best compromise to guarantee the vehicle stability while running on a straight track, and to adopt radial positions under curving conditions. For this, the application of even yaw stiffness is typically modified or complemented by suspensions with appropriate dynamic characteristics (usually by provision of hydraulic damping or friction in the elastic elements) [72, 73]; advanced bogies design can also address the conflict [70].

2.3.2.1.2 The inerter and inerter-based novel devices The introduction of the *missing mechanical circuit element* as published in [12] to refer to the *inerter* expanded the views on translational passive networks and their implementation, which were certainly limited. It enabled the design of new forms of passive mechanical control. Later, the inerter concept was introduced to the design of hydraulic suspensions whose dynamic characteristic can be approximated by mechanical networks comprising springs, dampers and inerters.

Before the inerter, implementation of translational mechanical networks following classical networks theory was reduced to the use of rigid interconnections of springs, dampers, levers and masses, the two latter being quite inconvenient in the design of suspension systems due to the trade-off between lever length and the absolute values of the masses required to provoke large levels of inertia. Moreover, using springs and dampers only constrains the type of complex admittances describing the ratio between the device's developed force and the velocity at the terminals in the complex plane. The limitation was fundamentally in the allocation of the poles and zeros of the admittance function, these could be placed only on the negative real axis [74]. Introducing inerters into the suspension configuration together with springs and dampers forming a mechanical network (similar to what is done with electrical networks using inductors, resistors and ungrounded capacitors, according to the force-current analogy [3]) enables the placement of the zeros and poles of the suspension admittance in the left complex semi-plane, and not only on the real axis.

The ***technology*** of the inerter essentially consists of a two-terminal either mechanical or hydraulic device with kinetic energy storage capabilities. A mechanical inerter normally comprises a flywheel system like in the rack-and-pinion and the ball-screw inerters in Figures 2.2(a) and 2.2(b), respectively, to store kinetic energy due to the linear movement of the terminals of the device (see the Patent No. US 7316303 B2 [75] for a detailed description). On the other side, a hydraulic inerter

stores kinetic energy as means of the balance of mechanical forces caused by the mass of a liquid moving in a configuration of flow paths (e.g. helical paths) due to a piston-cylinder embodiment containing the liquid and causing the flow; a schematic of one of the configurations of the hydraulic inerter is shown in Figure 2.2(c) (refer to the Patents No. US 2012/0199428 A1 [76] and W0 2011/095787 A1 [77] for a detailed description of the hydraulic inerter, together with other novelties describing behaviours of arbitrary mechanical networks). Some other relevant inventions in passive suspensions using the inerter concept have been disclosed, it is worth mentioning: more general force-controlling mechanical devices as described also in [75], force-controlling hydraulic devices as in [76], the fluid inerter claimed under the Patent No. WO 2011/089373 A1 [78], the screw-type inerter mechanism under Patent No. US 2009/0108510 A1 [79], the hydraulic inerter mechanism under Patent No. US 2009/0139225 A1 [77], and the mechatronic suspensions with inerter mechanisms under Patent US 2010/0148463 A1 [80]. In general, these attend the theory of passive networks [3] for the construction of arbitrary passive mechanical impedance including interconnected (linear) springs, dampers and inerters. For described methods see for example the patent on force-controlling mechanical devices [75] and the first formal publication about the inerter concept and device for the synthesis of mechanical networks [3]. Similar —although separated— concepts have been developed also for absorption of kinetic energy. An example of this is the two-terminal flywheel reported in [81] and [82] for vibration suppression, which using an inverse screw transmission mechanism for two-terminal manipulation of a flywheel, emulates a free two-terminal mass component with inertial mass equivalent to a magnified value of the gravitational mass of the flywheel. Another example is found in the absorption of kinetic energy of collisions as the EPAR technology [83]. In particular, a range of flywheel-based mechanisms with different applications can be widely found in the literature.

Practicalities around the inerter-based devices are discussed together with the patented inventions description in the referred claim documents. Experimental work on nonlinearities of a ball-screw mechanical inerter in vehicle suspension control was carried out by Wand and Su [84, 85], who determined the influence of nonlinearities of the device (i.e. friction, backlash and elastic effects) in the behaviour of a vehicle suspension. Wand and Su found some performance degradation due to the inerter nonlinearities although with still better performance than with the traditional suspensions. In particular, they model the elastic effects by placing a parallel spring damper arrangement in series with the inerter with backlash (contact/no-contact model) and static friction. The latter resulted in almost a square wave in response

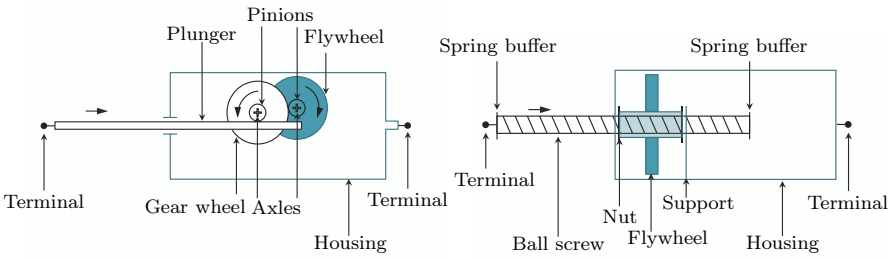

(a) Mechanical inerter: rack and pinion configuration [75]

(b) Mechanical inerter: ball screw configuration [75]

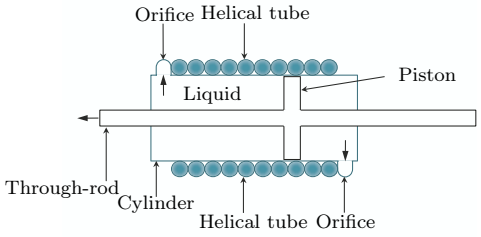

(c) Hydraulic inerter [76, 77]

Figure 2.2: Examples of inerter technologies.

to low frequency sinusoidals. Papageorgiou et al. [86] identified the backlash characteristic of a rack-and-pinion and a ball-screw mechanical inerter which caused unstable interaction with the control system of the testing platform; they proposed to place a buffer network consisting of a parallel combination spring damper to avoid the instability and to enable the identification of the mechanical admittance of the mechanical devices. Jiang et al. [87] performed experimental testing and modelling of an inerter-based compensator for motorcycle steering. They found that friction and backlash models were necessary to match the device performance at low and high frequencies, respectively. Smith and Wang [88] tested a rack-and-pinion prototype for a series arrangement damper inerter with centring springs for which a correction of the ideal model was provided by incorporation of stiction nonlinearities for the damper and inerter devices as parallel stiction forces defined also as square waves determined by the sign of the velocity of the correspondent elements (i.e. damper and inerter). Among the most relevant aspects of the practicalities, only elastic effects and linear friction were considered for this study.

In common, the inerter technology was first researched for automotive ***applications*** [12, 88, 89, 84, 90], and in particular it has been deployed in racing cars[1]. Also in the vehicle dynamics field, passive networks using inerters have been investigated in the

[1]Indeed, one of the biggest suppliers of shock absorbers components for Formula 1 teams entered in 2008 on a license agreement with Cambridge Enterprise, the commercialisation office of the University of Cambridge where theoretical work on the inerter began. : Luke, Penske Inerter Deal. August 22, 2008, Racecar Engineering.

compensation of the main oscillatory modes of high performance motorcycles [91, 13] and in passive control of different dynamical behaviours in railway vehicles with single and double stage suspensions [16, 17, 18, 19, 20, 21, 22] , proving benefits in all cases. Among these studies for railway vehicles, beneficial effects on enhancing ride quality in the vertical and lateral direction, on improving stability at a nominal speed, and on increasing the vehicle critical speed have been shown through results from computational simulation. Some of these authors have considered only the quarter vehicle (for which some experimental test was performed), and/or simple secondary suspensions models (i.e. a parallel configuration spring damper); furthermore, others included three-dimensional (3D) simulation in advanced modelling software. In all these tests, inerter-based configurations have proven some potential for the particular dynamics studied although not comparable to results attained with active solutions. The work presented in [20, 21] employed the same models used in this research as these were part of the outcomes from the collaborative activity of the author and this thesis' supervisors with the University of Cambridge undertaken in parallel with this project to investigate the inerter potential in passive suspensions only. Nevertheless, in every case, previous research was concentrated on the potential for the inerter with passive suspensions only. Other outside applications of the inerter have been explored in buildings suspensions [15].

The ***design*** of inerter-based mechanical networks may be based in the formulation or determination of a general positive-real admittance to be synthesised by using springs, dampers and inerters following networks synthesis methods [92, 3]. To pose the problem under this methodology for optimal suspensions design, previous research (e.g. [12] for automotive, [17] for trains) has defined a problem of Bilinear Matrix Inequalities (BMI). The BMI problem is formulated for the closed-loop system according to the norms of interest (e.g. $\mathcal{H}_2$-norms of the performance indices for [12, 17]) to restrict the set of stabilising controllers that achieve a desired set of performance indices upper bounds, together with the passivity condition (real-positivity constraint [3]) which converts the conventional Linear Matrix Inequality (LMI) problem (for unrestrained suspensions, i.e. rather active) into a BMI. Afterwards, specialised computational algorithms for solving BMIs are used (e.g. YALMIP [93]). Classical synthesis methods for electrical networks like Brune synthesis and Darlington synthesis can then be translated from the synthesis of one-ports electrical networks in terms of resistors, inductors and capacitors, to the synthesis of this type of one-port mechanical networks [3], [12] once the admittance function is defined. The interconnection and number of resistive (dampers) and reactive (springs and inerters) elements that systematically synthesise the resultant or formulated passive network admittance, however, is normally unknown *a priori*, is constrained and depends on the chosen method and intermediate assumptions. In this direction, recent

research by Jiang and Smith [94, 95] has extended former work on the formal classification of certain classes of one-port low-complexity passive networks realisable for positive-real functions, as a revived interest after the inerter concept. Moreover, introduction of models approximating practicalities of the physical devices will not result from this methodology.

As an alternative to network synthesis, the design could focus on the empirical formulation of the one-port mechanical network [88, 91, 17, 20, 21]. In this case, the design relies on knowledge and experience of defining an also feasible mechanical network whose admittance could passively control the vibrational system by predefining the number and type of elements and their interconnection. This method of design also enables to model approximated inherent effects of the physical device through linear mechanical equivalents. For optimal performance, an optimisation problem may be formulated and solved using numerical algorithms for tuning the parameters defining the elements characteristics [20, 21] to achieve optimal performance. This approach was adopted in this research.

2.3.2.2 Semi-active suspensions

Semi-active suspension has been an accepted technology owing to its fail-safe property since some years ago; their reliability is comparable to passive suspensions [96]. Their adaptability without power sources requirements make them an option for vehicle performance improvement, although not normally with the same achievements as with active suspensions. Semi-active suspensions are typically associated to the regulation of the damper characteristic, but also to stiffness modification in air suspensions. Goodall and Mei in [10] make a brief comment on an interesting option of implementing electronically-controllable springs whose existence is yet unknown. Similar configurations are semi-passive, adjustable passive and adaptive passive suspensions. These are associated with a rapid variation of the passive element controlled characteristic based on measurements which are not necessarily a variable of the system dynamics [10].

As a real case example, in Shinkansen trains (regarded as some of the most advanced trains in the world) the controlled characteristic of the suspensions provided improvements on the ride comfort in the lateral direction [97], prior to the implementation of full-active suspensions. Lateral semi-active suspensions counteract the worsening ride quality arising in the progress of the trains speeding-up. The requirements description for this was as follows: small damping in the lateral secondary suspension for high frequency conditions (track irregularities), and large damping to dissipate the movements provoked by aerodynamic forces actuating directly on the carbody. To achieve it, dampers with rapidly switching characteristic in a range of steps were

effectively installed and controlled by a skyhook control law.

Examples of semi-active devices are dampers with controllable fluids such as electro-rheological and magneto-rheological fluids, devices with controllable friction, and variable orifice dampers. Wang and Liao [98] modelled a full-scale vehicle with integration of semi-active controlled magneto-rheological dampers in the secondary suspension for the vehicle lateral, yaw, and roll motions compensation showing effectiveness over passive suspensions for random track irregularities. The semi-active dampers were controlled by a Linear Quadratic-Gaussian (LQG) control law using acceleration feedback. A pertinent example of semi-active implementation is the airspring with controllable damping and/or stiffness tested for automotive and railway applications (e.g. [99, 100]). Liang and Wang [100] presented a design of a semi-active airspring suspension with adjustable damping, controlled by an adaptive feed-forward control law, showing effectiveness of the control strategy and the implementation through the provision of a wider range of frequencies at which the airspring can isolate the vehicle from vibration. Several other examples of research on semi-active solutions include the use of control strategies based on intelligent algorithms [101, 102], robust control strategies [103], 'skyhook' based strategies [104], sliding mode control [105], PID control [106], for improving vertical ride comfort and handling through stiffness control using carbody accelerations feedback), and mixed strategies.

2.3.2.3 Active suspensions and steering

Extensive work has been done already on active suspensions, being of great interest due to their capabilities to outperform passive and semi-active systems. Active solutions, including suspension and steering, can provide better solution to the different conflicts arising from vehicles dynamics by extracting but also introducing energy into the system. This creates, however, design conflicts regarding the physical size of the actuators and the amounts of power required to drive them to implement the active solutions. Moreover, the clearance required by active suspensions for operation under deterministic conditions imposes an additional issue to the design; typically, the suspension clearance is of 3.5 [cm] [5]. Important aspects on active suspensions and steering design were discussed in [4], by Goodall and Mei.

Active solutions in railway vehicles cover mainly three distinct categories: tilting, active secondary suspensions, and active primary suspensions and steering. Notwithstanding the conservativeness of the rail industry, Iwnicki [107] mentioned in his paper on future trends in railway engineering in 2009 that mechatronic technology has started to be adopted and envisages that even if small at the time being, further incremental improvements on railway vehicle dynamics by these means will continue.

In fact, tilting trains technology is nowadays in widespread use. Primary and secondary active solutions on the other hand yet require more established reliability and confidence to accompany the big improvements these offer. The most recent version of the state-of-the-art in the field was undertaken in 2007 by Bruni et al. [10]. More recently, in 2010, Orvnäs [49] surveyed methods for reducing vibrations in the vehicle body of a railway vehicle, discussing on active suspensions achieving between 30 and 50% of ride comfort enhancement. The trade-off between ride comfort and suspension deflection is commonly reported for active suspensions, the same than a reduced ride quality improvement due to the real actuator dynamics. A more updated review performed by the author evidenced the novelty of this research on the use of inerter-based devices to simplify the design of active secondary suspensions and active stability control.

Among the control strategies typically researched, a diversity of configurations has been proposed on the basis of the intuitive, classical, output-based, skyhook damping concept, as proposed by Karnopp [108] in 1973 for attenuating carbody accelerations by virtual energy dissipation based on absolute velocity measurements [5, 109, 110, 44, 41, 111, 112, 45, 113]. Also, (model-based) linear and nonlinear optimal control techniques have been extensively studied for different dynamical problems; optimal control techniques provide the advantage of directly accounting for the design trade-offs. Examples reported in the literature for different applications in suspension design are [5, 41, 114, 115, 116]. Although strategies such as Linear Quadratic Gaussian (LQG) Regulator considering the suspension deflections as one of the design objectives can produce up to 50% of ride quality improvement, still large deflections are obtained [5]. Other approaches based on modal control [5, 4], classical compensation (which include filtering considerations in many cases) [5], sliding control [117, 118, 119], $\mathcal{H}_2$, $\mathcal{H}_\infty$, and mixed $\mathcal{H}_2/\mathcal{H}_\infty$ control [41, 45, 120], model predictive control [121], intelligent control [122, 123], linear parameter-varying control (LPV) [124], constitute also the type of control techniques commonly investigated for railway suspensions design.

As for implementation of active suspensions, electrohydraulic, electromechanical and electromagnetic actuators are normally the class of actuators employed [5, 42]. Real actuators are limited in different static and dynamical aspects. Regarding the static aspects, the main restriction is in the range of forces these can develop. From the dynamic point of view, the most fundamental practical consideration in active suspensions design is about making an 'almost perfect' force-tracking real actuator, which is difficult to achieve as the actuator internal dynamics normally affect the frequency performance of the designed ideal active suspension scheme [5]. Md Yusof [42], for example, researched the improvement of real actuator dynamics by integrating internal control loops for force-tracking control.

2.3.2.4 Integrated suspensions

As introduced through this thesis objectives, the aim is to evaluate the performance of synergetic —cooperative— suspensions for a railway vehicle so that passive and active suspensions help each other rather than compete. In that sense, this is similar to what was discussed by Fijalkowski in [125] for hybrid suspensions in automotive, and earlier by Smith et al. in [126] for the optimisation of vibrating structures. The common and main objective of these combined suspensions is to reduce power demands and actuator size in terms of maximum forces demanded (see, for example, Corriga et al. [58] and Guia et al. [59]). Some work has been done in this direction for suspension systems in general, by supplementing the actuators with simple arrangements of springs and dampers, or even redesigning the system parameters to constitute the passive part of the suspension as in [126]. References on this can be found by searching on keywords such as "hybrid suspensions", "combined suspensions", "tandem passive-active suspensions", "mixed suspensions", and so on. Moreover, for railway suspensions, most of the applications of active suspensions have been investigated to work together with the conventional passive suspensions [5, 45], and may be further aided by springs in the modification of the actuators bandwidth, for example, when considering real actuator dynamics [42]. However, no attempt to create cooperation between inerter-based suspensions (which have proven some benefits for passive suspensions as stated before) and active suspensions have been found as reported in the literature. The only previous work on developing mechatronic solutions using the inerter concept is the mechatronic network system proposed by Wang and Chan [90, 127, 80], who developed an inerter-based mechanical network combined with a permanent magnet electric machinery (PMEM) for the implementation of high-order networks for vehicle suspensions. The mechatronic device comprises a ball-screw type inerter and high-order electrical circuits. Nevertheless, this differs from what is studied in this thesis.

2.4 Research Contribution and Publications

2.4.1 Research Contribution

At present, there is a great opportunity to research the conventional passive suspensions of a railway vehicle, as introducing active solutions —excluding tilting— is still at a maturing stage. Following the success of the inerter technology for racing cars passive mechanical control, and the demonstrated benefits it can bring to railway vehicle dynamics, this work investigates potentialities of inerter-based mechatronic solutions.

The specific contributions of this research to the railway dynamics control field are:

- Development of a synergetic concept consisting in the integration of inerter-based mechanical suspensions and active solutions.
- Formulation and investigation of different configurations integrating inerter-based suspensions with different control strategies for ride quality enhancement.
- Integration between the capabilities of the 'absolute yaw stiffness' stability control strategy [1] and novel suspensions replacing the conventional longitudinal passive stiffness.
- Design of a nonlinear active control strategy for regulating secondary suspension deflection inspired by the passivity of the system; *'adaptive stiffness'* is the name adopted for the strategy.
- Analytical investigation of the proposed synergy for ride quality solutions.

The diagram in Figure 2.3 illustrates the proposed synergy with distinctions on the novel mechanical suspensions and the class of active solutions considered in the research.

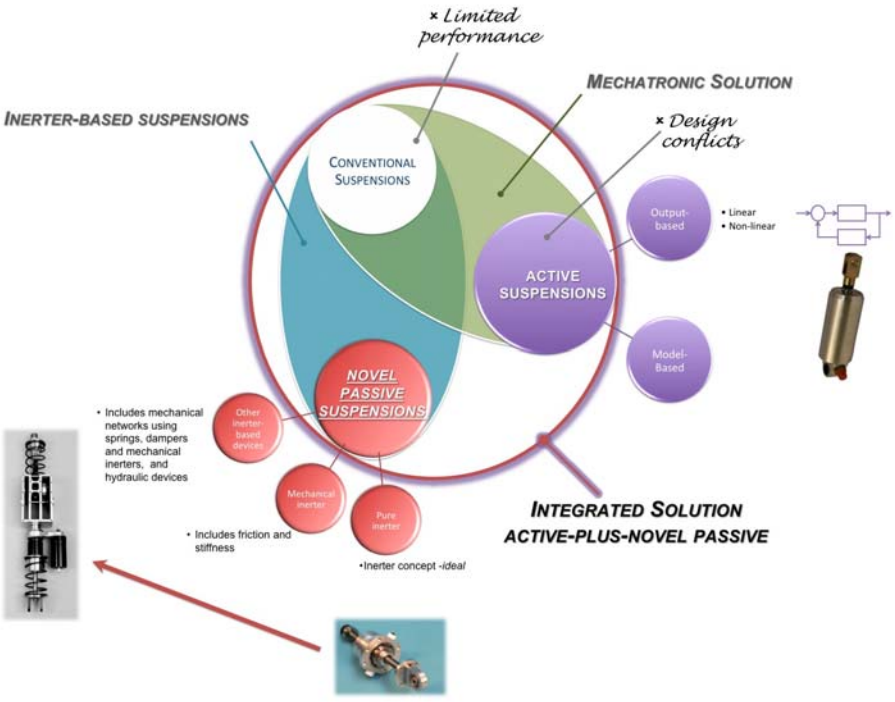

FIGURE 2.3: General diagram of the study on *active-plus-novel passive*.

2.4.2 Publications

In Book:

- Jiang J. Z., ***Matamoros A. Z.*** , Goodall R. M. and Smith M.C. *Performance Benefits in Two-Axle Railway Vehicle Suspensions Employing Inerters*, in: Developments in Control Theory towards Glocal Control. United Kingdom: Institute of Engineering and Technology (IET), 2012, pp. 99–107.
- ***Matamoros-Sánchez A. Z.***, Sira-Ramírez H., Goodall R. *Estimación y Control por Realimentación de los Estados de la Salida Plana de un Vehículo utilizando un Observador GPI*, in: Aplicaciones de Control, Automatización, Robótica y Visión Artificial. Venezuela: Universidad de Los Andes, 2011, pp. 97–112.

In Journal:

- Jiang, Z., ***Matamoros-Sanchez, A.***, Goodall, R., Smith, M. "Passive Suspensions Incorporating Inerters for Railway Vehicles". Vehicle System Dynamics., vol. 50 (Suppl. 1), pp. 263-276, January 2012.

In Proceedings:

- ***Matamoros-Sanchez, A. Z.***, Goodall, R. M., Zolotas, A. C., Jiang, J. Z. and Smith, M. C. "Stability control of a railway vehicle using absolute stiffness and inerters". UKACC International Conference in Control, Cardiff, UK. September, 2012.
- ***Matamoros-Sanchez, A. Z.***, Jiang, J. Z., Goodall, R. M. and Smith, M. C. "Effects of inertance in railway vehicles with active control". 23rd International Congress of Theoretical and Applied Mechanics. Beijing, China. 2012.
- ***Matamoros-Sanchez A.***, and Goodall R.M. "The Optimisation Problem in the Enhancement of Railway Vehicles Performance using Novel Suspension Systems ". CIMENICS 2012, Porlamar –Venezuela.
- Sira-Ramirez, H., ***Matamoros-Sanchez, A.***, and Goodall, R.M. "Flatness Based Control of a Suspension System: A GPI Observer Approach". IFAC World Congress 2011, Milan –Italy.

In progress: (tentative title)

- Jiang, Z., ***Matamoros-Sanchez, A.***, Zolotas, A., Goodall, R., Smith, M. "Passive Suspensions for ride quality improvement of two-axle railway vehicles" (to be submitted as a journal publication).

2.5 Summary of the Chapter

A survey on relevant concepts around the modelling, simulation, analysis and design of compensation systems for vehicles dynamics was presented. A review on ride quality and lateral stability is provided as the relevant aspects of railway vehicle dynamics for this thesis. A survey on studies on power management and optimisation problems around power and energy functions for active suspensions was performed as a background for analytical aspects studied in Chapter 4 based on energy functions. Much research have been developed during the past decades for enhancing vehicles performance by introducing different forms of compensation. Particular emphasis was done on the frequency dependent characteristic of airsprings and on the inerter as a new concept, its current technology and practicalities, and to the design of translational mechanical networks. Passive suspensions using inerters have demonstrated benefits for different dynamics in railway vehicles, apart from other type of vibrational systems. Also, combination of conventional passive structures with active suspensions have proven beneficial in previous research, but considerations on introducing inerters in the passive part have not been done in the past. The mechatronic inerter [90, 127, 80] is the most similar idea although yet far from what is studied here. The closest concept to incorporation of inerters to realise mechanical suspension systems is the old concept of the dynamic vibration absorber and the tuned mass damper, for which analytical studies on optimal solutions are widespread. As for semi-active and active suspensions design strategies, feedback of the absolute velocity of the suspended mass, commonly denominated 'skyhook damping' pioneers the research on ride quality, but several output-based and model-based control techniques have been also investigated. The contribution of this research has been placed in context.

3

Mathematical Modelling of the Side-View and Numerical Assessment Methods

In the analysis and control systems design for railway vehicles, as a result of the complexity of the overall dynamical system, representing the high-dimensional dynamics of the vehicle with simpler models is a well accepted practice. The degree of simplification is subject to the accuracy levels desired for studying particular phenomena appearing in the vehicle dynamics. This chapter develops mathematical modelling of the vertical and pitch modes of a railway vehicle for decentralised control design. Towards the end of this thesis, Chapter 7 presents a more sophisticated model assisted by multibody simulation software, and Chapter 8 presents the mathematical model for the simulation of lateral and yaw motions.

The main aim of this thesis is to complement the secondary suspension of a bogied vehicle via integrated solutions comprising inerter-based devices and active control for enhancing the vehicle ride quality. This chapter is dedicated to the mathematical modelling of this type of vehicle. Although during the development of this research some effort was also devoted to the design of passive suspensions using inerters for non-bogied vehicles, modelling and results are excluded from this manuscript. For a control treatment in the vertical dynamics of a two-axle vehicle see [128] for some achievements using inerters.

This work concerns on the dynamics of the passenger cabin of a single vehicle and, hence, inter-vehicle dynamics are omitted. Also, detailed geometry of the vehicle bodies, aerodynamic factors, body flexibilities, non-linearities of the wheel/rail interaction forces, are some of the factors not accounted for in the model. In this chapter, the reader will discover the main features describing the vertical dynamics

one is most interested on for vertical vibrations control design, and moreover for the aim of studying the potential of inerter-based integrated solutions.

The first section of this chapter describes a railway vehicle as a multibody system, discusses the modelling of the vehicle's elastic and rigid components, and formulates the Euler-Lagrange equations of motion with a short sub-section alluding to the state-space representation and to the model in the Laplace domain. Validation of the model is achieved by a comprehensive analysis on the kinetic modes and the step responses. Later, in Chapter 7, a validation with a more sophisticated model is provided. Also, the model of an electromechanical actuator is presented together with a discussion on the effects of its mechanical part in the suspension performance. The last section of the chapter describes the methods used to assess the vehicle performance in the analysis and design chapters.

3.1 A Railway Vehicle as a Multibody System

In a multibody system representation framework, a railway vehicle comprises several bodies linked together through suspension connections [34]. Normally in two layer vehicles, two bogies support the vehicle body joined by secondary suspensions. A bogie is a rigid frame on which the running equipment of a modern vehicle is mounted, i.e. those components guaranteeing safe motion of the train along the track, including wheelsets and linkages (see [70] for a detailed description). Wheelsets conventionally comprise two profiled wheels rigidly connected by a common axle. Wheelsets are allowed to rotate by axle-boxes which also provide the support for primary suspensions. In particular, a vehicle with a pair of wheelsets per bogie is considered in this work and the axle boxes are assumed to be part of the wheelsets due to their rigid connection.

For assessment of bounce and pitch modes only, the model constrains the lateral, yaw and roll motions of the vehicle, while the longitudinal dynamic is assumed stationary at a nominal travelling speed. This turns the representation into a planar model, the *side-view* model of the vehicle introduced in Figure 1.1 on page 3. Also, because the bodies are considered to be ideally rigid, the bending modes are neglected.

Accordingly, the multibody system comprises seven elements: the vehicle body, two bogies and four wheelsets. In a contribution to the studies on noise and vibration arising from high-speed trains [129], Remington discussed the wheel/rail interaction forces and wheel and rail roughness modelling. In particular, a contact impedance[1]

[1]The term 'impedance' describes the ratio of deflection to force, i.e. $Z = z/F$, following the electrical terminology according to the force-current analogy [3] between mechanical and electrical networks.

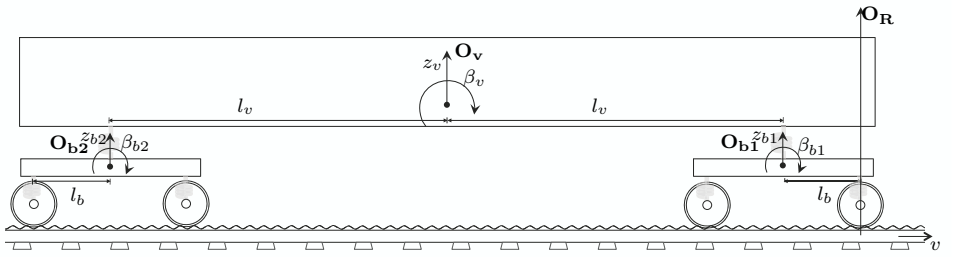

Figure 3.1: Side-view multibody representation of a railway vehicle with detail on the local coordinates and bodies DoF.

model approximates the interaction forces arising from the contact region between wheel and rail at low frequency and that such contact impedance is typically modelled as a spring whose stiffness equals the contact stiffness. The contact stiffness is the receptance[2] of the wheel when it is forced by the nominal load onto the rail. This simplification through the contact impedance model is valid for the description of the vehicle dynamics required for both fundamental dynamics of the vehicle-track system and ride quality assessment —as the frequencies to which the human body is more sensitive are low (below 20 [Hz] [29, 23]). Furthermore, the contribution of the contact forces to the upper body dynamics can be neglected because the contact stiffness is normally much higher than the vehicle's suspensions stiffness (e.g. for a wheel load of 10 [tonne] for a typical characterisation wheel/rail contact, the contact stiffness is of the order of 10^9 [Nm^{-1}] ; see [130]). Therefore, it is assumed here that the wheelsets follow the track and wheel surface irregularities. This results in a model describing the dynamic of three rigid bodies only, i.e. vehicle body and the two bogies.

Figure 3.1 shows a schematic of the railway vehicle described above. The reference coordinates system is identified by $\mathrm{O_R}$ and is located at the front wheel position; the local coordinates systems $\mathrm{O_v}$, $\mathrm{O_{b1}}$, and $\mathrm{O_{b2}}$ are placed at the centre-of-gravity (c.o.g.) of the bodies for the vehicle equilibrium position. The DoF in the vertical and pitch directions, respectively z_v, z_{b1} , z_{b2} , and β_v , β_{b1} , β_{b2}, symbolise variations around the equilibrium position of the bodies due to external excitations. The model developed here is an incremental model which assumes initial equilibrium conditions, i.e. the c.o.g. of the bodies is placed at the origin of their own local coordinates. Notice that the vehicle is perfectly symmetric about an imaginary vertical axis passing through $\mathrm{O_v}$; this symmetry should be preserved also in the suspensions design.

According to the description above for the vehicle side-view incremental model, three

[2]The term 'receptance' is used here to refer to the ratio of force to deflection, i.e. $\mathrm{Y}' = {}^{F}/_{z}$. Although the terms *receptance* and *mechanical impedance* in many cases are interchangeable (e.g. [The Mechanics of Vibration By R. E. D. Bishop, D. C. Johnson]), in this manuscript 'admittance' refers to the ratio of force to velocity, i.e. $\mathrm{Y} = {}^{F}/_{v}$.

stores of kinetic energy are defined for the system given in the three rigid bodies. The kinetic energy stored by the bodies is defined as

$$U_v = \frac{1}{2} m_v \, \dot{z}_v^2 + \frac{1}{2} I_{vy} \dot{\beta}_v^2 \tag{3.1}$$

$$U_{b,\,i} = \frac{1}{2} m_b \, \dot{z}_{b,\,i}^2 + \frac{1}{2} I_{by} \dot{\beta}_{b,\,i}^2, \text{ for i} = 1,\, 2. \tag{3.2}$$

There is also another form of kinetic energy storage in the suspensions which will be discussed briefly. Thus, the total kinetic energy of the system can be written as

$$U_T = U_v + \sum_i \left(U_{b,\,i}\right) + U_{\text{suspensions}} \tag{3.3}$$

On the other hand, roughness of the wheels and track are combined in a single one-dimensional mathematical model $\delta_z(t)$, presented later in this chapter. The model employed for assessing vertical dynamics corresponds to a 'moving irregularity model', i.e. the vehicle is modelled in a fixed frame and it is supposed that wheel/rail irregularities are contained in an imaginary strip (as described by [131]) which is hauled forwards below the vehicle model at the travelling speed. Excitations to the vehicle dynamics given by deterministic track profiles also enter the model under the same concept, as a moving track. From the modelling point of view, this imposes holonomic constraints at the wheels-track contact points, i.e.

$$z_{w,i}(t) = \delta_z(t - \tau_i) \tag{3.4}$$

$$\dot{z}_{w,i}(t) = \dot{\delta}_z(t - \tau_i), \text{ for } i\text{= 1, 2, 3, 4.} \tag{3.5}$$

with $\tau_i = {}^{d_i}/_{v}$ for v the vehicle speed, and d_i the horizontal distance from the reference frame, O_R, to the i-th wheelset:

$$d_1 = 0 \tag{3.6}$$

$$d_2 = 2l_b \tag{3.7}$$

$$d_3 = 2l_v \tag{3.8}$$

$$d_4 = 2\left(l_b + l_v\right) \tag{3.9}$$

according to the schematic of the vehicle in Figure 3.1.

3.2 Vertical Dynamic of the Suspension Systems

One-dimensional models of the primary and secondary suspensions are considered here. The primary suspension is modelled as a linear stiffness element with some dissipation. Thus, a parallel spring-damper arrangement with linear characteristics is placed between the wheel-points and the bogies front and rear ends in Figure 3.1. Secondary suspensions however are more complicated sub-systems to model.

The vehicle studied in this work has airsprings in the secondary suspension stage. One of the difficulties arising in airsprings modelling is the frequency-dependent behaviour they exhibit which is important in ride quality assessment. Although there is still not consensus on which is the most appropriate model for an airspring, a diversity of well approximated models has been proposed, as reported by Bruni et al. in [39] where a review on existing models for railway vehicle suspension components is presented.

In the description of an airspring system dynamic (see Figure 3.2), the main factors to consider are those associated with the airbag deformation. Internal dynamics developed by the air mass inside the surge reservoir and the pipework are also relevant for low-damped airspring systems. The dynamic of the air mass is even more important for those systems with long connecting pipes and no damping means rather than the losses naturally occurring inside the pipe. Hence, an airspring system stores both kinetic and potential energy. The stored kinetic energy, $U_{\text{suspensions}}$ in Equation 3.3, is associated to the fluid inertance of the air mass dynamics in the front and rear airsprings of the vehicle (thus, $U_{\text{suspensions}} = \sum_i U_{\text{airspring},\,i}$, for $i = 1, 2$). The potential energy, $T_{\text{airspring},\,i}$, is associated to the airbag and reservoir deformation due to the dynamic pressure applied onto the i-th airbag ($i = 1, 2$).

In general, the models developed towards calculation of airsprings dynamic stiffness can be grouped into 'lumped parameter models' and 'thermodynamical models', according to Facchinetti et al. in [36]. In particular, lumped parameter models associate equivalent lumped mechanical parameters to every physical element and some thermodynamical transformations. By using springs and dashpots, models like the Nishimura model (Figure 3.3(a), [39]), the Vampire model (Figure 3.3(b), [39], [6], [9]), and the SIMPACK linear model [39], approximate the frequency-dependent characteristic of the airspring. Similarly, by also including a lumped mass and non-linear damping, the Berg model ([37],[39]), the Vampire model and some more sophisticated models by SIMPACK provide a more accurate representation of the airspring dynamic.

The simplest representation of the dynamic stiffness of an airspring system is the Nishimura model (Figure 3.3(a)), which exhibits a monotonic transition from low-

frequency to high-frequency stiffness. Such well damped transition in the Nishimura model excludes the internal resonances due to the fluid inertance of the accelerated air in the air bag-reservoir interchange phase. It does account, however, for the damping effects given by a damping orifice placed in the connecting pipe.

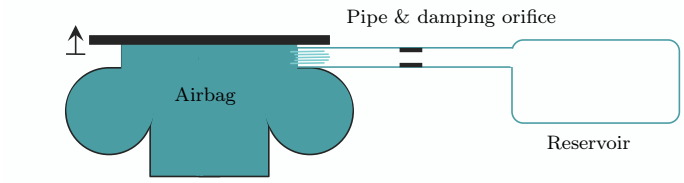

Figure 3.2: Schematic of an airspring with reservoir.

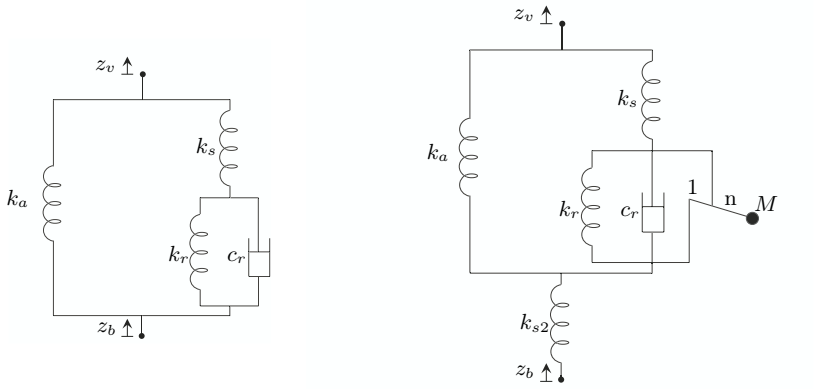

(a) Nishimura model (b) Vampire model

Figure 3.3: Typical airspring lumped parameter models.

3.2.1 Modelling the vertical dynamic of an airspring via springs, dampers and inerters

The mathematical model of the vehicle side-view dynamics employed in this research uses the Nishimura model [5]. However, because this work is focused on studying the effects of including inerters with the conventional secondary suspensions, it was considered that the airspring inertial effects should be also modelled and analysed.

In order to avoid including complex models that could distract the analyses from the original objective, and to follow the same order of ideas introduced with the inerter concept, another equivalent model of the airspring was formulated. It simulates the inertial effects due to the air mass oscillation in the pipe through an inerter element

in series with a linear damper accounting for losses in the pipe; as shown in the schematic in Figure 3.4. This model will be referred from here as the 'inerter-based airspring model'. The model is strictly linear, and is deduced in the following.

3.2.1.1 Approximation to the frequency response of an actual airspring

This inerter-based airspring model was deduced after studying the experimental frequency response of an actual airspring and the thermodynamical model reported both in [36]. Blocks of biquadratic real-rational functions of zero relative degree were designed to shape the underdamped peaks in the airspring force-deformation characteristic response. The structure of every i-block is described by $G_i(s)$ as follows

$$G_i(s) = \left(\frac{s^2/(2\pi f_{1,\,i})^2 + 2\,\zeta_{1i} s/(2\pi f_{1,\,i}) + 1}{s^2/(2\pi f_{2,\,i})^2 + 2\,\zeta_{2i} s/(2\pi f_{2,\,i}) + 1} \right) \tag{3.10}$$

Although the receptance defined by two and three blocks in cascade resulted in more accurate approximations for the airspring dynamic stiffness (see Appendix A), a model consisting of a single block characterising only the main transition from low to high stiffness was adopted. This one-block approximation would allow a direct comparison with the already well-known and accepted mechanical equivalents of the airspring, e.g. those shown in Figures 3.3(a) and 3.3(b).

3.2.1.2 Mechanical network synthesis and analysis

Integration in the Laplace domain of the attained real-rational function in Equation 3.10 (i.e. multiplication by s^{-1}) resulted in a real-rational function $\mathrm{Y}_a(s)$ which is equivalent to the one considered in [3],

$$\mathrm{Y}_a(s) = k \frac{a_0 s^2 + a_1 s + 1}{s\,(b_0 s^2 + b_1 s + 1)} \tag{3.11}$$

Moreover, for the 'shaping parameters' (see Appendix A) $\mathrm{Y}_a(s)$ resulted positive real and thus according with Smith in [3], Theorem 2, there would exist a one-port mechanical network whose admittance equals $\mathrm{Y}_a(s)$ consisting of an interconnection of springs, dampers, and inerters. Furthermore, the realisation of such positive real-rational function was not possible with only springs and dampers as in the Nishimura model because $\mathrm{Y}_a(s)$ does not hold the spring-damper admittance conditions also reported in [3]. Two mechanical configurations were obtained in [3] via Brune synthesis; the topology of those passive networks, however, did not allow to establish a complete analogy with the airspring physical parameters and phenomena. Therefore,

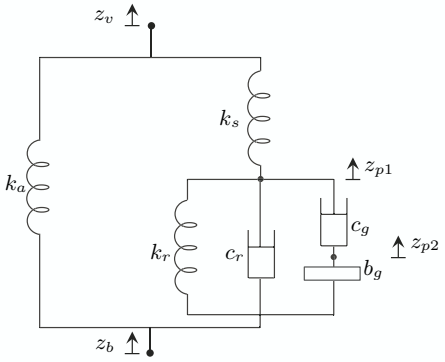

Figure 3.4: Inerter-based airspring model.

the equivalent network shown in Figure 3.4 was derived in attempt to achieve the required analogy.

According to Figure 3.4, the low and high frequency stiffness values, K, are the same as for the Nishimura model, i.e.

$$K_{s\to 0} = \frac{k_r k_a + k_s\,(k_r + k_a)}{k_s + k_r} \tag{3.12}$$

$$K_{s\to \infty} = k_s + k_a \tag{3.13}$$

Also, by using Equation 3.11, preserving the frequency characteristic of the short-length pipe airspring in [36] (i.e. retaining the values for a_0, a_1, b_0, and b_1 obtained by shaping), and adjusting $K_{s\to 0}$ and $K_{s\to \infty}$ through the values of k_s and k_r for the Bombardier model used by Zolotas [132], the parameters for the inerter-based model are defined as

$$k_a = \frac{k_s}{k_s + k_r}\left(\alpha_0 - \frac{a_0}{\alpha_3}k_r\right),\ c_r = \alpha_0\alpha_1,\ c_g = \frac{\alpha_0\alpha_2}{\alpha_4},\ b_g = \frac{\alpha_0\alpha_2}{\alpha_3} \tag{3.14}$$

with

$$\alpha_0 = \frac{b_0}{a_0 - b_0}\,(k_s + k_r) \tag{3.15}$$

$$\alpha_1 = a_1 - b_1 \tag{3.16}$$

$$\alpha_2 = \big(a_0\,(a_0 - (2\,b_0 + b_1\,(a_1 - b_1))) + b_0\,\big(a_1^2 + b_0 - a_1 b_1\big)\big) \tag{3.17}$$

$$\alpha_3 = a_0 - b_0 \tag{3.18}$$

$$\alpha_4 = (a_0 b_1 - a_1 b_0) \tag{3.19}$$

From this, the value of k_a resulted very close to the one reported in [132] for the Nishimura model (see Table 3.1). However, the damping value c_r differs as the

Table 3.1: Parameter values for the inerter-based airspring

Sym.	Parameter	Value
k_a	Change of area stiffness $\left[\mathrm{Nm}^{-1}\right]$	1.56×10^5
k_s	Airspring stiffness $\left[\mathrm{Nm}^{-1}\right]$	6.2×10^5
k_r	Reservoir stiffness $\left[\mathrm{Nm}^{-1}\right]$	2.44×10^5
c_r	Airspring damping $\left[\mathrm{Nsm}^{-1}\right]$	3.31×10^3
c_g	Pipework losses coefficient $\left[\mathrm{Nsm}^{-1}\right]$	4.22×10^5
b_g	Air inertance $[kg]$	4.14×10^2

airspring in [36] does not account for a damping orifice in the connecting pipe as seems to be the case for the model in [132] which was well damped. Figures A.2–A.4 in Appendix A depict the frequency response behaviour when some parameters from the model in Figure 3.4 vary. The plots demonstrate that changes in the damping and inertance parameters in the inerter-based model can be accordingly associated to changes in the connecting pipe dimensions, i.e. length and/or diameter, and/or to adjustments in the orifice damping, following results in [71]. It is not a surprising result, as the fluid inertance depends on the fluid density and the pipe's length and cross-sectional area [11]. The damping c_r, at certain levels of magnitude, can be considered as an intentional design parameter. The model in Figure 3.4, therefore, allows to approximate the functions for energy storage and dissipation of the airspring system. It also simplifies the synthesis of the airspring model in the Laplace domain while considering also the possibly oscillatory transition from low to high stiffness derived from its internal dynamics, already explained.

3.3 Equations of Motion for the Railway Vehicle Side-View Dynamics

Figure 3.5 depicts the mechanical model of the railway vehicle side-view accounted here for mathematical modelling. Euler-Lagrange equations are used here to derive the equations of motion. The model assumes that components of the gravitational forces are balanced by the static forces of the airsprings. Although it was already mentioned that only the bounce and pitch motions are to be considered and also that linear characteristics describe the system components, effects of other motions and/or nonlinear characteristics could be easily added to the model derived here for further investigations. The motivation for starting the mathematical model for the side-view dynamics from the Euler-Lagrange equations is to set the context for energy-based analyses performed in Chapter 4.

From variational analysis [11], the system's Lagrangian is defined as:

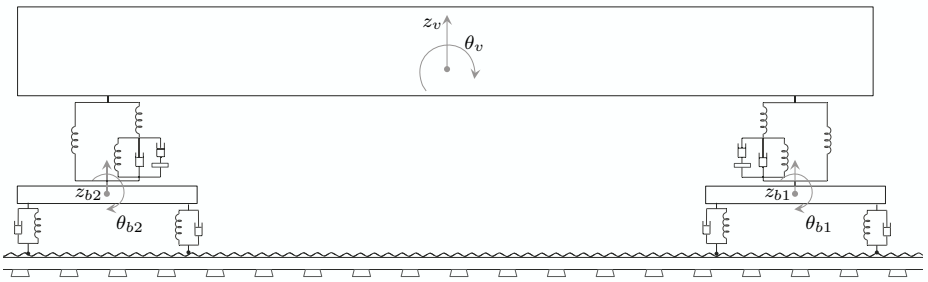

FIGURE 3.5: Side-view model with detail of the suspension models.

$$\mathcal{L} = U_T^* - T_T \tag{3.20}$$

where U_T^* is the co-content of total kinetic energy stored in the system which equals the total kinetic energy content (Equation 3.3 on page 37) as it is assumed that the constitutive relations associated to the masses (Newtonian masses) and mechanical inertance are linear; T_T is the total potential energy content. The energy stored/dissipated by every component adds up for the total energy stored/dissipated in the system. For this, once the suspension components have been described with their approximated models, and by defining the generalised coordinates vector of the system as

$$\begin{aligned}\left[\underline{q}\middle|\,\underline{w}\right]^T = [\,&z_v,\ \beta_v,\ z_{b1},\ \beta_{b1},\ z_{p11},\ z_{p21},\ z_{b2},\ \beta_{b2}, \ldots \\ &z_{p12},\ z_{p22}\middle|\ z_{w1},\ z_{w2},\ z_{w3},\ z_{w4}]^T\end{aligned} \tag{3.21}$$

one has:

- Primary Suspension:
  - Stored kinetic energy:

$$U_P = 0 \tag{3.22}$$

  - Stored potential energy:

$$T_P = \sum_{i=1}^{2} \sum_{j=2i-1}^{2i} T_{P,\,i,\,j} \tag{3.23}$$

    for

$$T_{P,\,i,\,j} = \frac{1}{2} k_p \left(z_{w,\,j} - \left(z_{b,\,i} + (-1)^{j-1}\, l_b \beta_{b,\,i} \right) \right)^2 \tag{3.24}$$

– Rayleigh dissipation function:

$$J_P = \sum_{i=1}^{2} \sum_{j=2i-1}^{2i} J_{P,i,j} \tag{3.25}$$

for

$$J_{P,i,j} = \frac{1}{2} c_p \left(\dot{z}_{w,j} - \left(\dot{z}_{b,i} + (-1)^{j-1} l_b \dot{\beta}_{b,i} \right) \right)^2 \tag{3.26}$$

- Secondary Suspension:

– Stored kinetic energy:

$$U_S = \sum_{i=1}^{2} U_{\text{airspring},i} \tag{3.27}$$

for

$$U_{\text{airspring},i} \simeq \frac{1}{2} b_g \left(\dot{z}_{b,i} - \dot{z}_{p2,i} \right)^2 + \frac{1}{2} m_p \dot{z}_{p1,i}^2 + \frac{1}{2} m_p \dot{z}_{p2,i}^2 \tag{3.28}$$

with m_p a very small mass defined here for representing the 'massless' points whose DoFs are illustrated in Figure 3.4. The choice of $m_p \neq 0\,[\text{kg}]$ eases later the handling of numerical issues appearing in numerical simulation using time-domain models.

– Stored potential energy:

$$T_S = \sum_{i=1}^{2} T_{S,i} \tag{3.29}$$

for

$$\begin{aligned} T_{S,i} \simeq & \frac{1}{2} k_a \left(z_{b,i} - \left(z_v + (-1)^{i-1} l_v \beta_v \right) \right)^2 \\ & + \frac{1}{2} k_r \left(z_{b,i} - z_{p1,i} \right)^2 \\ & + \frac{1}{2} k_s \left(z_{p1,i} - \left(z_v + (-1)^{i-1} l_v \beta_v \right) \right)^2 \end{aligned} \tag{3.30}$$

– Rayleigh dissipation function:

$$J_S = \sum_{i=1}^{2} J_{S,i} \tag{3.31}$$

for

$$J_{S,i} \simeq \frac{1}{2} c_r \left(\dot{z}_{b,i} - \dot{z}_{p1,i} \right)^2 + \frac{1}{2} c_g \left(\dot{z}_{p2,i} - \dot{z}_{p1,i} \right)^2 \tag{3.32}$$

Notice that in the equations above, $\sin\beta \to \beta$ $(\cos\beta \to 1)$, which is valid due to the fact that the pitch angles are normally very small. Now, with the definitions above, together with Equations (3.1) and (3.2) for the kinetic energy stored in the bodies, the total kinetic energy results in:

$$\begin{aligned} U_T^* &= U_T \\ &= U_{\text{vbody}} + \sum_{i=1}^{2} \left(U_{\text{bogie},\,i}\right) + U_P + U_S \\ &\simeq \frac{1}{2} m_v\, \dot{z}_v^2 + \frac{1}{2} I_{vy} \dot{\beta}_v^2 + \sum_{i=1}^{2} \Bigg(\frac{1}{2} m_b\, \dot{z}_{b,\,i}^2 + \frac{1}{2} I_{by} \dot{\beta}_{b,\,i}^2 \\ &\qquad + \frac{1}{2} b_g \left(\dot{z}_{b,\,i} - \dot{z}_{p2,\,i}\right)^2 \\ &\qquad + \frac{1}{2} m_p \dot{z}_{p1,\,i}^2 + \frac{1}{2} m_p \dot{z}_{p2,\,i}^2 \Bigg) \end{aligned} \tag{3.33}$$

and the total potential energy,

$$\begin{aligned} T_T &= T_P + T_S \\ &\simeq \sum_{i=1}^{2} \Bigg(\sum_{j=2i-1}^{2i} \frac{1}{2} k_p \left(z_{w,\,j} - \left(z_{b,\,i} + (-1)^{j-1}\, l_b \beta_{b,\,i} \right) \right)^2 \\ &\qquad + \frac{1}{2} k_a \left(z_{b,\,i} - \left(z_v + (-1)^{i-1}\, l_v \beta_v \right) \right)^2 \\ &\qquad + \frac{1}{2} k_r \left(z_{b,\,i} - z_{p1,\,i} \right)^2 \\ &\qquad + \frac{1}{2} k_s \left(z_{p1,\,i} - \left(z_v + (-1)^{i-1}\, l_v \beta_v \right) \right)^2 \Bigg) \end{aligned} \tag{3.34}$$

which then allows to calculate the Lagrangian function of the approximated system as

$$\begin{aligned} \mathcal{L}_{app} = \frac{1}{2} m_v\, \dot{z}_v^2 + \frac{1}{2} I_{vy} \dot{\beta}_v^2 + \sum_{i=1}^{2} \Bigg(& \frac{1}{2} m_b\, \dot{z}_{b,\,i}^2 + \frac{1}{2} I_{by} \dot{\beta}_{b,\,i}^2 + \frac{1}{2} b_g \left(\dot{z}_{b,\,i} - \dot{z}_{p2,\,i}\right)^2 \\ & - \sum_{j} \frac{1}{2} k_p \left(z_{w,\,j} - \left(z_{b,\,i} + (-1)^{j-1}\, l_b \beta_{b,\,i} \right) \right)^2 \\ & - \frac{1}{2} k_a \left(z_{b,\,i} - \left(z_v + (-1)^{i-1}\, l_v \beta_v \right) \right)^2 \\ & - \frac{1}{2} k_r \left(z_{b,\,i} - z_{p1,\,i} \right)^2 \\ & - \frac{1}{2} k_s \left(z_{p1,\,i} - \left(z_v + (-1)^{i-1}\, l_v \beta_v \right) \right)^2 \Bigg) \end{aligned} \tag{3.35}$$

for $\mathcal{L} \simeq \mathcal{L}_{app}$.

In addition, the total Rayleigh dissipation function results in

$$\begin{aligned} J_T &= J_P + J_S \\ &\simeq \sum_{i=1}^{2} \Bigg(\sum_{j=2i-1}^{2i} \frac{1}{2} c_p \left(\dot{z}_{w,\,j} - \left(\dot{z}_{b,\,i} + (-1)^{j-1} \, l_b \dot{\beta}_{b,\,i} \right) \right)^2 \\ &\qquad + \frac{1}{2} c_r \left(\dot{z}_{b,\,i} - \dot{z}_{p1,\,i} \right)^2 + \frac{1}{2} c_g \left(\dot{z}_{p2,\,i} - \dot{z}_{p1,\,i} \right)^2 \Bigg) \end{aligned} \tag{3.36}$$

Consequently, the Euler-Lagrange equations of motion can be derived from

$$\frac{d}{dt} \left(\frac{\partial}{\partial \dot{q}_i} \mathcal{L}_{app} \right) - \frac{\partial}{\partial q_i} \mathcal{L}_{app} + \frac{\partial}{\partial \dot{q}_i} J_T = F_i \tag{3.37}$$

with i=1, 2, ..., 10 and F_i the i-th entry of the generalised forces vector, and whose form is

$$\underline{F} = \left(F_{u1} + F_{u2},\, l_v \left(F_{u1} - F_{u2} \right),\, -F_{u1},\, 0,\, 0,\, 0,\, -F_{u2},\, 0,\, 0,\, 0 \right)^T \tag{3.38}$$

where F_{u1} and F_{u2} are control forces applied by the secondary suspension which can be developed by either the novel passive devices, by the actuators in active suspensions configurations, or both. Evaluating the derivatives in (3.37) yields

$$m_v \ddot{z}_v + k_a \left(2z_v - z_{b1} - z_{b2} \right) + k_s \left(2z_v - z_{p11} - z_{p12} \right) = F_1 \tag{3.39}$$

$$I_{vy} \ddot{\beta}_v + k_a l_v \left(2l_v \beta_v - z_{b1} + z_{b2} \right) + k_s l_v \left(2l_v \beta_v - z_{p11} + z_{p12} \right) = F_2 \tag{3.40}$$

for the vehicle body dynamics,

$$\begin{aligned} m_b \ddot{z}_{b,\,i} + b_g \left(\ddot{z}_{b,\,i} - \ddot{z}_{p2,\,i} \right) + k_p \left(2z_{b\,i} - z_{w,\,(2i-1)} - z_{w,\,2i} \right) \\ + k_a \left(z_{b,\,i} - \left(z_v + (-1)^{i-1} \, l_v \beta_v \right) \right) + k_r \left(z_{b,\,i} - z_{p1,\,i} \right) \\ + c_p \left(2\dot{z}_{b,\,i} - \dot{z}_{w,\,(2i-1)} - \dot{z}_{w,\,2i} \right) + c_r \left(\dot{z}_{b,\,i} - \dot{z}_{p1,\,i} \right) = F_{4i-1} \end{aligned} \tag{3.41}$$

$$\begin{aligned} I_{by} \ddot{\beta}_{b,\,i} + k_p l_b \left(2l_b \beta_{b,\,i} - z_{w\,(2i-1)} + z_{w,\,2i} \right) \\ + c_p l_b \left(2l_b \dot{\beta}_{b,\,i} - \dot{z}_{w\,(2i-1)} + \dot{z}_{w,\,2i} \right) = F_{4i} \end{aligned} \tag{3.42}$$

for the bogies' dynamics, with i=1, 2 for front and rear bogie, respectively, and

$$m_p \ddot{z}_{p1,\,i} + k_r \left(z_{p1,\,i} - z_{b,\,i}\right) + c_r \left(\dot{z}_{p1,\,i} - \dot{z}_{b,\,i}\right) + k_s \left(z_{p1,\,i} - \left(z_v + (-1)^{i-1}\, l_v \beta_v\right)\right) + c_g \left(\dot{z}_{p1,\,i} - \dot{z}_{p2,\,i}\right) = F_{4i+1} \tag{3.43}$$

$$m_p \ddot{z}_{p2,\,i} + b_g \left(\ddot{z}_{p2,\,i} - \ddot{z}_{b,\,i}\right) + c_g \left(\dot{z}_{p2,\,i} - \dot{z}_{p1,\,i}\right) = F_{4i+2} \tag{3.44}$$

for the states $z_{p1,\,i}$ and $z_{p2,\,i}$(complementing the description of the i-th airspring internal dynamic (for i=1, 2).

The four remaining equations, i.e. those for $w = (z_{w1},\, z_{w2},\, z_{w3},\, z_{w4})^T$, were not derived as the associated states are constrained according to Equation (3.4). The Equations (3.39)—(3.44) can be rewritten in a compact form once considering the constraints on $z_{w,\,i}$ (i=1, 2, 3, 4):

$$\mathbf{M}\,\underline{\ddot{q}}(t) + \mathbf{C}\,\underline{\dot{q}}(t) + \mathbf{K}\underline{q}(t) = \mathbf{Q}_m\,\underline{\delta_m}(t) + \dot{\mathbf{Q}}_m\,\underline{\dot{\delta}_m}(t) + \underline{F}(t) \tag{3.45}$$

with matrices $\mathbf{M}$, $\mathbf{C}$, $\mathbf{K}$, $\mathbf{Q}_m$, $\dot{\mathbf{Q}}_m$ as defined in Appendix B, $\underline{q}$ the vector of unconstrained generalised coordinates

$$\underline{q} = [z_v,\, \beta_v,\, z_{b1},\, \beta_{b1},\, z_{p11},\, z_{p21},\, z_{b2},\, \beta_{b2},\, z_{p12},\, z_{p22}]^T \tag{3.46}$$

with velocity $\underline{\dot{q}}$ and acceleration $\underline{\ddot{q}}$, and $\underline{\delta_m}(t)$ the excitation vector

$$\underline{\delta_m}(t) = \left[\ \delta_z(t-\tau_1)\ ,\, \delta_z(t-\tau_2),\, \delta_z(t-\tau_3),\, \delta_z(t-\tau_4)\right]^T \tag{3.47}$$

with velocity $\underline{\dot{\delta}_m}(t)$.

3.3.1 State-space representation

For a representation in the state-space for the system, by defining the state vector

$$\underline{x}(t) = \left[\ \underline{q}^T(t)\ \middle|\ \underline{\dot{q}}^T(t)\ \middle|\ \underline{w}^T(t)\ \right]^T \tag{3.48}$$

the state equation is

$$\begin{aligned} \underline{\dot{x}}(t) &= \mathbf{A}\,\underline{x}(t) + \mathbf{B}_u\,\underline{F}(t) + \mathbf{B}_{\dot{\delta}}\,(t)\,\underline{\dot{\delta}_m}(t), \\ \underline{x}(t) &= \underline{x}(t_0) \end{aligned} \tag{3.49}$$

which has a system matrix whose structure is defined from the compact form matrices as

$$\mathbf{A} = \left[\begin{array}{c|c|c} \mathbf{0}_{10\times10} & \mathbf{I}_{10\times10} & \mathbf{0}_{10\times4} \\ \hline -\mathbf{M}^{-1}\mathbf{K} & -\mathbf{M}^{-1}\mathbf{C} & \mathbf{M}^{-1}\mathbf{Q}_m \\ \hline \mathbf{0}_{4\times10} & \mathbf{0}_{4\times10} & \mathbf{0}_{4\times4} \end{array}\right] \tag{3.50}$$

and has the input matrices

$$\mathbf{B}_{\mathrm{u}} = \left[\begin{array}{c} \mathbf{0}_{10\times n_u} \\ \hline \mathbf{M}^{-1} \\ \hline \mathbf{0}_{4\times n_u} \end{array}\right], \text{ and } \mathbf{B}_{\dot{\delta}} = \left[\begin{array}{c} \mathbf{0}_{10\times4} \\ \hline \mathbf{M}^{-1}\dot{\mathbf{Q}}_m \\ \hline \mathbf{I}_{4\times4} \end{array}\right] \tag{3.51}$$

given that $\mathbf{M}^{-1}$ exists. The output vectors are written accordingly in a linear algebraic form for the variables needed for performance assessment of the open-loop system, $\underline{y_o}$, and for the 'measured' variables needed for feedback according to the control strategy, $\underline{y_m}$,

$$\underline{y_o}(t) = \mathbf{C}_{\mathrm{y}}\,\underline{x}(t) \tag{3.52}$$

$$\underline{y_m}(t) = \mathbf{C}_m\,\underline{x}(t) \tag{3.53}$$

with $\mathbf{C}_y$ and $\mathbf{C}_m$ defined by the control strategy. It is assumed that the measurements required by the control strategies are all available, otherwise, that state estimation is implemented.

The synergy of *active-plus-novel-passive* solutions incorporating linear control strategies is modelled in the state-space as

$$\underline{\dot{x}_{cl}} = \boldsymbol{\mathcal{A}}\,\underline{x_{cl}} + \boldsymbol{\mathcal{B}}_{\dot{\delta}}\,\underline{\dot{\delta}_m} \tag{3.54}$$

$$\underline{y_{cl}} = \boldsymbol{\mathcal{C}}\,\underline{x_{cl}} \tag{3.55}$$

with direct feedthrough matrix $\boldsymbol{\mathcal{D}} = 0$ provided both the active control strategy and the admittance of the passive network are functions strictly proper. For the augmented state vector of closed-loop,

$$\underline{x_{cl}} = \left[\begin{array}{c|c|c|c|c} \underline{x}^T & \underline{x_{af1}}^T & \underline{x_{af2}}^T & \underline{x_{pf1}}^T & \underline{x_{pf2}}^T \end{array}\right]^T \tag{3.56}$$

The output vector $\underline{y_{cl}}$ for performance assessment is re-written accordingly. In 3.56, $\underline{x_{af1}}$ and $\underline{x_{af2}}$ are the state vectors of the identical sub-systems ($\mathbf{A}_{af}$, $\mathbf{B}_{af}$, $\mathbf{C}_{af}$, $\mathbf{D}_{af}$) generating the active forces, F_{act1} and F_{act2}, in response to the measurements $\underline{y_{m(1)}} = \mathbf{C}_{m(1,*)}\,\underline{x}$, $\underline{y_{m(2)}} = \mathbf{C}_{m(2,*)}\,\underline{x}$, respectively. Similarly, $\underline{x_{pf1}}$ and $\underline{x_{pf2}}$ are the state vectors of the identical sub-systems ($\mathbf{A}_{pf}$, $\mathbf{B}_{pf}$, $\mathbf{C}_{pf}$, $\mathbf{D}_{pf}$) generating the passive forces, F_{pn1} and F_{pn2}, in response to the suspension relative velocity, i.e.

$y_{m(3)} = \mathbf{C}_{m(3,*)}\,\underline{x} = \dot{z}_{b1} - \left(\dot{z}_v + l_v\,\dot{\beta}_v\right)$, $y_{m(4)} = \mathbf{C}_{m(4,*)}\,\underline{x} = \dot{z}_{b2} - \left(\dot{z}_v - l_v\,\dot{\beta}_v\right)$. The sub-systems identified with the sub-index 'af' correspond to a canonical representation of the active control strategy implemented at the front and rear suspensions; similarly, the sub-systems identified with the sub-index 'pf' correspond to a canonical representation of the novel passive network including inerters integrated to the front and rear suspensions. The structure of these sub-systems, as considered in this thesis, is specified in Chapter 5. The closed-loop system matrices are defined as

$$\boldsymbol{\mathcal{A}} = \left[\begin{array}{c|c} \mathbf{A} + \mathbf{B}\,\boldsymbol{\Lambda}^u_{\mathrm{D}}\,\mathbf{C}_m & \mathbf{B}\,\boldsymbol{\Lambda}^u_{\mathrm{C}} \\ \hline \boldsymbol{\mathcal{A}}_{21} & \boldsymbol{\Lambda}^u_{\mathrm{A}} \end{array}\right], \tag{3.57}$$

$$\boldsymbol{\mathcal{B}} = \left[\begin{array}{c|c|c|c} \boldsymbol{B}_{\delta^T} & 0 & 0 & 0 \end{array}\right], \tag{3.58}$$

$$\boldsymbol{\mathcal{C}} = \left[\begin{array}{c|c|c|c} \boldsymbol{C}_o & 0 & 0 & 0 \end{array}\right] \tag{3.59}$$

where

$$\boldsymbol{\Lambda}^u_{\mathrm{A}} = \mathrm{diag}\left(\mathbf{A}_{af},\, \mathbf{A}_{af},\, \mathbf{A}_{pf},\, \mathbf{A}_{pf}\right) \tag{3.60}$$

$$\boldsymbol{\Lambda}^u_{\mathrm{C}} = \mathrm{diag}\left(\mathbf{C}_{af},\, \mathbf{C}_{af},\, \mathbf{C}_{pf},\, \mathbf{C}_{pf}\right) \tag{3.61}$$

$$\boldsymbol{\Lambda}^u_{\mathrm{D}} = \mathrm{diag}\left(\mathbf{D}_{af},\, \mathbf{D}_{af},\, \mathbf{D}_{pf},\, \mathbf{D}_{pf}\right) \tag{3.62}$$

and

$$\boldsymbol{\mathcal{A}}_{21} = \left[\begin{array}{c|c|c|c} \mathbf{C}^T_{m(1,*)}\mathbf{B}^T_{af} & \mathbf{C}^T_{m(2,*)}\mathbf{B}^T_{af} & \mathbf{C}^T_{m(3,*)}\mathbf{B}^T_{pf} & \mathbf{C}^T_{m(4,*)}\mathbf{B}^T_{pf} \end{array}\right]^T \tag{3.63}$$

The zero entries in the matrices define zero vectors/matrices of appropriate dimension, and $\mathbf{C}_{m(i,*)}$, corresponds to the i-th set of measurements according to matrix $\mathbf{C}_m$ and the feedback configuration for the active control strategies. On the other hand, formulating the model of the closed-loop system by using network synthesis —following next— resulted more convenient for the formulation of frequency-based suspensions, and to perform classical frequency-based analyses.

3.3.2 Vehicle modelling via network synthesis

The vehicle structure represented in Figure 3.5 can be also modelled by using network synthesis. This is possible under consideration that the model of the controlled vehicle is linear and, again, incremental.

From network synthesis, the model of the system can be synthesised as

$$s^2 m_v \hat{z}_v = \hat{F}_{\mathrm{a}1} + \hat{F}_{\mathrm{a}2} + \hat{F}_{u1} + \hat{F}_{u2} \tag{3.64}$$

$$s^2 I_{vy} \hat{\beta}_v = l_v \left(\hat{F}_{\mathrm{a}1} - \hat{F}_{\mathrm{a}2} + \hat{F}_{u1} - \hat{F}_{u2} \right) \tag{3.65}$$

$$s^2 m_b \hat{z}_{b,\,i} = -\hat{F}_{\mathrm{a},\,i} - \hat{F}_{u,\,i} + \hat{F}_{p,\,i,\,(2i-1)} + \hat{F}_{p,\,i,\,2i} \tag{3.66}$$

$$s^2 I_{by} \hat{\beta}_{b,\,i} = l_b \left(\hat{F}_{p,\,i,\,(2i-1)} - \hat{F}_{p,\,i,\,2i} \right) \tag{3.67}$$

where

$$\hat{F}_{\mathrm{a},\,i} = \mathrm{Y}_a(s)\, s \left(\hat{z}_{b,\,i} - \left(\hat{z}_v + (-1)^{i-1} l_v \hat{\beta}_v \right) \right) \tag{3.68}$$

$$\hat{F}_{u,\,i} = \mathrm{Y}_{pn}(s)\, s \left(\hat{z}_{b,\,i} - \left(\hat{z}_v + (-1)^{i-1} l_v \hat{\beta}_v \right) \right) + \hat{F}_{\mathrm{act},\,i} \tag{3.69}$$

$$\hat{F}_{p,\,i,\,j} = \mathrm{Y}_p(s)\, s \left(\hat{z}_{w,\,j} - \left(\hat{z}_{b,\,i} + (-1)^{j-1} l_b \hat{\beta}_{b,\,i} \right) \right) \tag{3.70}$$

with $j = 1,\, 2$ for $i = 1$, and $j = 3,\, 4$ for $i = 2$; $\mathrm{Y}_a(s)$ is as defined in Equation (3.11) for the inerter-based model, or

$$\mathrm{Y}_a(s) = \frac{s\,\gamma_c + \gamma_k}{s\,(s + \alpha)} \tag{3.71}$$

with $\gamma_c = k_s + k_a$, $\gamma_k = \frac{k_s(k_r+k_a)+k_r k_a}{c_r}$, and $\alpha = \frac{k_s+k_r}{c_r}$ for the Nishimura model; $\mathrm{Y}_p(s) = \left(k_p s^{-1} + c_p\right)$; $\mathrm{Y}_{pn}(s)$ is the mechanical admittance of the inerter-based network, and $\hat{F}_{\mathrm{act},\,i}$ is the i-th active control force applied by a controlled ideal or real actuator placed in parallel to the conventional front and rear airsprings ($i = 1,\, 2$). Both $\mathrm{Y}_{pn}(s)$ and $\hat{F}_{\mathrm{act},\,i}$ are presented later in Chapter 5.

The transfer functions for the system are obtained by using the equations system defined by (3.64)–(3.67) after substitution of the expressions of force, and rearranging the resulting equations to obtain

$$\mathbf{G_q}(s)\, \underline{\hat{q}} = \mathbf{G_\delta}(s)\, \underline{\hat{w}}. \tag{3.72}$$

In this way, $\mathbf{G_q}^{-1}(s)\, \mathbf{G_\delta}(s)$ is the matrix of transfer functions from $\underline{\hat{\delta}_z}$ to $\underline{\hat{q}}$ after introducing the constraints over $\underline{\hat{w}}$, i.e. $\underline{\hat{w}} = \underline{\hat{\delta}_m}$, and hence

$$\frac{s^2\,\hat{z}_v}{s\,\hat{\delta}_z} = s\sum_{i=1}^{4}\left(\frac{\hat{z}_v}{\hat{z}_{w,\,j}}e^{-\tau_i s}\right) \tag{3.73}$$

$$\frac{s^2\,\hat{\beta}_v}{s\,\hat{\delta}_z} = s\sum_{i=1}^{4}\left(\frac{\hat{\beta}_v}{\hat{z}_{w,\,i}}e^{-\tau_i s}\right) \tag{3.74}$$

$$\frac{\hat{z}_{b1}-\hat{z}_{v1}}{s\,\hat{\delta}_z} = \frac{1}{s}\sum_{i=1}^{4}\left(\frac{\hat{z}_{b1}-\hat{z}_{v1}}{\hat{z}_{w,\,i}}e^{-\tau_i s}\right) \tag{3.75}$$

$$\frac{\hat{z}_{b2}-\hat{z}_{v2}}{s\,\hat{\delta}_z} = \frac{1}{s}\sum_{i=1}^{4}\left(\frac{\hat{z}_{b2}-\hat{z}_{v2}}{\hat{z}_{w,\,i}}e^{-\tau_i s}\right) \tag{3.76}$$

for $\hat{z}_{v,\,j} = \hat{z}_v + (-1)^{j-1}\,l_v\hat{\beta}_v$, and $j = 1,\,2$. This model allows to readily obtain the closed-loop system equations and simplifies the assessment of performance variables, which will be discussed in the next chapter. It is worth mentioning that given the high degree of complexity of the system, *Mathematica*® was used not only for symbolic and numerical manipulation, but also for simulation, optimisation and to export models to MATLAB® when required.

3.4 Modelling and Airspring Consideration: the Nishimura versus Inerter-Based Dilemma

The starting point considered here for suspension design, involving the insertion of extra components to the conventional airspring systems, was that no better ride quality could be attained attending typical considerations. In that sense, the damping coefficient associated to the losses in the pipe of the air supply system due to its cross-sectional area, c_r, was re-adjusted. This parameter can be regulated in practice by inserting orifice plates in the pipe like in [133], for example.

Figure 3.6 shows the receptance of the airspring according to the Nishimura model contrasted with the receptance derived from the inerter-based model, both with parameters values as in Table 3.1, excepting for the damping value c_r which was now set to a quasi-optimal value of 50 $\left[\mathrm{kNsm}^{-1}\right]$. It shows that the resonance in the airspring vertical response caused by the air-mass dynamics, as observed in the model obtained by 'shaping' a real airspring response (see Annex A), can be compensated with good damping. Hence, the need for a better modelling of the transition from low to high stiffness loses importance for this investigation objectives. Plots attained on quantities measured at the middle position illustrate no significant difference with respect to the Nishimura model. Figure 3.7 shows the power spectral density (p.s.d.) plot of the vehicle body acceleration to stochastic inputs, and Figure 3.8 depicts the phase plot of the zero-input vehicle body bounce evolution. Therefore, for the sake

of simplicity, the Nishimura model is adopted in this thesis, i.e. active and passive suspensions will be incorporated to the system in Figure 3.5 with the series damper-inerter in the secondary suspensions removed. It means that the dynamic associated to the generalised coordinates z_{p21} and z_{p22} is neglected, thus, Equation (3.44) is not required. This agrees with the model used by Pratt [5].

Parameter values of the side-view model are listed in Table 3.2; these are adapted from Pratt [5], in conjunction to parameters in Table 3.1 but with a high airspring damping value.

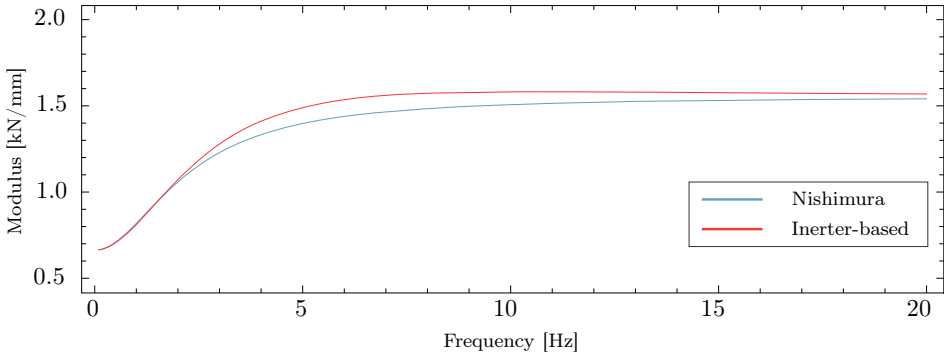

Figure 3.6: Dynamic stiffness of the Nishimura and the inerter-based models, with c_r =50 $\left[\text{kNsm}^{-1}\right]$.

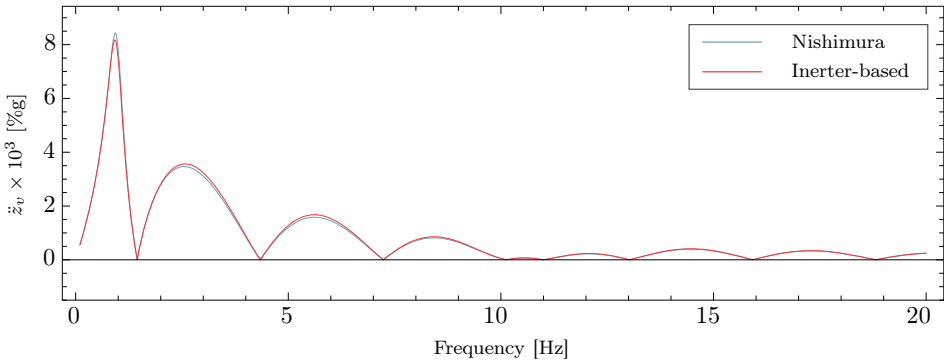

Figure 3.7: Acceleration p.s.d. plot of the vehicle body middle position bounce. Comparison between the Nishimura and the inerter-based model, for a speed of 55 $\left[\text{ms}^{-1}\right]$, and c_r =50 $\left[\text{kNsm}^{-1}\right]$.

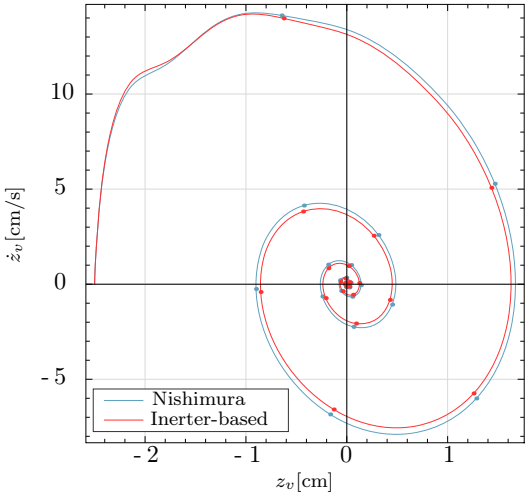

FIGURE 3.8: Phase plot for the vehicle body bounce at the middle position contrasting the vehicle response with the Nishimura and the inerter-based model with $z_v(t_0) = z_{b1}(t_0) = z_{b2}(t_0) = -2.5$cm, at a speed of 55m/s, with c_r =50 $\left[\text{kNsm}^{-1}\right]$.

TABLE 3.2: Parameter values for the Side-View model

Sym.	Parameter	Value
m_v	Vehicle body mass [kg]	38×10^3
m_b	Bogie mass [kg]	2.5×10^3
I_{vy}	Vehicle pitch inertia $\left[\text{kgm}^2\right]$	2.31×10^6
I_{by}	Bogie pitch inertia $\left[\text{kgm}^2\right]$	2×10^3
l_v	Semi-longitudinal spacing of secondary suspension [m]	9.5
l_b	Semi-longitudinal spacing of wheelsets [m]	1.25
k_a	Change of area stiffness (×2) $\left[\text{Nm}^{-1}\right]$	3.13×10^5
k_s	Airspring stiffness (×2) $\left[\text{Nm}^{-1}\right]$	1.24×10^6
k_r	Reservoir stiffness (×2) $\left[\text{Nm}^{-1}\right]$	4.88×10^5
c_r	Airspring damping (×2) $\left[\text{Nsm}^{-1}\right]$	1×10^5
k_p	Primary suspension stiffness(×2) $\left[\text{Nm}^{-1}\right]$	5×10^6
c_p	Primary suspension damping (×2) $\left[\text{Nsm}^{-1}\right]$	3.58×10^4
v	Vehicle speed $\left[\text{ms}^{-1}\right]$	55

[a] For this planar model symmetry about the longitudinal axis is also considered. Thus, both sides suspensions are concentrated in a planar suspension model by duplicating (×2) the suspension parameters.

3.5 Verification of the Side-View Model

The vibration modes of the system are listed on Table 3.3; differences in relation to results presented by Pratt [5] are justified by the difference in the airspring parameters values. Even though, similarity is preserved. The system has six vibration modes, although due to the assumption of perfect symmetry, and the fact that the front and rear bogies and suspensions are identical, only four modes appear as seen on Table 3.3. Due to the high damping in the airspring, the artificial masses m_p inserted for the time-domain model do not add extra vibration modes even if the inerter-based model is used; the eigenvalues due to the artificial masses dynamics are over-damped. Moreover, those modes relate to high frequencies (around 80 [Hz]) and do not affect the validity of the model at the frequencies of interest (up to 20 [Hz]).

Table 3.3: Vibration modes of the vehicle (Side-View DoF)

Mode	Frequency [Hz]	Damping [%]	DoF associated
1st	0.99	19.3	Vehicle body bounce
2nd	1.25	22.0	Vehicle body pitch
3rd	10.8	21.9	Bogies bounce
4th	14.1	31.6	Bogies pitch

The frequency response plots in Figure 3.9 obtained for the velocity of the DoF of the actual bodies complement the information in Table 3.3 for model verification purposes. Those were obtained for the vehicle excited at the leading wheelset only and consist of the gain response of the corresponding transfer functions. It is observed that the bouncing motion at the centre of the vehicle body is more influenced by the first and third vibrational modes, while the pitching motion by the second and third. It implies that the bouncing motion at the body ends is also affected by the second mode, which can be associated to the riding degradation normally experienced at the ends of a vehicle with passive suspensions compared with the ride quality experienced at the centre. Moreover, input frequency components of around 1 [Hz] affect the vehicle body bouncing motion more than those around 10.8 [Hz]. It can be also observed how the front bogie bounce and pitch motions are more affected than the rear bogie, as one would expect in a full-scale vehicle. The front bogie bounce at the centre is more influenced by the third vibrational mode and with greater gain than for the vehicle body vertical motion and the rear bogie. The plots illustrate how the strong effects of an input with frequency components of around the bogie vibration mode (i.e. 10.8 [Hz]) are dissipated in the flow from the front bogie to the rear bogie (conversely from rear to front if excited through the third or fourth wheelset). Transmissibility of the vehicle body dynamics to the front bogie can be

barely noticed because its own vibration mode is obviously stronger, but it is more evident for the rear bogie bounce as no excitation was applied at the rear wheelsets. The fourth mode, on the other hand, affects more the front bogie pitch and does not cause any rotational motion in the rear bogie, as a natural result due to the fact that transmissibility goes from body to body through the suspensions. That is, according to the system configuration, the secondary suspensions are not affected by the bogies pitching motion. The same analysis on the transmissibility effects applies accordingly for an excitation inserted through any other wheelset.

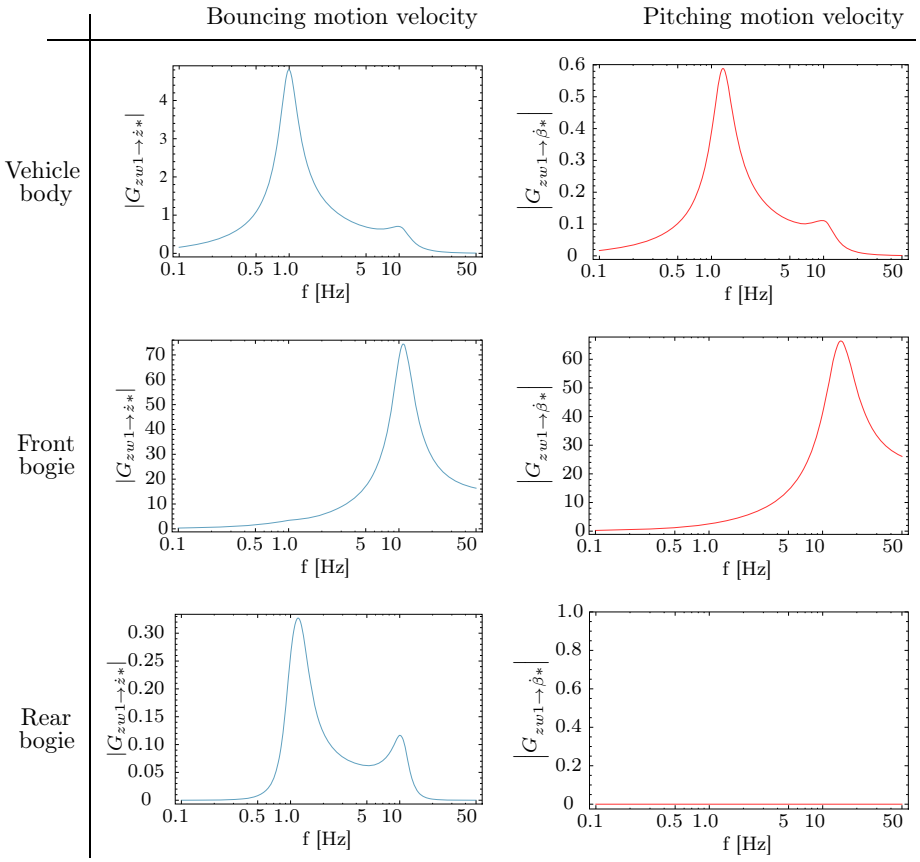

Figure 3.9: Gain frequency response for the system dynamics w.r.t. the leading wheelset excitation.

Plots in Figure 3.10 illustrate this transmissibility and equilibrium recovery through the system's step response. The system was excited by a step input of 5 [cm] applied to the wheelsets at a low speed of 5.5 [ms^{-1}] for a better inspection of the input delay effects due to the wheelsets separation.

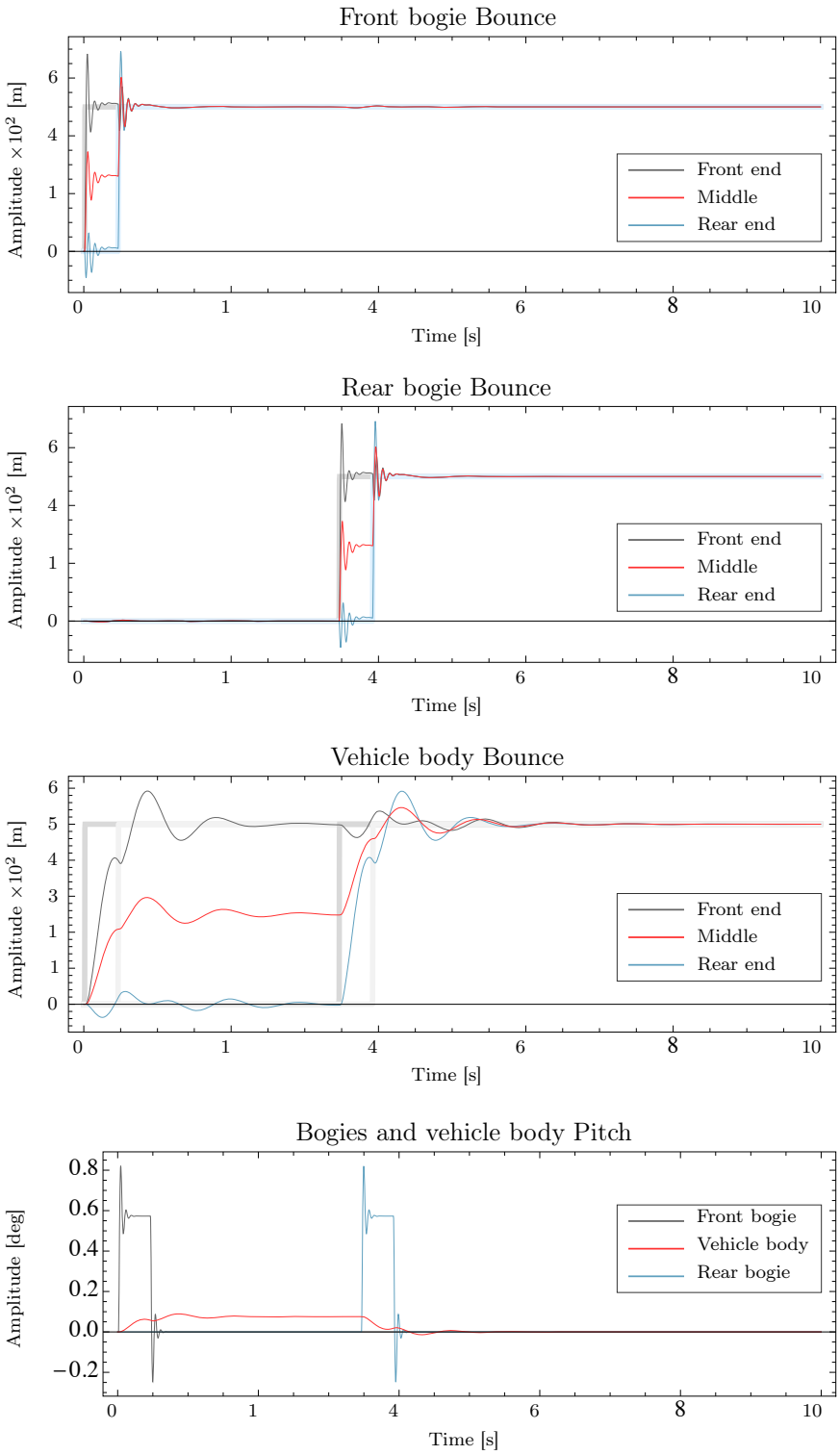

Figure 3.10: Time-response to a 'continuous step' input.

As stated by Pratt in [5], a geometric property of the vehicle causes the vehicle body and bogie to behave as semi-dividers which can be seen in the intermediate settlings of the bodies centre before settling at 5 [cm] and recovering the horizontal position in Figure 3.10.

Finally, the vehicle schematic in Figure 3.11 shows the stationary state achieved by the vehicle when a step force of 500 [kN] is applied through an ideal actuator placed in parallel to the front airspring (the magnitude of the validation force, although unrealistic, was chosen for illustrative purposes and given the fact that the model of the vehicle is linear; a more realistic value would be of 5 [kN]). As it was expected due to the action/reaction connection of the actuator and to the reaction of the airsprings, the transitory state of all the bodies in the bounce and pitch directions is nonzero. The steady state is a permanent elongation of the front airspring only, i.e. a positive rotation of the vehicle body, with also a permanent displacement of the centre of the vehicle body. The bogies return to the origin of their own local coordinates system with no rotation after settling from the transitory state, and the rear end of the vehicle returns to its natural equilibrium position, which is also expected.

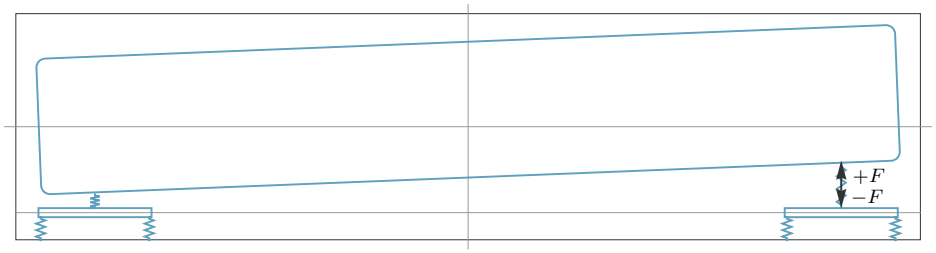

Figure 3.11: Steady state of the vehicle in response to a force step input of 5 [kN].

3.6 Effects of an Electromechanical Actuator in Active Suspension Design

Active control in a suspension system relies on the actuator dynamics which normally degrades the ideal control system behaviour. A recent research carried out by Md Yusof [42] was devoted to the control of actuators of different technology so that active suspensions in a railway vehicle behave close to the desired ideal. Most of the work in this thesis is focused on the use of ideal actuators. However, a research on the inertial effects of electromechanical actuators was found of interest to contrast with the effects of the inertance of the inerter concept.

In particular, an electromechanical actuator as the one in Figure 3.12(a) with electrical and mechanical sub-systems represented as in Figure 3.12(b), was considered.

It consists basically of a controlled motor driving a lead screw; the lead screw dynamics —and so the actuator applied force— however, is affected by the vehicle body and bogie dynamics to which the active suspension is attached. This imposes a difficulty in the design of active suspensions and solutions for this were addressed in [42].

A simplified and linear model of this electromechanical actuator [5, 42, 128] is given by the motor rotation equation

$$\begin{aligned} J_m\,\ddot{\theta}_m &= \tau_m - \tau_l - \tau_f \\ \ddot{\theta}_m &= \frac{K_t}{J_m}\,i_m - \frac{n_{sc}^2 k_c}{J_m}\,\left(\theta_m - n_{sc}^{-1} z_m\right) - \frac{c_m}{J_m}\,\dot{\theta}_m \end{aligned} \tag{3.77}$$

for which the induced current dynamic is defined as

$$\dot{i}_m = -\frac{R_{arm}}{L_{arm}} i_m - \frac{K_e}{L_{arm}} \dot{\theta}_m + \frac{1}{L_{arm}} v_c \tag{3.78}$$

and the lead screw travel equation of motion as

$$\ddot{z}_m = -\frac{k_{sc}}{m_{sc}}\,\left(z_m - z_{act}\right) - \frac{c_{sc}}{m_{sc}}\,\left(\dot{z}_m - \dot{z}_{\mathrm{act}}\right) + \frac{k_c}{m_{sc}}\,\left(n_{sc}\,\theta_m - z_m\right) \tag{3.79}$$

where: τ_m, τ_l, and τ_f, are, respectively, the motor torque, the torque due to the load and the torque due to the friction in the motor; J_m is the rotor inertia, K_t is the motor torque constant, k_c is the linear stiffness of the coupling between the motor and the screw, c_m is the coefficient of friction in the motor, R_{arm} and L_{arm} are the armature resistance and inductance, K_e is the back–emf gain, v_c is the voltage applied to the motor, m_{sc} is the screw mass (assumed concentrated), k_{sc} and c_{sc} are the stiffness and friction coefficients of the lead screw, and n_{sc} is the screw pitch. Hence, the active force applied on the vehicle body is given by

$$F_{\mathrm{act}} = k_{sc}\,\left(z_m - z_{\mathrm{act}}\right) + c_{sc}\,\left(\dot{z}_m - \dot{z}_{\mathrm{act}}\right) \tag{3.80}$$

with z_{act} the extension of the actuator. For an actuator installed in parallel to the i-th airspring, $z_{\mathrm{act},\,i} = z_{b,\,i} - \left(z_v + (-1)^{i-1} l_v \beta_v\right)$ affects, accordingly, the active force $F_{\mathrm{act},\,i}$.

The actuator dynamic is therefore one of the practicalities of great importance associated to active suspension design. In particular, in the study of the inerter applications for railway vehicle active suspensions, the following queries are of relevance,

1. What is the effect of the motor rotating parts inertia in the active suspension?

2. Can a passive network using inerters externally compensate for the deteriorating

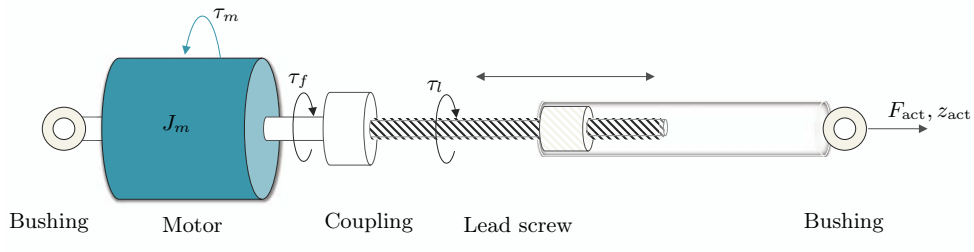

(a) Electromechanical actuator diagram.

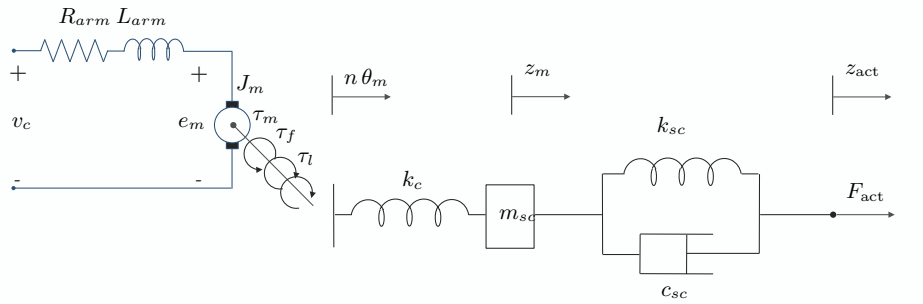

(b) Electrical and mechanical subsystems in the electromechanical actuator.

Figure 3.12: Electromechanical actuator.

internal dynamics of the electromechanical actuator?

To address those queries, a schematic of the equivalent linear mechanical network was developed for the diagram in Figures 3.12(a)–3.12(b), and is shown in Figure 3.13. It represents the relative inertia of the rotating parts in the motor as an inerter in parallel to a controlled force source concentrating the electrical sub-system (equivalent force developed by the motor) and a linear friction element associated to the friction in the motor. This allows to illustrate analogies between the actuator's subsystems mechanical phenomena and the three types of elements, namely: springs, dampers and inerters. These elements including inerters define the novel passive devices treated in this thesis.

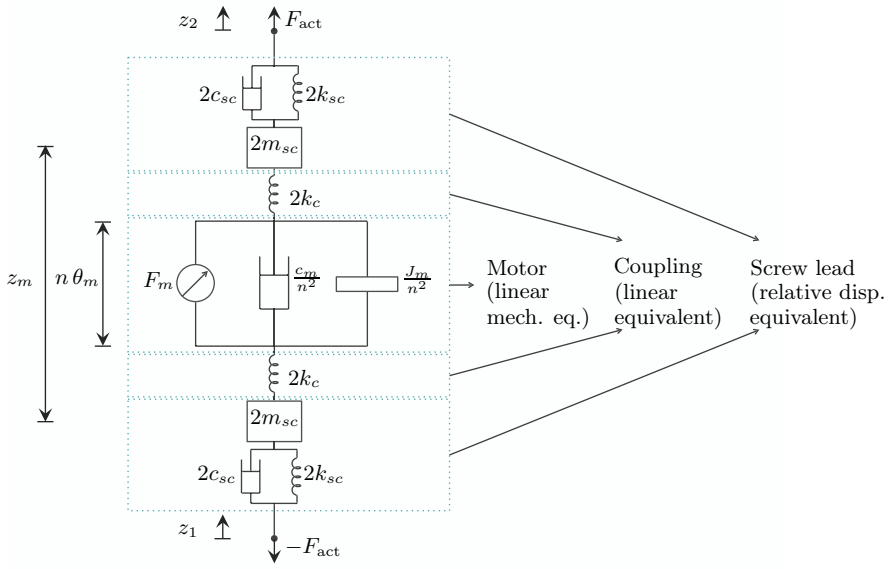

Figure 3.13: Linear mechanical equivalent of the electromechanical actuator.

A test for an electromechanical actuator placed in parallel to every airspring in the vehicle model in Figure 3.5 was performed to provide an answer to the first query. Firstly, it was assumed that the motor induced current i_c required to produce a desired control torque $\tau_c = K_t\, i_c$ is generated by an inner controller fast enough as to neglect the induced current dynamic and thus $i_m = i_c$ (therefore, $\tau_m = \tau_c$). The actuators are driven by a local 'skyhook' damping with complementary filtering control strategy with fixed parameters (refer to Chapter 5 for the strategy description). The control force resulting from the control scheme, F_c, is transformed into torque through the screw pitch value as $\tau_c = n_{sc}\, F_c$. It is also assumed that all the measurements are available and that no compensation for the effects of z_{act} and $\dot{z}_{\text{act}}$ is introduced. With all those considerations, the parameters J_m and c_m were tuned by optimising for ride quality assessed at the middle position of the vehicle (the next section describes the methods for assessing ride quality). Although this does not follow the conventional procedures for commercial actuators sizing, the idea here was to determine the potential of the rotor inertia and friction as design parameters. The outcome of this test was that neither friction nor inertia can provide any beneficial effect to the actuator dynamic, as it was possibly expected. This can be readily extracted from the p.s.d. plots for the vehicle body central acceleration excited through the four wheelsets in Figure C.1, Appendix C. The friction of the motor degrades the vehicle dynamics' first and third mode of vibration, while the rotor inertia degrades the third mode –without affecting the main mode– and adds an extra vibrational mode at higher frequencies. Moreover, it was found that the

friction in the motor eases the mode inserted by the rotor inertia.

In this way, the first query concerning the potential of the rotor inertia to produce similar results to those achieved by incorporating a passive network with inerters to the vehicle secondary suspension system was addressed. The answer to this depends on the possibility of modifying the inertial effects of the rotor so that its linear mechanical equivalent is distinct from a pure inerter. In the knowledge of this thesis' author, this is not possible at least for a conventional electromechanical actuator motor. Thus, the answer to the first question would be that inertial effects of the rotor are, in fact, deteriorating.

The second query is addressed in Chapter 6 for the same electromechanical actuator, accordingly sized (Appendix C), with an outer loop for actuator force control. Because the motor is controlled by the voltage input, v_c, either a static or a dynamic controller is required to provide the actuator with the force command resulting from the control of the active suspension. For the interest of this thesis a conventional Proportional–Integral (PI) actuator force control law for a closed-loop configuration was adopted, i.e.

$$G_{\mathrm{PI}}(s) = k_{pc}\left(1 + \frac{1}{T_{ic}\, s}\right) \tag{3.81}$$

Its parameters were manually tuned to provide an acceptable actuator force-response in terms of: accuracy to follow the desired force F_c, higher bandwidth, and less sensitivity to mechanical disturbances $\dot{z}_{\mathrm{act}}$. On this basis, the PI controller parameters were set to be $k_{pc} = 0.014$ and $T_{ic} = 0.08\,[\mathrm{s}]$. For illustrative purposes, the performance of the PI implemented in closed-loop as in Figure 3.14 is contrasted here with that of a static open-loop controller for which $v_c = K\,F_c$ (with K so that it provides an unitary force-to-force actuator gain). In Figure 3.14, $G^o_{vc}(s) = {}^{\hat{F}^{\mathrm{o}}_{\mathrm{act}}}/_{\hat{v}_c}$ and $G^o_{\dot{z}\mathrm{act}}(s) = {}^{\hat{F}^{\mathrm{o}}_{\mathrm{act}}}/_{s(\hat{z}_b - \hat{z}_v)}$ derive from Equations (3.77)—(3.80), considering F^o_{act} the output of the uncontrolled actuator.

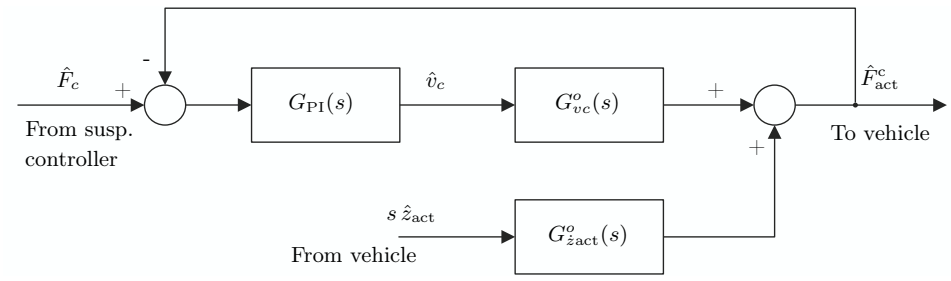

Figure 3.14: Block diagram of the i-th actuator force control loop (i=1, 2).

The performance of the controlled actuator alone is shown in Figures 3.15–3.16. The frequency response in Figure 3.15 shows a bandwidth increase in the actuator with closed-loop PI control in comparison to the open-loop unitary gain control configuration. It also depicts a reduced influence of the mechanical disturbance $\dot{z}_{\text{act}}$ on the actuator force. Plots in Figure 3.16 show the time-response of the actuator to a square-wave force command of $F_c = 1\,[\text{kN}]$ and to a step disturbance of $\dot{z}_{\text{act}} = 0.01\,[\text{ms}^{-1}]$. The effectiveness of the closed-loop PI controller is evidenced, i.e. a faster accurate response to the force command and a reduced sensitivity to disturbances. It has to be acknowledged here that more advanced strategies as these studied in [42] have already proven to drive the in-service actuator towards a performance closer to the ideal. However, designing in-service actuator control goes beyond the scope of this thesis and studies including actuator dynamics in this research were based on the model of PI-controlled actuators.

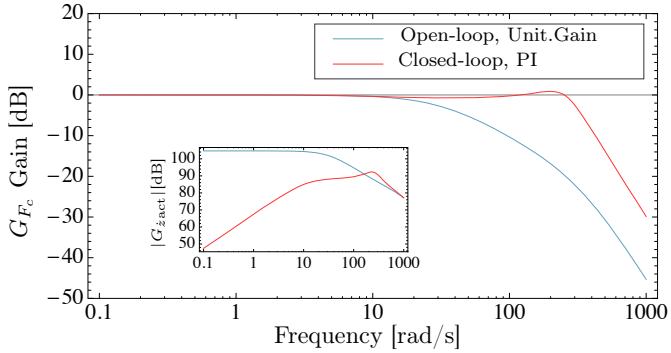

Figure 3.15: Bode plots for the actuator dynamics: $G_{F_c} = \hat{F}_{\text{act}}/\hat{F}_c$, and $G_{\dot{z}\text{act}} = \hat{F}_{\text{act}}/\hat{\dot{z}}_{\text{act}}$.

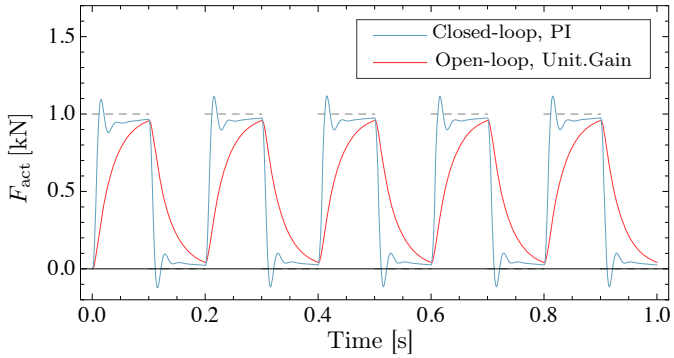

(a) Response to a square-wave reference force of $F_c = 1\,[\text{kN}]$ at $10\,[\text{Hz}]$ without mechanical disturbance, i.e. $\dot{z}_{\text{act}} = 0$.

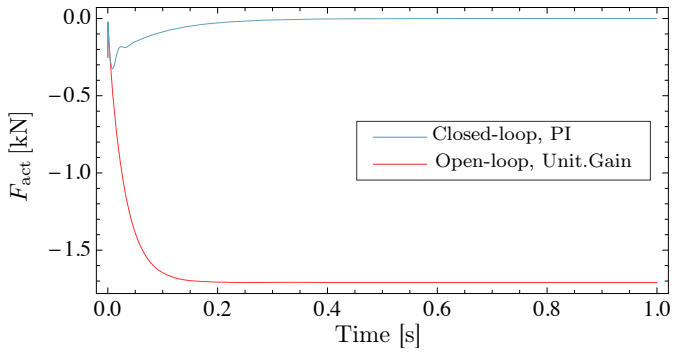

(b) Response to a step disturbance $\dot{z}_{\text{act}} = 0.01\,[\text{ms}^{-1}]$ and $F_c = 0\,[\text{kN}]$.

Figure 3.16: Actuator force time-response to different conditions.

3.7 Numerical Methods for Performance Assessment

The concern in this thesis while studying the vertical and inherited dynamics using the side-view model of the vehicle, is specifically to enhance ride quality. As a first study on the potential of the integrated suspensions using inerters, the assessment of the ride quality indices considered the vehicle response evenly for a range of frequencies to which the human body is normally more sensitive (below $20\,[\text{Hz}]$). Further studies should include the use of weighted norms for particular cases of ride comfort assessment, not considered here. Notwithstanding, results presented in the next chapters are well supported by the frequency response of the vehicle to track irregularities, and hence, a comparison with the ride comfort weighting curves can

still provide qualitative information about the ride comfort for the human body under specific travelling conditions.

3.7.1 Track profile for ride quality assessment and accomplishment of physical constraints

The track geometry model imposes holonomic constraints on the railway vehicle model and define the primary excitation ports of the vehicle given by both stochastic and deterministic features, as described earlier.

A definition for track geometry is given in [47] in terms of the type of track irregularities, among them, vertical surface profile which is the average elevation of the left and right rail. As stated by Garg and Dukkipati [47], it is impossible to gather the track irregularities in a detailed analytical description. Thus, a statistical representation containing irregularities amplitudes (roughness) and information on the wavelengths for characteristics as rail joints, for example, is more feasible for a satisfying model of track irregularities. Conversely, isolated track geometry variations (e.g. those in [47]) are more prone to be modelled analytically. A particular deterministic condition was considered for assessment of suspensions performance and actuators demand. Track models employed in this thesis are described next.

3.7.1.1 Stochastic irregularities

For assessment of vertical ride quality, a simplified stochastic model can be used to determine the response of the vehicle to nominal track surface irregularities whose variation $\dot{\delta}_z$ was described by a "white" random stationary process with a Gaussian distribution, i.e. the spatial spectral density of the irregularities variation in the space (and so in time for a constant speed) is uniform with "infinite" bandwidth. This flat characteristic excludes periodic features of the track. Even though the "infinite" connotation results slightly unrealistic for a real track, this simplification —as compared in [5] with realistic data of track elevation and with a fourth order spatial power spectrum *best fit* model— is yet valid and useful for suspension design purposes. In favour of simplicity, the wheels surface was assumed perfect and so only track irregularities are introduced in the performance indices assessment.

The above mentioned flat spectral density approximating the rate of the track irregularities, $\dot{\delta}_z(z)$, is derived from the mean spectral density, $S_s^{\delta z}(\omega_s)$, of the spatial elevation of the track, $\delta_z(z)$ [5] [3], which can be thought of a random stationary process of zero mean (i.e. $\bar{\delta}_z = 0$) with:

[3] Disambiguation: $\delta_z(t)$ denotes track profile; $\delta(t)$ is the normal Dirac delta function.

$$S_s^{\delta_z}(\omega_s) = \frac{2\pi\,\Omega_z}{\omega_s^2} \quad \left[\mathrm{m}^2\,(rad/\mathrm{m})^{-1}\right] \tag{3.82}$$

Ω_z is the vertical roughness coefficient of the track, taken along this thesis as 2.5×10^{-7} [m] which is a typical value for a good quality track [5, 110, 44, 41]; ω_s is the spatial circular frequency.

Recalling what was addressed previously in the mathematical modelling of the system, the prediction of the vehicle dynamics is assessed in this work using a moving irregularity model, and thus the track model clearly depends on the vehicle's travelling speed after performing appropriate conversions from the space domain to the time domain (the reader is invited to refer to Appendix D for a complete derivation).

Assuming a constant travelling speed v, the spectral density of $\delta_z(z)$ has the equivalent time-domain relation $S_t^{\delta_z}(\omega_t)$ for $\delta_z(t)$:

$$S_t^{\delta_z}(\omega_t) = \frac{2\pi\,\Omega_z\,v}{\omega_t^2} \quad \left[\mathrm{m}^2\,(\mathrm{rad/s})^{-1}\right] \tag{3.83}$$

where ω_t is the temporal circular frequency. Thus, the p.s.d. of time-variation of the track irregularities, $\dot{S}_t^{\dot{\delta}_z}(\omega_t)$, is readily obtained by multiplying $S_t(\omega_t)$ by ω_t^2, in accordance with the time-derivative property of the Fourier Transform, resulting in

$$\dot{S}_t^{\dot{\delta}_z}(\omega_t) = 2\pi\,\Omega_z\,v \quad \left[(\mathrm{m/s})^2\,(\mathrm{rad/s})^{-1}\right] \tag{3.84}$$

or equivalently, in temporal linear frequency,

$$\dot{S}_t^{\dot{\delta}_z}(f_t) = (2\pi)^2\,\Omega_z\,v \quad \left[(\mathrm{m/s})^2\,(\mathrm{Hz})^{-1}\right] \tag{3.85}$$

for which the autocorrelation function is the Dirac delta function,

$$R_\omega^{\dot{\delta}_z}(0) = \frac{p}{2\pi}\,\delta(t,\,t_1) \quad \left[(\mathrm{m/s})^2\right] \tag{3.86}$$

for the circular frequency, and

$$R_f^{\dot{\delta}_z}(0) = p\,\delta(t,\,t_1) \quad \left[(\mathrm{m/s})^2\right] \tag{3.87}$$

for the linear frequency, with

$$p = (2\pi)^2\;\Omega_z\,v \;\left[(\mathrm{m/s})^2\right] \tag{3.88}$$

and

$$\delta(t,\, t_1) = \begin{cases} 1, & \text{for } t = t_1 \\ 0, & \text{otherwhise.} \end{cases}$$

Nevertheless, because a flat spectrum may cause unrealistic results in some cases, due to modelling assumptions, the track input modelled as described above was modified by introducing a first order low-pass filter with corner frequency of 20 [Hz] .

3.7.1.2 Deterministic profile

Different track features can be modelled analytically. It is of interest for suspensions design the modelling of deterministic features of the track which can develop critical conditions in the vehicle dynamics. In particular, special attention should be given to the suspension deflection due to limitations in the suspensions clearance, and to the maximum active forces due to actuator limitations. A typical deterministic profile producing extreme conditions for those physically constrained variables is a railway gradient with a superimposed acceleration limit in the transition of 0.4 [ms^{-2}] (i.e. of approximately 4 [%g]) for a nominal speed of 55 [ms^{-1}], resulting in a transitional section of 1 [s] [5, 134] as in Figure 3.17. Thus,

$$\dot{\delta}_z(t) = \dot{f}(t) = 0.4 \int_{-\infty}^{t} \left(1\left(\tau_1 - t_0\right) - 1\left(\tau_1 - (t_0 - 1)\right)\right) d\tau_1 \quad [\text{ms}^{-1}] \tag{3.89}$$

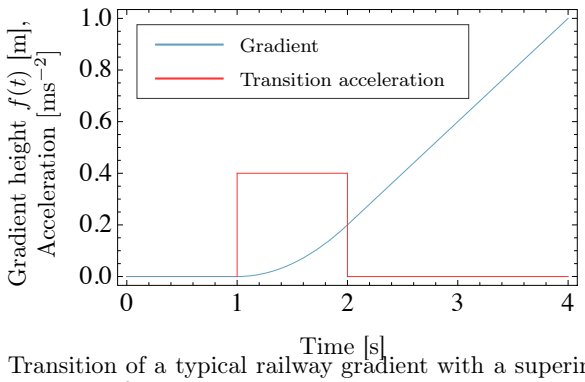

Figure 3.17: Transition of a typical railway gradient with a superimposed acceleration of 0.4 [ms^{-2}].

3.7.2 Assessment of the ride quality index, J_1

Ride quality is typically assessed by calculation of the root-mean-square (r.m.s.) of the vehicle body acceleration measurement, $\underline{J_1}$, at specific points along the vehicle

body, developed in response to track irregularities as described in the previous subsection. In particular, $\underline{J_1}$ is here a vector of values presented in percentage of gravity units, $\underline{J_1} = \begin{bmatrix} J_{1L} & J_{1M} & J_{1T} \end{bmatrix}^T$ [%g], where the subindices L, M, T stand for leading, middle and trailing positions (the leading and trailing positions are located above the centre of gravity of the front and rear bogies). For analyses based on the quarter vehicle model, for which the vehicle pitching mode is dismissed, $\underline{J_1}$ becomes the scalar J_1 and is equivalent to J_{1M} according to the calculation procedures described in the following. For optimisation problems, the worst case of ride quality among the three positions, $\underline{J_1}^{sup}$, is taken as the main design objective.

The mean-square of a zero-mean stationary process $z(t)$, $\mathrm{E}[z^2]$, can be obtained by knowledge of either the autocorrelation function $R^z_\omega(t)$ —following the equivalence given by Equation (D.7) in Appendix D— obtained from time based analysis, or by knowledge of the spectral density $S^z_t(\omega)$[4] from frequency based analysis which would allow the calculation of $\mathrm{E}[z^2]$ by using Equation (D.6) in Appendix D. These methods, however, are developed for linear systems only .

An alternative for nonlinear systems is to directly perform the conventional r.m.s. calculation on the output data obtained from simulations over the time to determine $\underline{J_1}$. This results in more inaccuracies and is computationally expensive; it is less convenient for performing numerical optimisation tasks over the other two methods, and thus it was avoided for the linear cases. In the next chapters, ride quality was assessed using the time history only when nonlinearities were introduced to the suspensions design. In the following, the frequency based and the state-space based (time-domain) methods are described [135, 5].

3.7.2.1 Spectral density: Frequency based method

If h_1(t) is the impulse response of a stable process whose Fourier transform is given in $H_1(j\,\omega)$, then the spectral density of the process response $z(t)$ to an excitation given as in Equation (3.84), according to the Wiener-Khintchine Equations (D.4)–(D.5), the convolution integral, and some interpretation of the resulting expressions, leads to the algebraic relation [136]:

$$\begin{aligned} S^z_t(\omega) &= H_1(-j\,\omega)\, H_1(j\,\omega)\, \dot{S}^{\delta z}_t(\omega) \\ &= |H_1(j\,\omega)|\, \dot{S}^{\delta z}_t(\omega) \end{aligned} \tag{3.90}$$

Thus, calculation of the mean square for $z(t)$ can be performed from

[4] From here, ω is adopted to refer to temporal circular frequency.

$$\sigma_z^2 = \int_{-\infty}^{\infty} |H_1(j\,\omega)|\ \dot{S}_t^{\delta z}(\omega)\, d\omega \tag{3.91}$$

Moreover, if the output of the process is the vector of accelerations

$$\underline{z}_{acc}(t) = [\ddot{z}_{vL}(t)\ \ddot{z}_{vM}(t)\ \ddot{z}_{vT}(t)]^T \tag{3.92}$$

$$= \left[\ddot{z}_v(t) + l_v\ddot{\beta}_v(t)\ \ddot{z}_v(t)\ \ddot{z}_v(t) - l_v\ddot{\beta}_v(t)\right]^T \tag{3.93}$$

for assessment of vehicle accelerations at the front, middle and rear positions of the vehicle body, then by using Equations (3.73)–(3.74), it is possible to find the r.m.s. of the vehicle accelerations as

$$\underline{J_1} = \underline{\sigma_{zacc}} = \sqrt{\int_{-\infty}^{\infty} \left|\underline{H_1}(j\,\omega)\right|\ \dot{S}_t^{\delta z}(\omega)\, d\omega} \tag{3.94}$$

where

$$\underline{H_1}(j\,\omega) = \begin{bmatrix} (j\,\omega)\sum_{i=1}^{4}\left(\frac{\hat{z}_v(j\,\omega)}{\hat{z}_{w,\,i}(j\,\omega)} + l_v\frac{\hat{\beta}_v(j\,\omega)}{\hat{z}_{w,\,i}(j\,\omega)}\right)e^{-\tau_i(j\,\omega)} \\ (j\,\omega)\sum_{i=1}^{4}\left(\frac{\hat{z}_v(j\,\omega)}{\hat{z}_{w,\,i}(j\,\omega)}e^{-\tau_i(j\,\omega)}\right) \\ (j\,\omega)\sum_{i=1}^{4}\left(\frac{\hat{z}_v(j\,\omega)}{\hat{z}_{w,\,i}(j\,\omega)} - l_v\frac{\hat{\beta}_v(j\,\omega)}{\hat{z}_{w,\,i}(j\,\omega)}\right)e^{-\tau_i(j\,\omega)} \end{bmatrix} \tag{3.95}$$

3.7.2.2 Covariance analysis: State-Space based method

This analysis applies for the state-space representation of the system and is based on the solution of the Lyapunov stability equation for the stationary process, which results in the autocovariance matrix of the states. The autocovariance matrix of the states —equivalent to the non-normed autocorrelation matrix of the states for $\tau = 0$ as in Equation (D.7)— was solved in MATLAB®. The computational solution of the Lyapunov equation is a more efficient procedure than performing the integration implied in the calculation of the autocorrelation vector from the frequency based method. Therefore, this method was in general preferred for numerical optimisation tasks.

A generic notation $\mathbf{A}^\flat$, $\mathbf{B}_{\hat{\delta}}^\flat$, $\mathbf{C}^\flat$, for the system matrices is used here for the description of the covariance method implementation. This is suitable to any linear structure of the system: open-loop —Equations (3.49)–(3.52), or closed-loop —Equations (3.54)–(3.63). Hence, the state-space representation of the vehicle dynamics excited

by the vector of random inputs $\underline{\dot{\delta}}_m(t)$ according to Equation (3.47), for which $\dot{\delta}_z(t)$ has the spectrum density in Equation (3.85), is given as

$$\underline{\dot{x}}^{\flat}(t) = \mathbf{A}^{\flat}\,\underline{x}^{\flat}(t) + \mathbf{B}^{\flat}_{\dot{\delta}}\,(t)\,\underline{\dot{\delta}_m}(t), \tag{3.96}$$

$$\underline{x}^{\flat}(t_0) = \underline{0},\ t_0 = 0 \tag{3.97}$$

$$\underline{y^{\flat}}(t) = \mathbf{C}^{\flat}_{\mathrm{y}}\,\underline{x}^{\flat}(t) \tag{3.98}$$

With the track irregularities applied at every wheelset as the inputs $\underline{\dot{\delta}_m}(t)$ related through time-delays between every pair of entries of $\underline{\dot{\delta}_m}(t)$ through an auto-correlation $\mathbf{R}_{\dot{\delta}}(t,\,\tau)$ matrix (Appendix D, Equation (D.13) for $n = 4$), p as in Equation (3.88), and $\tau_1 = 0\,[\mathrm{s}]$, the statistically stationary covariance matrix $\mathbf{P}(t) = \mathbf{P}$ (i.e. $\dot{\mathbf{P}}(t) = \mathbf{0}$) is the Lyapunov-type equation

$$\begin{aligned}\mathbf{A}^{\flat}\,\mathbf{P} + \mathbf{P}\,\mathbf{A}^{\flat T} = &-p\,\mathbf{B}^{\flat}_{\dot{\delta}}\mathbf{B}^{\flat T}_{\dot{\delta}} - p\sum_{\substack{j=1\\ j>i}}^{4}\sum_{i=1}^{4}\underline{B}^{\flat}_{\dot{\delta}j}\,\underline{B}^{T}_{\dot{\delta}i}\mathbf{\Phi}(\tau_j-\tau_i)^T \\ &-\left(p\sum_{\substack{j=1\\ j>i}}^{4}\sum_{i=1}^{4}\underline{B}^{\flat}_{\dot{\delta}j}\,\underline{B}^{T}_{\dot{\delta}i}\mathbf{\Phi}(\tau_j-\tau_i)^T\right)^T\end{aligned} \tag{3.99}$$

(For a derivation of Equation (3.99), refer to Appendix D). By solving the Lyapunov equation, the state stationary covariance (symmetric and positive-definite) matrix $\mathbf{P}$ is obtained provided the system is stable. Thus, the covariance vector for the outputs in $\underline{y^{\flat}}(t) = \underline{z_{zacc}}(t)$ is readily calculated as

$$\underline{\sigma^2_{zacc}} = \mathbf{C}^{\flat}_{y}\,\mathbf{P}\,\mathbf{C}^{\flat T}_{y} \tag{3.100}$$

with $\underline{\sigma_{zacc}}$ the root-mean-square vector of stochastic accelerations.

Again, for a result evaluated only for positive frequencies, the ride quality vector is obtained as $J_1 = \underline{\sigma^{+}_{zacc}} = {}^1\!/_2\,\underline{\sigma_{zacc}}$.

3.7.3 Assessment of other physical indices, J_2–J_4

In the design of railway vehicle suspensions, some physical constraints conflict with the achievement of the most desired levels of ride quality. In particular, special attention is given here to the trade-off defined between ride quality and secondary suspension deflection, and ride quality and active forces. Those impose difficulties

in the suspension design which justify this investigation on the use of novel mechanical devices with active suspensions. The indices associated to suspension deflection and active forces were assessed for the vehicle response to both, stochastic and deterministic features of the track and were considered in the suspension system parameters tuning. In addition, the calculation of the stochastic mean power ideally consumed/extracted by the actuators was performed to complete the comparative analyses later.

- ***Suspension deflection index, J_2:***

  The definition of the suspension deflection index, J_2, is a well accepted practice by railway dynamicists. For this, the three-sigma rule [137] on the standard deviation of the suspensions' deflection about their equilibrium condition, due to track irregularities, is considered as a measure of confidence added to the peak response to the gradient $f(t)$ from Figure 3.17.

  For the leading and trailing secondary suspension deflection vector, z_{DL} and z_{DT}, respectively,

$$\underline{z_D}(t) = \left[\begin{array}{cc} z_{DL}(t) & z_{DT}(t) \end{array} \right]^T = \left[\begin{array}{cc} z_{D1}(t) & z_{D2}(t) \end{array} \right]^T \tag{3.101}$$

$$= \left[\begin{array}{c} z_{b1}(t) - (z_v(t) + l_v\beta_v(t)) \\ z_{b2}(t) - (z_v(t) - l_v\beta_v(t)) \end{array} \right] \tag{3.102}$$

  the performance index J_2 is defined as

$$J_2 = \max_{i=1,\,2} \left[M_{D,\,i} + 3\,\sigma_{D,\,i} \right] \tag{3.103}$$

  where $M_{D,\,i}$ is the $i-th$ entry of the vector

$$\underline{M_D} = \left[\begin{array}{cc} \max\limits_{\dot{f}(t),\,t>0} |z_{D1}(t)| & \max\limits_{\dot{f}(t),\,t>0} |z_{D2}(t)| \end{array} \right]^T \tag{3.104}$$

  which is the vector of the maximum deflection of the leading and trailing secondary suspensions developed during the transitional response to the deterministic track input, $\dot{f}(t)$, defined in Equation (3.89). On the other hand, $\sigma_{D,\,i}$ in Equation (3.103) is the root-mean-square of the entries of z_D in Equation (3.102) in response to the stochastic track irregularities $\delta_z(t)$ and is calculated by using the same methods defined for ride quality assessment in Subsection 3.7.2. A typical value for the suspension deflection index J_2 is 3.5 [cm], see Pratt [5].

- ***Active force index,*** J_3***:***

  Similarly to the calculation of J_2, for the vector of measurements of the active forces required by the control systems of the leading and trailing active suspensions to the actuators, F_{cL} (F_{c1}) and F_{cT} (F_{c2}), respectively,

$$\underline{F_c}(t) = \left[\begin{array}{cc} F_{cL}(t) & F_{cT}(t) \end{array} \right]^T = \left[\begin{array}{cc} F_{c1}(t) & F_{c2}(t) \end{array} \right]^T \tag{3.105}$$

  the performance index J_3 is defined as

$$J_3 = \max_{i=1,\,2} \left[M_{Fc,\,i} + 3\,\sigma_{Fc,\,i} \right] \tag{3.106}$$

  where $M_{Fc,\,i}$ is the $i-th$ entry of the vector

$$\underline{M_{Fc}} = \left[\begin{array}{cc} \max\limits_{\dot{f}(t),\,t>0} |z_{Fc1}(t)| & \max\limits_{\dot{f}(t),\,t>0} |z_{Fc2}(t)| \end{array} \right]^T \tag{3.107}$$

  which is the vector of the peak forces required by the control systems to the leading and trailing actuators during the transitional response to the deterministic track input, $\dot{f}(t)$, in Equation (3.89). $\sigma_{Fc,\,i}$ is the root-mean-square of $F_{c,\,i}$ in response to the stochastic track irregularities and is calculated by using the same methods defined for ride quality assessment.

- ***Stochastic mean power,*** J_4***:***

  The stochastic mean power extracted by *perfect* actuators was assessed in J_4 to examine the potential of using novel mechanical devices to reduce the supply requirements. This is usually another challenge in active suspensions design, although for a bogied railway vehicle, the levels of power associated to the secondary suspensions are significantly low in comparison to the power dissipated by the primary suspensions. Moreover, the external power requirements would depend on the actuators technology. That was not particularly a fact considered for tuning the parameters of the different suspensions configurations, but for comparison purposes. The signs convention adopted considers a positive J_4 value as the average power (ideally) extracted by the actuators. For perfect actuators, that would be the mean power required to drive the actuators to produce active forces in a direction opposite to the relative velocity at its terminals.

  The stochastic mean power extracted/virtually dissipated in a suspension is given in general by the expected value of the product force-suspension deflection velocity, as

$$\mathcal{P} = \mathrm{E}\left[F_c\,(\dot{z}_2 - \dot{z}_1)\right] \tag{3.108}$$

For a single input system (i.e. a quarter vehicle model), with $r(t)$ the impulse response from $\dot{\delta}_z(t)$ to $F_c(t)$, and $h_2(t)$ the impulse response from $\dot{\delta_z}(t)$ to $\dot{z}_2(t) - \dot{z}_1(t)$, $\mathcal{P}$ is derived by using the convolution integral and the fact that $\mathrm{E}\left[\dot{\delta}_z(\tau_2)\dot{\delta}_z(\tau_1)\right] = p\,\delta\,(\tau_2 - \tau_1)$ (following and adapting [60]) as

$$\begin{aligned}
\mathcal{P} &= \int_{-\infty}^{t}\int_{-\infty}^{t} r(t-\tau_1)h_2(t-\tau_2)\,\mathrm{E}\left[\dot{\delta}_z(\tau_2)\,\dot{\delta}_z(\tau_1)\right] d\tau_1 d\tau_2 && (3.109)\\
&= q\,(r(t) * h_2(-t))(0) && (3.110)\\
&= q\int_{-\infty}^{\infty} R(j\omega)\,H_2(-j\omega)\,d\omega && (3.111)\\
&= q\int_{-\infty}^{\infty}\left(\sum_{i=1}^{n} G_{c,\,i}(j\omega)\,M_i(j\omega)\right)|H_2(j\omega)|^2 d\omega && (3.112)
\end{aligned}$$

where the summation term refers to the transfer function from the suspension deflection velocity to the active force, i.e.

$$\begin{aligned}
\sum_{i=1}^{n} G_{c,\,i}\,M_i &= \frac{F_c}{(\dot{z}_2 - \dot{z}_1)}\\
&= \sum_{i=1}^{n}\left(\frac{F_c}{\mu_i}\cdot\frac{\mu_i}{(\dot{z}_2 - \dot{z}_1)}\right) && (3.113)
\end{aligned}$$

and where the set of μ_i's are the measurements fed-back by the active control system of the suspension. Thus, $G_{c,\,i} = {}^{F_c}\!/_{\mu_i}$, and $M_i = {}^{\mu_i}\!/_{(\dot{z}_2 - \dot{z}_1)}$.

For the side-view model with two active suspensions (i.e. front and rear) and four wheelsets through which the track irregularities disturb the system,

$$J_4 = \mathcal{P} = \mathrm{E}\left[F_{c1}\,\dot{z}_{D1} + F_{c2}\,\dot{z}_{D2}\right] \tag{3.114}$$

For Equation (3.114), the impulse response functions used in Equation (3.109) become in matrices of appropriate dimension relating the active forces and suspension deflection velocity to every track input, and the formulation has to include the correlation matrix relating the track inputs. Here, for brevity, the derivation is based on the results in (3.112) with the time-delays included appropriately into the transfer functions, resulting in

$$J_4 = \int_{-\infty}^{\infty} \underline{\upsilon}^T(-\tau)\,\mathbf{H}_2^*\,(j\omega)\,\mathbf{\Gamma}(j\omega)\,\mathbf{H}(j\omega)\,\underline{\upsilon}(\tau)\,d\omega \tag{3.115}$$

where

$$\mathbf{\Gamma}(j\omega) = \sum_{i=1}^{n} \left(\mathbf{G}_{c,\,i}\,(j\omega) \begin{bmatrix} \mathbf{M}_{1,\,i}\,(j\omega) & 0 \\ 0 & \mathbf{M}_{2,\,i}\,(j\omega) \end{bmatrix} \right) \tag{3.116}$$

because the front and rear control configurations are assumed identical, $\underline{\upsilon}^T$ is

$$\underline{\upsilon}^T(\tau) = \begin{bmatrix} e^{-j\omega\tau_1} & e^{-j\omega\tau_2} & e^{-j\omega\tau_3} & e^{-j\omega\tau_4} \end{bmatrix} \tag{3.117}$$

the dynamic associated to the time delays $\tau = \{\tau_1,\, \tau_2,\, \tau_3,\, \tau_4\}$.

3.8 Summary of the Chapter

This chapter presented the mathematical model of the vehicle side-view and the geometric characteristics of the vertical track profile used for analysis and control design in later chapters. The suspension configurations proposed in those chapters are to be compared through the system's performance indices: ride quality ($\underline{J_1}$), suspension deflection index (J_2), active force index (J_3), and stochastic mean power, J_4, for which numerical assessment methods were also described in this chapter. It also examined the influence of the inertance effects appearing in the different components of the secondary suspension even though those are different in nature to the novel mechanical devices this work investigates. That was the case of the air fluid inertance in the airspring, whose equivalent was developed in this chapter using the concept of an ideal inerter, and the relative inertia of the electromechanical actuator which also admits a pure inerter as a linear mechanical equivalent. It was found from analysis that the inertance effects of the airspring system can be removed by provision of appropriate damping, and that the inertia of an electro-mechanical actuator deteriorates the suspensions performance.

4

Analytical Assessment on the Inerter Potential

Studies in this chapter identify the potential of adding inertance to railway vehicle secondary suspensions by placing an inerter in parallel to the conventional airspring, i.e. $\mathrm{Y}_{pn}(s) = b\,s$ [1]. The first assessment is on the contour plots of the inertance and vehicle parameters for variations in the ride quality index. The second part of the analyses goes beyond the typical assessment indices and focuses on energy functions and power dissipation. The pattern of the evolution of the vehicle body vertical dynamic is studied in energy-based 2D plots for deterministic excitations. Also, the levels of kinetic energy stored by the vehicle body and the inerter for periodic inputs are analysed. The last part of the chapter appraises the influence of the inerter and other characteristics of the passive suspensions on the levels of mean dissipated power for stochastic irregularities. Outcomes from this chapter sustain the numerical results obtained later in Chapter 6 for active suspensions with virtual dissipation, integrated with inerter-based devices.

4.1 Preliminars

The study investigates the fundamentals of the structural modification caused by the insertion of a new kinetic energy storage device into a suspension system. For this, a quarter vehicle model as in Figure 4.1 was employed, where: $m_{qv} = {}^{m_v}/_2$, $k_{qp} = 2\,k_p$, and $c_{qp} = 2\,c_p$. The force $F_s = F_a + F_u$ groups the force applied by

[1] The improperness of $\mathrm{Y}_{pn}(s)$ is recognised and this fact is considered later in the suspensions design.

the airspring and that by the inerter and the active suspension, where applies. F_p is the force applied by the primary suspension comprising a parallel arrangement spring (k_{qp}) and damper (c_{qp}). Thus, effects on the vehicle response due to its longitudinal geometry (side-view model) are obviated in the study. From analysis on such simpler structure, this assessment offers a projection on the effects of inerters for the implementation of active suspensions with 'dissipative' character.

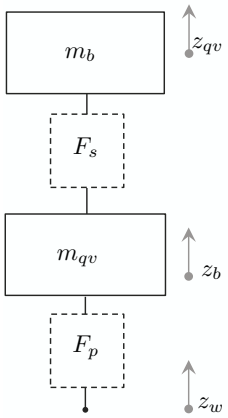

Figure 4.1: Quarter vehicle model.

4.2 Contour plots on the ride quality index variation, ΔJ_1

Contour plots for percentage changes in the ride quality in reference to the nominal index value, J_1^*, were obtained for different parameter settings of the quarter-vehicle model with an ideal inerter placed in the secondary suspension[2]. More specifically, this analysis was based on the calculation of the ride quality index, J_1, using the covariance method described in Subsection 3.7.2.2, as a function of a pair (a_1, a_2) where a_1 and a_2 are two of the following system parameters:

- those associated to the vehicle kinetic energy storage, i.e. the vehicle body mass m_{qv}, the inertance b of the ideal inerter, and the bodies mass ratio $\beta_m = {}^{m_b}/_{m_{qv}}$, and
- the airspring design parameters: airspring stiffness k_s, and airspring orifice damping c_r (the change of area and reservoir associated stiffness were assumed fixed to the values in Table 3.2).

[2] *Improvement* in the ride quality in the contour plots is indicated by a *positive* change.

The assessed $J_1(a_1, a_2)$ indices resulted from a respective real-rational function of high-degree polynomials in a_1 and a_2. $J_1(m_{qv}, b)$, $J_1(m_{qv}, k_s)$, and $J_1(b, \beta_m)$ would allow to contrast the effects of the bodies mass variation with the effects of the inerter; the manner that $J_1(b, k_s)$ and $J_1(b, c_r)$ change would become indicators to anticipate how modifying the kinetic energy of the system by using inerters could benefit the design of active suspensions in a railway vehicle. An analytical view of this is presented in the following supported by contour plots for:

$$\Delta J_1(a_1, a_2) = 100\% \times \left(1 - \frac{J_1(a_1, a_2)}{J_1^*}\right) \tag{4.1}$$

Contour plot for $\Delta J_1(m_{qv}, b)$:

The contour plot for ΔJ_1 in Figure 4.2(a) illustrates the dependency of the ride quality on the quarter-vehicle body mass, m_{qv}, and the inertance value, b. It depicts the existence of a nonzero finite value of inertance for which an optimal ride quality improvement (near 10%) can be obtained for the system with a nominal value of quarter-vehicle body mass, i.e. with $m_{qv} = 19$ [tonne]. It also shows what it is normally expected for an increased value of the upper mass of a suspended system as the quarter vehicle, i.e. the bigger the inertia of the body, the better the vibration attenuation. What it is most distinctive, however, is the particular fact that for achieving about 9.5% of improvement in the ride quality, for example, by introducing an inerter to the nominal system, an inertance of less than 500 [kg] is needed. Conversely, for achieving the same ride quality level without the inerter, the quarter-vehicle body mass should have to be increased by about 2.5 [tonne] (i.e. 5 [tonne] for the whole vehicle) which is unacceptable for high-speed trains. Moreover, the mass of an inerter with $b \approx 500$ [kg] could be of about 3 [kg] (neglected in the model) which is substantially more convenient than increasing the vehicle body mass for aiming such improvement through kinetic energy storage elements.

Contour plot for $\Delta J_1(b, \beta_m)$:

An analysis based on the bodies mass ratio $\beta_m = {}^{m_b}/_{m_{qv}}$ and the inertance, b, was also performed. Similarly to the analysis in [89] for automotive suspensions, it was assumed that the total mass of the quarter-vehicle $m_{qv} + m_b$ was constant and that the mass ratio β_m was varied. Figure 4.2(b) shows the contour plot for this analysis on the percentage variation of J_1. It confirms that for the ride quality interest, the lower the mass ratio the better, thus evidencing also the influence of the bogie mass on this performance measurement. It is also noticed that even the previous conclusion is normally known in railway suspensions assessment, the inclusion of an

inerter allows to increase the ratio β_m to maintain the nominal ride quality level J_1^* (with the possibility of slightly improving it); for the nominal parameters of the vehicle, $\beta_m = 0.13$. The conclusion obtained from Figure 4.2(b) could benefit lateral stability problems by a redistribution of the masses of the system.

Contour plot for $\Delta J_1\,(m_{qv},\, k_s)$:

The contour plot attained for percentage variations in m_{qv} and k_s (Figure 4.2(c)) illustrates the common trade-off between ride quality and suspension deflection. For a range of realistic values of the parameters, it evidences the existence of an optimal —rather soft— airspring stiffness finite value, k_s, whose level of improvement monotonically depends on a minimum quarter-vehicle body mass value, m_{qv}. As an example, the nominal ride quality attained with $k_s = 1.24 \times 10^6 \left[\mathrm{Nm}^{-1}\right]$ and $m_{qv} = 19\,[\mathrm{kg}]$ can also be achieved with a minimum value of suspension stiffness $k_s = 0.9 \times 10^6 \left[\mathrm{Nm}^{-1}\right]$ for which the quarter-vehicle body mass is also *slightly* smaller: 18.7 [tonne]. However, reducing the suspension stiffness for this small change in the vehicle mass would degrade the suspension deflection index, J_2. The contours also confirm that: a) increasing the suspension stiffness for a constant value of m_{qv} degrades the ride quality starting from a reasonable stiffness value (about $1 \times 10^6 \left[\mathrm{Nm}^{-1}\right]$) which agrees with the fact that softer suspensions provide better quality; and b) that increasing the vehicle body mass improves the ride quality —also observed from Figure 4.2(a).

Contour plot for $\Delta J_1\,(b,\, k_s)$:

The contour plot for the percentage of improvement/degradation of the ride quality index with different settings of the inertance b, and the airspring stiffness k_s, is shown in Figure 4.2(d). It depicts the existence of an optimal value of improvement of J_1 (even though not substantial for vertical ride quality enhancement) in a range of realistic values of b and k_s: an improvement of 9.5% can be attained with $b = 462\,[\mathrm{kg}]$, and $k_s = 1.34 \times 10^6 \left[\mathrm{Nm}^{-1}\right]$, which is slightly greater than the nominal stiffness of the airspring. Moreover, around this optimal setting, there are sets of *contiguous* pairs $(b,\, k_s)$ defining closed contours —although meaning lower ride quality enhancement— which reveal that the suspension stiffness value can be varied with the inertance value following a nonlinear relation without affecting the ride quality level defined by the contour. Increasing k_s is normally in favour of the suspension deflection index J_2 (described in Subsection 3.7.3). This outcome might be advantageous for the design of secondary active suspensions as the degradation of J_2 is normally a consequence of the improvement of J_1 in conventional passive suspensions as will be discussed later.

Contour plot for $\Delta J_1\,(b,\, c_r)$:

Figure 4.2(e) shows the contour plot for $\Delta J_1\,(b,\, c_r)$. Oval-shaped contours relating the inertance, b, and the airspring orifice damping parameters, c_r, for the J_1 modification function are observed. For a realistic range of the parameters values, a maximum improvement of 9.75% is attained for $c_r = 88.6 \times 10^3 \ \left[\mathrm{Nsm}^{-1}\right]$ and $b = 435$ [kg]. The plot evidences that for a constant damping coefficient and an inertance value greater than zero, but in a certain range, a higher level of improvement can be attained. This occurs specially for the range of damping values $(65 - 120) \times 10^3 \ \left[\mathrm{Nsm}^{-1}\right]$ for which improvements of $(7.5 - 9.5)\,\%$ can be obtained. Figure 4.2(e) also depicts limitations in the airspring orifice damping (as modelled here) in the provision of ride quality. Those limitations are in general displayed by the oval shape of the contours pointing to the c_r growing direction: for a constant inertance value, increasing c_r over certain value might not be beneficial. Moreover, for damping coefficients greater than the nominal, $c_r = 100 \times 10^3 \ \left[\mathrm{Nsm}^{-1}\right]$ for $b = 0$ [kg], for example, degradation contours are obvious.

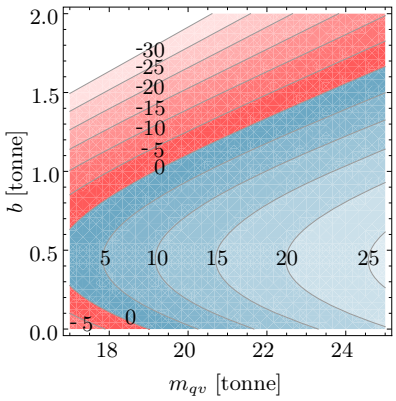

(a) Vehicle body mass and inertance

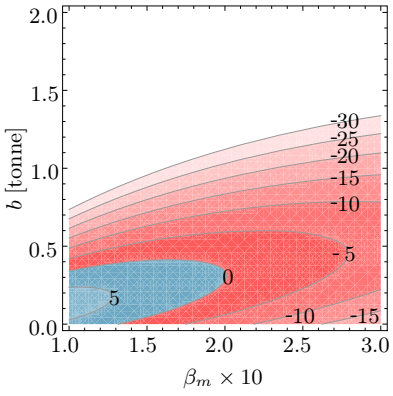

(b) Inertance and the bodies mass ratio, β_m

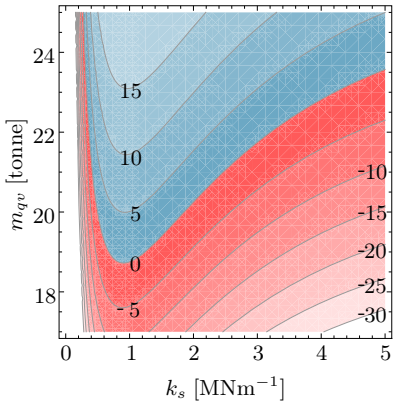

(c) Vehicle body mass and airspring stiffness

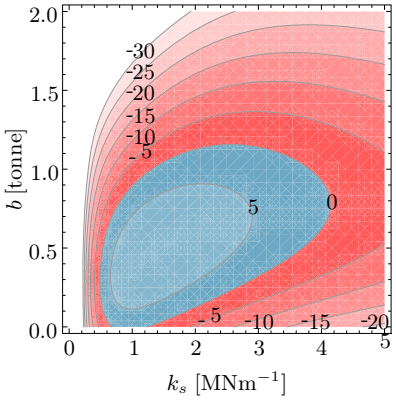

(d) Inertance and the airspring stiffness

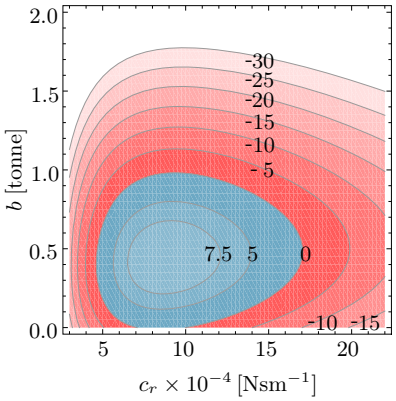

(e) Inertance and the airspring damping

Figure 4.2: Contour plot of specific pairs of parameters for ride quality percentage variation, ΔJ_1. Blue contours show improvement; red contours show degradation.

Further remarks on the contour plots:

The contour plots in Figure 4.2 depicted ride quality enhancement for optimal settings of the inertance and the vehicle parameter values. The influence of the kinetic energy storage elements on the ride quality of the vehicle (i.e. body mass and inertance) was compared in the contour plots in Figure 4.2(a). Particularly, enhancements in the ride quality are monotonic with (unrealistic) increased values of the vehicle body mass. Introducing inerters could overcome at some extent the need for a heavier body mass for this aim. Therefore, a finite optimal value of inertance which allows for improvement, enables also to:

1. Increase the airspring stiffness without causing degradation (Figure 4.2(d))
2. Reduce the damping of the airspring without causing degradation (Figure 4.2(e))
3. Reduce the vehicle body mass without causing degradation (Figure 4.2(a))
4. Increase the bogie mass without causing degradation (Figure 4.2(b))

That suggests that the inerter should cause either a better attenuation of the vibrations transmitted to the vehicle body, an improved dissipation in the suspensions, or both. This envisages a positive test of the research hypothesis. A more dedicated energy-based study is presented in the following; practical results including active suspensions and more realistic inerter-based devices are presented later to complete the hypothesis' test.

4.3 The kinetic energy storage function

The analysis based on the system kinetic energy storage functions provided here, searches for a relation with the enhanced ride quality evidenced in the previous section. Instead of a direct assessment of the ride quality index, however, it is supported by the evolution of the vehicle body acceleration. Specifically, this provides an examination based on the physics of the system about the existence of some inertance values $b > 0$ for which the ride quality of the vehicle could be improved to some extent when a pure and ideal inerter is placed in parallel to the airspring. This establishes an analytical framework for studying the potential of modifying the kinetic energy storage function of the vehicle body for simplifying the design of 'dissipative' active suspensions. By 'dissipative' active suspensions one refers here to those whose control law: 1) contains a term which allows to modify appropriately the damping of the system; 2) does not inject energy to the system. For instance, control

strategies as these based on the 'skyhook' damping concept are normally dissipative; in fact, this concept comes naturally from the passivity of the system.

An insight on the kinetic energy storage function for individual components of the vehicle undergoing periodic inputs is also developed. Hence, the analysis is developed in two parts; it employs the system's time-domain solution trajectories to deterministic inputs.

4.3.1 Vehicle body stored kinetic energy versus rate of change

Introducing passive networks into the secondary suspensions of the vehicle presumes an interconnection between passive subsystems. The inerter (and any mechanical network realised by using springs, dampers and inerters only) is a passive device by definition [3], and the dynamic of a railway vehicle with passive suspensions can be completely determined by using Euler-Lagrange equations as in Subsection 3.3, therefore the passivity concepts apply to the interconnection [3] [138]. Although the models employed in this research are linear simplifications of the vehicle dynamics, the analysis presented here was inspired by the most relevant concepts and objectives behind energy-based methodologies for nonlinear control design, to mention: Passivity-Based-Control (PBC) —see for example [138, 139]—, energy-shaping plus damping injection —see for example [140]—, the controlled Lagrangians —see for example [141, 142, 143, 144]—, and Lewis' differential geometric approach for kinetic and potential energy shaping [145]. In these methodologies, the design is concentrated in the definition of the system's closed-loop total energy; Lyapunov stability theory and Euler-Lagrange and/or Hamiltonian systems properties can be said to be part of their conceptual foundations. Even if those energy-based control design methodologies have been interestingly applied to a variety of dynamical problems, no dedicated analysis tools in this area were found by the author in the literature suitable for the interest of this analysis. Even though, concepts like 'available storage' and 'required supply' treated in analysis of dissipative systems [146] influenced this assessment. In general, those methods for defining the desired closed-loop total energy function consist basically of the following stages: reshaping the potential energy of the system to achieve desired equilibrium conditions, modification of the dissipation function through damping injection, and reshaping the kinetic energy of the system (although not always performed) which, according to Ortega et al. in [138], plays a role in the control task for regulation in some underactuated problems and the modification of the transient performance of stabilisation tasks.

[3] Although mathematical formalities are not derived, it is almost a direct conclusion due to the system's nature.

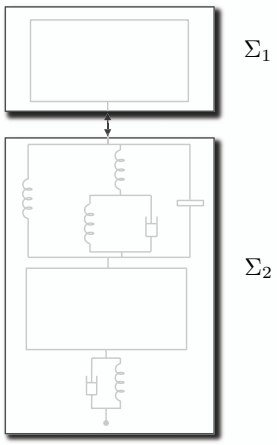

Figure 4.3: Separation of the quarter-vehicle model in Figure 4.3 into two subsystems. Notice that an ideal inerter was inserted in the secondary suspension.

Given the interest of this analysis on the vehicle body behaviour, a separation of the vehicle as two interconnected subsystems: Σ_1 and Σ_2, as in Figure 4.3, was performed. In this way, the vehicle body was considered as a subsystem Σ_1 excited by the subsystem Σ_2 through the interconnection, at which the energy interface between the two subsystems occurs. Due to the system nature and modelling assumptions (3.3 on page 42), it is clear that the vehicle body —subsystem Σ_1— stores kinetic energy only, whilst the passive subsystem Σ_2 stores potential energy in the (conventional) primary and secondary suspensions, and kinetic energy in the supporting bogie and the inerter (Figure 4.3). Remark: recall here that all the studies in this thesis are developed on the basis of incremental models around an equilibrium condition, thus, potential energy terms due to gravity do not appear in the analysis. Notice also that Σ_2 dissipates energy, and it is the subsystem through which: a) the energy due to the track profile enters the system, and b) some energy from the controlled actuator for the case of active suspensions, would enter/leave the system. Notice that an actuator driven by a control law in general may inject and/or remove mechanical energy to/from the system. In particular, a 'dissipative' active suspension, as defined here, will not inject energy to the system but only remove, i.e. virtually dissipate.

This analysis was prompted by energy-based methodologies featuring kinetic energy reshaping, and supported by the method of 'minimised kinetic energy' studied by Zilletti et al. [68], briefly discussed in Chapter 2. The analysis is based on the facts that the ideal inerter is a kinetic energy store and that ride quality is assessed on the subsystem Σ_1, which only stores kinetic energy. Specifically, it concentrates on how the kinetic energy storage function U_1 of the subsystem Σ_1 is effected by the insertion of an inerter in the subsystem Σ_2, which can reveal important features of

the system with inerters. To justify the interest on the energy function of Σ_1 only, the reader is invited here to remember that the objective is to minimise the ride quality index, which is based on the vehicle body accelerations. To see more clearly the inerter influence on the evolution of U_1, also the first time-derivative of U_1 is analysed, i.e. the kinetic energy rate $\dot{U}_1$.

Energy-2D plots for U_1 versus $\dot{U}_1$ are produced for the analysis. These are contrasted with parametric 2D plots for $\dot{z}_{qv}$ versus $\ddot{z}_{qv}$; notice that this differs from the normal phase curves z_{qv} versus $\dot{z}_{qv}$ employed, for example, in qualitative stability analyses. It is well known that the storage function U_1 is a quadratic function of $\dot{z}_{qv}$, i.e. $U_1 = \frac{1}{2} m_{qv} \dot{z}_{qv}^2$, and one has that the rate of change $\dot{U}_1$ is related to the vehicle body acceleration $\ddot{z}_{qv}$ through the gradient of U_1 with respect to the vehicle body velocity $\partial U_1 / \partial \dot{z}_{qv}$, which is characterised by $\pm\sqrt{2\, m_{qv}\, U_1}$, as: $\dot{U}_1 = \partial U_1 / \partial \dot{z}_{qv}\, \ddot{z}_{qv}$. This enables a parametrisation of U_1 versus $\dot{U}_1$ in terms of the acceleration $\ddot{z}_{qv}$, which sets the basis for a comparison between the two types of aforementioned plots. Although this parametrisation deserves some theoretical work, this goes beyond the scope of this thesis.

The *energy portrait* concept has been introduced in few different applications and its interpretation has been adapted according to the particular case of study, e.g. [147, 148]. Nevertheless, here we do not derive portrait plots but instead generate a single curve of the portrait for the response of the vehicle going from an equilibrium condition to another for different parameter settings. The parametric plot for the kinetic energy function and its time-derivative introduces a qualitative tool to illustrate the outstanding geometric feature of the curve U_1 versus $\dot{U}_1$ for the system with an optimal value of inertance. This aims an analytical understanding of the potential of the inerter for reorganising the system energy and how it could benefit active suspensions designed to minimise the body accelerations. It is worth noting that this form of representation does not display the time dependency of the curves, its definition stems from the trajectories of the system which are its unique solution for a time interval $[0,\, t]$ in response to the excitation (applied either through the track input port or through the actuator port). However, depending on the nature of the excitation, characteristics associated to the transitory and stationary states of the system response could be identified from the plot (e.g. it is direct to associate the maximum kinetic energy stored by Σ_1 with the maximum peak of the vehicle velocity response).

Two cases associated to the system's input ports were examined. In both cases, an exponentially decreasing function $g(t) = e^{-t/T}$ with $T = 0.01\,[\mathrm{s}]$ was set to dominate a specified input signal. $g(t)$ decays more than ten times faster than the system's fastest response and thus provides a quasi-zero input response. The system initial conditions are, in every case, the equilibrium of the system for the input initial

condition defined as a factor of $g(0)$. The examined cases were:

1. Excitation through the wheelset (displacement/velocity of the wheelset/track contact point): $z_w(t) = \delta_z(t) = 0.025\, g(t)\,[\mathrm{m}]$ (and $\dot{z}_w(t) = \dot{\delta}_z(t)$), with $F_{\mathrm{act}}(t) = 0$. (Figure 4.4).

2. Excitation through an ideal actuator (force): $F_{\mathrm{act}}(t) = 10^3 g(t)\,[\mathrm{N}]$, with $z_w(t) = \mathrm{const.} = 0$. (Figure 4.5).

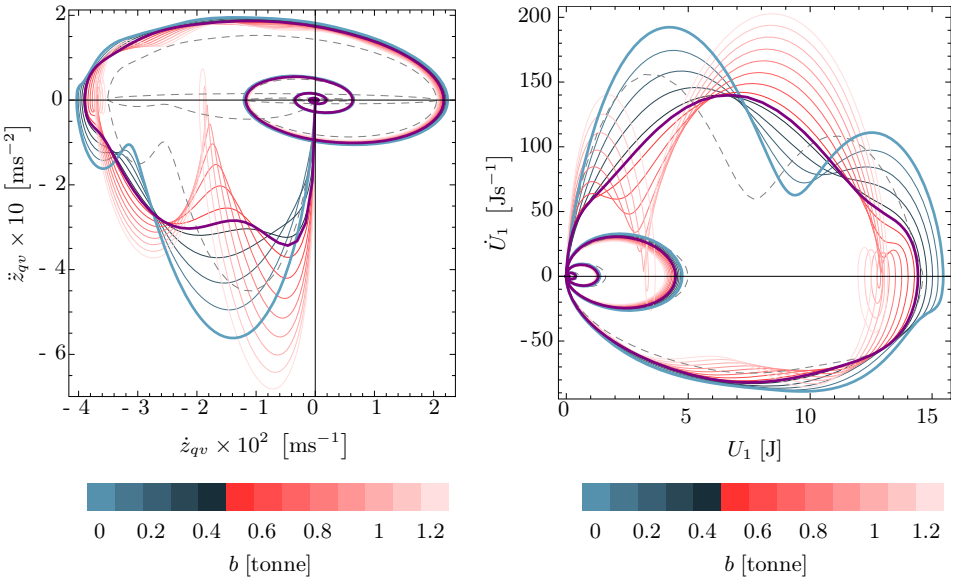

Figure 4.4: Plots resulting for the track input. Left: Phase graph, $\dot{z}_{qv}$ vs. $\ddot{z}_{qv}$; Right: Energy graph, U_1 vs. $\dot{U}_1$.

The referred plots generated with the quasi-zero input trajectories are shown in Figures 4.4–4.5. There, the purple thick curves are for the optimal inertance value obtained for ride quality to stochastic irregularities ($b = 443\,[\mathrm{kg}]$ for 9.4% of ride quality improvement, not illustrated), and standard parameter values for the bodies and the suspensions. The blue and red curves were generated also for the standard quarter-vehicle but with arbitrary inertance values, according to the colour scale underneath the plots. The gray dashed curves are, on the other hand, for zero inertance and 25% heavier vehicle body. The analysis on the plots follows:

Firstly, the system stability and dissipation properties result obvious as all the curves in Figures 4.4–4.5 converge to the origin of the plots, which is an attractor point by nature, i.e. the system goes from one equilibrium condition to another.

Secondly, a direct observation from the purple thick curve in Figure 4.4–Right, for the first case, is that with an inerter with optimal inertance value, the maximum kinetic energy stored by the vehicle body in an equilibrium-to-equilibrium transition, is reduced if compared with the system without the inerter (blue thick curve). This is consonant with the reduction in the maximum amplitude of the vehicle body velocity, $\max|\dot{z}_{qv}|$, depicted in Figure 4.4–Left through the corresponding thick curves. An immediate remark derives from here and is the fact that a lesser kinetic energy stored in Σ_1 is indication of either a better dissipation in the suspensions or a convenient redistribution of the energy among the system's elements (i.e. better vibration isolation). Hence, it is evident that less energy would have to be removed to further improve the vehicle body dynamics. Thus, if a 'dissipative' control strategy is implemented for a secondary active suspension, the maximum levels of energy that the controlled —ideal— actuator would have to remove from the system to achieve a ride quality, say J_1^{a} , are lower as compared to the vehicle without the inerter to achieve the same ride quality J_1^{a}. In contrast, the gray dashed curves illustrate that without inerter, a 25% heavier vehicle body (which also implies a better ride quality —16% better— not represented in the plots) stores lower levels of kinetic energy and has lower gain/loose (positive/negative) energy rate, in absolute value.

Thirdly, a reduction in the maximum amplitude of $|\ddot{z}_{qv}|$ is observed from the purple thick curve (i.e. with b optimal) of Figure 4.4–Left, and so in the maximum amplitude of $\left|\dot{U}_1\right|$ of the energy plot (Figure 4.4–Right).

Fourthly, it is easy to note apart from a reduced $\max\left|\dot{U}_1\right|$ for the system trajectories, that the inerter has a direct influence on determining the shape of the rate of energy transition associated to how the interface between Σ_1 and Σ_2 occurs. This shows that the inerter has some 'authority' on the energy management: the set of red and blue curves illustrates a *reshaping* for different values of inertance. It can be checked that an optimal inertance value produces a smoother energy curve (purple thick curve in Figure 4.4–Right) with the waviness mostly removed, and indeed without saddle points. A smoother curve appears to be in favour of a reduced variance in $\ddot{z}_{qv}$ at frequencies related to secondary vibration modes of the system, and hence to the ride quality. However, not all the curves with $b > 0\,[\mathrm{kg}]$ seem to be favourable for the shape of the energy-2D plot and the vehicle dynamics assessed through the variance of $\ddot{z}_{qv}$. For instance, inertance values greater than $1000\,[\mathrm{kg}]$ are known to degrade the ride quality of this system; such degradation can be associated to the 'deteriorated' shape (high peaks and sharp saddle points) of the corresponding curves in Figure 4.4, as compared to these for optimal inertance and with no inertance (purple and blue thick curves, respectively). Conversely to the 'reshaping' caused by the inerter, the gray dashed curves are more alike the curves for the conventional configuration with a saddle point in the initial dynamic region but with different amplitude, which settles

a 'redimensioning' effect due to a parameter change in the conventional structure.

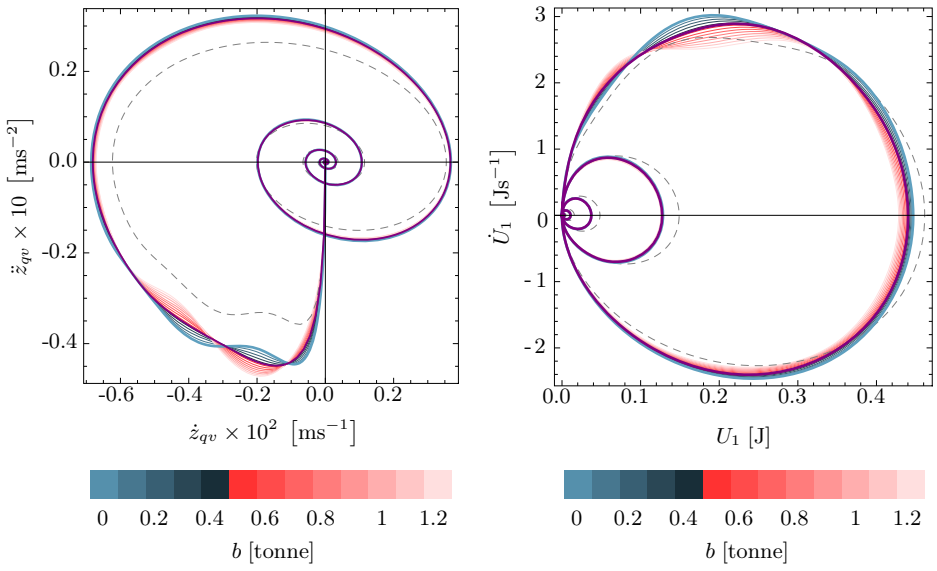

Figure 4.5: Plots resulting for the force input. Left: Phase graph, $\dot{z}_{qv}$ vs. $\ddot{z}_{qv}$; Right: Energy graph, U_1 vs. $\dot{U}_1$.

On the other hand, by comparing the plots in Figures 4.4–4.5 it can be extracted that the inerter would effect more the response to the track input than the response to active control force. The curve $\dot{U}_1(U_1)$ for the optimal value of b in Figure 4.5 results also smoother. The plot suggests that the energy interface between Σ_1 and Σ_2 in this case is barely effected by the inerter, the vehicle body would store about the same levels of kinetic energy U_1 than without the inerter and with similar gain/loss rate $\dot{U}_1$. In other words, the kinetic energy stored in Σ_1 in response to the dynamic caused by the track profile is reduced by the inerter in comparison with the conventional suspensions, which is desirable for vibrations attenuation and better transient response. In addition, the kinetic energy stored in the vehicle body (subsystem Σ_1) in response to the dynamic caused by the actuator remains almost the same with and without inerter, which is also desirable for the effectiveness of the active suspension. Thus, the inerter should not affect the control action. The small reduction of the storage rate associated to the initial dynamic trajectories is a result of the smoothing of the curve, and because it occurs for the energy storage rate stage (i.e. $\dot{U}_1 > 0$), this should not be a negative effect at least for the response to a control action intended to remove vibrational energy.

This analysis suggests the following on the potential of the inerter (with optimal

inertance value) integrated with active suspensions:

1. the vehicle body stores less kinetic energy, thus less energy needs to be removed for a better ride quality;

2. the energy extraction rate by a virtually dissipative active suspension can be lower, i.e. providing no energy is injected to the system through the active suspension;

3. the inerter does not affect significantly the shape of the kinetic energy loss rate assessed for the vehicle body, so should not affect significantly the extraction —virtual dissipation— rate;

4. the inerter improves the high frequency vibrational modes (outcome extended in the next analysis), which is beneficial to simplify the active suspension design. Indeed, the active suspension is normally designed to reduce the primary mode but the actuators normally have low bandwidth, thus the insertion of an inerter could complement the implementation of active suspensions;

5. the inerter should not interfere in the active control tasks, but instead should provide the system with better dynamical conditions;

6. due to the redistribution of the energy in the system, it can be envisaged that some extra potential energy store may be allowed to be introduced to the system for reducing J_2 without deterioration of the ride quality level, J_1, improved mostly by active suspensions.

The merits of this qualitative analysis are expected to be consolidated in future work. The objective here was to get a good picture of the potential of the inerter for passive and active suspensions before tackling numerical studies.

4.3.2 Frequency dependence of the inerter kinetic energy storage

The second part of the analysis is based on Figure 4.6 which shows how the levels of kinetic energy stored by the inerter, U_b, are frequency dependent. This is an immediate outcome from the admittance function of the ideal inerter.

Here, a periodic input $\delta_z(t) = 0.01\,\mathrm{Sin}\,(2\pi f\,t)$ [m] ($F_{\mathrm{act}}(t) = 0$) is provided for different values of frequency f. Figure 4.6 contains the plots for the stationary response for every case, depicting U_1 vs. U_b, both normalised by $\max(U_1)$ with $b = 0$ [kg]. The frequency dependency of the kinetic energy storage in the inerter is mainly determined by the phase difference between $\dot{z}_b$ and $\dot{z}_v$, as $U_b = \frac{1}{2}b\,(\dot{z}_b - \dot{z}_v)^2$; the radii of the ellipses in the plots are determined by the phase difference between

the stationary, periodic, trajectories in t described by $\dot{z}_v$ and $(\dot{z}_b - \dot{z}_v)$ and the ratio between their amplitudes. It is noticed that for frequencies bellow 1 [Hz], the inerter stores very low levels of kinetic energy; for higher frequencies, the stored energy can be much higher than the energy stored by the vehicle body. In particular, the plot for $f = 10$ [Hz] clearly depicts that the range of values containing the optimal value of b is so that an outside inertance value would cause the vehicle body to store more energy than with b optimal. Moreover, the energy stored by the vehicle body tends to be zero for such frequency. This allows to interpret the existence of inertance values for ride quality enhancement as the possibility of causing a frequency dependent redistribution of the kinetic energy so that the vehicle body stores less energy when excited at certain frequencies, which directly relates to the body motion. The relation $\max\left(\bar{U}_1\right) : \max\left(\bar{U}_b\right)$ for b optimal varies from being about $1 : 10^{-4}$ for $f = 0.25$ [Hz] to be $0.1 : 60$ for $f = 10$ [Hz], and $1 : 1600$ for $f = 15$ [Hz]. It is worth to mention that for a configuration with optimal inertance value, frequencies $f = 15$ [Hz] and above are amplified as compared to the vehicle without inertance (according to Bode plots not provided here for brevity), hence, indicating poor response to high frequencies.

It is remarkable that for suspension design based on the introduction of inerter-based mechanical networks, frequency-based methods are more appropriate. This way, the inerter can be conveniently combined with springs and dampers to build a passive structure with certain frequency response characteristics to avoid undesirable effects at higher frequencies4.6. This also enables to add extra compensation benefits. Furthermore, a mechanical inerter has some limitations which makes the characteristic of the inerter response to be frequency dependent. Chapter 5 makes some considerations for modelling a real inerter.

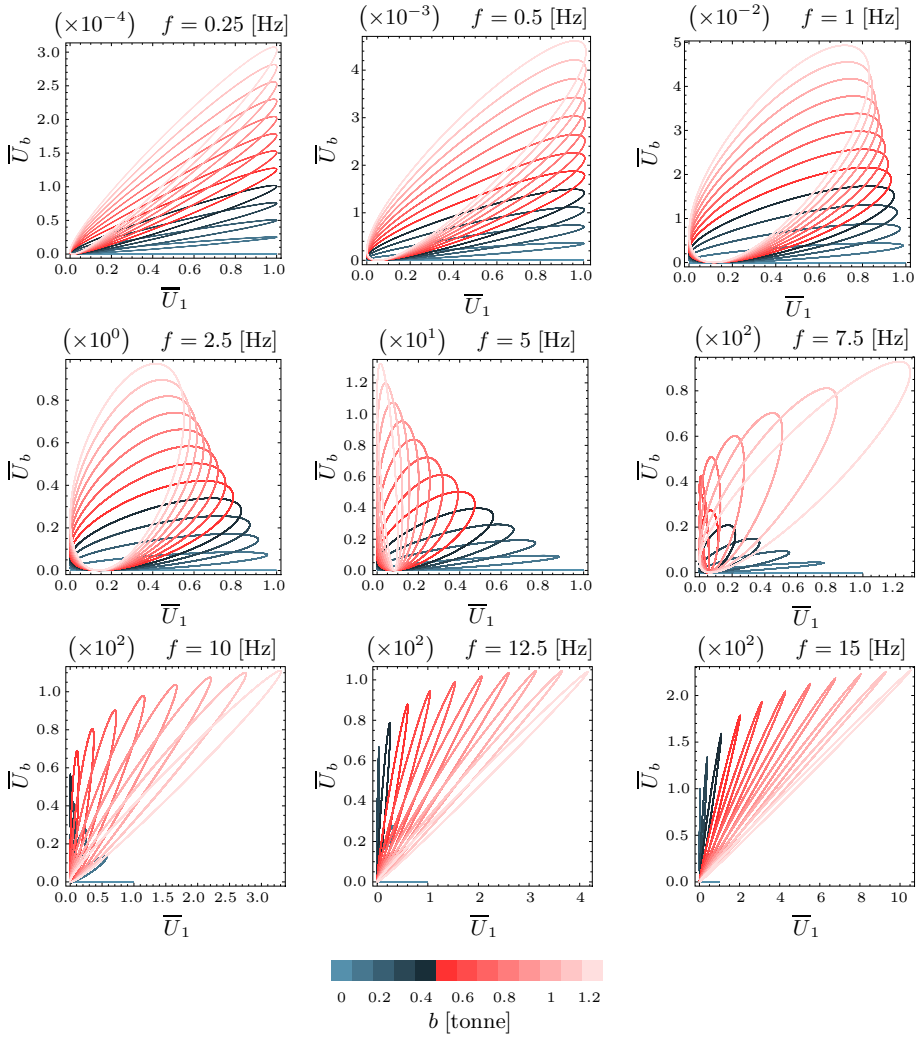

Figure 4.6: Kinetic energy stored by the vehicle body versus kinetic energy stored by the inerter in the stationary response to periodic inputs.

What is deduced from this analysis might be indicative of a contribution of the inerter to the energy dissipation and extraction efficiency by the resulted energy redistribution. The *efficiency* term has, in this thesis, a merely intuitive character, no attempt to measure the energy dissipation/extraction efficiency is made. Instead, the next subsection discusses the mean power dissipated by the passive suspensions, and in the following chapters the J_4 index assesses the mean power extracted by the active suspensions.

4.4 Stochastic mean power dissipated by the passive suspensions

Here, the mean dissipated power is assessed for the 'bounce quarter-vehicle' excited by stochastic irregularities to determine how the inerter effects the dissipation in the primary and secondary passive suspensions, contrasted with the effect of other suspension parameters. The calculation is based on Equation 3.108, for which following [60], one has:

$$\mathcal{P}_p = p \int_{-\infty}^{\infty} \mathrm{Y}_p(j\omega)\,|H_p(j\omega)|^2 \frac{1}{(\epsilon^2\omega^2+1)} d\omega \tag{4.2}$$

$$\mathcal{P}_s = p \int_{-\infty}^{\infty} \mathrm{Y}_s(j\omega)\,|H_s(j\omega)|^2 \frac{1}{(\epsilon^2\omega^2+1)} d\omega \tag{4.3}$$

for the mean dissipated power in the primary and secondary suspensions, respectively, and where: $\mathrm{Y}_p(s)$ is the admittance of the primary suspension, $\mathrm{Y}_p(s) = \left(k_p s^{-1} + c_p\right)$, $H_p(s)$ is the transfer function from the track irregularities rate, $\dot{\delta}_z$ (defined by a white noise power spectrum as in Equation 3.84), to primary suspension deflection velocity, $\dot{z}_w - \dot{z}_{b1}$ (with $\dot{z}_w = \dot{\delta}_z$). Similarly, $\mathrm{Y}_s(s)$ is the admittance of the airspring $\mathrm{Y}_a(s)$ (Equation 3.71) augmented by the inerter admittance, $b\,s$, and $H_s(s)$ is the transfer function from the track irregularities rate, $\dot{\delta}_z$, to secondary suspension deflection velocity, $\dot{z}_{b1} - \dot{z}_v$. The common term $\frac{1}{(\epsilon^2\omega^2+1)}$ comes from a low-pass filter assumed for the disturbance signal, $\dot{\delta}_z$, which is introduced to avoid an infinite –and unrealistic– power result for $\mathcal{P}_p$ [60]. The value of ϵ is set to $\epsilon = 0.008$ to give a cut-off frequency of 20 [Hz] as referred in Chapter 3 for assessing the performance indices of the system.

Figures 4.7–4.9 contain the 3D plots obtained for the power dissipated in the primary and secondary suspensions (individual and total), for variations in the airspring damping coefficient, c_s, and the inertance, b. Figure 4.7, in particular, depicts that for damping values ranging from 0 to 200 $[\mathrm{kNsm}^{-1}]$ (and any value of $b > 0\,[\mathrm{kg}]$), the total dissipated power, $\mathcal{P}_p + \mathcal{P}_s$, is relatively constant —although not exactly— as found also by Smith and Swift [60] for a similar assessment on automotive suspensions, due to the transfer of power between $\mathcal{P}_p$ and $\mathcal{P}_s$. Increasing the damping value c_s up to 50 $\left[\mathrm{kNsm}^{-1}\right]$ reduces the dissipation in the primary suspension (Figure 4.8), but increases it in the secondary one (Figure 4.9); the converse occurs for $c_s > 50\,\left[\mathrm{kNsm}^{-1}\right]$ although with a much lower gradient.

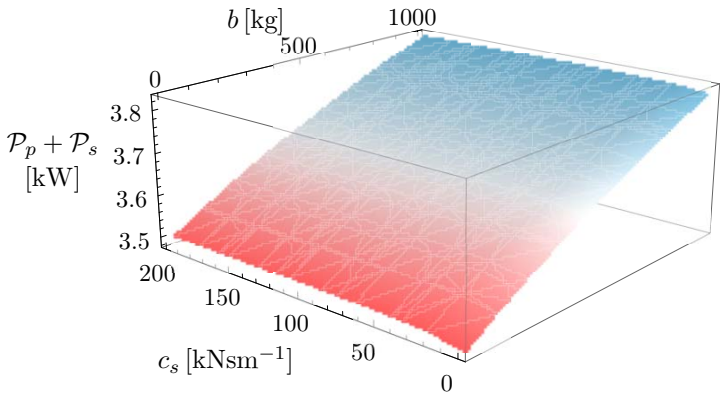

Figure 4.7: Total mean power dissipated in the vehicle passive suspensions as a function of b and c_s.

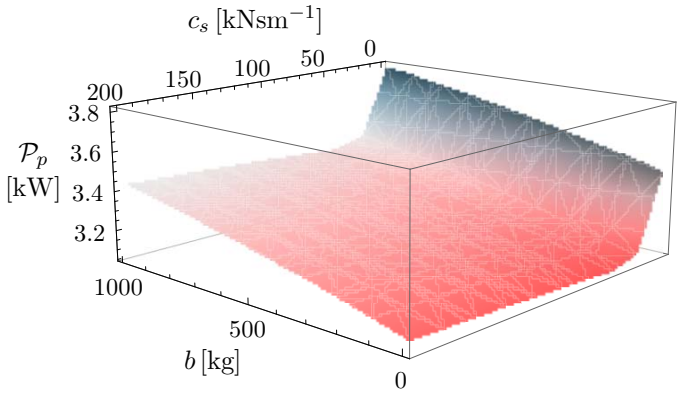

Figure 4.8: Mean power dissipated in the primary suspension as a function of b and c_s.

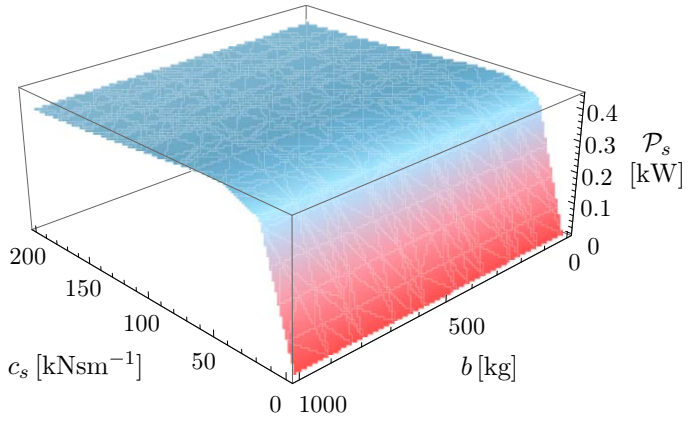

Figure 4.9: Mean power dissipated in the secondary suspension as a function of b and c_s.

Interestingly, for the inertance variation, b, this phenomenon on the value of $\mathcal{P}_p + \mathcal{P}_s$ appears to be different (Figure 4.7). The redistribution of the energy caused by an inerter in the system for a fixed value of $b > 0$ [kg] induces a higher power dissipation in the primary suspension (Figure 4.8), while the power dissipated in the secondary suspension reports a relatively very small variation (Figure 4.9). Therefore, an increment of the inertance, b, results in a higher value of total stochastic mean power dissipated in the system, $\mathcal{P}_p + \mathcal{P}_s$, which at certain degree is beneficial for the improvement of ride quality, J_1. A similar condition was observed in $\mathcal{P}_p + \mathcal{P}_s$ for variations in m_{qv} (not included here for brevity), with a total dissipated power also ranging from 3.5 to 3.8 [kW]. In addition, the effects of the airspring stiffness, k_s, resulted very small compared to the effects of b (about 300 [W] for any value of k_s): for a range $0 - 3 \times 10^6$ [Nm^{-1}] an —almost linear— increment of 40 [W] for $b = 0$ [kg] in the total dissipated power is attained (and is even smaller for $b > 0$ [kg]) and the plots were not considered of relevance for the analysis presented here. An important fact to highlight is that even if the value of total power dissipation increases with the inertance value, it does not necessarily imply that the index J_1 for ride quality is monotonically dependent on the value of the inertance b. In fact, the existence of a finite value of inertance ($b = 443$ [kg]) for the nominal parameters of the quarter-vehicle for which the dissipation is optimal in the context of J_1 improvement, was

already discussed.

An additional verification was performed: varying the airspring's change of area stiffness, k_a (which is equivalent to place a spring in parallel to the inerter from the modelling viewpoint), as in Figure 4.10. This case also reported an increment in the dissipated power with k_a, which is further raised by an increment in the inertance value. While a good damping value of c_s is beneficial to dissipate the vibrational energy caused by track irregularities, it is known that increasing the potential energy storage normally deteriorates the ride quality.

The fact of obtaining a higher mean power dissipation value in the primary suspension and nearly unchanged levels of mean power dissipated in the secondary suspension by introducing an inerter in the secondary suspension, complements the observations extracted from Figures 4.4–4.5. That is, the evidences found on the reduced levels of kinetic energy stored by the vehicle body are due to the following facts: 1) some kinetic energy is stored by the inerter, which reduces the levels of energy transported to the vehicle body specially at certain frequencies, and 2) the inerter leads to a higher disturbance dissipation in the primary suspension, which for the ride quality problem results of some benefit but may not be necessary the case for other aspects of the vehicle dynamics. Nevertheless, analyses above suggest that the inerter should enhance the vehicle vertical behaviour without affecting the performance of the secondary suspension itself.

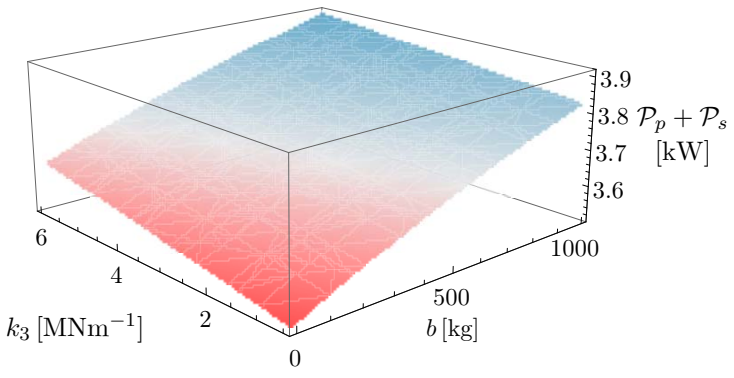

Figure 4.10: Total mean power dissipated in the vehicle passive suspensions as a function of b and k_3.

4.5 Summary of the Chapter

This analytical chapter examined the potential of the inerter for railway vehicle suspensions. The effects of an ideal inerter on the vehicle ride quality were assessed by analysis of contour plots for variation in the parameters of a quarter-vehicle system. It was shown that improvements of no more than 10% can be achieved by insertion of an inerter together with the modification of one parameter of the airspring system. This justifies the need for complementing the inerter to further enhance the vehicle ride quality, e.g. by provision of active suspensions. An energy-based framework to get a good picture on the potential of the inerter for the design of passive and active suspensions was established. Analyses showed that the insertion of kinetic energy stores in the secondary suspension, as the inerter, could provide an advantageous modification of the kinetic energy function of the vehicle body. A reduction of the levels of kinetic energy stored by the vehicle body mass, a faster and smoother dissipation rate, and higher levels of stochastic power dissipated mostly in the primary suspension, were some of the features extracted on the inerter potential. Moreover, interesting suggestions for the effects of the inerter on 'dissipative' active suspensions derived from the analyses. The need for considering novel devices with frequency-dependent characteristics was also discussed. Overall, the outcomes from this chapter suggest a positive test of the research hypothesis.

5

Passive and Active Secondary Suspension Design

This chapter defines the structure of the suspension systems selected to investigate the synergy active-plus-novel-passive. It begins with relevant background necessary for tackling design tasks and describes the selection and design criteria for the passive and active control structures. Given the open range of control possibilities, it was necessary to select very carefully an adequate closed set of passive and active structures to draw a conclusion based on the research hypothesis. Otherwise, studying the effects of novel mechanical devices (inerter-based networks) for railway vehicles with active secondary suspensions could result in a very extensive work.

An extensive number of passive networks modelled by interconnection of springs, dampers and inerters with passive mechanical control capabilities can be thought of as candidates for novel devices. Also, a wide variety of experiential, classical and advanced control strategies for actuated suspensions in the solution of ride quality problems can be formulated (e.g. linear/non-linear, output-based/model-based, etcetera). Moreover, it is acknowledged that active suspension control laws could include the passive network equivalent control structure model, typically consisting of a complex admittance function. Nevertheless, complex admittance functions and different control laws for active suspensions are defined separately for this research purposes. These are presented in this chapter to model passive and active suspension structures. The control parameters are tunned later in Chapter 6 to cause a synergetic work for the accomplishment of optimal performance.

Along this chapter, the structure of different active suspension configurations including well established, adapted and novel control strategies is presented. 'Adapt-

ive Stiffness' is introduced here as an appealing control strategy and is considered a contribution to the field of active suspension control design. The last section of this chapter discusses the methodology for designing inerter-based passive suspension structures and defines the proposed candidate layouts.

5.1 Background for the Design of Secondary Suspensions

This section discusses aspects of fundamental relevance to the analysis for suspension design. To start with, an important phenomenon to bear in mind is the so-called geometric filtering effect, derived by Zhou et al. in [149]. It appears in the analysis of the frequency response and ride quality assessment of the railway vehicle. Given the nature of this phenomenon, the filtering frequencies depend on the vehicle geometry and speed, and define two separated geometric effects: the 'wheelbase filtering effect' and the 'bogie spacing filtering effect'. These have particular influence in the behaviour of the vehicle body, with prominence at positions away from the centre of the passenger cabin —where its linear and rotational modes are combined. This phenomenon is unavoidable, regardless of the suspension design.

Other relevant aspects of the side-view model for designing towards ride quality improvement are: the 'simplicity' of the model for decoupled analysis and design, and the mathematical nature of the trade-off between ride quality and suspension deflection. The following subsections concern these two aspects.

5.1.1 Decoupling of the vehicle body dynamic modes by 'simplicity'

Decoupling the model of the vehicle body dynamic enables a simplification in the analyses and control structure formulation. For instance, modal control is one of the very well known control strategies for suspension design as will be presented later [5, 4].

Given the nominal symmetry of the side-view of a railway vehicle, the model in Equations 3.64–3.67 can be structurally decoupled into two simpler —quarter-vehicle— models whose excitations can be easily separated (Figure 5.1). This separation derives in a 'bounce' quarter-vehicle model and a 'pitch' quarter-vehicle model equivalent to the 'generic' model shown in Figure 5.2. The 'inputs of the separated modes', as defined in [149], are described as: $(z_{b1} + z_{b2})$ for the excitation of the vehicle body bouncing mode, z_v, and $(z_{b1} - z_{b2})$ for the excitation of the pitching mode, β_v (Figure 3.1).

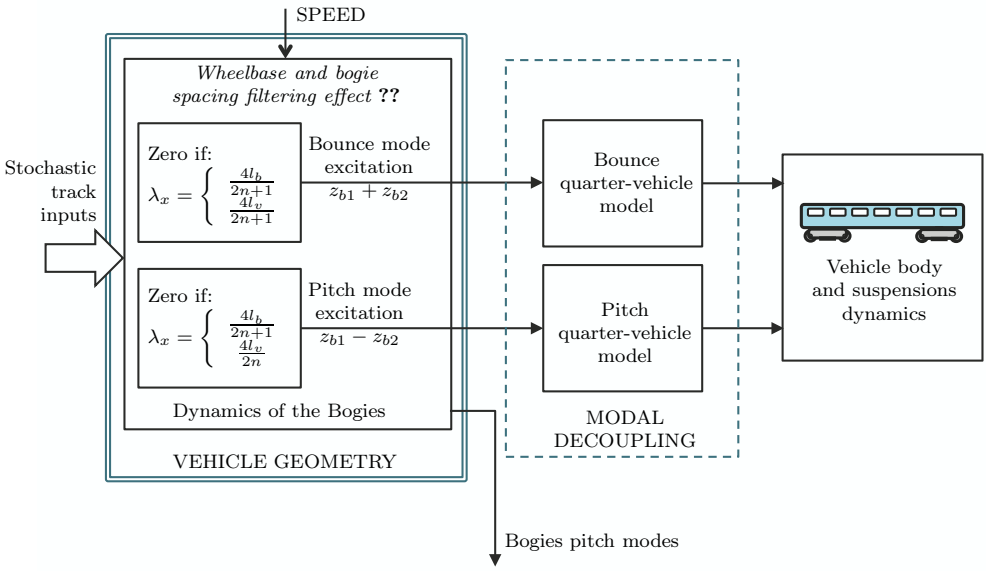

Figure 5.1: Scheme for the geometric filtering and the modal decomposition of the vehicle body dynamics.

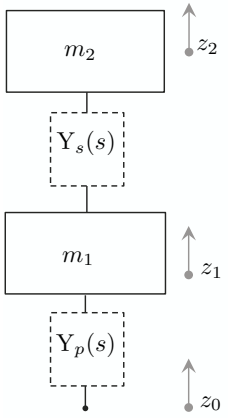

Figure 5.2: Generic quarter vehicle model.

Following the decoupling by 'simplicity' performed by Smith and Wang in [150] for an automotive application, here the definition of 'simple' directly holds due to the vehicle's symmetry. The transformation applied for the railway vehicle model should consider the four excitation ports and the internal excitation of the vehicle body caused by the bounce mode of the bogies. Also due to symmetry, the pitch modes of the bogies —to which the fourth vibration mode of the system is associated— do

not affect the vehicle body dynamics nor the secondary suspensions performance. So, the equations of motion for β_{b1} and β_{b2} do not appear naturally in the decoupled model and for the interest of this thesis on the side-view dynamics, those are not included.

The decoupled model is formally derived in Section D.3, Appendix D, and is employed from here for the modal control strategies. The representation is also useful for analysis and coding simplification, even for the implementation of other output-based control strategies. Although this decoupled model does not define the bogies' pitch motion, it does completely define the ride quality and suspension deflection performance indices, J_1 and J_2, respectively. In general, this fact should not affect either the active force index J_3 as the bogies' pitching is not normally considered for feedback in active suspension control strategies. An exception appears for model-based control strategies with full state feedback.

The correspondences between the 'bounce' and 'pitch' quarter-vehicle models from Figure 5.1 and the 'generic' quarter-vehicle from Figure 5.2, are summarised in Table 5.1. Recall here from Appendix D that for all the variables, the subindex 'b' is used to denote bouncing component, and the subindex 'ρ' for pitching component (e.g. $(z_b)_b$ and $(z_b)_\rho$ correspond, respectively, to the bounce and pitch components of $\underline{z_b}$; with $\underline{z_b} = \begin{bmatrix} z_{b1} & z_{b2} \end{bmatrix}^T$). Also from Appendix D, recall that the bouncing components of the wheelsets, which define the excitation due to the track profile, are: $(\hat{z}_{w12})_b = \frac{\hat{z}_{w1}+\hat{z}_{w2}}{2}$ and $(\hat{z}_{w34})_b = \frac{\hat{z}_{w3}+\hat{z}_{w4}}{2}$.

Table 5.1: Correspondences between the 'generic' quarter-vehicle (QV) and the decoupled side-view model

QV—Generic	QV—Bounce	QV—Pitch
m_1	m_b	$m_b\, l_v^2$
m_2	$m_v/2$	$I_{vy}/2$
$\mathrm{Y}_p(s)$	$2\,\mathrm{Y}_p(s)$	$2\,\mathrm{Y}_p(s)\, l_v^2$
$\mathrm{Y}_s(s)$	$\mathrm{Y}_s(s)$	$\mathrm{Y}_s(s)\, l_v^2$
z_0	$1/2\ (z_{w12} + z_{w34})$	$1/2l_v\ (z_{w12} - z_{w34})$
z_1	$(z_b)_b$	$(z_b)_\rho$
z_2	z_v	β_v
F_{act}	$(F_{\mathrm{act}})_b$	$(F_{\mathrm{act}})_\rho\, l_v^2$

5.1.2 The decoupled invariant equations: J_1 versus J_2

Hedrick and Butsuen in their paper on the invariant properties of automotive suspensions [151], developed a full analysis on the constraining equations of a quarter-car model which establish that there is a part of the system dynamics which cannot be influenced. This mathematically justifies the trade-offs normally holding for the vehicle suspension design. Similarly, the analysis of the trade-off J_1 versus J_2 for the side-view model of a railway vehicle can be derived. For this, the two quarter-vehicle models obtained for the decoupled system are used here (Section D.3, Appendix D). If one extracts the *invariant equations* of the decoupled system, will easily find that the secondary suspension does not influence the constrained bounce and pitch behaviours of the vehicle. This is discussed in the following with the transfer functions of the system.

For $(\hat{z}_{w14})_b = {}^1\!/_2\,(\hat{z}_{w12} + \hat{z}_{w34})$, and $(\hat{z}_{w14})_\rho = {}^1\!/_{2l_v}\,(\hat{z}_{w12} - \hat{z}_{w34})$, define $(H_{J_1}(s))_b = \frac{s^2\hat{z}_v}{s\,(\hat{z}_{w14})_b}$ as the transfer function for assessing the ride quality index at the middle position of the vehicle body, and $(H_{J_2})_b = \frac{(\hat{z}_b)_b - \hat{z}_v}{(\hat{z}_{w14})_b}$ as the transfer function for assessing the bounce component of the suspension deflection index, J_2. Also, define $(H_{J_1}(s))_\rho = \frac{s^2\hat{\beta}_v}{s\,(\hat{z}_{w14})_\rho}$ as the transfer function for obtaining the acceleration of the vehicle body pitch, required in the assessment of the ride quality index at the leading and trailing positions of the vehicle body, respectively, J_{1L} and J_{1T}, and $(H_{J_2})_\rho = \frac{(\hat{z}_b)_\rho - \hat{\beta}_v}{(\hat{z}_{w14})_\rho}$ as the transfer function for the relative pitch motion. Therefore, the *invariant equations* can be written in terms of the transfer functions as:

$$(H_{J_2}(s))_b = \frac{2\mathrm{Y}_p(s)}{m_b s + 2\mathrm{Y}_p(s)} - \frac{1}{s}\left(\frac{{}^1\!/_2 m_v s}{m_b s + 2\mathrm{Y}_p(s)} + 1\right)(H_{J_1}(s))_b \tag{5.1}$$

$$(H_{J_2})_\rho = \frac{2\mathrm{Y}_p(s)}{(m_b s + 2\mathrm{Y}_p(s))} - \frac{1}{s}\left(\frac{{}^1\!/_2 I_{vy} s}{l_v^2\,(m_b s + 2\mathrm{Y}_p(s))} + 1\right)(H_{J_1}(s))_\rho \tag{5.2}$$

Clearly, only one of the transfer functions, either $(H_{J_1}(s))_*$ or $(H_{J_2}(s))_*$, can be independently influenced whilst the other is completely defined (and constrained) by the respective invariant equation. It is readily to see from the previous subsection that $(H_{J_1})_b\,(\hat{z}_{w14})_b \pm l_v\,(H_{J_1})_\rho\,(\hat{z}_{w14})_\rho$ and $(H_{J_2})_b\,(\hat{z}_{w14})_b \pm l_v\,(H_{J_2})_\rho\,(\hat{z}_{w14})_\rho$ define the leading/trailing vehicle body acceleration and the deflection of the leading/trailing suspension. Thus, no matter how the secondary suspension structure is designed for improving the ride quality, these will always have a behaviour which cannot be directly influenced, but only through considerations in the design of the 'ride quality' transfer functions (or vice versa).

5.2 Selection of Control Strategies

After recognising the advantages of modal decomposition and the nature of the trade-off between ride quality (assessed in J_1) and suspension deflection (assessed in J_2), a selection of control strategies with application to suspension systems was performed. Physically, the trade-off implies that softening the suspensions for ride quality improvement produces large deflections and may violate the restriction on the suspensions' clearance space. To simplify this trade-off, regulation actions considering also suspension deflection may be included in the design. It is almost intuitive that the conflict becomes important in active suspension design, but not in passive suspensions in general. The latter can easily recover the suspension deflection natural condition.

Figure 5.3 shows a classification of the strategies for the suspension configurations selected in the development of this thesis. Active and passive control strategies for ride quality enhancement are identified in the first level of the diagram in Figure 5.3. These are implemented according to a specific scheme and complemented, if required, by control strategies for suspension deflection regulation (e.g. complementary LPF for the local implementation of HPF skyhook damping). On the other hand, passive control strategies are directly associated here to mechanical networks. Although in this chapter the control strategies for active and passive suspensions are described separately, it is important to recall here that the investigation on the synergy active-plus-novel-passive starts with the integration of active and passive configurations as shown in the general scheme from Figure 1.8. Results on the cooperative work between the two suspension technologies are obtained in Chapter 6, after performing optimal tuning of the configuration parameters.

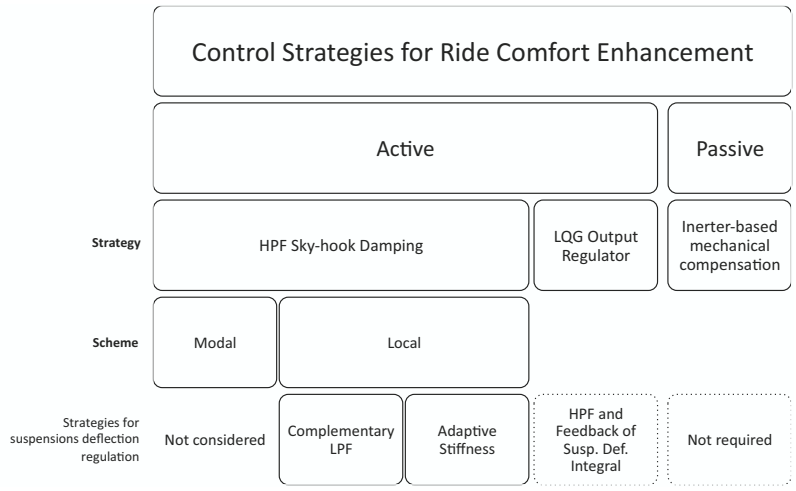

Figure 5.3: Classification of the control strategies.

For active suspensions, the selection in Figure 5.3 is led by modifications of the well known 'skyhook' damping strategy [108], which is an intuitive output-based suspension design strategy. Most of the variants of the skyhook damping implementation in Figure 5.3 are well known configurations, which have been already reported in the literature for railway suspension applications (Chapter 2). In addition, this thesis proposes another form of implementation of the local HPF skyhook damping. This consists of complementing the basis strategy for ride quality with the hereon so-called 'Adaptive Stiffness' control law for suspension deflection regulation, as will be extended later. 'Adaptive Stiffness' is a slightly intuitive strategy inspired by the passivity of the system. It was created to complement the set of skyhook damping-based strategies and the kinetic energy-based analyses presented in Chapter 4. This is a nonlinear strategy conceived as a modification of the potential energy function of the mechanical (Euler-Lagrange) system based on the assessment of the vehicle's absolute velocity. This would fulfil the need for testing the effects of inerter-based devices with nonlinear strategies and would complete at the same time the study on the three key elements of the total energy function of the Euler-Lagrange system: dissipation, and kinetic and potential energy storage functions modification.

Besides skyhook damping-based control strategies, a convenient modification of the standard implementation of LQR-output feedback —from the branch of model-based control strategies— is also proposed. In this manner, a significant set of control configurations to drive the actuated suspensions for the enhancement of the vehicle's vertical ride quality with regulation of the suspensions' deflection was considered to be well defined for the purposes of this study. The individual active control strategies for both ride quality and suspension deflection regulation are described in the next section, and the methodology for passive control design and the chosen candidate mechanical networks are presented subsequently.

5.3 Active Control Strategies

This section presents a description of the active control strategies for ride quality and suspension deflection regulation selected for the study.

5.3.1 Control Strategies for Ride Quality

5.3.1.1 *Skyhook Damping* (Absolute Velocity Feedback) with High-Pass Filtering

Referred in Figure 5.3 as HPF Skyhook Damping, this is an absolute velocity feedback with high-pass filtering strategy which implements Karnopp's idea on providing

the vehicle with a form of damping which is somehow acting between the damped mass and the 'sky' [108] as in Figure 5.4(a). The pure skyhook damping intuitive idea consisted, therefore, on virtually applying a force, F_c, onto the damped mass only, defined as $F_c = -c_{sky}\dot{z}_2$, with c_{sky} the absolute damping coefficient. However, the mechanical implementation of this strategy results almost impractical and the analogy with the idea of providing the vehicle with damping acting between the damped mass and the 'sky' is not exact. Regardless this, the use of the term is fairly common in vehicle dynamics and thus, it is also adopted here. The control configuration driven by F_c is instead normally implemented by placing an actuator between the primary and secondary mass (correspondingly, bogie and vehicle body for this particular application case), as shown in Figure 5.4(b). As a drawback, a pure skyhook damping create a steady-state offset in the suspension deflection when the vehicle transverses deterministic tracks with non-zero profile velocity, e.g. a gradient as the one described in Chapter 3 by Equation 3.89. That is readily explained by calculation of the coordinates of the equilibrium point, $\underline{z}_*$, of the quarter vehicle model in Figure 5.4(b), excited by a constant velocity profile $\dot{\delta}_z = \vartheta$, for which $\dot{z}_{1*} = \vartheta$, $\dot{z}_{2*} = \vartheta$, $\dot{z}_{3*} = \vartheta$. These result in

$$\begin{aligned} z_{1*} &= \vartheta\, t \\ z_{2*} &= \vartheta\, (t - \varrho\, c_{sky}) \\ z_{3*} &= \vartheta\, (t - \varrho\, c_{sky}) \end{aligned}$$

with $\varrho = {c_{sky}(k_r+k_s)}/{k_r k_s + k_a(k_r+k_s)}$, evidencing an offset in the secondary suspension deflection equilibrium which is proportional to the damping coefficient, c_{sky}:

$$z_1^{\text{ss}} - z_2^{\text{ss}} = \varrho\, c_{sky} \tag{5.3}$$

Because of this issue, previous research [5, 109] proposed filtering the low-frequency components (usually below 0.1 [Hz]) of the absolute velocity $\dot{z}_2$. This way, the active force applied between the bogie and the vehicle body would respond mainly to high frequency excitations and is the response to the commanded force $F_c = -c_{sky}\dot{\tilde{z}}_2$, with $\dot{\tilde{z}}_2$ the high-pass filtered measurement of $\dot{z}_2$ for the system in Figure 5.5.

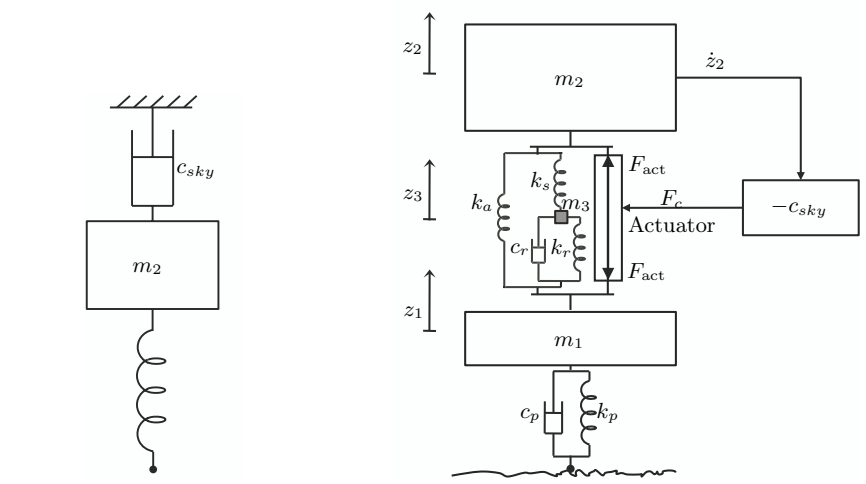

(a) Skyhook damping concept. (b) Skyhook damping implementation.

Figure 5.4: Schematic of skyhook damping implementation.

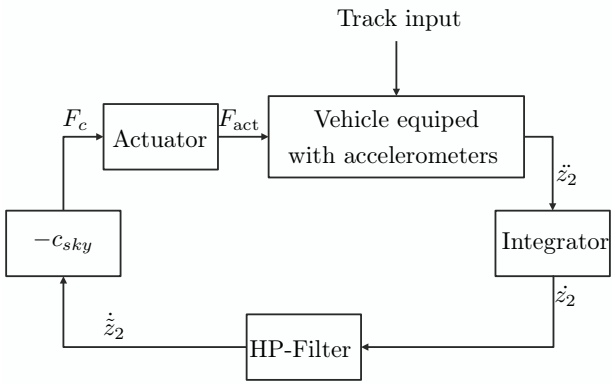

Figure 5.5: HPF Skyhook Damping.

Here, the high-pass filter chosen for all the implementations was as a second order Butterworth filter, with a corner frequency f_c defined accordingly in each configuration. Moreover, although high-pass filtering the feedback variable avoids the offset problem, the maximum amplitude experienced by the suspension deflection depends on the implementation scheme and the damping coefficient value, c_{sky}.

HPF Skyhook Damping configuration can be implemented in different ways; among them, the most common are local and modal implementations [5].

Local Implementation Local implementation feeds back the high-pass filtered local —i.e. measured at the actuator location— velocity of the vehicle body with a (damping) gain $c_{sky} = K_l$, i.e. $\dot{z}_L$ ($\dot{z}_T$) is high-pass filtered to drive the actuator placed between the leading (trailing) bogie and the vehicle body. That is,

$$\hat{F}_{cL}^{J_1} = -K_l\, G_{\mathrm{HPF}}(s) s \left(\hat{z}_v + l_v \hat{\beta}_v\right) \tag{5.4}$$

$$\hat{F}_{cT}^{J_1} = -K_l\, G_{\mathrm{HPF}}(s) s \left(\hat{z}_v - l_v \hat{\beta}_v\right) \tag{5.5}$$

Here, the notation $\hat{F}_{cL,T}^{J_1}$ is used to refer to the additive component of the active control law designed to enhance the ride quality indices, $\underline{J_1}$ (defined in Chapter 3). It is worth noting that implementing local HPF skyhook damping strategy produces larger suspension deflection for deterministic track profiles than, for example, the modal implementation discussed below. Thus, it requires to be complemented by a suspension deflection regulation strategy so that the control law of the total active forces accounts for the trade-off ride quality, J_1, versus suspension deflection, J_2, problem. Therefore, the total control forces are defined by these two components: $\hat{F}_{cL} = \hat{F}_{cL}^{J_1} + \hat{F}_{cL}^{J_2}$, and $\hat{F}_{cT} = \hat{F}_{cT}^{J_1} + \hat{F}_{cT}^{J_2}$, with $\hat{F}_{cL,T}^{J_2}$ as defined later in this chapter.

Figure 5.6 shows a block diagram of the HPF Skyhook Damping local configuration for the vehicle with passive suspensions (i.e. with/out novel passive devices).

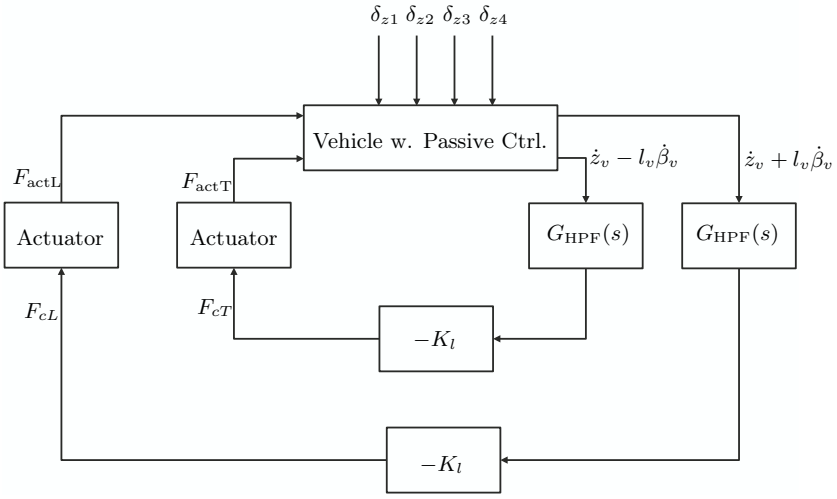

Figure 5.6: Block diagram for the local implementation of HPF Skyhook Damping.

Modal Implementation As its name suggests, for modal implementation the bounce and pitch modes of the vehicle are considered separately. HPF skyhook damping as described in Figure 5.4(b) is equivalently applied on the 'bounce quarter-vehicle model' and the 'pitch quarter-vehicle model' discussed for the vehicle's side-view modes decoupling in Subsection 5.1.1. That is, by obtaining and feeding back through different loops the measurements of the vehicle body bounce and pitch velocities. This allows the definition of different values for the bounce and pitch damping coefficients, c_{sky_b} and c_{sky_ρ} (or K_b and K_ρ to avoid confusion with passive parameters), respectively, as well as for the corner frequency of the respective high-pass filter, f_{c_b} and f_{c_ρ}. This way, the active forces bounce and pitch components from Equations D.24–D.27, $\left(\hat{F}_c\right)_b$ and $\left(\hat{F}_c\right)_\rho$, respectively, can be written in the Laplace domain as:

$$\left(\hat{F}_c\right)_b = -K_b G_{\mathrm{HPF}}^{f_{cb}}(s) s\, \hat{z}_v$$
$$\left(\hat{F}_c\right)_\rho = -K_\rho G_{\mathrm{HPF}}^{f_{c\rho}}(s) s\, \hat{\beta}_v$$

for active forces commanded to the leading and trailing suspension actuators given, respectively, as

$$\hat{F}_{cL} = \hat{F}_{c1} = \left(\hat{F}_c\right)_b + l_v \left(\hat{F}_c\right)_\rho \tag{5.6}$$
$$\hat{F}_{cT} = \hat{F}_{c2} = \left(\hat{F}_c\right)_b - l_v \left(\hat{F}_c\right)_\rho \tag{5.7}$$

Figure 5.7 shows a schematic of the decoupled configuration, with forces $F_{\mathrm{act}L}$ and $F_{\mathrm{act}T}$ applied by electromechanical actuators whose dynamic was described in Chapter 3. Figure 5.8 is a block diagram of the configuration implemented for the vehicle with passive suspensions (i.e. with/out novel passive devices).

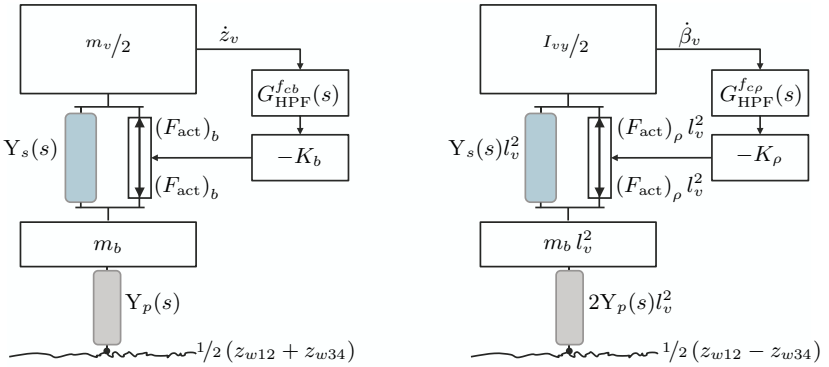

HPF Skyhook Damping on the QV Bounce Model

HPF Skyhook Damping on the QV Pitch Model

Figure 5.7: Schematic of the decoupled (Modal) HPF Skyhook Damping (Table 5.1).

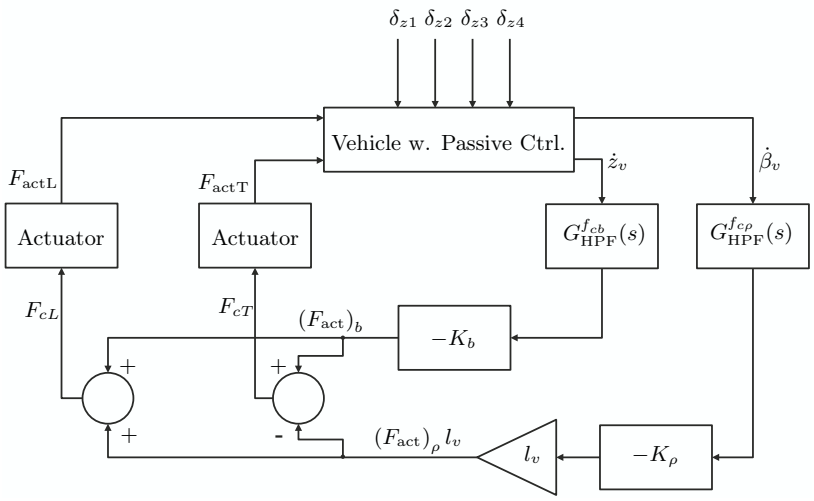

Figure 5.8: Block diagram for the Modal Implementation of HPF Skyhook Damping.

5.3.1.2 Linear-Quadratic Gaussian (LQG) HPF-Output Feedback Regulator

As mentioned in Chapter 2, optimal (linear and nonlinear) control strategies, to which LQG belongs, have been widely explored for active and semi-active suspension design. LQG constitutes an appealing method which has shown benefits for multi-objective optimal design problems arising in railway vehicle dynamics [5, 41]. So by exploiting the linear structure of the approximated model of the railway vehicle side-view dynamics (with and without novel passive suspensions) —Equations 3.54–3.63, a linear optimal feedback control structure was implemented here for the ride quality enhancement objective and the conflicting problems with suspension deflections and active control force magnitudes.

***Optimal Regulator Problem*:**

In particular, given the Gaussian characteristic of the track irregularity change rate model, the structure of a classical optimal output-feedback linear regulator with Gaussian estimator was initially adopted for the design of the leading and trailing suspensions' active control forces $\underline{F_c}(t) = \begin{bmatrix} F_{cL} & F_{cT}(t) \end{bmatrix}^T$. This would solve the linear-quadratic output regulator problem formulated as the minimisation of the performance measure given in the expected value of a quadratic function in terms of the system's assessment output and the control input. That is

$$J_{\mathrm{LQR}} = \lim_{t\to\infty} \mathrm{E}\left[\left\|\underline{\chi}(t)\right\|^2 + \rho\left\|\underline{F_c}(t)\right\|^2\right] \tag{5.8}$$

which can be rewritten as

$$J_{\mathrm{LQR}} = \lim_{t\to\infty} \mathrm{E}\left[\underline{\chi}^T(t)\,\mathbf{Q}\,\underline{\chi}(t) + \rho\,\underline{F_c}^T(t)\,\mathbf{R}\,\underline{F_c}(t)\right] \tag{5.9}$$

for $\mathbf{Q}$ and $\mathbf{R}$ defined both as real-positive definite weighting matrices (as specified in the next chapter with the respective numerical settings and results), and ρ a real-positive value determining the particular case of solving a 'cheap control problem' [152]. Under this formulation, the vector $\underline{\chi}(t)$ is the assessment output vector consisting of the acceleration at both longitudinal ends of the vehicle body (where the ride quality is worst), together with the time-domain integral of the suspensions' deflection (introduced as new states in the system's linear model, $x_{iD1,2}(t)$) to prevent excessive suspension deflection, and assumed available for measurement:

$$\underline{\chi}(t) = \begin{bmatrix} \ddot{z}_{vL}(t) \\ \ddot{z}_{vT}(t) \\ \int_0^t z_{DL}(t)\,dt \\ \int_0^t z_{DT}(t)\,dt \end{bmatrix} = \begin{bmatrix} \ddot{z}_{vL}(t) \\ \ddot{z}_{vT}(t) \\ x_{iD1}(t) \\ x_{iD2}(t) \end{bmatrix} \tag{5.10}$$

Introducing the time-domain integral of the suspensions' deflection in the control accuracy measurement (first quadratic term of the performance measure J_{LQR}), as well as omitting the acceleration measurement at the middle position of the vehicle body, were found to produce a better trade-off between the assessed performance indices: $\underline{J_1}$, J_2, and J_3 (ride quality, suspension deflection and active forces indices) —compared with including simply the suspensions' deflection as in [5, 41].

By defining the states of the system as

$$\underline{x'}(t) = \left[\begin{array}{c|c|c|c|c} \underline{x^T}(t) & x_{iD1}(t) & x_{iD2}(t) & \underline{x_{pf1}^T}(t) & \underline{x_{pf2}^T}(t) \end{array} \right]^T \tag{5.11}$$

the describing mathematical model corresponds to the one in Equation 3.49 (Chapter 3), extended with the suspensions' deflection integral states and the states corresponding to the dynamic of the novel passive suspensions installed on the system (i.e. $\underline{x_{pf1}}$ and $\underline{x_{pf2}}$ with applied forces $\underline{F_{pn}}$ according to the passive network structure).

Given the fact that not all the states of the system are to be measured and available for feedback for the system with state vector $\underline{x'}(t)$, and whose assessment output is given by $\underline{\chi}(t) = \mathbf{C}_\chi \underline{x'}(t) + \mathbf{D}_\chi \underline{F_c}(t)$, the solution of the optimal regulator problem consists in finding the feedback control law for the suspension's active forces minimising Equation 5.9, defined as

$$\underline{F_c}(t) = -\mathbf{K}_u\, \underline{\tilde{x}'}(t) \tag{5.12}$$

with $\underline{\tilde{x}'}(t)$ the optimal estimate of $\underline{x'}(t)$.

***Optimal Estimator Problem*:**

For a stochastic system:

$$\underline{\dot{x}'}(t) = \mathbf{A}\, \underline{x'}(t) + \mathbf{B}_u\, \underline{u}(t) + \underline{\xi}(t) \tag{5.13}$$

$$\underline{y_m}(t) = \mathbf{C}_m\, \underline{x'}(t) + \mathbf{D}_u\, \underline{u}(t) + \underline{\theta}(t) \tag{5.14}$$

where $\underline{x'}(t)$ is the state vector and $\underline{y}_m(t)$ the measured output, the behaviour of the estimated state vector, $\underline{\tilde{x}'}(t)$, is defined by an equivalent model of the behaviour of $\underline{x'}(t)$, driven by the output estimation error, $\underline{\overline{y_m}}(t) = \left(\underline{y_m}(t) - \mathbf{C}_m\, \underline{\tilde{x}'}(t)\right)$ through

the Kalman estimator design gain matrix, $\mathbf{K}_e$. In Equations 5.13–5.14, $\underline{u}(t)$ a deterministic input vector, $\underline{\xi}(t)$ and $\underline{\theta}(t)$ uncorrelated Gaussian, zero-mean, white-noise random vectors denoting process and measurement additive noises, respectively. The matrix $\mathbf{K_e}$ is therefore the solution of the minimisation problem for the expected value of the state estimation error $\underline{\bar{x}'}(t) = \left(\underline{x'}(t) - \underline{\tilde{x}'}(t)\right)$, under consideration that $\underline{\xi}(t)$ and $\underline{\theta}(t)$ have the autocorrelation matrices $\mathrm{E}\left[\underline{\xi}(t)\,\underline{\xi}^T(\tau)\right] = \mathbf{W}\,\delta(\mathbf{t}-\tau) \geq \mathbf{0}$ and $\mathrm{E}\left[\underline{\theta}(t)\,\underline{\theta}^T(t)\right] = \mathbf{V}\,\delta(\mathbf{t}-\tau) \geq \mathbf{0}$, respectively.

The equivalence of the vehicle model with Equations 5.13–5.14 can be completed by recalling Equation 3.49 from Chapter 3. The additive process noise in Equation 5.13 is given by $\underline{\xi}(t) = \mathbf{B}_{\dot{\delta}}(t)\,\underline{\dot{\delta}_m}(t)$, where $\underline{\dot{\delta}_m}(t)$ is the change rate of the track irregularities. The measurement noise vector $\underline{\theta}(t)$ in Equation 5.14, however, is a consideration not included in any of the control configurations studied in this thesis, and thus received low importance in the estimator design. The vector $\underline{u}(t)$ in Equations 5.13–5.14 is equivalent to the active control force vector, $\underline{u}(t) :\triangleq \underline{F_c}(t)$ from Equation 5.12. The matrices $\mathbf{A}$, $\mathbf{B}_u$, $\mathbf{C}_m$, $\mathbf{D}_u$ are defined accordingly to the states $\underline{x'}(t)$, and the estimator feedback output $\underline{y_m}(t)$:

$$\underline{y_m}(t) = \underline{z_{acc}}(t) = \left[\ddot{z}_v + l_v\ddot{\beta}_v,\ \ddot{z}_v,\ \ddot{z}_v - l_v\ddot{\beta}_v\right]^T \tag{5.15}$$

Solution and Implementation:

The structure of the side-view model of the railway vehicle with conventional and novel passive suspensions defined as above is controllable and observable[1]— hence, the feasibility of designing $\underline{F_c}$ to minimise J_{LQR}. For this, individual problems were formulated to calculate the optimal regulator gain matrix $\mathbf{K}_u$ and the optimal estimator gain matrix $\mathbf{K}_e$ of the railway vehicle equipped with different novel passive suspensions. Accordingly, the separation principle [152] was used and corresponding Riccati equations were computationally solved.

For the ride quality problem concerning the major part of this research, a good fidelity of the process noise estimation was desirable. A drawback of this classical structure comes, however, from its merely 'regulation' nature, which accounts only for the system's behaviour to stochastic irregularities. Similar to the skyhook damping strategy, the classical configuration is not designed to discern between irregularities and deterministic track profile. The *regulator* classical configuration would take a deterministic input —defining for this problem the track profile, e.g. the railway gradient in Figure 3.17— also as a disturbance to which it is not designed to respond,

[1]Including extra states to define the track displacement variables as in Equation 3.48 may numerically change this condition; positive 'epsilons' may be incorporated in the matrices of the system to avoid this problem, although this is not actually derived from the vehicle dynamic.

changing possibly the equilibrium of the system and resulting in sustained suspension deflection. Therefore, for practical implementation, a consideration on removing the low-frequency components of the measured outputs $\underline{y_m}$ was performed. Hence, the inclusion of the 'HPF' acronym in the configuration name.

Figure 5.9 illustrates the configuration for the LQG HPF-Output Feedback Regulator. This way, the feedback on the system's dynamic states is implemented on the filtered estimated states, $\tilde{\tilde{x}}'_z$ (from $\tilde{\tilde{x}}' = \left[\begin{array}{c|c} \tilde{\tilde{x}}'_z & \tilde{\tilde{x}}'_{iD} \end{array} \right]^T$), throughout the regulator gain sub-matrix, $\mathbf{K}_{cz}$ (from $\mathbf{K}_c = \left[\begin{array}{c|c} \mathbf{K}_{cz} & \mathbf{K}_{ciD} \end{array} \right]$). On the other hand, the feedback associated with the gain sub-matrix $\mathbf{K}_{ciD}$ to regulate the suspension travel is directly performed on the time-integral of the measured suspension's deflection; i.e. the estimation of $\underline{x_{iD}}(t)$ is not used for feedback. As an alternative, the estimated variables for $\underline{x_{iD}}(t)$ can be extracted before performing high-pass filtering on the estimated states and used for feedback; this would be determined by practical implementations convenience. The drawback of doing this modification after designing the gain estimation matrix $\mathbf{K}_e$ is that the estimation error is increased and thus the solution is sub-optimal and relies on suitable choice of the filter corner frequency value, f_c. The actuators were considered ideally perfect, i.e. $\underline{F_c} = \underline{F_{\text{act}}}$.

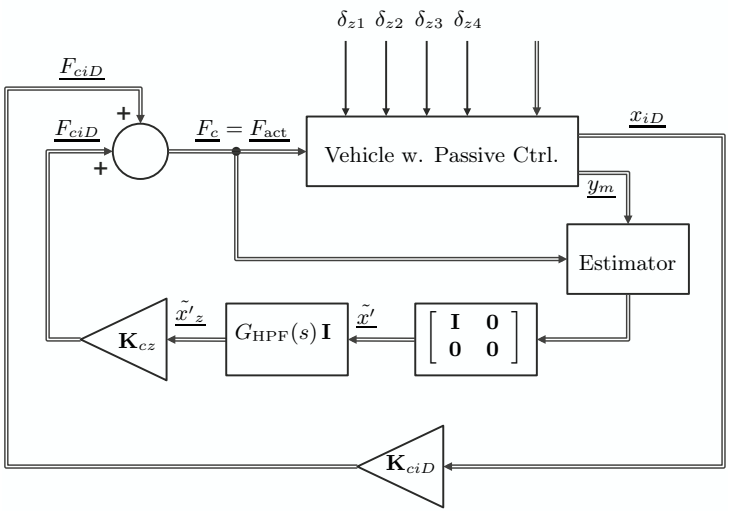

Figure 5.9: Block diagram for the LQG HPF-Output Feedback Regulator.

5.3.2 Control strategies for suspension deflection regulation

5.3.2.1 Complementary Low-Pass Filter (LPF)

Given the fact that the HPF Skyhook Damping Strategy does not completely eliminate its action on frequency components of the vehicle body velocities below the corner frequency f_c, undesirable softening of the suspensions in response to low frequency inputs (commonly deterministic) still occurs. This effect obviously depends on the order of the high-pass filter, but realistically a very high order filter would have to be used to avoid the situation. Moreover, it results in some deterioration for the local implementation of the HPF Skyhook Damping Strategy due to the coupling of the bouncing and pitching modes in the control law. To compensate for these effects, one solution is stiffening the suspension at the low frequency range by definition of additive active forces $F_{cL,T}^{J_2}$ in favour of reducing the assessment index J_2 (i.e. to care for physical practicalities related to the suspensions clearance).

For this, previous investigators (e.g. [113, 5]) have shown that formulating a complementary low-pass filter for the suspension deflection measurements provides an acceptable regulation. That is, a filter with transfer function $G_{\mathrm{LPF}}(s)$ so that

$$G_{\mathrm{HPF}}(s) + G_{\mathrm{LPF}}(s) = 1$$

for the definition of the active forces $F_{cL,T}^{J_2}$:

$$\hat{F}_{cL}^{J_2} = K_l \, G_{\mathrm{LPF}(s)} \hat{z}_{DL} = K_l \, G_{\mathrm{LPF}(s)} \left(\hat{z}_{b1} - \hat{z}_v - l_v \hat{\beta}_v \right) \tag{5.16}$$

$$\hat{F}_{cT}^{J_2} = K_l \, G_{\mathrm{LPF}(s)} \hat{z}_{DT} = K_l \, G_{\mathrm{LPF}(s)} \left(\hat{z}_{b2} - \hat{z}_v + l_v \hat{\beta}_v \right) \tag{5.17}$$

for complementing the forces defined in Equations 5.4–5.5 (which have K_l as absolute *damping* coefficient). The block diagram in Figure 5.10 depicts the implementation of the configuration for $\underline{F_c} = \underline{F_c^{J_1}} + \underline{F_c^{J_2}}$, for the vehicle with passive suspensions (i.e. with/out novel passive devices) and with electromechanical actuators as described in Chapter 3.

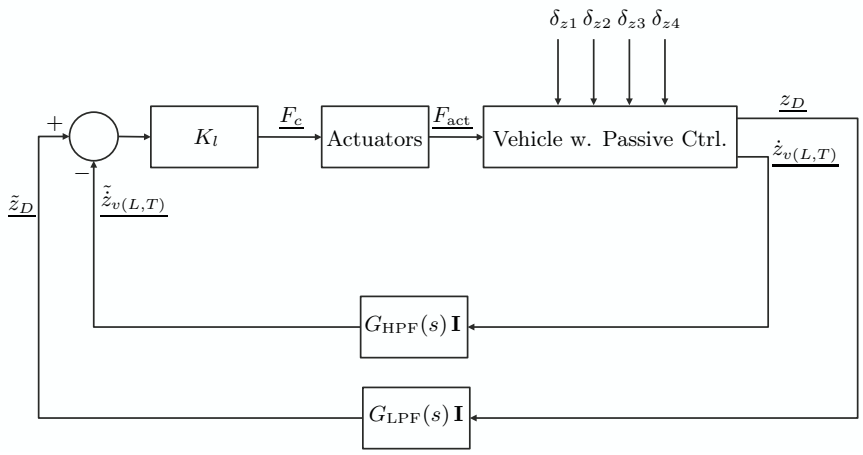

Figure 5.10: Block diagram for the Skyhook Damping with Complementary Filtering strategy.

5.3.2.2 Adaptive Stiffness –*A Novel Approach*

Inspired by the energy management analyses presented in Chapter 4, and also acknowledging the need for stiffening the suspensions for certain conditions, as discussed with the Complementary LPF strategy, an also intuitive strategy was proposed. It consists of a virtual modification of the potential energy function of the system.

To understand the concept, consider only a quarter vehicle model. The regulating strategy consists of the definition of a nonlinear control law so that it corrects the large suspension deflection caused by the HPF skyhook damping configuration with low impact on the vehicle vibrations control.

Proposition: To complement the dissipative control law $F_c^{J_1}$ with an additive force $F_c^{J_2}$ defined as

$$F_c^{J_2}(t) = \kappa \left|\dot{z}_2(t)\right| \left(z_1(t) - z_2(t)\right) \tag{5.18}$$

so that the suspension deflection compensation law explicitly depends upon the vehicle body absolute velocity, producing a total control force given by

$$F_c(t) = -c_{sky}\dot{\tilde{z}}_2(t) + \kappa \left|\dot{z}_2(t)\right| \left(z_1(t) - z_2(t)\right) \tag{5.19}$$

From the proposition above, the term added to the skyhook damping strategy in $F_c^{J_1}$ interestingly will make the suspension stiffer for faster bouncing of the vehicle body, while softer otherwise. Notice that the extraction of the absolute value of $\dot{z}_v$ is needed for guaranteeing a positive stiffness factor for the second term in order to preserve the stability of the system. A feature of the 'stiffening term' is that it knows the degree of instantaneous damping that the suspension is providing to the system. Moreover, the multiplying factor $\kappa\,|\dot{z}_v(t)|$, with $\kappa > 0$, could be thought as the stiffness coefficient in a spring with *adaptive stiffness*. Hence, the title given to the configuration. However, as the author of this thesis is unaware of the existence of such device, its implementation will continue being part of the active suspension configuration.

Furthermore, a control force $F_c(t)$ as in Equation 5.19 would modify both the total energy of the system according to the absolute value of the velocity of the vehicle body and the suspensions' deflection, and the Rayleigh dissipation function through the skyhook damping. It incorporates the new term in the total energy function of the system,

$$T_{Fabs} = \frac{1}{2}\kappa\,|\dot{z}_2(t)|\,(z_1(t) - z_2(t))^2 \tag{5.20}$$

which effects the energy time-variation towards equilibrium recovery with the term

$$\dot{T}_{Fabs} = \begin{cases} \kappa\,(z_1(t) - z_2(t))\left(|\dot{z}_2(t)|\,(\dot{z}_1(t) - \dot{z}_2(t)) + \frac{1}{2}\ddot{z}_2(t)\right), \text{ for } \dot{z}_2(t) > 0 \\ \kappa\,(z_1(t) - z_2(t))\left(|\dot{z}_2(t)|\,(\dot{z}_1(t) - \dot{z}_2(t)) - \frac{1}{2}\ddot{z}_2(t)\right), \text{ for } \dot{z}_2(t) < 0 \end{cases} \tag{5.21}$$

Although mathematically $\dot{T}_{Fabs}$ does not exist for the stationary constant position $z_2(t)$, no further analysis was developed in this regard as this does not affect the computational simulations. That is expected to be extended in the near future. What is important to recall here is that for $\dot{z}_2(t) \neq 0$, the performance variable $\ddot{z}_2(t)$ also effects the energy time-variation (instantaneous power). It was shown in Chapter 4 that modifying the inertia matrix of the system (e.g. using inerters) could provide some benefit to the ride quality problem; similarly, this appears in the time-variation of the total energy function as a function of the second derivative of the involved variables. This is an appealing technique which would require deeper theoretical and practical analysis. For the interests of this research, it is enough to consider the technique by taking Equation 5.19 for the implementation of local control laws for the leading and trailing suspensions, and to understand that part of the effects of the nonlinear term are towards the benefit of suspension deflection and the ride quality at the same time. However, it works much better combined with the HPF Skyhook Damping strategy and thus the configuration in Figure 5.11 (with

ideal actuators) was adopted for the vehicle with passive suspensions (i.e. with/out novel passive devices).

The additive active forces implemented under this strategy are given by

$$F_{cL}^{J2}(t) = \kappa \left|\dot{z}_{vL}(t)\right| z_{DL}(t) \tag{5.22}$$

$$= \kappa \left|\dot{z}_v(t) + l_v\dot{\beta}_v(t)\right| \left(z_{b1}(t) - z_v(t) - l_v\beta_v(t)\right) \tag{5.23}$$

$$F_{cT}^{J_2}(t) = \kappa \left|\dot{z}_{vT}(t)\right| z_{DL}(t) \tag{5.24}$$

$$= \kappa \left|\dot{z}_v(t) - l_v\dot{\beta}_v(t)\right| \left(z_{b1}(t) - z_v(t) + l_v\beta_v(t)\right) \tag{5.25}$$

for regulating the effects of the forces defined in Equations 5.4–5.5, respectively.

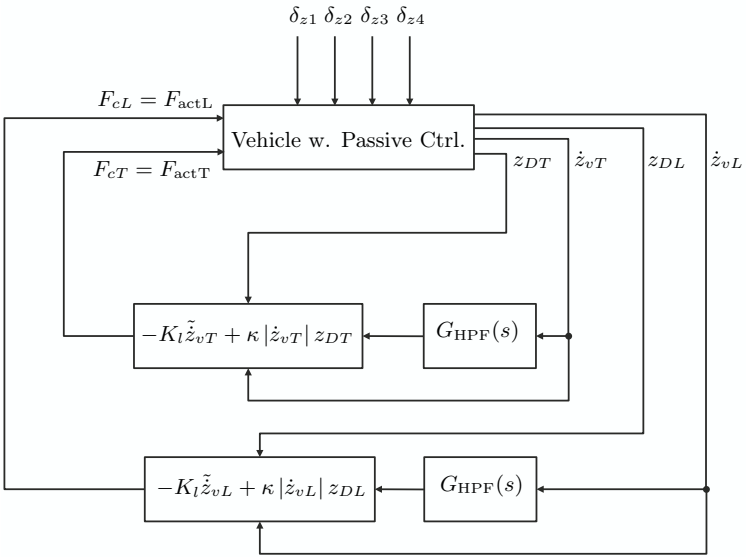

Figure 5.11: Block diagram for the Adaptive Stiffness strategy integrated with HPF Skyhook Damping.

Until here, the skyhook damping concept is known to modify the 'dissipation' (energy extraction by active means) in the system, whilst the insertion of inerters is known to change the function of the kinetic energy stored by the system and therefore, the energy management. Other mechanical elements as springs and dampers inserted through the proposed structures contribute also to the modification of the energy functions. Feeding back suspension deflection measurements either by complementary filtering or by LQG, translates into a potential energy function virtual

modification, although still with linear characteristics which may limit the possibilities of the suspension. The formulation and exploration of the strategy proposed above considering a distinct way of modifying the potential energy function of the system by active means, set a complete revision on the effects of modifying the system's energy functions through the design of active-plus-novel-passive secondary suspensions. This is founded on acknowledgement of the passivity of the system.

5.4 Passive Mechanical Control: Novel *Inerter-Based* Suspensions

The previous chapter analysed the potential of the inerter for improving the bounce mode of a railway vehicle and the secondary suspension performance by considering the inerter as a pure device. These analytical assessments have indeed provided an abstraction on the prospects for the combined suspensions studied in this work. However, given the modelling fact that an inerter is mathematically represented by an improper admittance, and also due to the realistic fact that its inertance property is normally accompanied by the mounting end-stiffness and parasitic damping coming from internal frictions of the device, for example, a more reasonable manner of discussing its use was in inerter-based passive networks. This would guarantee properness and would include designed stiffness and damping properties that might cancel to some extent the effect of those parasitic unmodelled ones, ergo increasing the number of what we have called *novel mechanical devices* to be appraised.

As anticipated earlier in this thesis, empirical formulation of the one-port mechanical network [88, 91, 17, 20, 21] was adopted for this research. Several passive networks layouts for mechanical compensation including springs, dampers and inerters were proposed[2]. Some of these structures resemble the dynamics of some of the damping and inertial hydraulic devices proposed in [77].

The layouts chosen for this study on the potential of inerter-based devices are in Figure 5.12 labeled as Si', with 'i' identifying the structure number. The figure illustrates the mechanical networks for the novel devices Si' placed in parallel to the airspring model, S0. The spring k_1, common to the layouts S2–S6, includes implicitly the end-stiffness k_e of the bushes that would be attached to both ends of the novel device (typically $k_e = 3.5 \times 10^6\,[\mathrm{Nm}^{-1}]$ and thus $k_1 \leq 3.5 \times 10^6\,[\mathrm{Nm}^{-1}]$) and the vehicle body and bogies. The parasitic effects of the inerter itself, in terms of damping or frictions and stiffnesses, depend on the physical implementation of

[2]The formulation of the candidate layouts resulted from the experience acquired from the collaborative activity with Professor Malcolm Smith and Dr. Jason Z. Jiang, from University of Cambridge, on design of railway vehicle passive suspensions.

the inerter device which is not explicitly treated in this thesis. As an example, the layout S1' (illustrated in Figure 5.12 as S1: S0//S1') represents a mechanical inerter device whose parasitic damping/friction and stiffness are modelled, respectively, as a damper, $c_{b1} = 1 \times 10^4 [\mathrm{Nsm}^{-1}]$, and a spring, $k_{b1} = k_e$, in series with the pure inerter element. Moreover, layout S2' implicitly considers the parasitic characteristics of the mechanical inerter modelled this way in c_1 and k_1 and allows to include more damping and to design the series stiffness. Layouts S3' and S4', on the other hand, are the mechanical equivalents of two of the embodiments presented with the damping and inertial hydraulic device invention [77, Figures 16 and 20], with end-stiffness modelled in series. Layout S6 was chosen to investigate the effects of using identical structures —with possibly different parameter values— installed in parallel.

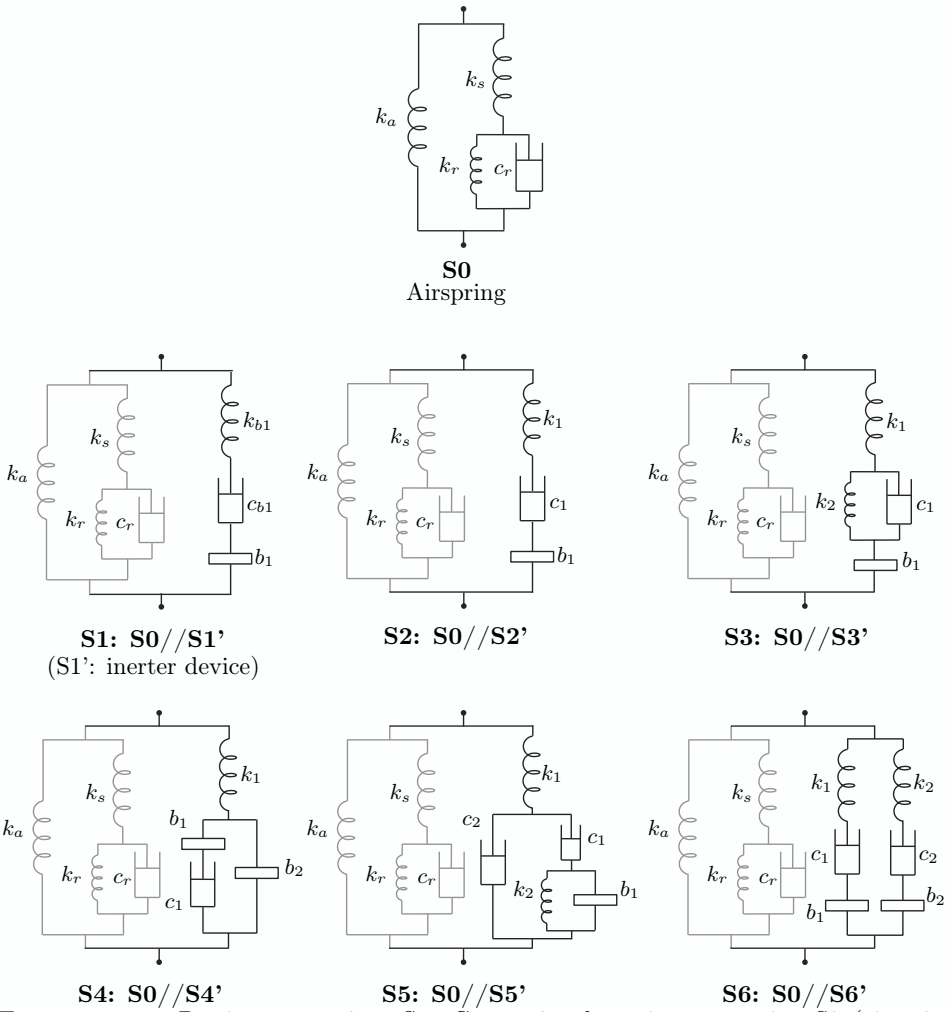

Figure 5.12: Passive suspensions Si: Conventional passive suspension S0 (airspring) with inerter-based candidate layouts Si' in parallel (for i the structure identifier).

The corresponding admittances for the proposed layouts —which are low degree unconditional positive-real functions[3]— are expressed in Table 5.2. It can be checked from Table 5.2 that the admittance of the passive network S3' can also be synthesised by S4'. An important point to make regarding the type of compensation that an inerter-based mechanical network can provide is that the Bode plot slopes of general positive-real admittances do not have fundamental restrictions [3]. Indeed, the frequency response may exhibit phase lead and under-damped characteristics. Thus, all the poles and zeros of an inerter-based mechanical network are in the left-hand side complex semi-plane. In contrast, all the zeros and poles of the admittance of a mechanical network comprising springs and dampers only, are simple and alternate on the negative real axis of the complex plane, with a pole being the rightmost and possibly placed at the origin [74] . The zeros and poles placement (and therefore the gains, frequencies and damping ratios of the structures) is defined by the parameter values of the suspension elements, which are obtained in Chapter 6 from numerical optimisation.

Table 5.2: Complex Admittance Function of the Mechanical Networks

PN	Complex Admittance	Coefficients
S1'	$k_{b1}\frac{s}{s^2+\beta_1 s+\beta_0}$	$\beta_1 = {}^{k_{b1}}/_{c_{b1}}$, $\beta_0 = {}^{k_{b1}}/_{b_{b1}}$
S2'	$k_1\frac{s}{s^2+\beta_1 s+\beta_0}$	$\beta_1 = {}^{k_1}/_{c_1}$, $\beta_0 = {}^{k_1}/_{b_1}$
S3'	$k_1\frac{s(s+\alpha_0)}{s^3+\beta_2 s^2+\beta_1 s+\beta_0}$	$\alpha_0 = {}^{k_2}/_{c_1}$, $\beta_2 = {}^{(k_1+k_2)}/_{c_1}$, $\beta_1 = {}^{k_1}/_{b_1}$, $\beta_0 = {}^{k_1}/_{b_1}\alpha_0$
S4'	$k_1\frac{s(s+\alpha_0)}{s^3+\beta_2 s^2+\beta_1 s+\beta_0}$	$\alpha_0 = {}^{b_2}/_{k_1}\left({}^{b_1}/_{b_2}+1\right)\beta_0$, $\beta_2 = \alpha_0$, $\beta_1 = {}^{k_1}/_{b_2}$, $\beta_0 = {}^{c_1}/_{b_1}\beta_1$
S5'	$k_1\frac{s^2+\alpha_1 s+\alpha_0}{s^3+\beta_2 s^2+\beta_1 s+\beta_0}$	$\alpha_1 = c_1c_2\nu$, $\alpha_0 = {}^{k_2}/_{b_1}$, $\beta_2 = \alpha_1 + b_1k_1\nu$, $\beta_1 = \alpha_0 + c_1k_1\nu$, $\beta_0 = k_1k_2\nu$, $\nu = \left(b_1c_2\left({}^{c_1}/_{c_2}+1\right)\right)^{-1}$
S6'	$k_1\frac{s}{s^2+\beta_{11}s+\beta_{10}} + k_2\frac{s}{s^2+\beta_{21}s+\beta_{20}}$	$\beta_{11} = {}^{k_1}/_{c_1}$, $\beta_{10} = {}^{k_1}/_{b_1}$, $\beta_{21} = {}^{k_2}/_{c_2}$, $\beta_{20} = {}^{k_2}/_{b_2}$

[3]See Theorem 3 from [3] for the properties of a definition on conditional positive-real functions, as opposite.

5.5 Summary of the Chapter

This chapter presented the passive and active control configurations used in Chapter 6 to investigate the possible synergy active-plus-novel-passive in the secondary suspensions of the railway vehicle. Three fundamental aspects of the vehicle vertical and pitch dynamics were discussed: geometric filtering —an unavoidable phenomenon, simplicity —enabling modal decoupling, and the invariability of the transfer functions employed for assessing ride quality and suspension deflection —describing the formalities of the normal design conflicts.

The passive configurations comprise six mechanical networks as candidate layouts of inerter-based novel devices, together with the conventional secondary suspension. Two well established active control strategies for ride quality enhancement were presented for implementation within different configurations, namely: Skyhook damping and LQG. Configurations for modal and local implementation of the well-known intuitive strategy, skyhook damping, were developed. Those with local implementation, in particular, are complemented by strategies for the suspensions' deflection regulation. Also, a modification of the classical LQG output regulator configuration was formulated attending practicalities for the implementation. Finally, a novel nonlinear strategy for regulating suspension deflection was proposed; it was called 'Adaptive Stiffness' following its role in the suspension and the control law structure.

6

Integration of Inerter-based Devices with Active Suspensions

This chapter presents numerical results and discussions on the integration of the inerter-based passive networks with active suspensions using the control strategies presented in Chapter 5. A complete study for the well established strategies: 'modal skyhook damping with high-pass filtering' and 'local skyhook damping with complementary filtering' is performed, using the candidate layouts for the passive suspensions shown in Figure 5.12. Later, a sub-set of inerter-based suspensions is chosen accordingly to further discuss their effects in the synergy with active suspensions developed with the remaining control strategies from those chosen for this research. The dynamic of the electromechanical actuator introduced in Chapter 3 is included in some of the analyses. The analysis methodology described in the first section provides a guidance to what is presented in the following sections.

6.1 Analysis Methodology

The assessment methods as discussed in Chapter 3 were employed to set optimisation problems for tuning the parameters of the passive and active components of the (ideal) suspensions, described in Chapter 5. Results from the optimisation were then used to study other important aspects of the system performance with the proposed configurations.

Optimal tuning of the parameters was performed computationally on each configuration, with the exception being on the configuration integrating the LQG HPF-output

regulator strategy. For numerical optimisation, a multiobjective optimisation problem subject to a set of realistic physical constraints was defined as:

$$obj: \; min\left(\underline{J_1}^{sup},\, J_3,\, J_2\right) \tag{6.1}$$

when active control strategies were integrated with novel devices, with $\underline{J_1}$, J_2 and J_3 as defined in Section 3.7. $\underline{J_1}^{sup}$ is the least ride quality index among the three points assessed along the vehicle, i.e. leading, middle, and trailing positions: $\underline{J_1}^{sup} = sup\begin{pmatrix} J_{1L} & J_{1M} & J_{1T} \end{pmatrix}$.

For the case of tuning parameters for suspensions comprising passive elements only, the scalar objective:

$$obj: \; min\left(\underline{J_1}^{sup}\right) \tag{6.2}$$

was defined instead.

The optimisation problems defined that way were solved for the parameters of every configuration, as specified in the corresponding section of this chapter, by using a genetic algorithm from the *Global Optimization Toolbox* from MATLAB®, `gamultiobj` [153], which finds a local Pareto set for the objective functions (or an optimal point for the scalar objective —passive— case). It is recognised that a more flexible alternative for the optimisation problem in Equation 6.1 was to set a constraint on J_2 and leave it out of the objective functions, however, the attained results are considered satisfactory.

Furthermore, the analysis on the integration of inerter-based devices with active suspensions was supported by a methodology consisting of a set of relevant analysis tools as depicted in the diagrams in Figures 6.1–6.2. As introduced earlier, a complete study was performed on the well established skyhook damping modal and local strategies. To this end, multiobjective optimisation problems were defined and solved as stated above, and the subsequent analyses followed the three-phases schematic in Figure 6.1. Once a first conclusion was drawn and the several potentials of inerter-based suspensions were explored and understood, the analysis of the results for other control strategies was concentrated to Phases I and II only (schematic in Figure 6.2). This would allow validation of the outcomes related to the main problem formulated for this thesis, i.e. to investigate the potential of inerter-based devices for simplifying the design of active suspensions (with ideal actuators). Moreover, a selection of two of the 'best' inerter-based layouts was performed for the validation.

From here, the labels F&S0, F&S1, F&S2, and so on, are adopted to refer to an integrated configuration active-plus-passive with the passive suspensions S0, S1, S2, and so on, respectively, according to the candidate layouts $\mathrm{S0}-\mathrm{S6}$ described in

Chapter 5, Figure 5.12. Therefore, the identifier 'F' stands for 'active forces applied', and the control strategy employed will be specified accordingly in the corresponding section.

The following sections are dedicated to the application of the analysis methodologies on the integrated configurations. It is worth noting from here that pre-optimisation procedures, run for the configurations with modal skyhook damping and local skyhook damping with complementary filtering, revealed that the optimal value for the series stiffness k_1 (and k_2 in S6) is greater than the bush stiffness ($k_e = 3.5 \times 10^6 [\mathrm{Nm}^{-1}]$). Therefore, k_1 (and k_2 in S6) were set to be equal to k_e, as any lower value caused the algorithm to find low-quality sub-optimal solutions. This was adopted for all the strategies whose results are presented in this chapter. Nevertheless, the loss in ride quality caused by the constraint on k_1 with respect to a stiffer suspension normally does not exceed 3%.

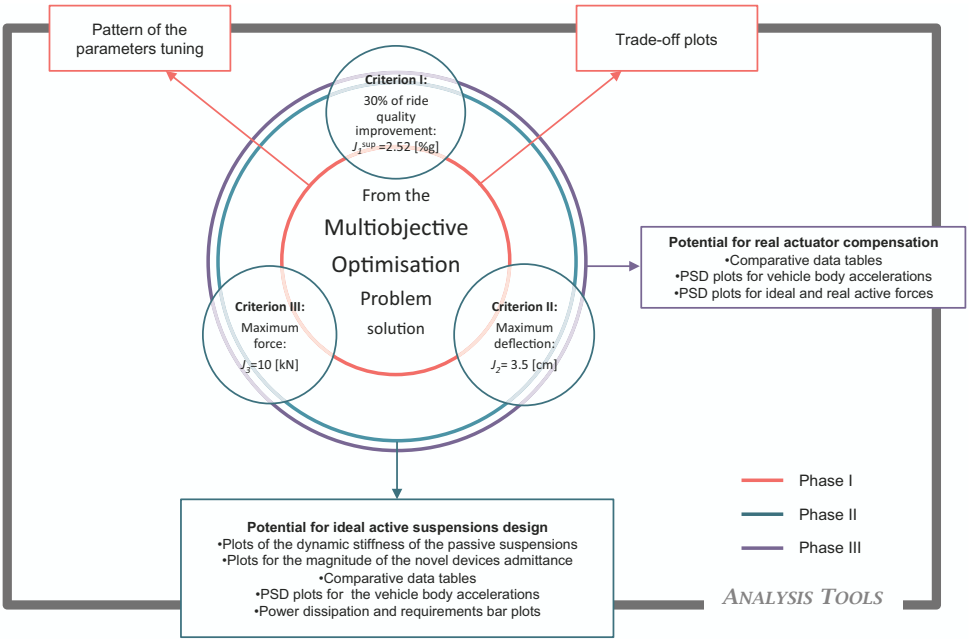

FIGURE 6.1: Diagram for the methodology employed for studying the inerter-based devices several potentials.

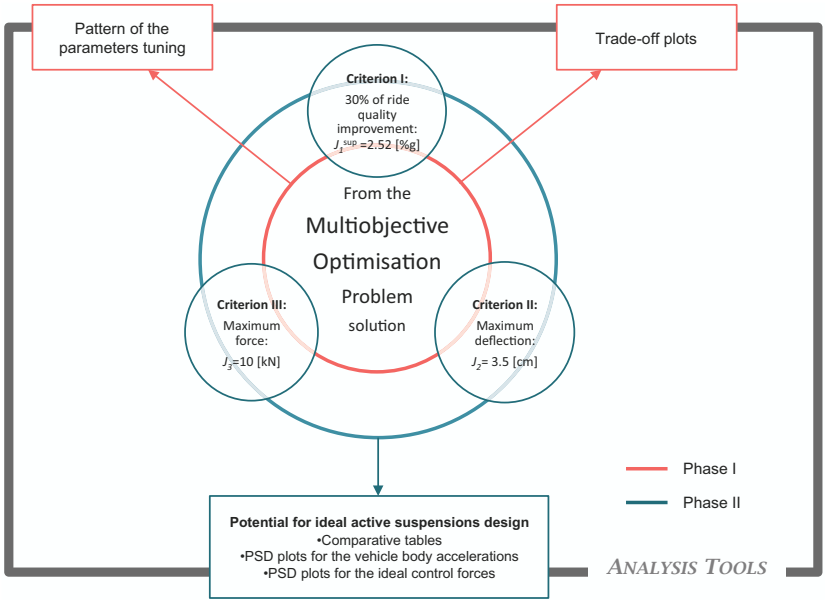

FIGURE 6.2: Diagram for the methodology employed for validation.

6.2 Passive System Performance

The performance of the railway vehicle equipped with passive suspensions only in the secondary suspensions is as depicted in Table 6.1. The candidate suspensions layouts were grouped by similarity as follows: S1 and S2 as these have the same modelling structure but different constraints, S3 and S4 as these have the same admittance function but different constraints apply because of the difference in the realisation, S5 and S6 for being more complex structures. It can be checked from Table 6.1 that all the configurations with S1–S6 provide a certain level of enhancement on the vehicle ride quality, as compared with the results for the system with conventional secondary suspensions, S0. In particular for S1 compared with S2, it can be noted that further improvement can be provided if dedicated damping is introduced in series with the inerter device. Another observation is regarding the suspension deflection, which is reduced by all the inerter-based configurations contrasted with S0. This provides an advantage for the active suspensions design and will be evidenced in the following sections.

Table 6.1: Optimisation results for the passive suspensions

	Ride quality			Other Indices
Config.	J_{1L}[%g]	J_{1M}[%g]	J_{1T}[%g]	J_2[cm]
S0	3.09	1.36	**3.60**	3.4
S1	2.95	1.35	**3.19**(11%)[a]	2.8
S2	2.69	1.39	**2.92**(19%)[a]	2.9
S3	2.74	1.59	**2.93**(19%)[a]	3.1
S4	2.66	1.32	**3.08**(14%)[a]	3.2
S5	3.00	1.41	**3.13**(13%)[a]	2.6
S6	3.10	1.35	**3.31**(8%)[a]	2.7

[a] Percentage of improvement in the ride quality index, $\underline{J_1}^{sup}$, with respect to the passive conventional suspension: $\underline{J_1}^{sup} = 3.60$[%g].
[b] Optimal settings are provided in Table E.1.

6.3 Integration with Modal Skyhook Damping

As discussed in Chapter 5, modal skyhook damping feeds back to the system the high-pass filtered measurements of the bounce and pitch modes of the vehicle body through the active suspensions. The filters cut-off frequencies were set to be, respectively, $f_{cb} = 0.225\,[\text{Hz}]$, and $f_{c\rho} = 0.179\,[\text{Hz}]$, after decisions on results attained from a pre-optimisation stage where optimisation over f_{cb}, and $f_{c\rho}$ was included. In the strategy, the bounce and pitch feedback gains can be regulated so that the bigger the gain, the better the vehicle performance in terms of ride quality, $\underline{J_1}^{sup}$. However, increasing the control gains consequently increases the suspension deflection index, J_2, and the required force index, J_3, even though the filtering of the low frequency components of the fed back variables reduces the problem. Therefore, attempting to enhance the ride quality of the vehicle while reducing the suspension deflection and, most importantly, the actuator requirements is subject to the design trade-offs: $\underline{J_1}^{sup}$ versus J_2, and $\underline{J_1}^{sup}$ versus J_3. Figure 6.3(a)[1] depicts this tendency through normalised optimal curves for the aforementioned trade-offs and for the behaviour of the controller bounce and pitch gains, K_b and K_ρ, in the conflicting tuning. Here, the normalisation was performed individually for each conflicting index (i.e. J_2, J_3) and each control parameter (i.e. K_b, K_ρ) with respect to the corresponding average values $\overline{J_2}$, $\overline{J_3}$, $\overline{K_b}$, $\overline{K_\rho}$, extracted for the set of values producing the range $\underline{J_1}^{sup}$ illustrated in Figure 6.3(a).

[1] Disambiguation: In the plot, the hat symbol ˆ over a parameter symbol means normalised value of the parameter, whilst ˆ over a variable symbol refers to the Laplace transform of the variable.

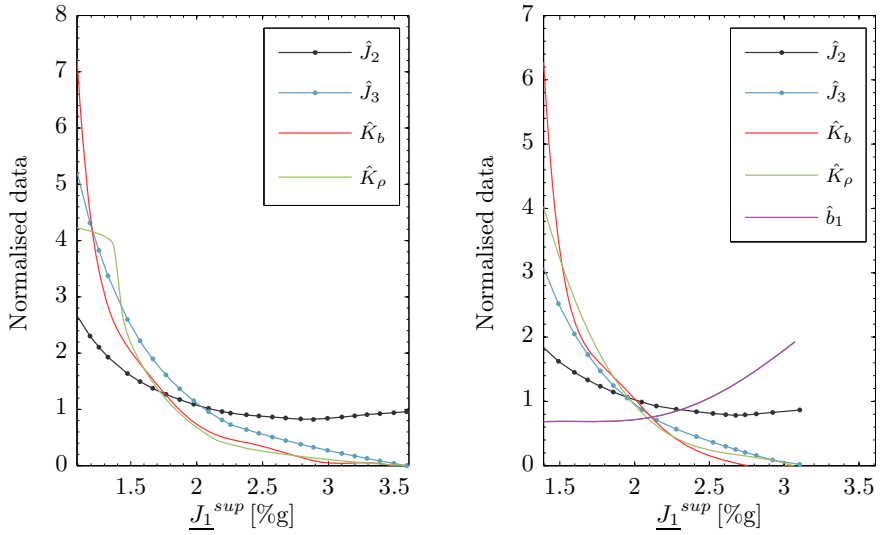

(a) F&S0 [2] (b) F&S1 [3]

Figure 6.3: Optimisation results for the active configurations F&S0 and F&S1 with respect to the least ride quality.

Once the active configuration was integrated with every candidate layout from Figure 5.12 into the vehicle model, the multiobjective optimisation problem defined above was solved. A condition established for the optimisation algorithm was to penalise all the solutions worsening the performance achievable by introducing the inerter-based suspension to the conventional suspensions (i.e. following $\underline{J_1}^{sup}$ from Table 6.1). This defined the least performance of every synergetic suspension.

6.3.1 Analysis Phase I: Optimal solution for the integration using Modal Skyhook Damping

Due to linear considerations on the models of the novel devices, it is natural to associate the settings of their parameters to the definition of particular frequency characteristics according to their structure as a passive network (Table 5.2). However, to complement the view of the passive device simply as a 'passive mechanical controller', a review on the patterns of the optimal setting of the individual components of the mechanical networks with respect to the ride quality index $\underline{J_1}^{sup}$ achieved with the synergetic solution is provided here.

[2] with $\hat{J}_2 = J_2/3.5\,[\text{cm}]$, $\hat{J}_3 = J_3/10\,[\text{kN}]$, $\hat{K}_b = K_b/(\overline{K}_b)$, $\hat{K}_\rho = K_\rho/(\overline{K}_\rho)$, for the mean parameters values for the obtained data range: $\overline{K}_b = 1.89 \times 10^4$ and $\overline{K}_\rho = 1.52 \times 10^5$.

[3] with $\hat{J}_2 = J_2/3.5\,[\text{cm}]$, $\hat{J}_3 = J_3/10\,[\text{kN}]$, $\hat{K}_b = K_b/\overline{K}_b$, $\hat{K}_\rho = K_\rho/\overline{K}_\rho$, $\hat{b}_1 = b_1/\overline{b}_1$, for the mean parameters values: $\overline{K}_b = 9.31 \times 10^3$, $\overline{K}_\rho = 9.96 \times 10^4$, and $\overline{b}_1 = 2581[\text{kg}]$.

The multiobjective optimisation algorithm found for every configuration a Pareto-suboptimal[4] solution defined by parameter tuning curves with oscillations around clear and smoother patterns. These patterns were extracted by performing a selective smoothing process and approximated by either polynomial or shape-preserving interpolant functions using MATLAB® 's graphical interface. The resultant approximated optimal (normalised) tuning for the active configuration with S1 (i.e. F&S1) —chosen from among the rest to highlight the tendency of the inertance values tuning curve— is shown in Figure 6.3(b); Figures F.1–F.3 in Appendix F show the equivalent results for the system with this active suspension and the layouts S2–S6. These figures include the normalised tuning of every parameter and the normalised trade-off curves re-calculated with the interpolated parameters functions, displayed together in the same plots (the same treatment was given to obtain the plots in Figure 6.3(a)). For the integrated configurations, the normalisation of the index/control parameter was performed with respect to the average value of the index/control parameter producing $\underline{J_1^{sup}}$ in the corresponding plot. The plots in Figure 6.4 comparing every two different configurations with the results of combining the active suspension with S0, also display the actual outputs from the optimisation algorithm whose data points are mostly on the new (smoothened) trade-off curves for which more data is available for analysis.

The tuning pattern of the parameters in Figure 6.3(b) illustrates the trend for the feedback gains and the inertance value in the overall suspension conflicting performance. In common —and in general for most of the ride quality range— for the configurations F&S1–F&S5, the pattern of the setting curves for the inertance values and the active suspensions gains opposed each other in the improvement of the ride quality, $\underline{J_1}^{sup}$. The inertance resulted higher with respect to its mean value for low active feedback gains, and decreased for higher feedback gains until almost settling to a constant value (as well as the parameters of the other passive elements). This suggests that the beneficial autonomy of the inerter as a kinetic storage device, discussed in Chapter 4, holds true mainly for ideal suspensions with low active feedback gains. Due to the nature of the control strategy, this is equivalent to interpret the inerter as being more beneficial for ride quality enhancement if the system is provided with low —virtual— dissipation. Moreover, it was found that for the configurations F&S2–F&S4 (Figures F.1–F.2(b) in Appendix F), the parameters associated to the inerters were more influential for the synergy —according to their variability with ride quality— than the other passive suspension elements (springs and dampers). Conversely, parameters associated to dissipation in the novel devices (i.e. passive damping parameters) did not show important variation for the suspensions F&S1–F&S4, whilst for F&S5 presented a similar trend to the inertance value setting. The

[4]Although adopted from here as 'optimal' for terminology simplicity.

stiffness coefficient k_2 in F&S3 showed a trend similar to the inertance value b_1. For the suspension with S6 (Figure F.3(b), Appendix F), constant *optimal* settings of the passive parameters along the ride quality range provided the optimal results for the synergy. Nevertheless, the particular forms of energy storage and dissipation defined by the structure and settings of the novel devices translate into specific frequency characteristics as mentioned earlier.

The statement about the inerter benefits, envisaged from analyses in Chapter 4, is confirmed for the layouts S1–S4 with ideal actuators as represented in Figures 6.4(a) and 6.4(c). There, the most noticeable difference in the trade-off plots of ride quality, $\underline{J_1}^{sup}$, versus force index, J_3, with the insertion of the novel suspensions is depicted for ride quality indices above around 2.1 [%g], i.e. for up to 40% of ride quality improvement. The optimal settings of the parameters of the passive elements cause the trade-off curves $\underline{J_1}^{sup} - J_3$ to get closer to the one with S0 only as K_b and K_ρ further increase. Plots for the $\underline{J_1}^{sup} - J_2$ (ride quality versus suspension deflection index) trade-off curves show that the inclusion of inerter-based suspensions S1–S4 to the active suspensions regulates the suspension deflection so that J_2 does not exceed the maximum deflection allowed, typically 3.5 [cm]. In contrast, suspensions including either S5 or S6 are more limited in the level of improvement achievable without exceeding the suspension deflection constraint. Moreover, S5 and S6 will deteriorate the $\underline{J_1}^{sup} - J_3$ trade-off curve for improvements in the ride quality over 30% (2.52 [%g]) as can be depicted in the plots in Figure 6.4(e).

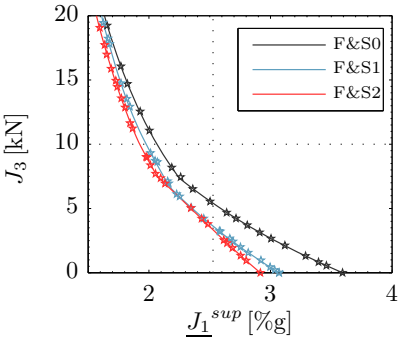

(a) Least ride quality, $\underline{J_1}^{\text{sup}}$, versus active force index, J_3, for the conventional active suspension, F&S0, compared with the synergies F&S1 and F&S2.

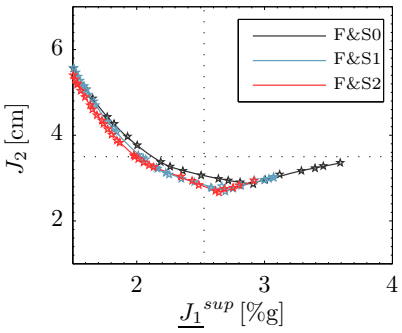

(b) Least ride quality, $\underline{J_1}^{\text{sup}}$, versus suspension deflection index, J_2, for the conventional active suspension, F&S0, compared with the synergies F&S1 and F&S2.

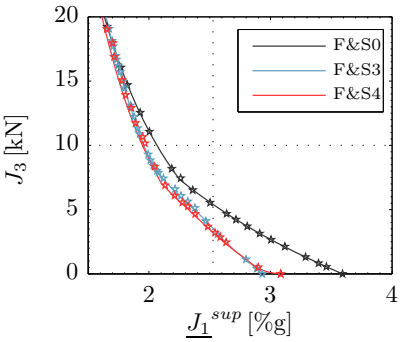

(c) Least ride quality, $\underline{J_1}^{\text{sup}}$, versus active force index, J_3, for the conventional active suspension, F&S0, compared with the synergies F&S3 and F&S4.

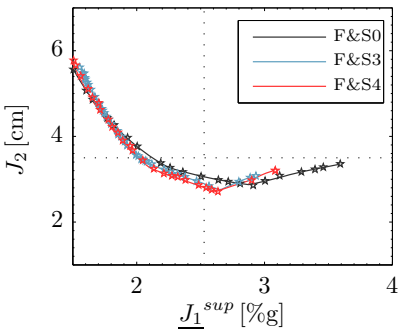

(d) Least ride quality, $\underline{J_1}^{\text{sup}}$, versus suspension deflection index, J_2, for the conventional active suspension, F&S0, compared with the synergies F&S3 and F&S4.

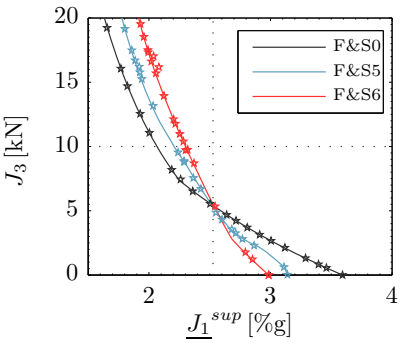

(e) Least ride quality, $\underline{J_1}^{\text{sup}}$, versus active force index, J_3, for the conventional active suspension, F&S0, compared with the synergies F&S5 and F&S6.

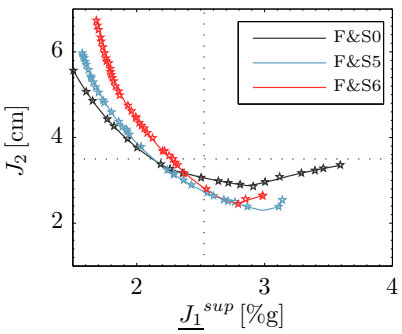

(f) Least ride quality, $\underline{J_1}^{\text{sup}}$, versus suspension deflection index, J_2, for the conventional active suspension, F&S0, compared with the synergies F&S5 and F&S6.

Figure 6.4: Comparison of the design trade-off curves for the vehicle with active suspensions and the candidate layouts S0–S6 from Figure 5.12.

6.3.2 Analysis Phase II: Potential of the integration using Modal Skyhook Damping

As depicted in the diagram for the methodology of analysis in Figure 6.1, three criteria were considered for selecting sets of data from the results presented in Figure 6.4. These were:

- **Criterion I (CI):** set of data for which the ideal suspensions would achieve 30% of improvement in the vehicle ride quality compared with 3.60[%g], which is the ride quality of the vehicle with conventional passive suspensions, S0. Thus, $\underline{J_1}^{sup} = 2.52$[%g] defines this criterion.
- **Criterion II (CII):** set of data for which the suspension deflection index reaches $J_2 = 3.5$[cm] which is the typical maximum allowable suspension excursion in the vertical direction [5].
- **Criterion III (CIII):** set of data for which the (ideal) active force index is $J_3 = 10$ [kN], which is a typical value for the maximum force considered for the actuators sizing.[5]

Results for each criterion are depicted in Tables 6.2–6.4, and were illustrated in the trade-off curves in Figure 6.4 through the dotted lines on each plot. The corresponding parameter settings can be found in Appendix E, Tables E.2–E.4.

For the three criteria, Figures 6.5(a), 6.5(c), and 6.5(e) depict the dynamic stiffness gain for the passive part of the suspension (airspring in parallel to a novel device). There, the modulus of the dynamic stiffness for S1–S6 is importantly modified in contrast to the dynamic of the airspring (S0). These show how the insertion of inerter-based devices with optimal settings changes the transition between low and high frequency stiffness, magnifies the high frequency stiffness, and increases the highest dynamical frequency of the augmented passive suspension. Similarly, Figures 6.5(b), 6.5(d), and 6.5(f) show the magnitude of the frequency response of the inerter-based device complex admittance. The plots show the sort of —passive— compensation that every novel device with optimal parameters provides to the system for the different criteria. The magnitude curves for the admittances S1'–S4' and S6' resemble the frequency response of a band-pass filter, even if S3' and S4' show magnitude peaks at certain frequencies. In fact, it will be seen from the results discussed in the following that the resonant peaks in Figure 6.5(d) for the frequency response of the admittance function of S3', and S4' with more prominence, may be beneficial; the peaks display that greater damping is applied by the device at their

[5]For this planar model of the vehicle, the assumption of one actuator for the leading suspension and one actuator for the trailing suspension was done.

resonant frequency. Unlike the others, the novel device S5' does not display the inerter-like behaviour (i.e. positive first order slope) for low frequencies clearly identified for the other layouts. Instead, the parallel spring-inerter in the device in S5' causes a notch response around 1 [Hz] on the flat damping shown up to more than 10 [Hz].

Table 6.2: Optimisation results for Criterion I (CI): 30% of improvement in the ride quality with respect to the passive conventional suspension, i.e. $\underline{J_1}^{sup} = (2.52 \pm 0.01)$ [%g]

	Ride quality			**Other Indices**		
Config.	J_{1L}[%g]	J_{1M}[%g]	J_{1T}[%g]	J_2[cm]	J_3[kN]	J_4[W]
F&S0	2.40	1.31	**2.52**	3.1	5.44	132
F&S1	2.39	1.30	**2.52**	2.9	3.65 (33%)[b]	74
F&S2	2.41	1.36	**2.52**	2.8	3.38 (38%)[b]	54
F&S3	2.40	1.43	**2.53**	2.9	3.51 (35%)[b]	52
F&S4	2.38	1.32	**2.53**	2.8	3.21 (41%)[b]	57
F&S5	**2.52**	1.37	2.46	2.7	5.37 (1%)[b]	78
F&S6	**2.53**	1.42	2.44	2.8	5.51 (−1%)[b]	52

[b] Percentage of variation in the active force index, J_3, with respect to $J_3{}^{S0} = 5.44$[kN]

Table 6.3: Optimisation results for Criterion II (CII): $J_2 = (3.5 \pm 0.1)$ [cm]

	Ride quality			**Other Indices**		
Config.	J_{1L}[%g]	J_{1M}[%g]	J_{1T}[%g]	J_2[cm]	J_3[kN]	J_4[W]
F&S0	**2.12** (41%)[a]	1.27	2.04	3.5	9.09	145
F&S1	**2.04** (43%)[a]	1.26	1.95	3.5	8.92 (2%)[b]	95
F&S2	**1.99** (45%)[a]	1.23	1.94	3.5	8.77 (4%)[b]	96
F&S3	**2.02** (44%)[a]	1.23	2.00	3.5	8.66 (5%)[b]	89
F&S4	**2.01** (44%)[a]	1.24	1.95	3.5	8.74 (4%)[b]	83
F&S5	**2.13** (41%)[a]	1.32	1.93	3.5	11.25 (−24%)[b]	73
F&S6	**2.26** (37%)[a]	1.41	2.09	3.5	10.81 (−19%)[b]	26

[a] Percentage of improvement in the ride quality index, $\underline{J_1}^{sup}$, with respect to the passive conventional suspension: $\underline{J_1}^{sup} = 3.60$[%g].
[b] Percentage of variation in the active force index, J_3, with respect to $J_3{}^{S0} = 9.09$[kN]

In the following, discussions on results for each criterion.

Table 6.4: Optimisation results for Criterion III (CIII): $J_3 = (10 \pm 0.2)$ [kN]

Config.	Ride quality			Other Indices		
	J_{1L}[%g]	J_{1M}[%g]	J_{1T}[%g]	J_2[cm]	J_3[kN]	J_4[W]
F&S0	**2.06** (43%)[a]	1.26	1.93	3.6	10.17	143
F&S1	**1.97** (45%)[a]	1.25	1.85	3.7	10.15	91
F&S2	**1.92** (47%)[a]	1.21	1.82	3.7	10.14	91
F&S3	**1.96** (46%)[a]	1.22	1.90	3.7	10.06	92
F&S4	**1.94** (46%)[a]	1.23	1.83	3.7	10.17	74
F&S5	**2.20** (39%)[a]	1.34	2.02	3.3	10.05	78
F&S6	**2.30** (36%)[a]	1.41	2.13	3.4	10.10	33

[a] Percentage of improvement in the ride quality index, $\underline{J_1}^{sup}$, with respect to the passive conventional suspension: $\underline{J_1}^{sup} = 3.60$[%g].

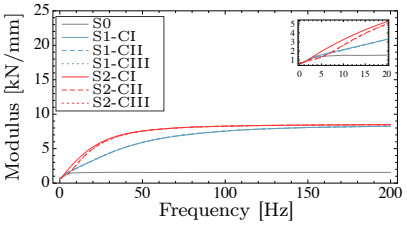

(a) Dynamic stiffness gain of S1 and S2, compared to S0.

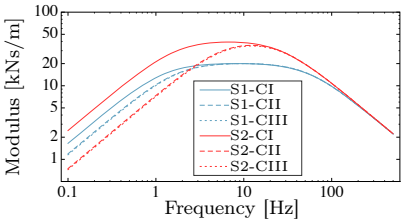

(b) Magnitude of the admittance for the novel device in S1 and S2.

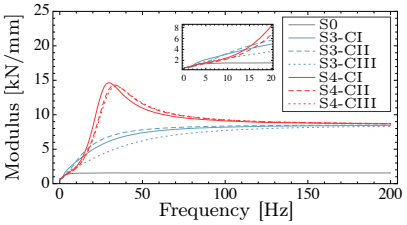

(c) Dynamic stiffness gain of S3 and S4, compared to S0.

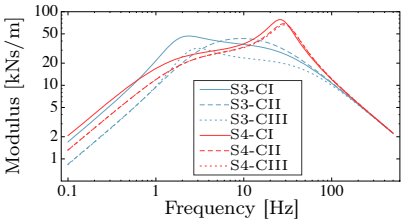

(d) Magnitude of the admittance for the novel device in S3 and S4.

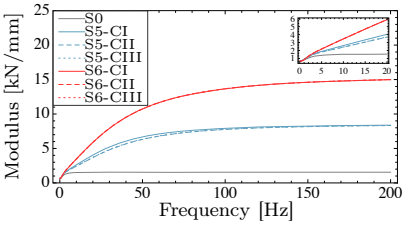

(e) Dynamic stiffness gain of S5 and S6, compared to S0.

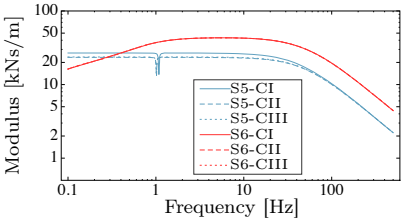

(f) Magnitude of the admittance for the novel device in S5 and S6.

Figure 6.5: Magnitude of the frequency response for: dynamical stiffness of the configurations S0–S6 (left column), and admittance of the mechanical networks S1′ – S6′ (right column), for the three criteria CI–CIII. Refer to Figure 5.12 for the candidate layouts.

Criterion I:

The power spectrum density plots for the accelerations at the leading, and trailing positions of the vehicle body, respectively $\ddot{z}_{vL}$ and $\ddot{z}_{vT}$, are shown in Figure 6.6 (p.s.d. plots for $\ddot{z}_{vM}$ are supplemented in Appendix F, Figure F.4). It can be checked that the inerter-based suspensions further attenuate low frequency vibrations (below 2–3[Hz]) but affect the attenuation of the high frequencies. This corresponds to the so-called "waterbed" effect, which comes from the robust control field in the study of the sensitivity transfer function of the system; it refers to the fact that a control designed to attenuate disturbances in one frequency range must be accompanied by amplification of the disturbance in other frequency range [154]. Nevertheless, the mechanical components response to the frequency is always limited; according to the experts, an inerter is normally not sensitive to frequencies over 20[Hz]. This fact from the devices practicalities should be examined in later research. Moreover, in the assessment of vertical ride quality according to the currently known weighted norms [46, 47, 48], the range of middle frequencies, below 20 [Hz], is the most important. The plots clearly show the already discussed geometric filtering effect occurring in the vehicle dynamics.

From the tabulated results in Table 6.2, an improvement of 30% in the ride quality can be achieved by assuming ideal actuators for which the index for the demanded force, J_3, is 41% lower when introducing an inerter-based suspension as described by S4. Also, a reduction of 38% in J_3 is attained with the optimal setting for the active configuration combined with S2, followed by S3 with 35% and S1 with 33%. More complex suspensions as S5 and S6 did not show any improvement in terms of J_3 for ideal suspensions. In every case, the suspension deflection index value, J_2 , is within the physical allowance.

In terms of the ride quality assessed at the other two positions of the vehicle body (other than the one showing the worst ride quality), it can be checked that S1–S4 do not affect the ride quality at the front by more than ± 0.02 [%g]. For S5–S6, conversely, a better ride quality is obtained at the rear of the vehicle as compared with the ride index at the front. A small deterioration (less than 10%) is caused at the middle of the vehicle when inserting S2–S6. A test of robustness to parameter variations was performed showing that combining any of the candidate layouts S1–S6 with the active suspensions will reduce the sensitivity to the active suspension parameters. Even so, the system is very robust with S0 inclusive; the maximum sensitivity index is 0.27 for the vehicle body acceleration assessed at the rear position with the configuration F&S0 for a variation in K_ρ of 10% with respect to the setting for Criterion I.

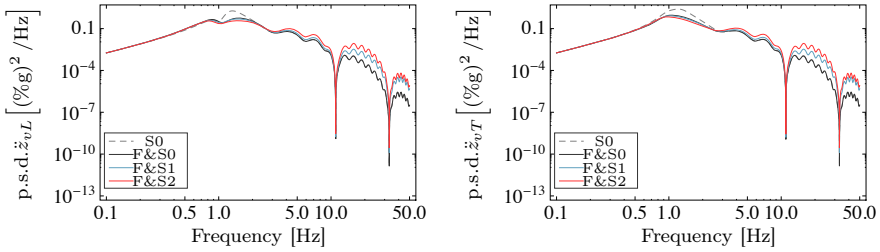

(a) *Leading position* with active and S1–S2, compared to S0 (airspring only) and the conventional active configuration, F&S0

(b) *Trailing position* with active and S1–S2, compared to S0 (airspring only) and the conventional active configuration, F&S0

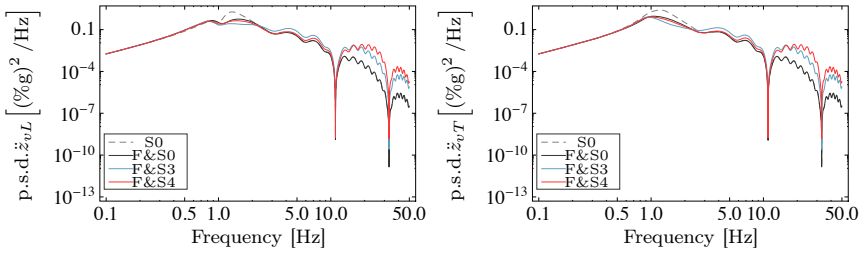

(c) *Leading position* with active and S3–S4, compared to S0 (airspring only) and the conventional active configuration, F&S0

(d) *Trailing position* with active and S3–S4, compared to S0 (airspring only) and the conventional active configuration, F&S0

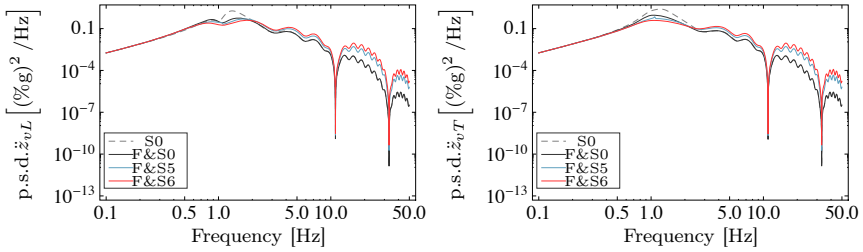

(e) *Leading position* with active and S5–S6, compared to S0 (airspring only) and the conventional active configuration, F&S0

(f) *Trailing position* with active and S5–S6, compared to S0 (airspring only) and the conventional active configuration, F&S0

Figure 6.6: p.s.d. plots for the vehicle body acceleration at the leading ($\ddot{z}_{vL}$) and trailing positions ($\ddot{z}_{vT}$) for configurations F&S0 – F&S6 with settings according to Criterion I, with ***ideal*** actuators.

Table 6.2 also shows a positive value for the average stochastic power J_4 for all the configurations, F&S0–F&S6, according to the sign convention adopted for Equation 3.114. Whether this is average power required to the source or average power that can be recovered, would depend on the actuator technology. The actuators, therefore, will either extract power from the system —as opposite to supply—, or demand this

average power to the source to produce active forces opposing the direction of the suspension's relative velocity. For instance, if 'double acting' technology is adopted, for example, introducing inerter-based suspensions would have also potential for reducing power requirements, following results in Table 6.2, upon consideration of perfect actuators. Following discussions on energy extraction rate in Chapter 4 (Subsection 4.3), which envisaged that 'the energy extraction rate by a virtually dissipative active suspension can be lower', it is found from results for J_4 for the different configurations that analytical (deterministic-based) and numerical results (stochastic-based) are in good agreement, at least for this active configuration. It should be recalled here that the skyhook damping strategy is, in essence, a virtually dissipative strategy according to the definition given in Chapter 4. In particular, the synergies F&S3 and F&S6 showed a reduction of 61% in J_4, followed by F&S2 (59%), F&S4 (57%), F&S1 (44%) and F&S5 (41%). Even if J_4 is of the order of the tens to few hundreds of watts, that still may be significant when real actuators efficiency enters into play, for example. Figure 6.7 shows in a bar plot the levels of stochastic mean power dissipated in the secondary passive suspensions (i.e. S1–S6), $\mathcal{P}_s$, and the stochastic mean power extracted by the ideal actuators, $\mathcal{P}_a = J_4$ (blue and red bars, respectively). It is observed that for the conventional active suspensions, F&S0, the total mean power dissipated in the airsprings $\mathcal{P}_s$ is reduced when active suspensions are implemented. Conversely, the blue bars depict that incorporating inerter-based devices in the suspensions increases the power dissipated in the passive suspensions S1–S6, as compared with the dissipation in the airsprings in either the passive (S0) or the active configuration (F&S0). This is due to the damping provided by c_1 (and c_2 where applies) and the inerter effects on power dissipation, as studied in Chapter 4 (Subsection 4.4) for the passive quarter vehicle model. Moreover, the height of the combined bars reveals higher total stochastic mean power ($\mathcal{P}_s + \mathcal{P}_a$) dissipated/extracted by the secondary suspensions for all the active configurations combined with S1–S6.

Thus, results for J_3 and J_4 for Criterion I suggest that incorporating passive structures as S1–S4 have a potential for reducing the actuator requirements in terms of size and power for a configuration enhancing the vehicle ride quality by 30%. Besides this, a direct relation between the amount of dissipated/extracted power and the ride quality levels does not seem obvious. Further work deeply considering the actuators' dynamic for particular technologies would be necessary to fully understand the findings on power dissipation.

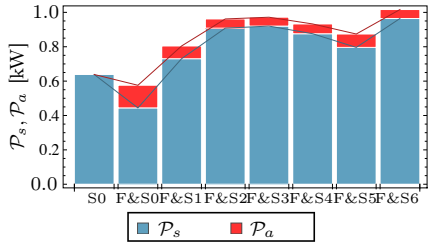

FIGURE 6.7: Stochastic mean power dissipated/extracted by the passive and active suspensions, with settings according to Criterion I.

Criteria II and III:

Not surprisingly for Criteria II and III, for which the ride quality is further improved as compared with Criterion I, the feedback gains get increased (see Table E.3 and E.4 in Appendix E for reference). In such cases, no important benefit is attained with the insertion of inerter-based devices with the ideal active suspensions, as discussed earlier on the trade-off plots for high feedback gains. Numerical results are shown in Tables 6.3 and 6.4, respectively. For the $J_2 = 3.5\,[\text{cm}]$ criterion (Criterion II), the percentage of improvement in the ride quality for the active suspension combined with S0 respect to the conventional passive suspension (i.e. S0 only) is of 41%. In contrast, the active configuration integrating S1–S4 enhances the ride quality assessment index $\underline{J_1}^{sup}$ by no more than 4%, with ride quality improvement along the vehicle of the same order. Also, a reduction of J_3 of less than 5% is attained for F&S1–F&S4. Moreover, introducing S5 or S6 in the suspensions will cause an increased value of J_3, respectively; S5 does not cause any benefit on $\underline{J_1}^{sup}$ and S6 deteriorates it. The potential of the inerter-based suspensions for high levels of improvement of ride quality seems to be therefore in the stochastic mean power required by the actuators. In those terms, the insertion of any of the candidate layouts enhances the stochastic mean power dissipated by the passive suspensions in comparison with the configuration F&S0. Substantial reductions (up to 50%) in the stochastic mean power extracted (and therefore ideally required) by active means is observed with respect to F&S0 for suspensions providing the same levels of ride quality, $\underline{J_1}^{sup}$, or even slightly better. This result suggests that for ideal implementation of active suspensions with the modal skyhook damping configuration designed under Criterion II, incorporating inerter-based suspensions are neither significantly beneficial in terms of ride quality nor in the maximum applied forces, but in terms of the —ideal— active suspensions power requirements (check the values for the mean power index $J_4 = \mathcal{P}_a$ in Table 6.3). The total power $\mathcal{P}_s + \mathcal{P}_a$ is depicted in the bar plot in Figure 6.8(a).

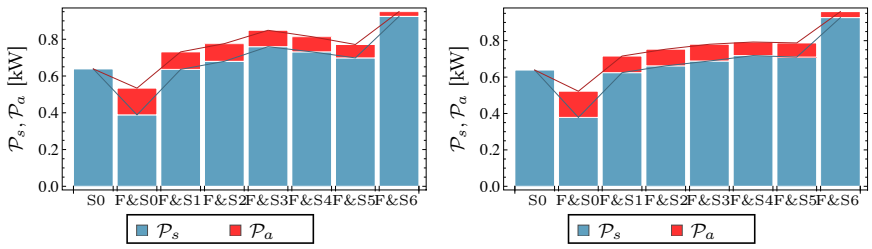

(a) Criterion II (b) Criterion III

Figure 6.8: Stochastic mean power dissipated by the passive suspensions and extracted/required by the active (ideal) suspensions for Criteria II and III.

The power spectrum density plots for the vehicle body accelerations, $\ddot{z}_{vL}$, $\ddot{z}_{vM}$, and $\ddot{z}_{vT}$, included in Appendix F, Figures F.5–F.7, are very similar to those for Criterion I, i.e. the inerter-based suspensions slightly improves the attenuation of low frequency vibrations (below 5 [Hz] for S1–S4, and below 3 [Hz] for S5–S6 for the leading and trailing positions) but worsen the high frequency components, counterbalancing to produce similar levels of ride quality as reported in the tables of data.

Similar observations to those for Criterion II in terms of ride quality and mean dissipated and extracted power derive from Table 6.4 for Criterion III. Given this, further analysis is developed from here only on results for Criteria I and II.

6.3.3 Analysis Phase III: Potential for real actuator compensation to implement Modal Skyhook Damping

This phase provides a non-exhaustive review on the results obtained when the dynamic of the actuator was also introduced. Outcomes from this phase should be considered as a simple exploration on another potentiality of the inerter-based devices for active suspensions, but not as conclusive results. The following is an assessment of the system with the electromechanical actuator model with PI controller presented in Chapter 3, which still has substantial bandwidth limitations. The suspension parameters obtained for the ideal configurations with Criteria I and II (Table E.2 and E.3 in Appendix E) were used in this phase, i.e. no re-tuning was performed.

The data presented in Tables 6.5 and 6.6 depict a potential of inerter-based suspensions for the compensation of the deteriorating effects of the actuator dynamic in the production of the active control forces for Criteria I and II. Indeed, for Criterion I, a deterioration of the ride quality index $\underline{J_1}^{sup}$ from 30% (ideal) to 14% (real) was obtained for the conventional active configuration F&S0. However, the compensation given by any of the novel suspensions S1–S6 could recover the ride quality

index to up to 28% as for S6, or to 26% with S3, for example. Also, a reduction in the required active force index, J_3^{c}, and the index for the applied (real) force, J_3^{ac}, was attained. This is remarkable for F&S1–F&S4. For Criterion II, similarly, the improvement of ride quality with the conventional active suspension, F&S0, was reduced from 41% for the ideal actuator to 27%, whilst inserting any of the inerter-based devices produces results closer to the ride quality achieved with ideal actuators (refer to Table 6.3 for results with ideal actuators, and to Table 6.6 for results with real ones). As an example, the configuration F&S1 achieves 43% of improvement with settings under Criterion II and ideal actuators, and 37% with real actuators for the same parameter settings. In terms of the force indices, the reduction observed for the ideal case with the configurations S1–S4 case holds for the demanded control force, J_3^{c}, and the applied active force, J_3^{ac}.

Table 6.5: Results for the system with electromechanical actuator for the settings in Table E.2 (Criterion I (CI)—30% of improvement with ideal suspensions: *ideal* $\underline{J_1}^{sup} = (2.52 \pm 0.01)$ [%g])

	Ride quality [%g]			**Other Indices**		
Config.	J_{1L}[%g]	J_{1M}[%g]	J_{1T}[%g]	J_2[cm]	J_3^{c}[kN]	J_3^{ac}[kN]
F&S0	3.00	1.52	**3.12**(14%)[a]	3.1	5.82	6.26
F&S1	2.73	1.39	**2.90** (20%)[a]	2.9	3.94 (32%)[b]	5.03
F&S2	2.54	1.36	**2.70** (25%)[a]	2.8	3.60 (38%)[b]	4.82
F&S3	2.47	1.44	**2.68** (26%)[a]	2.9	3.73 (32%)[b]	4.88
F&S4	2.55	1.33	**2.76** (24%)[a]	2.8	3.49 (40%)[b]	4.68
F&S5	**2.79** (23%)[a]	1.43	2.68	2.8	5.69 (2%)[b]	6.14
F&S6	**2.60** (28%)[a]	1.39	2.48	2.8	5.72 (2%)[b]	6.14

[a] Percentage of improvement in the ride quality index, $\underline{J_1}^{sup}$, with respect to the passive conventional suspension: $\underline{J_1}^{sup} = 3.60$[%g].
[b] Percentage of variation in the active force index, J_3, with respect to $J_3{}^{\mathrm{S0}} = 5.82$[kN]

Returning to Criterion I, Figure 6.9 contains the p.s.d. plots for the vehicle body accelerations assessed at the leading and trailing positions (plots for the middle position are provided in Appendix F, Figure F.8) obtained for the model with real actuators. The plots display the referred compensation for most of the frequency range, and mainly around the first vibrational mode and at high frequencies. Figures 6.10–6.11 contrast the p.s.d. for the active forces as applied at the front and rear suspensions, respectively, by the different configurations according to Criterion I. In the column at the left, the p.s.d. plots for the active forces applied by ideal actuators; in the column at the right, the p.s.d. for the command forces, F_{c}, and for the actual forces, F_{act}, for the system with real actuators, displayed in the same plot. A reduction in the p.s.d. of the active forces for the system with suspensions S1–S4

Table 6.6: Results for the system with electromechanical actuator for the settings in Table E.3 (Criterion II (CII)—maximum deflection: *ideal* $J_2 = (3.5 \pm 0.1)$ [cm])

	Ride quality [%g]			**Other Indices**		
Config.	J_{1L}[%g]	J_{1M}[%g]	J_{1T}[%g]	J_2[cm]	J_3^{c}[kN]	J_3^{ac}[kN]
F&S0	**2.62** (27%)[a]	1.48	2.50	3.5	9.71	9.31
F&S1	**2.28** (37%)[a]	1.34	2.16	3.5	9.49 (2%)[b]	9.13
F&S2	**2.17** (40%)[a]	1.28	2.10	3.5	9.36 (4%)[b]	9.05
F&S3	**2.10** (42%)[a]	1.25	2.08	3.5	9.10 (6%)[b]	8.85
F&S4	**2.11**(42%)[a]	1.26	2.03	3.5	9.27 (5%)[b]	8.93
F&S5	**2.34** (35%)[a]	1.39	2.05	3.5	11.90 (−23%)[b]	11.30
F&S6	**2.29** (37%)[a]	1.38	2.05	3.5	11.40 (−17%)[b]	10.80

[a] Percentage of improvement in the ride quality index, $\underline{J_1}^{sup}$, with respect to the passive conventional suspension: $\underline{J_1}^{sup} = 3.60$[%g].
[b] Percentage of variation in the active force index, J_3, with respect to ${J_3}^{\mathrm{S0}} = 9.71$[kN]

is evidenced at low frequencies compared to the forces for the conventional active suspension, F&S0, in both cases, ideal and real. Moreover, the p.s.d. curves for the command force, F_{c}, in the system with real actuators and S1–S4 show lower for all the assessed frequency range. For the suspensions with S5–S6, the p.s.d.s for F_{c} (front and rear) are closer to the p.s.d.s of the ideal forces, excepting at high frequencies for which the amplitude of the control forces is clearly reduced. This is mostly preserved for the real applied forces, F_{act}, in all the configurations. It can be checked that the dynamic of the actuator significantly reduces the wheelbase geometric filtering effect at high frequencies, appearing in the command force due to the modal feedback setting. The plots for the real active forces, F_{act}, show a major force attenuation at frequencies around 1.5 [Hz] and some near 10 [Hz] which are beneficial to the ride quality as evidenced in Figure 6.9. This statement on the active forces p.s.d. around 1.5 [Hz] excludes, however, the p.s.d. of the rear suspension active forces for the system with the candidate layouts S5 and S6. Even though, the attenuation of the vehicle body accelerations with the real configurations with S5 and S6 around 1.5 [Hz] holds, demonstrating the cooperative work between passive and active suspensions (regardless the fact that the parameters of the suspensions and controllers were not re-tuned).

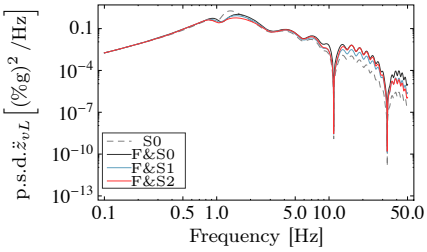

(a) *Leading position* with active and S1–S2, compared to S0 (airspring only) and the conventional active configuration, F&S0

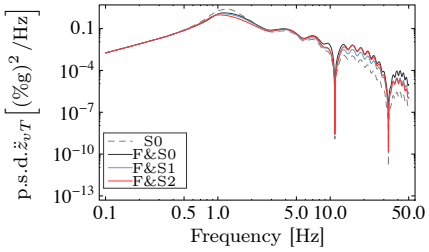

(b) *Trailing position* with active and S1–S2, compared to S0 (airspring only) and the conventional active configuration, F&S0

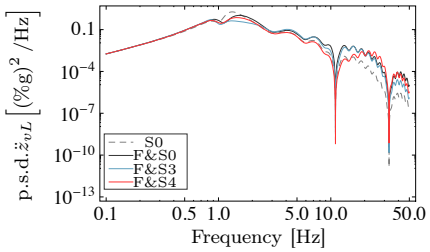

(c) *Leading position* with active and S3–S4, compared to S0 (airspring only) and the conventional active configuration, F&S0

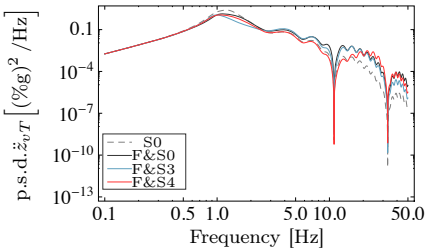

(d) *Trailing position* with active and S3–S4, compared to S0 (airspring only) and the conventional active configuration, F&S0

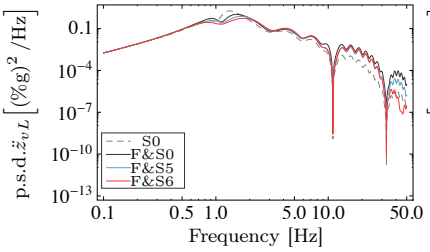

(e) *Leading position* with active and S5–S6, compared to S0 (airspring only) and the conventional active configuration, F&S0

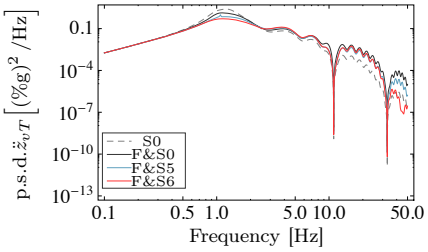

(f) *Trailing position* with active and S5–S6, compared to S0 (airspring only) and the conventional active configuration, F&S0

Figure 6.9: p.s.d. plots for the vehicle body acceleration at the leading and trailing positions ($\ddot{z}_{vL}$ and $\ddot{z}_{vT}$) for configurations F&S0 – F&S6 with settings according to Criterion I, with ***real*** actuators.

Findings on the p.s.d. plots for the vehicle body accelerations and the active (ideal and real) forces for Criterion II, were similar to those for Criterion I, with the main difference being in the frequencies at which the passive networks provide compensation of the real active forces (given for the range 1-5 [Hz], and also around 10[Hz]).

The plots are included in Appendix F, Figures F.9–F.10 for vehicle body accelerations, and Figures F.11–F.12 for the active forces.

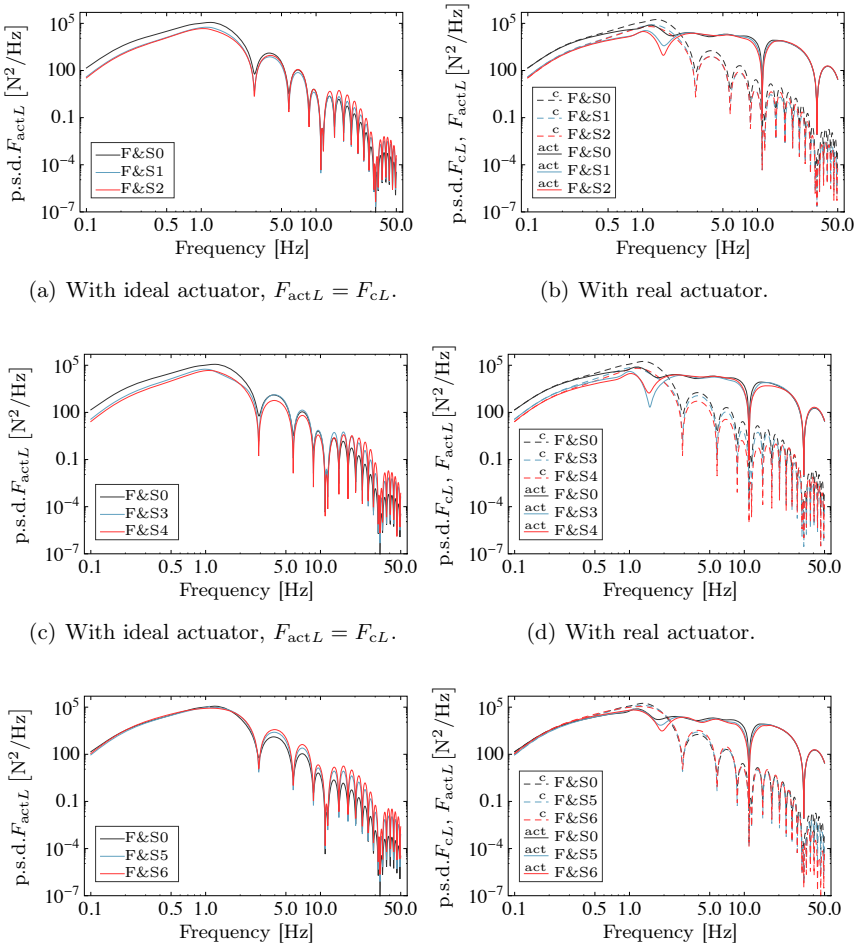

(a) With ideal actuator, $F_{\mathrm{act}L} = F_{\mathrm{c}L}$.

(b) With real actuator.

(c) With ideal actuator, $F_{\mathrm{act}L} = F_{\mathrm{c}L}$.

(d) With real actuator.

(e) With ideal actuator, $F_{\mathrm{act}L} = F_{\mathrm{c}L}$.

(f) With real actuator.

Figure 6.10: p.s.d. plots of the active forces applied at the leading suspension due to configurations F&S0 – F&S6 with settings according to Criterion I; left column: with ***ideal*** actuators, right column: with ***real*** actuators .

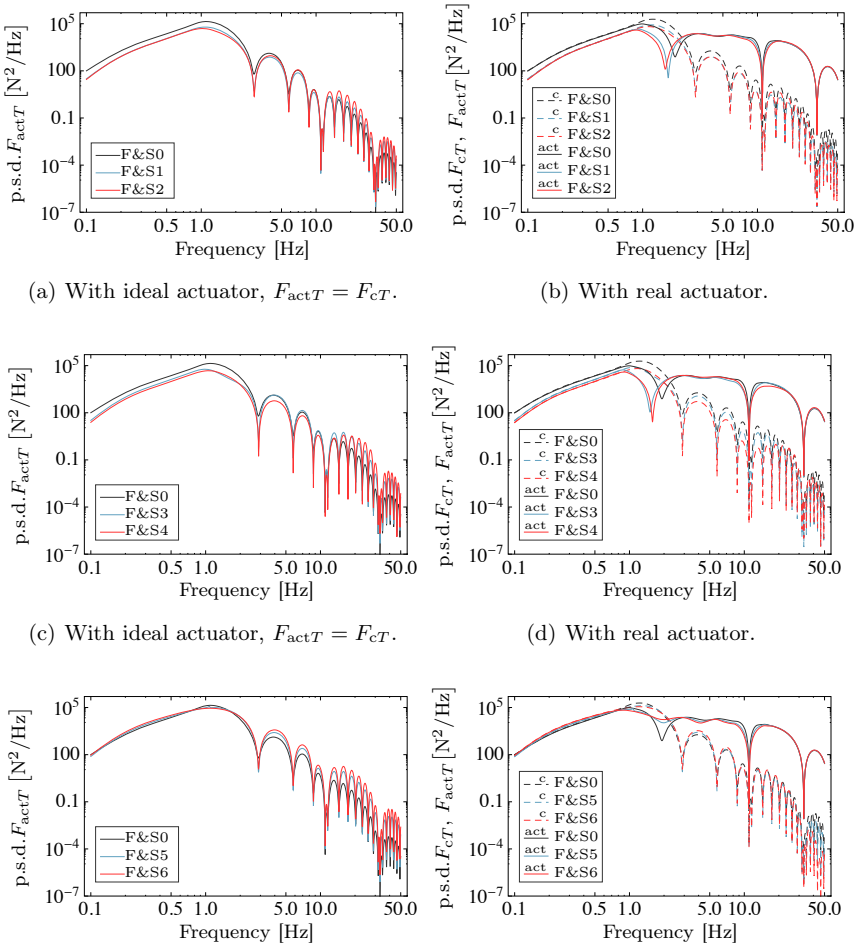

(a) With ideal actuator, $F_{\mathrm{act}T} = F_{\mathrm{c}T}$.

(b) With real actuator.

(c) With ideal actuator, $F_{\mathrm{act}T} = F_{\mathrm{c}T}$.

(d) With real actuator.

(e) With ideal actuator, $F_{\mathrm{act}T} = F_{\mathrm{c}T}$.

(f) With real actuator.

Figure 6.11: p.s.d. plots of the active forces applied at the trailing suspension due to configurations F&S0 – F&S6 with settings according to Criterion I; left column: with ***ideal*** actuators, right column: with ***real*** actuators.

6.4 Integration with Local Skyhook Damping and Complementary Filtering

Figure 5.6 in Chapter 5 illustrated the integration of local skyhook damping with complementary filtering for a vehicle provided with passive suspensions. Parameter tuning for this configuration integrated with novel devices followed also the definition and computation of the multiobjective problem solution described at the beginning of this chapter (fixed airsprings parameters were assumed as in all the configurations). This configuration incorporates two design parameters to the optimisation problem: the corner frequency of the complementary filters, f_c , and the design gain, K_l, apart from the novel-passive suspension parameters.

In general, increasing the skyhook damping gain K_l tends to improve the performance of the vehicle in terms of ride quality, $\underline{J_1}^{sup}$. It is also expected, at least for the conventional active configuration F&S0, that the corner frequency of the filters f_c tends to be smaller in order to get a better $\underline{J_1}^{sup}$ value. This assert is depicted in Figure 6.12, which corresponds to the normalised (hat) output of the multiobjective algorithm for the parameters and objectives for the vehicle with conventional active secondary suspensions, F&S0 [6]. From results in Figure 6.12, the optimal frequency f_c is almost constant for most of the range (around $\bar{f}_c = 0.28\,[\text{Hz}]$) whilst the optimal K_l monotonically increases towards a smaller value $\underline{J_1}^{sup}$ (i.e. for better ride quality). The effect of f_c is mostly evidenced for high gains K_l for which the algorithm returned an almost constant value: for a constant K_l, f_c should be importantly decreased in order to improve the ride quality. The latter has more impact on the compromise with the suspension deflection index J_2. These patterns were in fact expected for this configuration.

Similar to what was presented in the previous section for the modal configuration, the analyses on the potential of inerter-based devices followed the methodology described by the diagram in Figure 6.1.

[6] The curves in Figure 6.12 were obtained after performing a smoothing procedure as the described for the modal configuration, plotted against the output for the $\underline{J_1}^{sup}$ value.

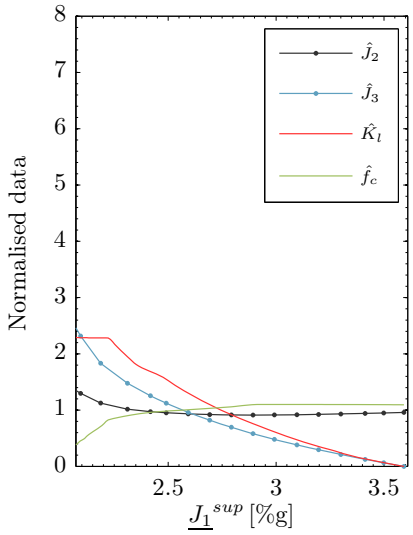

FIGURE 6.12: Optimisation results for the active configuration F&S0 [7].

6.4.1 Analysis Phase I: Optimal solution for the integration using Local Skyhook Damping with Complementary Filtering

For this practical configuration of skyhook damping, incorporating inerter-based devices seems to have reciprocal effects to the active part. Similar to what was attained for the parameter tuning in the modal implementation of the skyhook damping strategy, the inerter plays an important role in the tuning of the active parameters of the combined suspension.

Particularly, for the system with layouts S1–S4 and low 'dissipation' implemented by active means (i.e. low K_l), it was observed that high inertance values b_1, together with the other parameters of the novel-passive structure, contribute to the enhancement of the vehicle ride quality. To follow this assertion, refer to Figure 6.13, for example. Notice that what is considered here as 'high'/'low' depends upon the normalisation of the variable/parameter performed with respect to the corresponding average value for the set of data obtained for each configuration. Specifically, the following observations were extracted for the optimal parameter settings in configurations F&S1–F&S4:

- As well as for the modal implementation of skyhook damping with HPF, the pattern of the tuning curve for the inertance b_1 (and also b_2 for F&S4) reveals

[7] with $\hat{J}_2 = J_2/3.5\,[\text{cm}]$, $\hat{J}_3 = J_3/10\,[\text{kN}]$, $\hat{K}_l = K_l/\overline{K}_l$, $\hat{f}_c = f_c/\overline{f}_c$, for the mean parameters values: $\overline{K}_l = 3.19 \times 10^4$, and $\overline{f}_c = 0.28[\text{Hz}]$.

that the inerter can provide benefits to the ride quality of the vehicle mainly for low and intermediate active gain values, K_l. This pattern opposes the pattern of the K_l's tuning curve, i.e. K_l grows to achieve better ride quality index $\underline{J_1}^{sup}$ whilst b_1 (and b_2 for F&S4) decreases.

- It is common to all the structures that the tuning of the inertance value b_1 for settings producing a ride quality index $\underline{J_1}^{sup}$ better than about 2.5[%g] (i.e. $\underline{J_1}^{sup}$ below 2.5[%g]) barely changes and has the lowest value in the normalised tuning curve.

- Due to the frequency dependent characteristic of the candidate layouts, the pattern for the corner frequency f_c of the complementary filters of the active configuration is different in each structure. As an example, refer to the parameter tuning for the layouts F&S1 and F&S2 in Figure 6.13. Figure 6.13(a) for F&S1 shows that for low and intermediate gains K_l, the corner frequency f_c has a tuning pattern similar to the one for the inertance value b_1, which decreases with increasing K_l. In contrast, for low and intermediate gains K_l in the layout F&S2 (Figure 6.13(b)), the corner frequency f_c is lower than its average, increases to produce an intermediate range of $\underline{J_1}^{sup}$, and decreases again to allow further improvements with constant K_l. Therefore, it can be inferred from here that a device like S2' compensates for the suspension deflection for small values of K_l. F&S1, as opposite, results with a wider low-pass band for the implementation of $F_c^{J_2}$. This suggests, on the other hand, that the suspension deflection compensation required due to the skyhook implementation is not mainly provided by S1'. For the plots showing the parameter tuning for F&S3 and F&S4, refer to Figure in F.13, Appendix F.

- As for the damping parameters of the passive structures, these remain mostly constant for settings with high inertance. For active suspensions with the layouts $S2 - S3$, a slowly growing pattern with high values of K_l is attained. That shows that high improvements in $\underline{J_1}^{sup}$ for this configuration are mainly due to dissipative effects (active and passive) in the secondary suspensions.

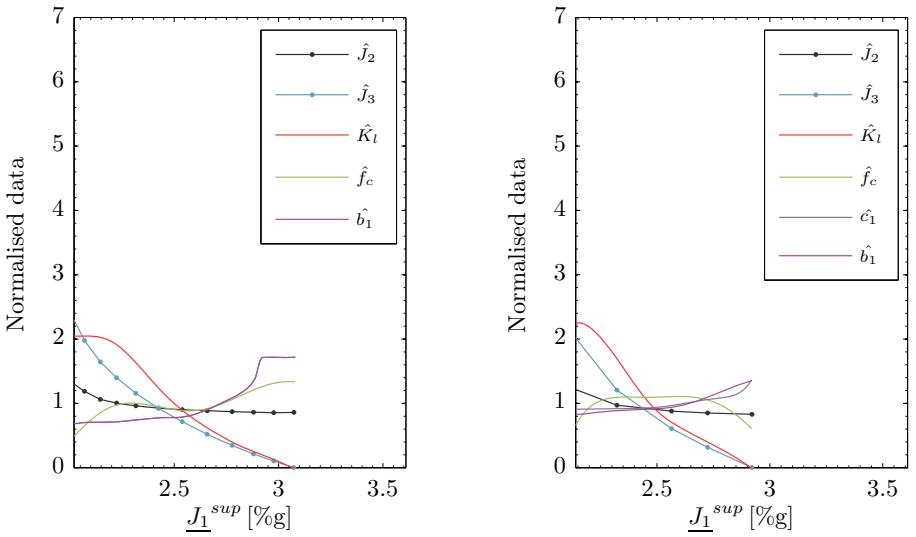

(a) F&S1 [8] (b) F&S2 [9]

Figure 6.13: Optimisation results for the integrations F&S1 and F&S2.

Conversely, the configurations F&S5 – F&S6 show distinct patterns for the parameter tuning. The inertance values are almost constant for most of the obtained optimal settings, whilst the passive damping coefficients appear to dominate the effects of the novel suspensions for ride quality improvement when the suspensions have low active gain K_l. That results in little change in the pattern of f_c for F&S5, for low and intermediate values of K_l. Figure 6.14 shows the tuning plots illustrating this different tendency.

[8] with $\hat{J}_2 = J_2/3.5\,[\text{cm}]$, $\hat{J}_3 = J_3/10\,[\text{kN}]$, $\hat{K}_l = K_l/\overline{K}_l$, $\hat{f}_c = f_c/\overline{f}_c$, $\hat{b}_1 = b_1/\overline{b}_1$, for the mean parameters values: $\overline{K}_l = 3.57 \times 10^4$, $\overline{f}_c = 0.25$[Hz], and $\overline{b}_1 = 2837$[kg].

[9] with $\hat{J}_2 = J_2/3.5\,[\text{cm}]$, $\hat{J}_3 = J_3/10\,[\text{kN}]$, $\hat{K}_l = K_l/\overline{K}_l$, $\hat{f}_c = f_c/\overline{f}_c$, $\hat{c}_1 = c_1/\overline{c}_1$, $\hat{b}_1 = b_1/\overline{b}_1$, for the mean parameters values: $\overline{K}_l = 3.01 \times 10^4$, $\overline{f}_c = 0.21$[Hz], $\overline{c}_1 = 3.59 \times 10^4\,[\text{Nsm}^{-1}]$ and $\overline{b}_1 = 4480$[kg].

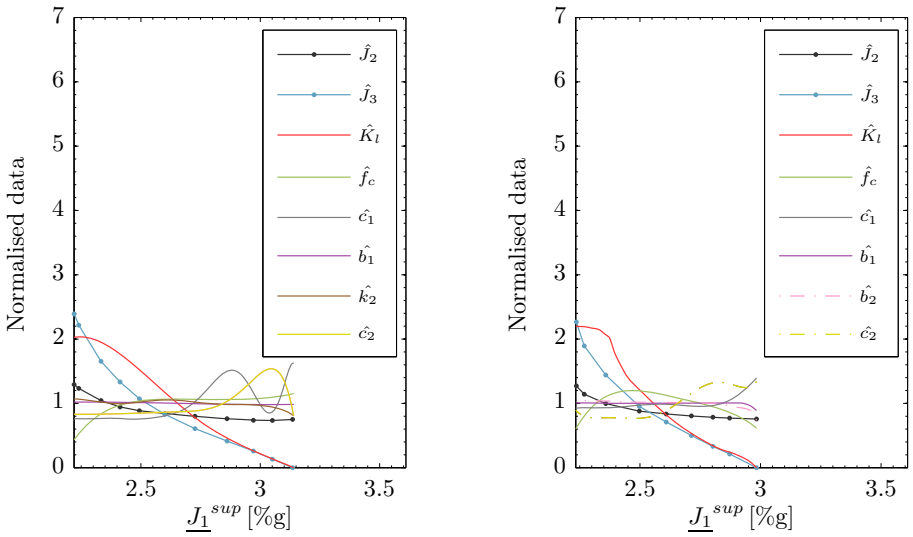

(a) F&S5 [10] (b) F&S6 [11]

Figure 6.14: Optimisation results for the integrations F&S5 and F&S6.

On the other hand, Figure 6.15 shows the trade-off plots for ride quality index versus active forces index ($\underline{J_1}^{sup}$ versus J_3), and ride quality index against suspension deflection index ($\underline{J_1}^{sup}$ versus J_2) —left and right-hand side columns, respectively. Similarly to what was obtained for the modal implementation of skyhook damping with HPF, and as it was briefly discussed earlier, the trade-off curves for the configurations with inerter-based devices, are better than the conventional (F&S0) for intermediate and low values of K_l. The curves corresponding to configurations with inerter-based devices get closer to the conventional active suspension with increased values of the active gain K_l, and in fact intersect it. By comparison between them, the configuration with S2 shows slightly better than S1 for low and intermediate values of K_l (Figure 6.15(a)), S4 shows even closer to S3 (Figure 6.15(c)), and S6 shows better than S5 (Figure 6.15(e)). Those configurations with $\mathrm{S1}-\mathrm{S4}$ intersect the '$\underline{J_1}^{sup}$ versus J_3' trade-off curve for the conventional configuration F&S0 at more than 15 [kN], producing a ride quality index of nearly 2 [%g]; configurations with $\mathrm{S5}-\mathrm{S6}$ intersect it at about 12 [kN] corresponding to about 2.4 [%g]. The trade-off curves considering the suspension deflection index (i.e. $\underline{J_1}^{sup}$ versus J_2) depicts,

[10] with $\hat{J}_2 = J_2/3.5\,[\mathrm{cm}]$, $\hat{J}_3 = J_3/10\,[\mathrm{kN}]$, $\hat{K}_l = K_l/\overline{K}_l$, $\hat{f}_c = f_c/\overline{f}_c$, $\hat{c}_1 = c_1/\overline{c}_1$, $\hat{b}_1 = b_1/\overline{b}_1$, $\hat{k}_2 = k_2/\overline{k}_2$, $\hat{c}_2 = c_2/\overline{c}_2$, for the mean parameters values: $\overline{K}_l = 3.57 \times 10^4$, $\overline{f}_c = 0.25$[Hz], $\overline{c}_1 = 1.14 \times 10^4\,[\mathrm{Nsm}^{-1}]$, $\overline{b}_1 = 6.2926 \times 10^4\,[\mathrm{kg}]$, $\overline{k}_2 = 2.27 \times 10^6\,[\mathrm{Nm}^{-1}]$, and $\overline{b}_2 = 1.66 \times 10^4$[kg].

[11] with $\hat{J}_2 = J_2/3.5\,[\mathrm{cm}]$, $\hat{J}_3 = J_3/10\,[\mathrm{kN}]$, $\hat{K}_l = K_l/\overline{K}_l$, $\hat{f}_c = f_c/\overline{f}_c$, $\hat{c}_1 = c_1/\overline{c}_1$, $\hat{b}_1 = b_1/\overline{b}_1$, $\hat{c}_2 = c_2/\overline{c}_2$, $\hat{b}_2 = b_2/\overline{b}_2$, for the mean parameters values: $\overline{K}_l = 3.27 \times 10^4$, $\overline{f}_c = 0.20$[Hz], $\overline{c}_1 = 1.19 \times 10^4\,[\mathrm{Nsm}^{-1}]$, $\overline{b}_1 = 3.95 \times 10^4\,[\mathrm{kg}]$, $\overline{c}_2 = 1.97 \times 10^4\,[\mathrm{Nsm}^{-1}]$, and $\overline{b}_2 = 7919$[kg].

on the other hand, that the suspensions integrating the active configuration with S5 – S6 produce lower suspension deflection than the other configurations for low control gain values.

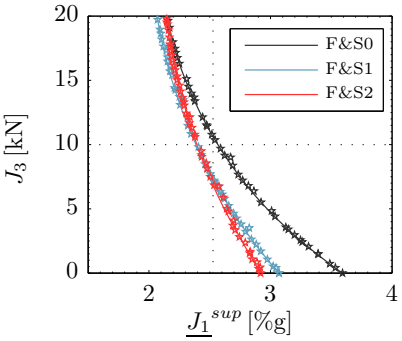

(a) $\underline{J_1}^{\text{sup}}$ versus J_3 for F&S0 compared with F&S1 and F&S2

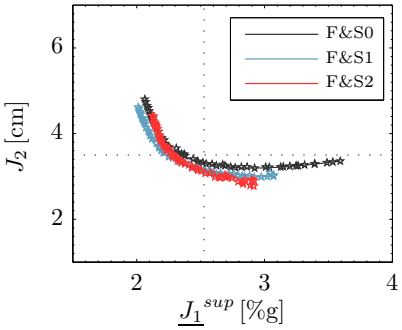

(b) $\underline{J_1}^{\text{sup}}$ versus J_2 for F&S0 compared with F&S1 and F&S2

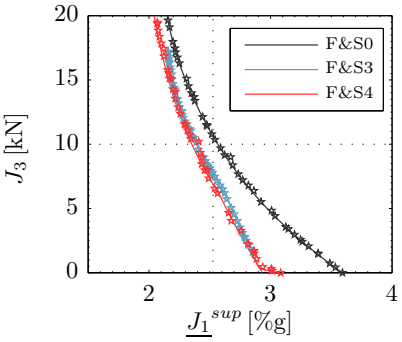

(c) $\underline{J_1}^{\text{sup}}$ versus J_3 for F&S0 compared with F&S3 and F&S4

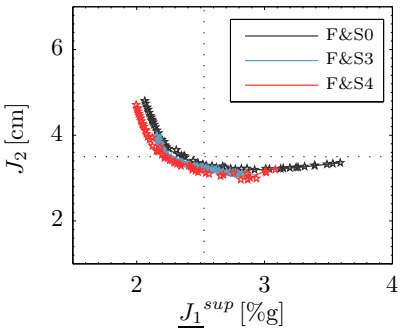

(d) $\underline{J_1}^{\text{sup}}$ versus J_2 for F&S0 compared with F&S3 and F&S4

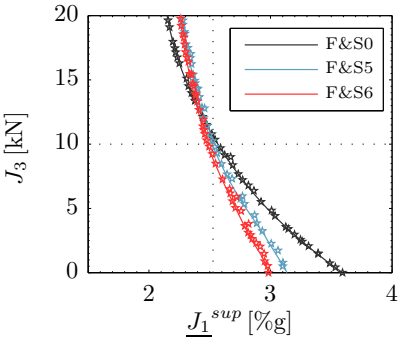

(e) $\underline{J_1}^{\text{sup}}$ versus J_3 for F&S0 compared with F&S5 and F&S6

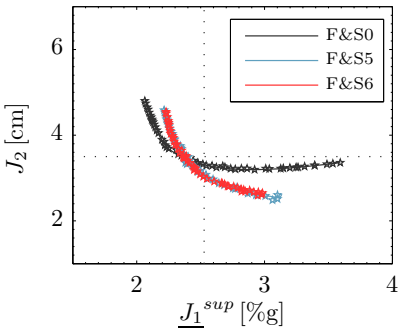

(f) $\underline{J_1}^{\text{sup}}$ versus J_2 for F&S0 compared with F&S5 and F&S6

Figure 6.15: Comparison of the design trade-off curves for the vehicle with active suspensions and the candidate layouts S0–S6 from Figure 5.12.

6.4.2 Analysis Phase II: Potential of the integration using Local Skyhook Damping with Complementary Filtering

This phase of the analysis was driven by the same three criteria discussed with the modal implementation of the skyhook damping with HPF configuration: Criterion I: $\underline{J_1}^{sup} = 2.52\,[\%g]$, Criterion II: $J_2 = 3.5\,[cm]$, and Criterion III: $J_3 = 10\,[kN]$. The results for each criterion are presented in Table 6.7, Table 6.8, and Table 6.9, respectively. The parameter settings can be found in Appendix E E.5–E.7.

Table 6.7: Optimisation results for Criterion I (CI): 30% of improvement in the ride quality with respect to the passive conventional suspension, i.e. $\underline{J_1}^{sup} = (2.52 \pm 0.01)\,[\%g]$.

	Ride quality			Other Indices		
Config.	J_{1L}[%g]	J_{1M}[%g]	J_{1T}[%g]	J_2[cm]	J_3[kN]	J_4[W]
F&S0	2.43	1.19	**2.52**	3.3	10.71	208
F&S1	2.39	1.20	**2.53**	3.2	7.37(31%)[b]	122
F&S2	2.48	1.26	**2.52**	3.1	7.00(35%)[b]	97
F&S3	2.33	1.18	**2.52**	3.2	7.73(28%)[b]	124
F&S4	2.36	1.21	**2.53**	3.2	6.89(36%)[b]	106
F&S5	**2.53**	1.28	**2.53**	3.0	9.73(9%)[b]	117
F&S6	**2.52**	1.27	**2.53**	3.0	8.78(18%)[b]	51

[b] Percentage of variation in the active force index, J_3, with respect to $J_3{}^{S0} = 10.71$[kN]

Table 6.8: Optimisation results for Criterion II (CII): $J_2 = (3.5 \pm 0.1)\,[cm]$.

	Ride quality			Other Indices		
Config.	J_{1L}[%g]	J_{1M}[%g]	J_{1T}[%g]	J_2[cm]	J_3[kN]	J_4[W]
F&S0	2.31	1.16	**2.35** (35%)[a]	3.5	13.93	229
F&S1	2.20	1.15	**2.23** (38%)[a]	3.5	13.75 (1%)[b]	169
F&S2	2.25	1.21	**2.28** (37%)[a]	3.5	13.40 (4%)[b]	133
F&S3	2.15	1.10	**2.24** (38%)[a]	3.5	13.20 (5%)[b]	159
F&S4	2.15	1.14	**2.21** (39%)[a]	3.5	13.66 (2%)[b]	147
F&S5	**2.37** (34%)[a]	1.24	2.34	3.5	15.13 (−9%)[b]	164
F&S6	**2.36** (34%)[a]	1.24	2.33	3.5	14.40 (3%)[b]	146

[a] Percentage of improvement in the ride quality index, $\underline{J_1}^{sup}$, with respect to the passive conventional suspension: $\underline{J_1}^{sup} = 3.60$[%g].
[b] Percentage of variation in the active force index, J_3, with respect to $J_3{}^{S0} = 13.93$[kN]

Figure 6.16 contains, in the left column, the plots for the magnitude of the dynamic stiffness of the configurations S1 − S6 contrasted with the corresponding plots for the

Table 6.9: Optimisation results for Criterion III (CIII): $J_3 = (10 \pm 0.1)$ [kN]

	Ride quality			Other Indices		
Config.	J_{1L}[%g]	J_{1M}[%g]	J_{1T}[%g]	J_2[cm]	J_3[kN]	J_4[W]
F&S0	2.46	1.19	**2.56** (29%)[a]	3.3	10.1	202
F&S1	2.30	1.18	**2.39** (34%)[a]	3.3	9.9	145
F&S2	2.33	1.23	**2.39** (34%)[a]	3.3	10.0	117
F&S3	2.26	1.14	**2.39** (34%)[a]	3.3	9.9	145
F&S4	2.25	1.17	**2.35** (35%)[a]	3.3	10.1	131
F&S5	**2.52**	1.28	**2.52** (30%)[a]	3.1	10.0	141
F&S6	**2.48**	1.27	**2.48** (31%)[a]	3.1	10.0	127

[a] Percentage of improvement in the ride quality index, $\underline{J_1}^{sup}$, with respect to the passive conventional suspension: $\underline{J_1}^{sup} = 3.60$[%g].

airspring in conventional configuration S0; in the right column, it shows the plots for the admittance of the corresponding novel devices ($S1' - S6'$), all according to the three criteria settings. It can be noticed that the frequency response of all the passive configurations, S1–S6, does not change much for the three different settings. Although this differs from what was obtained for the modal implementation of the skyhook damping with HPF strategy, that comes from the cooperative nature of the active-plus-novel-passive configurations. In this case, the novel devices compensate for suspension deflection at low frequencies even for higher control gains (e.g. Criteria II–III).

In the following, discussions on results obtained for each criterion.

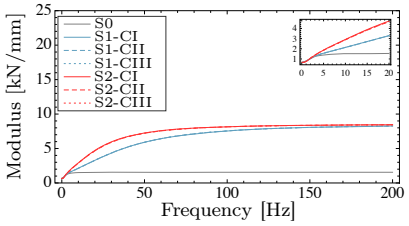

(a) Dynamic stiffness gain of S1 and S2, compared to S0.

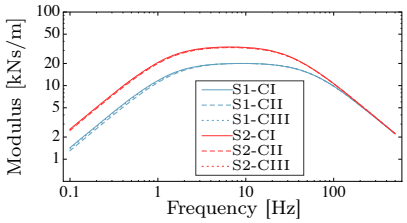

(b) Magnitude of the admittance for the novel device in S1 and S2 (i.e. S1' and S2').

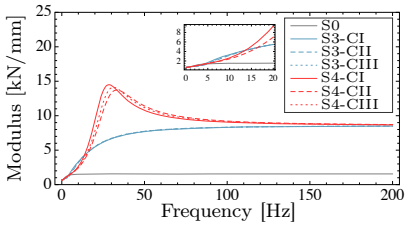

(c) Dynamic stiffness gain of S3 and S4, compared to S0.

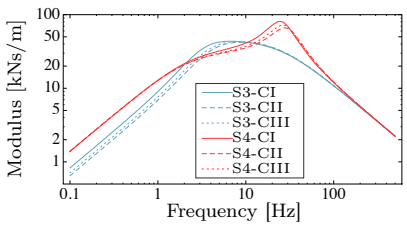

(d) Magnitude of the admittance for the novel device in S3 and S4 (i.e. S3' and S4').

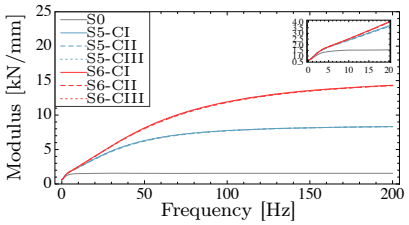

(e) Dynamic stiffness gain of S5 and S6, compared to S0.

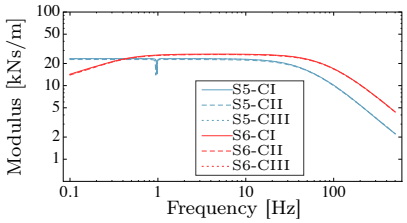

(f) Magnitude of the admittance for the novel device in S5 and S6 (i.e. S5' and S6').

Figure 6.16: Magnitude of the frequency response for: dynamical stiffness of the configurations S0–S6 (left column), and admittance of the mechanical networks $S1' - S6'$ (right column), for the three criteria CI–CIII. Refer to Figure 5.12 for the candidate layouts.

Criterion I:

This active configuration applies, in general, higher forces than the modal implementation presented in the Section 6.3. As depicted in Table 6.7, achieving 30% of improvement in the ride quality requires actuators capable of applying forces of at least 10.71 [kN] (recall here that the index J_3 considers both deterministic and stochastic forces). Incorporating inerter-based suspensions with this configuration may reduce the active forces index by at least 9% when using S5, and up to 35%–

36% when introducing S2 or S4. Moreover, introducing passive structures as S1, S3 and S4 slightly improves the ride quality at the leading position of the vehicle, whilst the ride quality at the middle position remains about the same. Structures like S2, S5 and S6 cause a small deterioration in the ride quality at these positions.

On the other hand, the power dissipation index, $J_4 = \mathcal{P}_a$, is importantly reduced for all the configurations introducing inerter-based devices. Configuration F&S6 shows a reduction of 75% in the mean power required by a perfect actuator for applying the active stochastic forces needed to achieve 30% of improvement in the ride quality of the vehicle. Similarly, configuration F&S4 showed a reduction of 49% in J_4; this result confirms layout S4 as the most favourable for vertical ride quality improvement, at least for the two control strategies presented until now. Even if F&S3 produces less reduction in terms of power demand, it still reduces the index by 40%. Furthermore, the bar plot in Figure 6.17 shows that the mean stochastic power $\mathcal{P}_s$ dissipated in the secondary passive suspensions with novel devices $\mathrm{S1}-\mathrm{S6}$ (with active suspensions implemented) is increased as contrasted with the dissipation in the airsprings S0, with and without active suspensions implemented (S0 and F&S0, respectively). In fact, for F&S0, the dissipation in the airsprings is reduced in comparison to the passive case, S0.

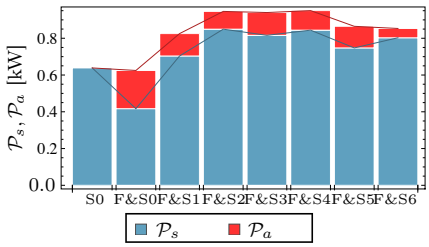

Figure 6.17: Stochastic mean power dissipated/extracted by the passive and active suspensions, with settings according to Criterion I. Local skyhook damping with complementary filtering configuration.

The power spectrum density plots for the vehicle body accelerations, $\ddot{z}_{vL}$, $\ddot{z}_{vM}$, and $\ddot{z}_{vT}$, showed very similar to these for Criterion I for the modal implementation, in terms of the effects of inerter-based suspensions. That is, the novel suspensions slightly improve the attenuation of low frequency vibrations but worsen the high frequency components, counterbalancing to produce similar levels of ride quality as reported in the tables of data. Figure 6.18(a) contains the p.s.d. plots for $\ddot{z}_{vT}$ for a vehicle with either suspensions F&S0, F&S3, and F&S4, chosen as an illustrative example.

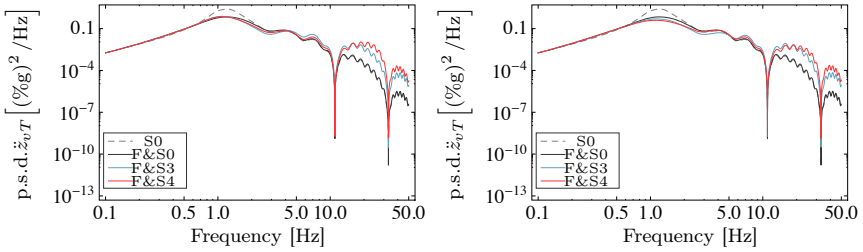

(a) Criterion I (b) Criterion II

Figure 6.18: p.s.d. plots for the vehicle body acceleration at the trailing position ($\ddot{z}_{vT}$) for configurations F&S0, F&S3, and F&S4 with suspensions settings according to Criteria I and II, and ***ideal*** actuators.

Criteria II and III:

According to results for Criterion II, shown in Table 6.8, improvements in the ride quality and the active force indices are fairly low in comparison to the conventional case of active implementation, F&S0. Again, the expected waterbed effect is observed in the p.s.d. plots, as illustrated for the vehicle body acceleration at the trailing position for configurations F&S0, F&S3, and F&S4 in Figure 6.18(b). Therefore, introducing inerter-based devices integrated with high gain active suspensions with the current configuration is not justified for these specific aims. Nevertheless, results in Table 6.8 are particularly favourable for the stochastic mean power index J_4, as depicted in Table 6.8. Beneficial configurations as F&S2 and F&S4 produce reductions of 42% and 36%, respectively, which, again, give suggestions on the potential of the inerter for the actuators efficiency. The bar plot in Figure 6.19(a) depicts the levels of stochastic mean power dissipated by the passive and active part of the integrated configurations. The suspensions F&S2, F&S4, and F&S6 show the highest level of total stochastic mean dissipated power, $\mathcal{P}_p + \mathcal{P}_a$. S1 dissipated —by passive means— about the same levels of power as the airsprings without active suspensions implementation, whilst S0 in the active configuration, again resulted with lower levels of passive dissipation.

For Criterion III, the active configuration integrated with either of the novel suspensions result in some benefit for the ride quality at the trailing position of the vehicle, as shown in Table 6.9. Once more, the suspensions with S4 are more beneficial, though with only 6% of benefit over the conventional implementation of the active suspensions F&S0. Furthermore, it also shows benefit in the ride quality at the leading and middle positions (9% and 4%, respectively). Benefits in terms of

power dissipation are again evident; these are shown in Table 6.9 and the bar plot in Figure 6.8(b). From here, analyses for Phase III will take only Criteria I and II as these reunite the trend of the results for Criteria III.

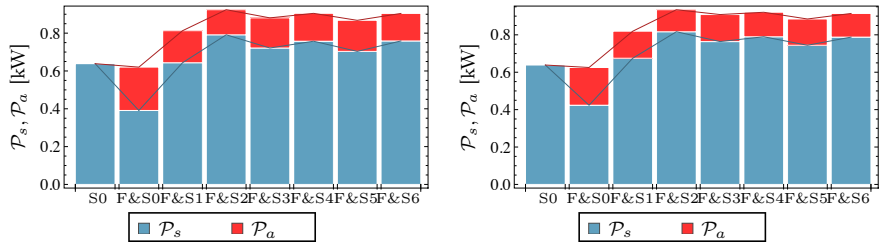

(a) Criterion II (b) Criterion III

Figure 6.19: Stochastic mean power dissipated/extracted by the passive and active suspensions, with settings according to Criteria II and III. Local skyhook damping with complementary filtering configuration.

6.4.3 Analysis Phase III: Potential for real actuator compensation to implement Local Skyhook Damping with Complementary Filtering

As it was done with the modal configuration of the skyhook damping with HPF, this phase provides a non-exhaustive review on the results obtained when the dynamic of the actuator was introduced to apply the active forces with the local skyhook damping with complementary filtering configuration.

Table 6.10 reports the results obtained with the suspensions with parameters as tuned for the ideal case according to Criterion I (an improvement of 30% in $\underline{J_1}^{sup}$). The findings are similar to these for the modal configuration. Whilst a deterioration in the performance of the suspension with F&S0 from 30% of improvement for $\underline{J_1}^{sup}$ for the ideal case, to 14% for the real case, the performance improvements for inerter-based suspensions can still be of 23%–24% as for the real implementation of F&S2–F&S4, and F&S6. Similarly, Table 6.11 presents results for Criterion II. From there, it can be noticed, for example, that the configuration F&S4 can still produce a 35% of improvement over $\underline{J_1}^{sup}$. That is a good result compared to the 39% of improvement obtained for the ideal case. Results for F&S1 – F&S4, contrasted with the reduction from 35% to 21% of ride quality enhancement with F&S0 (ideal versus real), verify the potential of the novel suspensions (and mostly S1′ – S4′) to mitigate the actuators dynamic deteriorating effects. Furthermore, results in Tables 6.10–6.11 suggest that the potential of inerter-based suspensions for reducing the actuators size may hold

Table 6.10: Results for the system with electromechanical actuator for the settings in Table E.5 (criterion of 30% of improvement for ideal suspensions: *ideal* $\underline{J_1}^{sup} = (2.52 \pm 0.01)\,[\%g]$).

	Ride quality			**Other Indices**		
Config.	J_{1L}[%g]	J_{1M}[%g]	J_{1T}[%g]	J_2[cm]	J_3^{c}[kN]	J_3^{ac}[kN]
F&S0	3.04	1.39	**3.09** (14%)[a]	3.3	7.16	7.44
F&S1	2.76	1.27	**2.90** (19%)[a]	3.2	4.38 (39%)[b]	5.61
F&S2	2.62	1.27	**2.74** (24%)[a]	3.1	4.20 (41%)[b]	5.51
F&S3	2.56	1.17	**2.79** (23%)[a]	3.3	5.32 (26%)[b]	5.99
F&S4	2.55	1.19	**2.76** (23%)[a]	3.2	4.52 (37%)[b]	5.56
F&S5	**2.85** (21%)[a]	1.35	2.81	3.0	6.30 (12%)[b]	6.75
F&S6	**2.79** (23%)[a]	1.32	2.77	3.0	5.45 (24%)[b]	6.13

[a] Percentage of improvement in the ride quality index, $\underline{J_1}^{sup}$, with respect to the passive conventional suspension: $\underline{J_1}^{sup} = 3.60$[%g].
[b] Percentage of variation in the active force index, J_3, with respect to ${J_3}^{S0} = 5.82$[kN]

for actual implementation of this active configuration, in particular for low active gain settings.

Table 6.11: Results for the system with electromechanical actuator for the settings in Table E.6 (Criterion II (CII)—maximum deflection: *ideal* $J_2 = (3.5 \pm 0.1)\,[cm]$).

	Ride quality			**Other Indices**		
Config.	J_{1L}[%g]	J_{1M}[%g]	J_{1T}[%g]	J_2[cm]	J_3^{c}[kN]	J_3^{ac}[kN]
F&S0	2.86	1.36	2.86 (21%)[a]	3.5	8.75	8.72
F&S1	2.49	1.23	**2.50** (31%)[a]	3.5	8.27 (5%)[b]	8.34
F&S2	2.41	1.22	**2.42** (33%)[a]	3.5	7.44 (15%)[b]	7.62
F&S3	2.36	1.10	**2.45** (32%)[a]	3.5	7.40 (15%)[b]	7.68
F&S4	2.29	1.13	**2.33** (35%)[a]	3.5	8.17 (7%)[b]	8.27
F&S5	**2.65** (26%)[a]	1.31	2.57	3.5	8.62 (1%)[b]	8.38
F&S6	**2.86**	1.36	**2.86** (21%)[a]	3.5	8.75 (0%)[b]	8.72

[a] Percentage of improvement in the ride quality index, $\underline{J_1}^{sup}$, with respect to the passive conventional suspension: $\underline{J_1}^{sup} = 3.60$[%g].
[b] Percentage of variation in the active force index, J_3, with respect to ${J_3}^{S0} = 8.75$[kN]

The comparative p.s.d. plots for the vehicle body accelerations are similar to those for the modal configuration, as depicted in Figure 6.20 for the chosen example: $\ddot{z}_{vT}$ for configurations F&S3 – F&S4, contrasted with F&S0, according to Criteria I and II. By observing the plots in Figures 6.18–6.20, it can be readily checked that the novel devices provide compensation at intermediate and high frequencies as compared with F&S0. This outcome opposes what was shown by results from the implementation with ideal actuators, for which an amplification of the high frequencies occurs, specially for F&S4. As for the active forces of the front and

rear suspensions, the p.s.d. plots in Figures 6.21–6.22 show the effects of every configuration with parameter settings according to Criterion I, on both command and applied forces, for ideal and real actuators. For all the configurations with novel devices, the plots in the left column of Figures 6.21–6.22 reveal a reduction in the ideal control forces along the frequency range $0.1 - 50\,[\text{Hz}]$ in comparison with the conventional active configuration, F&S0. This holds for the p.s.d. plots obtained for the command forces and the applied forces when the actuators dynamic is inserted (right column in Figures 6.21–6.22). In particular, the devices S4′ in the configuration F&S4 cause a further reduction of the content of the active forces observed more evidently for the frequency range $10 - 30\,[\text{Hz}]$. This appears to be a consequence of the admittance damped resonance occurring at $25.66\,[\text{Hz}]$ (Figure 6.16).

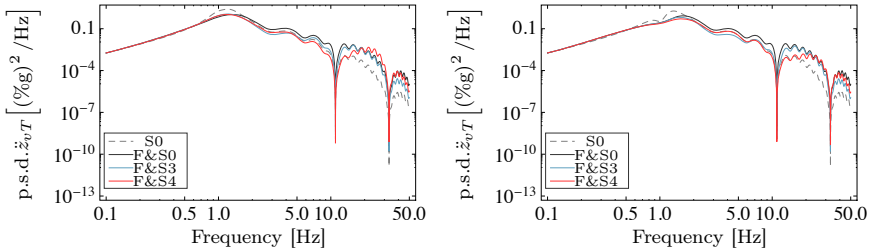

(a) Criterion I (b) Criterion II

Figure 6.20: p.s.d. plots of the vehicle body accelerations at the trailing position ($\ddot{z}_{vT}$) for configurations F&S0, F&S3, and F&S4 with suspensions settings according to Criteria I and II, and ***real*** actuators.

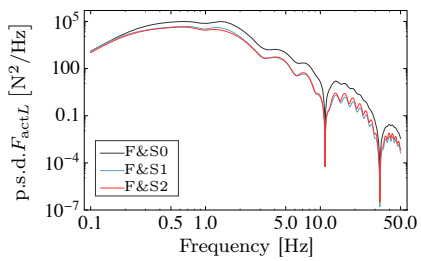

(a) With ideal actuator, $F_{\mathrm{act}L} = F_{\mathrm{c}L}$.

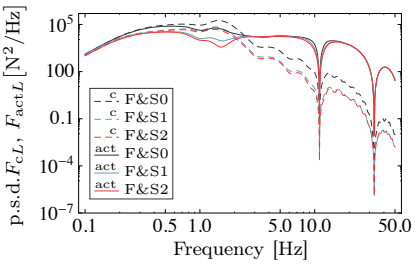

(b) With real actuator.

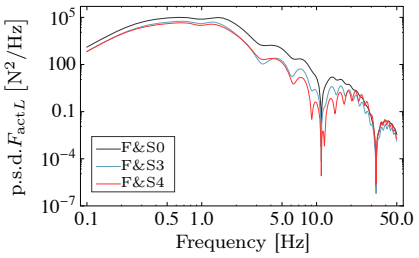

(c) With ideal actuator, $F_{\mathrm{act}L} = F_{\mathrm{c}L}$.

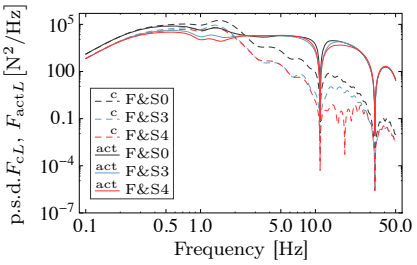

(d) With real actuator.

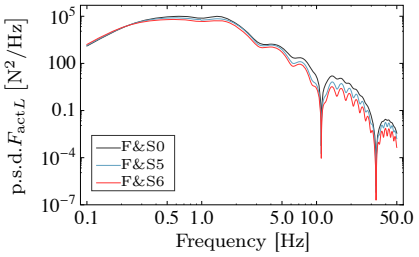

(e) With ideal actuator, $F_{\mathrm{act}L} = F_{\mathrm{c}L}$.

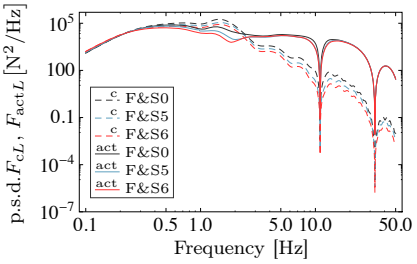

(f) With real actuator.

Figure 6.21: p.s.d. plots of the active forces applied at the leading suspension due to configurations F&S0 – F&S6 with settings according to Criterion I; left column: with ***ideal*** actuators, right column: with ***real*** actuators .

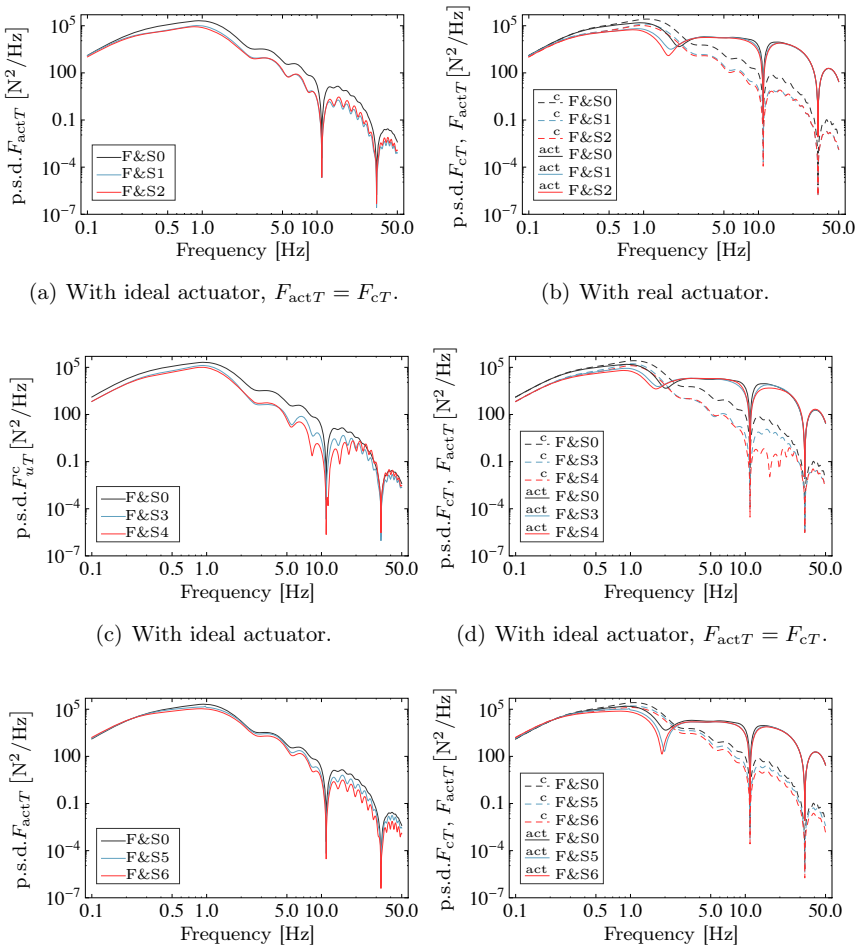

(a) With ideal actuator, $F_{\mathrm{act}T} = F_{cT}$.

(b) With real actuator.

(c) With ideal actuator.

(d) With ideal actuator, $F_{\mathrm{act}T} = F_{cT}$.

(e) With ideal actuator, $F_{\mathrm{act}T} = F_{cT}$.

(f) With real actuator.

Figure 6.22: p.s.d. plots of the active forces applied at the trailing suspension due to configurations F&S0 – F&S6 with settings according to Criterion I; left column: with ***ideal*** actuators, right column: with ***real*** actuators.

Notice, however, that the results presented here are with suspension parameters tuned for the configurations with ideal actuators, i.e. the parameters values were translated to this configuration considering the actuators dynamic without re-tuning. Results with optimal tuning of the parameters cannot be easily anticipated with the information known until here, although it is reasonable to accept the compensating effects of the inerter-based devices for the high-frequency modes inserted by the actuators dynamic as valid.

6.5 Integration with HPF Local Skyhook Damping with Adaptive Stiffness

This section validates the main results obtained from the two previous ones. It focuses on the potential of inerter-based suspensions for simplifying the design trade-off between ride quality enhancement, active forces, and suspension deflection, i.e. $\underline{J_1}^{sup}$, J_2 and J_3. For this, the methodology shown in Figure 6.2 was followed. Again, the three criteria previously considered were brought to here for discussing results on the configuration in Figure 5.11 with inerter-based devices. Two particular configurations of inerter-based devices were chosen from among the candidate layouts in Figure 5.12: S2 and S4, which were proven to be two of the most beneficial to the ride quality enhancement and active suspensions design. A high-pass filter with a corner frequency of $f_c = 0.23\,[\text{Hz}]$ was employed.

6.5.1 Analysis Phase I: Optimal solution for the integration using Local Skyhook Damping with Adaptive Stiffness

The optimal parameter settings attained for a vehicle provided with airsprings and ideal actuators driven by the HPF local skyhook damping strategy with adaptive stiffness are shown in Figure 6.23. This plot for the normalised data versus the ride quality index $\underline{J_1}^{sup}$, shows that the trend of the absolute damping coefficient, K_l, is similar to the other configurations based on skyhook damping. That result is sensible as significant improvements in the ride quality are normally achieved by increasing the dissipation/energy extraction in the system, as it was indeed proven by results from the two previous applications of skyhook damping. On the other hand, the coefficient κ for the suspension deflection regulatory part of the active strategy, which is based on adaptive stiffness, has a non-monotonic growing trend towards ride quality improvement (i.e. $\underline{J_1}^{sup}$ reduction); it reaches a maximum value together with increasing K_l and then decreases (yet for increasing K_l). This indicates that the virtual modification of the potential energy function by means of $F_{cL,T}^{J_2}$ as defined by Equations 5.23–5.25 is beneficial for high gains of the dissipative function, but within certain limits. The range at which κ optimal settings tend to decrease with increasing K_l, causes the suspension deflection index to increase rapidly with improved $\underline{J_1}^{sup}$, as one would expect with no extra aids for the suspension deflection regulation. However, this occurs for settings achieving more than 70% of improvement in the ride quality, whilst achieving still more than 50% of enhancement would not cause much modification in the suspension deflection index. The index for the control forces, J_3, also appears to be well regulated for the achievement of $\underline{J_1}^{sup}$ values above the best value achieved with the maximum value of κ. This allows to qualify

the proposed control law as an appealing strategy for improving the ride quality and a good candidate to test the potential of inerter-based devices to enhance this strategy achievements.

Once inerter-based devices are integrated to the configuration with active suspensions, again a multiobjective optimisation algorithm was employed to calculate the optimal parameter settings producing the Pareto fronts of the formulated design trade-offs. Plots in Figure 6.24 show the smoothened curves for the normalised parameters patterns defining optimal settings for each configuration, F&S2, and F&S4, and for the normalised trade-off curves, all versus $\underline{J_1}^{sup}$. As well as in the previous control configurations, the inerters parameters (i.e. b_1 for S2, and b_1 and b_2 for S4) dominate over the passive damping coefficient c_1. In fact, a pre-optimisation run suggested to keep c_1 constant to produce a better Pareto front for the configuration with S2, whilst b_1 showed a pattern similar to those observed in previous configurations. For the suspension with S4, the variability of c_1 in Figure 6.24(b) occurs mostly for low improvements of the ride quality index. b_1 starts with a high value with respect to its mean value in the range, and then starts to decrease for better ride quality. For intermediate to high improvements of $\underline{J_1}^{sup}$, b_1 shows, however, an alternating variation together with b_2 which may suggest a possibility of just needing constant values for that range of improvements (which was not tested).

To better illustrate the effects of the adaptive stiffness part of the active control law, Figure 6.25 shows the trade-off plots for the vehicle with active suspensions implementing the strategy with and without adaptive stiffness together with the conventional suspension S0 only. It also shows the trade-off plots for the strategy with skyhook damping and adaptive stiffness, integrated with S2 and with S4. The first observation is the comparison between the configurations with S0, with and without adaptive stiffness (F&S0 and F*&S0, respectively). The trend of the trade-off curves opposes the trend observed in the previous configurations integrated with inerter-based devices (see plots in Figure 6.15 for example). That is, inserting adaptive stiffness improves the trade-off curves for high values of absolute damping, K_l. When inerter-based devices are integrated to this newly proposed configuration, the trade-off curve $\underline{J_1}^{sup}$ versus J_3 shows a 'sort of' parallel displacement to the left with respect to the configuration F*&S0, i.e. without adaptive stiffness and conventional passive suspensions. Moreover, the suspension deflection index is kept for most of the ride quality improvement range, within the physical allowance. When compared to F&S0 (i.e. with adaptive stiffness), the configurations with inerter-based devices, F&S2 and F&S4, resulted more beneficial for low to intermediate improvements of ride quality, i.e. low to intermediate values of the dissipation gain, K_l, as it was found with the previous control configurations.

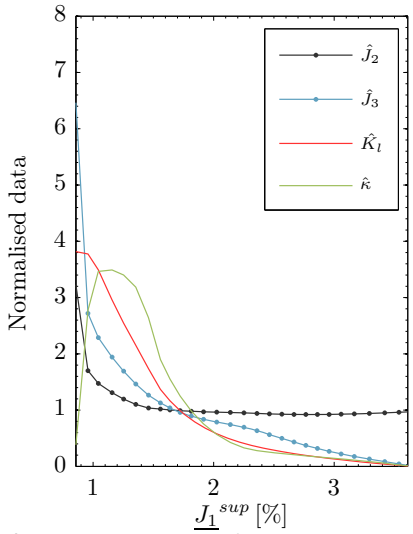

FIGURE 6.23: Optimisation results for the active configuration F&S0 [12].

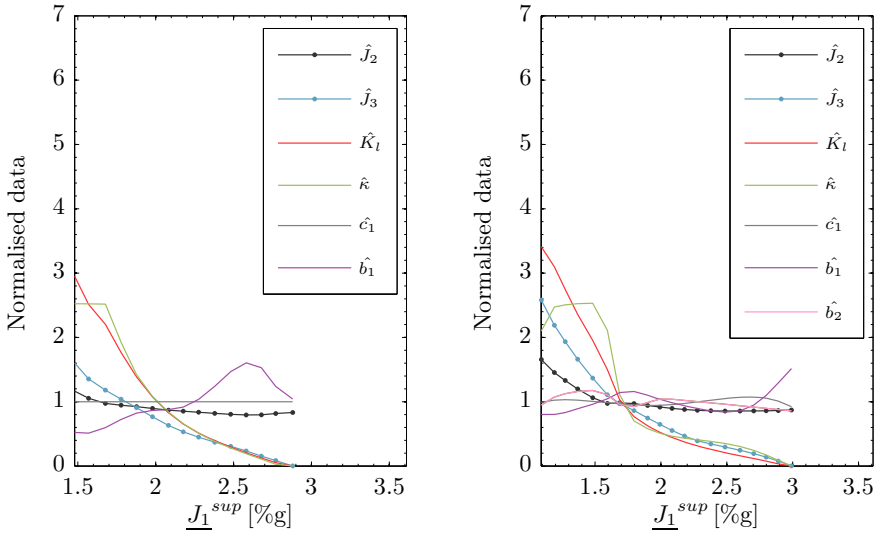

(a) F&S2 [13] (b) F&S4 [14]

FIGURE 6.24: Optimisation results for the active configurations F&S2 and F&S4.

[12] with $\hat{J}_2 = J_2/3.5$ [cm], $\hat{J}_3 = J_3/10$ [kN], $\hat{K}_l = K_l/\overline{K}_l$, $\hat{\kappa} = \kappa/\overline{\kappa}$, for the mean parameters values: $\overline{K}_l = 1.26 \times 10^5$, $\overline{\kappa} = 3.3 \times 10^6$.

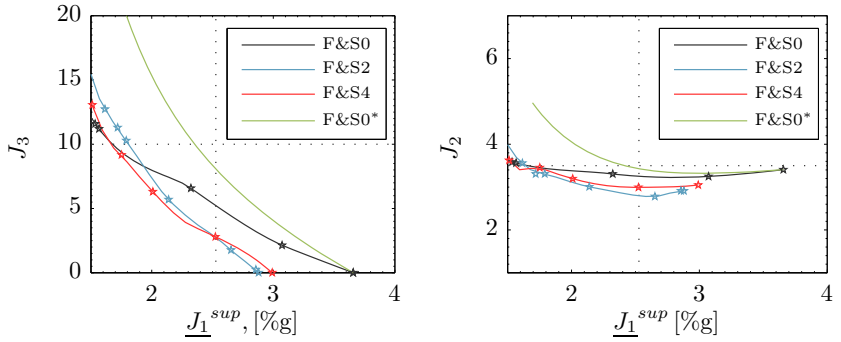

(a) $\underline{J_1}^{sup}$ versus J_3 for F&S0 compared with F&S2 and F&S4

(b) $\underline{J_1}^{sup}$ versus J_2 for F&S0 compared with F&S2 and F&S4

FIGURE 6.25: Comparison of the design trade-off curves for the vehicle with active suspensions and the candidate layouts S0, S2 and S4 from Figure 5.12.

6.5.2 Analysis Phase II: Potential of the integration using Local Skyhook Damping with Adaptive Stiffness

Results for Criteria I–III are presented in Tables 6.12–6.14; the corresponding parameter settings are provided in Appendix E, Tables E.8–E.10. In the first row of each table, relevant data for the configuration without adaptive stiffness, F*&S0, was included only for reference. The data in Table 6.12 shows that the active forces index can be reduced by 50% (i.e. from 5.65 [kN] to 2.81 [kN]) when including inerter-based devices as S2' in the secondary suspensions to produce 30% of improvement in the vehicle ride quality. Conversely, for designs allowing higher suspension deflection and active forces, the inerter-based devices did not show important benefit (see Tables 6.13–6.14). However, this is not a new result after having analysed the two other control configurations in Sections 6.3 and 6.4. What is even more remarkable from Tables 6.13–6.14 is that, within the physical constraints, it is possible to enhance the vehicle ride quality by slightly more than 50% with any of the configurations. Furthermore, from previous analyses with other control strategies, it was obtained that even if the inerter-based suspensions do not importantly benefit/deteriorate the effects of the active suspensions for settings following Criteria II and III, the devices could still be advantageous for reducing power requirements and for actuator

[13] with $\hat{J}_2 = J_2/3.5\,[\text{cm}]$, $\hat{J}_3 = J_3/10\,[\text{kN}]$, $\hat{K}_l = K_l/\overline{K}_l$, $\hat{\kappa} = \kappa/\overline{\kappa}$, $\hat{c}_1 = c_1/\overline{c}_1$, $\hat{b}_1 = b_1/\overline{b}_1$, for the mean parameters values: $\overline{K}_l = 1.038 \times 10^5$, $\overline{\kappa} = 4.4 \times 10^6$, $\overline{c}_1 = 4 \times 10^4\,[\text{Nsm}^{-1}]$ and $\overline{b}_1 = 5689[\text{kg}]$.

[14] with $\hat{J}_2 = J_2/3.5\,[\text{cm}]$, $\hat{J}_3 = J_3/10\,[\text{kN}]$, $\hat{K}_l = K_l/\overline{K}_l$, $\hat{\kappa} = \kappa/\overline{\kappa}$, $\hat{c}_1 = c_1/\overline{c}_1$, $\hat{b}_1 = b_1/\overline{b}_1$, $\hat{b}_2 = b_2/\overline{b}_2$, for the mean parameters values: $\overline{K}_l = 1.33\times10^5$, $\overline{\kappa} = 4.25\times10^6$, $\overline{c}_1 = 2.29\times10^4\,[\text{Nsm}^{-1}]$, $\overline{b}_1 = 2687[\text{kg}]$ and $\overline{b}_2 = 215[\text{kg}]$.

dynamics compensation. Analyses in this direction, however, did not enter on the objectives drawn for this strategy.

Table 6.12: Optimisation results for Criterion I (CI): 30% of improvement in the ride quality with respect to the passive conventional suspension, i.e. $\underline{J_1}^{sup} = (2.52 \pm 0.1)\,[\%g]$.

	Ride quality			Other Indices	
Config.	J_{1L}[%g]	J_{1M}[%g]	J_{1T}[%g]	J_2[cm]	J_3[kN]
F*&S0	2.29	1.14	**2.56**	3.42	7.79
F&S0	2.23	1.13	**2.46**	3.27	5.65
F&S2	2.37	1.31	**2.48**	3.06	2.81 (50%)[b]
F&S4	2.23	1.18	**2.49**	2.96	2.99 (47%)[b]

[b] Percentage of variation in the active force index, J_3, with respect to ${J_3}^{S0} = 5.65$[kN]

Table 6.13: Optimisation results for Criterion II (CII): $J_2 = (3.5 \pm 0.1)\,[\text{cm}]$.

	Ride quality			Other Indices	
Config.	J_{1L}[%g]	J_{1M}[%g]	J_{1T}[%g]	J_2[cm]	J_3[kN]
F*&S0	2.15	1.10	**2.35** (35%)[a]	3.6	10.0
F&S0	1.61	0.96	**1.65** (54%)[a]	3.5	10.2
F&S2	1.65	1.02	**1.68** (53%)[a]	3.4	11.8 (−15%)[b]
F&S4	1.63	0.98	**1.66** (54%)[a]	3.4	9.9 (3%)[b]

[a] Percentage of improvement in the ride quality index, $\underline{J_1}^{sup}$, with respect to the passive conventional suspension: $\underline{J_1}^{sup} = 3.60$[%g].
[b] Percentage of variation in the active force index, J_3, with respect to ${J_3}^{S0} = 10.22$[kN]

Figures 6.26–6.27 show the p.s.d. plots for the vehicle body accelerations at the leading and trailing positions, $\ddot{z}_{vL}$ and $\ddot{z}_{vT}$, which were extracted from time-simulation data obtained for the control configurations with settings according to Criteria I and II. As with the previous control configurations, the plots for the 30% of improvement in the ride quality (Criterion I, Figure 6.26) depict the attenuating effects of the novel devices for the low frequency range (below 3 [Hz]), together with amplification of the high frequencies. This effect can also be extracted from the plots in Figure 6.27, although low frequency benefits are not so evident. Figure 6.27, on the other hand, also shows the low frequency effects of including adaptive stiffness to the active suspensions control law. Adaptive stiffness noticeably attenuates the main vibrational mode of the system provided the active damping configuration has been set with a high gain value, K_l. Moreover, at high frequencies, adaptive stiffness causes less deteriorating effect on the vehicle body accelerations as compared with the water-

Table 6.14: Optimisation results for Criterion III (CIII): $J_3 = (10 \pm 0.1)$ [kN].

	Ride quality			Other Indices	
Config.	J_{1L}[%g]	J_{1M}[%g]	J_{1T}[%g]	J_2[cm]	J_3[kN]
F*&S0	2.15	1.10	**2.35** (35%)[a]	3.6	10.0
F&S0	1.63	0.96	**1.68** (53%)[a]	3.5	10.0
F&S2	1.78	1.08	**1.81** (50%)[a]	3.3	10.0
F&S4	1.63	0.98	**1.66** (54%)[a]	3.4	9.9

[a] Percentage of improvement in the ride quality index, $\underline{J_1}^{sup}$, with respect to the passive conventional suspension: $\underline{J_1}^{sup} = 3.60$[%g].

bed effect of inerter-based devices (or as it is expected from any linear compensator, either active or passive).

As for the control forces, Figures 6.28–6.29 show the p.s.d. plots of the active forces for the configurations F*&S0, F&S0, F&S2, and F&S4, with parameter settings according to Criteria I and II. Figures 6.30–6.31 show the corresponding deterministic active forces (in response to the deterministic profile in Equation 3.89). The p.s.d. plots show that the cost of implementing a control strategy with adaptive stiffness is that most of the frequency components of the active forces are increased in magnitude with respect to the active forces developed by the HPF skyhook damping strategy alone. This is more noticeable from the plots in Figure 6.31, for which the gain of the absolute damping coefficient, K_l, is higher. Even though, the reduction of the magnitude of control forces produced in response to the track gradient (deterministic) is considerable, specially for high improvements in $\underline{J_1}^{sup}$, as depicted in Figure 6.31. In fact, the active forces produced by this control strategy are characterised by having a low magnitude component at a particularly low frequency value, as depicted by the downside peak at about 0.2 [Hz] (Figures 6.28–6.29). Furthermore, Figure 6.28 illustrates the potential of inerter-based devices for improving the p.s.d. of the active forces for the range of low frequencies below 3 [Hz], when the optimal value of K_l acquires intermediate values, corresponding to intermediate improvements of $\underline{J_1}^{sup}$. However, Figure 6.31 shows that the novel devices do not have the same potential for high damping gains, an expected fact.

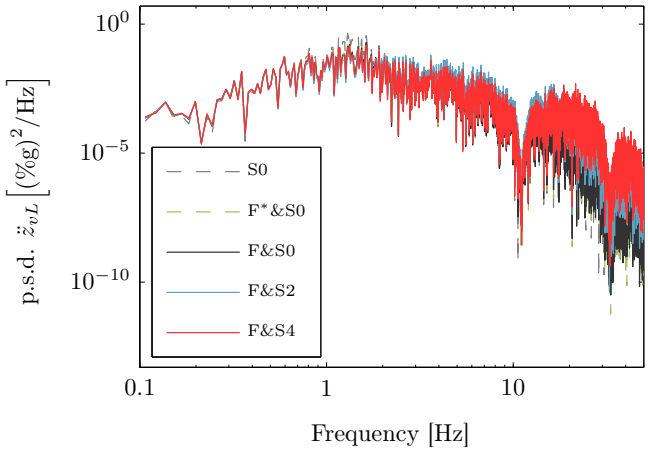

(a) Accelerations at the body leading position

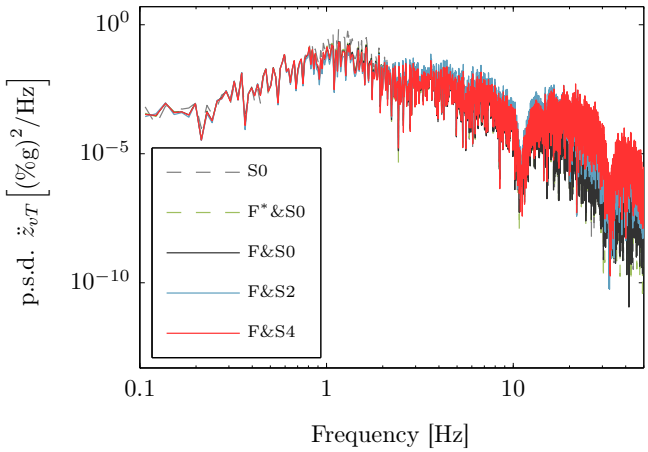

(b) Accelerations at the body trailing position

Figure 6.26: p.s.d. plots for the vehicle body acceleration at the leading and trailing position ($\ddot{z}_{vL}$ and $\ddot{z}_{vT}$, respectively) for suspension settings according to Criterion I, with ***ideal*** actuators.

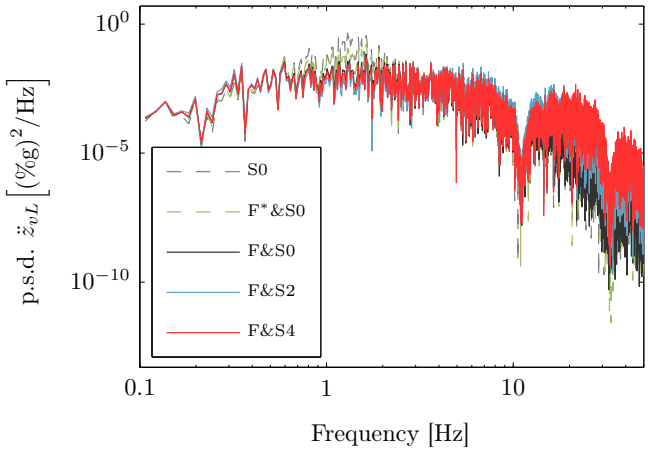

(a) Accelerations at the body leading position

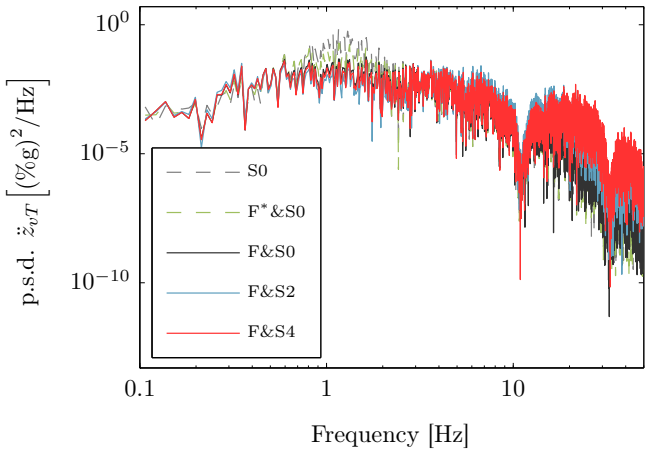

(b) Accelerations at the body trailing position

Figure 6.27: p.s.d. plots for the vehicle body acceleration at the leading and trailing position ($\ddot{z}_{vL}$ and $\ddot{z}_{vT}$) for suspension settings according to Criterion II, with ***ideal*** actuators.

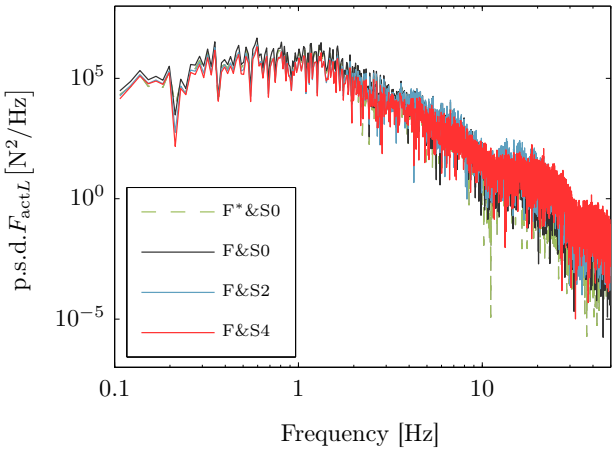

(a) Leading suspension active force

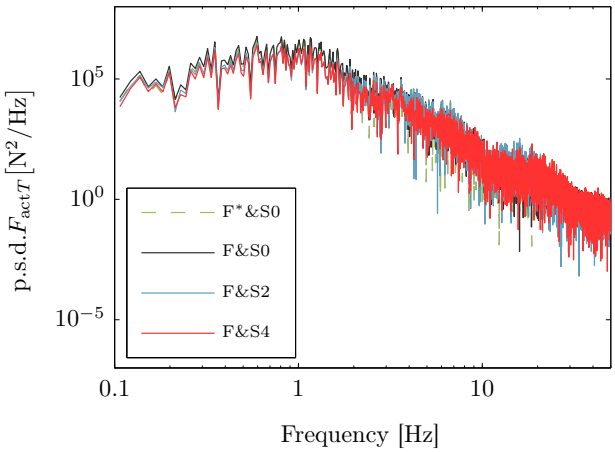

(b) Trailing suspension active force

Figure 6.28: p.s.d. plots of the active forces applied at the leading and trailing suspensions (F_L^c and F_T^c, respectively) for suspension settings according to Criterion I, with ***ideal*** actuators.

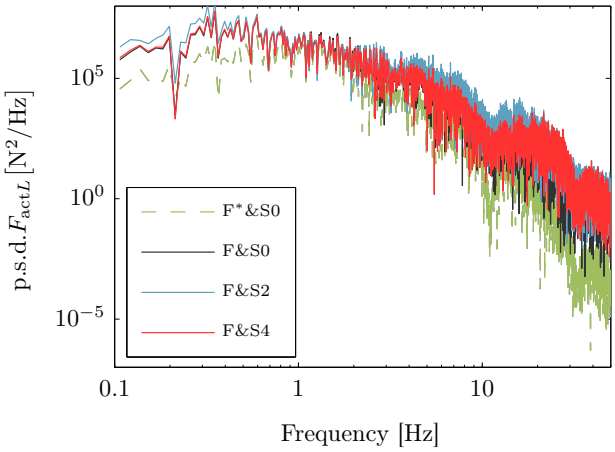

(a) Leading suspension active force

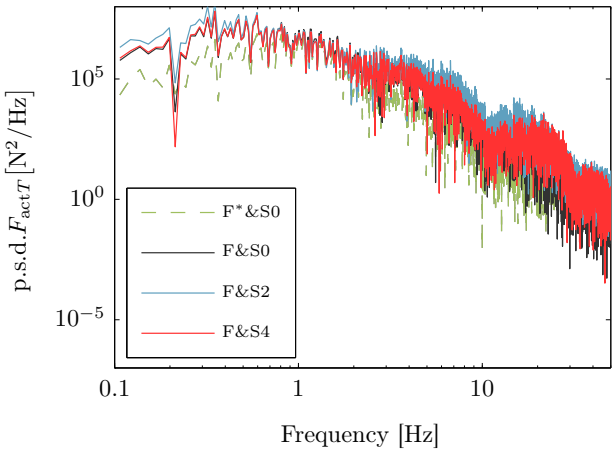

(b) Trailing suspension active force

Figure 6.29: p.s.d. plots of the active forces applied at the leading and trailing suspensions(F_L^c and F_T^c, respectively) for suspension settings according to Criterion II, with ***ideal*** actuators.

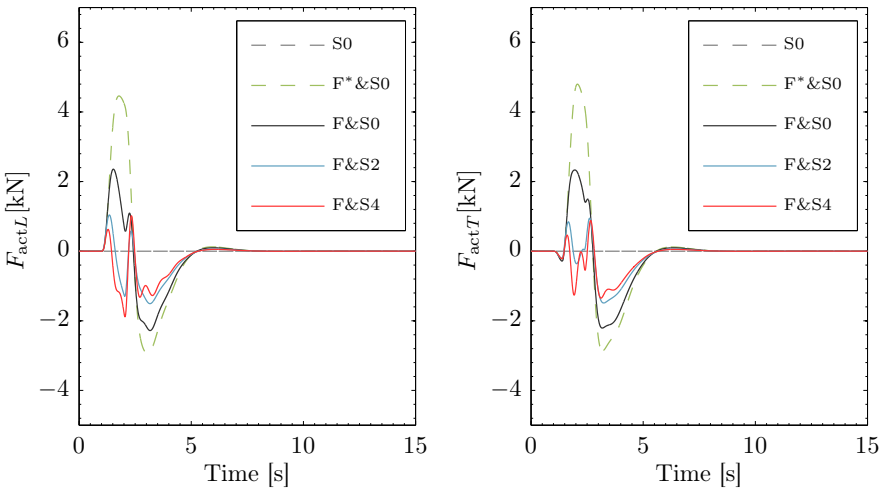

(a) Leading suspension, Criterion I (b) Trailing suspension, Criterion I

Figure 6.30: Deterministic ideal active forces applied at the leading and trailing suspensions with parameter settings for Criterion I.

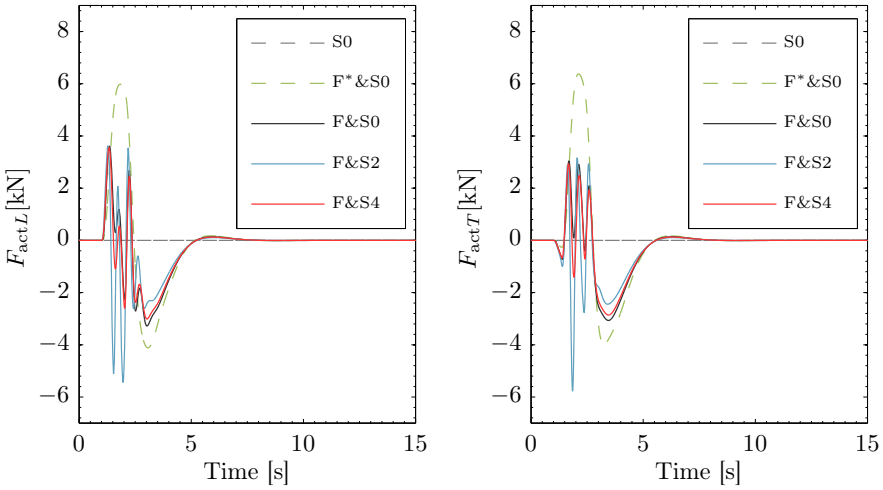

(a) Leading suspension, Criterion II (b) Trailing suspension, Criterion II

Figure 6.31: Deterministic ideal active forces applied at the leading and trailing suspensions with parameter settings for Criterion II.

6.6 Integration with LQG HPF-Output Feedback Regulator

The configuration shown in Figure 5.9 for implementation of a Linear-Quadratic Gaussian (LQG) HPF-output feedback regulator was employed as a model-based optimal control technique to validate the results associated to the design trade-off curves obtained in Sections 6.3–6.4. The inerter-based suspensions considered for this validation were S2 and S4, as it was also done for the validation presented in Section 6.5. As opposed to the previous configurations, here the parameters of the novel devices were not further optimised together with the parameters of the active control. The parameter settings for S2' and S4' were thus fixed to the optimal values attained for the vehicle with passive suspensions only, i.e. those producing behaviours as depicted in Table 6.1. Furthermore, results presented for this configuration assumed perfect actuators.

Following Equation 5.9, varying the value of the parameter ρ enables the adjustment of the control forces penalisation for the optimisation cost function. That would determine the flexibility on the control forces cost allowed in the design. Therefore, the design trade-off curves required for this analysis were obtained by assigning values of ρ within a reasonable range. It was varied from 0.25 to 10^4; a value of $\rho = 0.25$ allows high variance active forces, whilst $\rho = 10^4$ sets a very strong penalisation on the control forces amplitude causing them to be practically null. Hence, the trade-off curves resulted for a set of values for the assessment indices $\underline{J_1}^{sup}$, J_2, and J_3, obtained for the system with feedback gain matrix, $\mathbf{K}_u$, and estimation matrix, $\mathbf{K}_e$, calculated for the set of values ρ. The calculation of $\mathbf{K}_u$ and $\mathbf{K}_e$ was performed using the functions `LQOutputRegulatorGains` and `LQEstimatorGains`, respectively, from *Mathematica*®. For this, the assessment outputs and the control forces weighting matrices ($\mathbf{Q}$ and $\mathbf{R}$, respectively), appearing in the cost function J_{LQR} in Equation 5.9, were defined as

$$\mathbf{Q} = \mathbf{Q}^{\mathrm{S}} = \begin{bmatrix} \mathbf{Q}^{\mathrm{S}}_{J_1} & \mathbf{0} \\ \mathbf{0} & \mathbf{Q}^{\mathrm{S}}_{\sigma_{SDi}} \end{bmatrix} \tag{6.3}$$

with

$$\mathbf{Q}^{\mathrm{S}}_{J_1} = \begin{bmatrix} \frac{1}{\left(J^{\mathrm{S}}_{1L}\right)^2} & 0 \\ 0 & \frac{1}{\left(J^{\mathrm{S}}_{1T}\right)^2} \end{bmatrix} \text{ and } \mathbf{Q}^{\mathrm{S}}_{\sigma_{SDi}} = \begin{bmatrix} \frac{1}{\left(\sigma\left(x^{\mathrm{S}}_{iD1}\right)\right)^2} & 0 \\ 0 & \frac{1}{\left(\sigma\left(x^{\mathrm{S}}_{iD2}\right)\right)^2} \end{bmatrix}, \text{ and}$$

$$\mathbf{R} = \begin{bmatrix} \frac{1}{\left(\sigma^{\mathrm{Max}}_{Fc}\right)^2} & 0 \\ 0 & \frac{1}{\left(\sigma^{\mathrm{Max}}_{Fc}\right)^2} \end{bmatrix} \tag{6.4}$$

This basically follows Bryson's rule [155]. The super-index 'S' in Equation 6.3 (and therefore in the entries of $\mathbf{Q}^{\mathrm{S}}_{J_1}$ and $\mathbf{Q}^{\mathrm{S}}_{\sigma_{SDi}}$) was used to denote 'suspension layout', i.e. S0, S2, S4. Thus, for every configuration F&S0, F&S2, and F&S4, a different $\mathbf{Q}$ matrix was calculated; the indicated r.m.s. values $J^{\mathrm{S}}_{1L,\,T}$ and $\sigma\left(x^{\mathrm{S}}_{iD1,\,2}\right)$ were obtained for the vehicle with every candidate layout. Defining $\mathbf{Q}$ this way, normalises the assessment outputs according to their values for every particular case, and sets a standard for the calculation of the optimal solution to allow for comparisons. On the other hand, the value $\sigma^{\mathrm{Max}}_{F_c}$ for the definition of the matrix $\mathbf{R}$ was based on the consideration that the maximum value allowed for the variance of the control forces applied at the leading and trailing suspensions was $\sigma^{\mathrm{Max}}_{F_c} = 4\,[\mathrm{kN}]$. For the optimal estimator, the autocorrelation matrices of the input and measurement noises, were defined as $\mathbf{W} = p\,\mathbf{I}_{4\times4}$ (with $p = 5.43\times10^{-4}\,\left[\left(\mathrm{m\,s^{-1}}\right)^2\right]$ from Equation 3.88), and $\mathbf{V} = v_\theta^2\,\mathbf{I}_{4\times4}$, with v_θ arbitrarily defined as a very low value under assumption of almost 'perfect' measurements ($v_\theta = 5\times10^{-6}$).

6.6.1 Analysis Phase I: Optimal solution for the integration using LQG-HPF Output Regulator

The trade-off curves obtained from the recently described settings for the optimal control problems solved for every configuration are shown in Figure 6.32. The trend of the curves for $\underline{J_1}^{sup}$ versus J_3 (Figure 6.32–left), and $\underline{J_1}^{sup}$ versus J_2 (Figure 6.32–right) validates the results obtained in the previous sections. That is, further improvement of the design trade-offs is attained with the insertion of inerter-based devices (configurations S2 and S4) for low to intermediate improvements of $\underline{J_1}^{sup}$, associated with low to intermediate feedback gains (see Appendix E). For high improvements in the ride quality, however, the inerter-based devices fail to provide benefits in terms of the simplification of the design trade-offs. Nevertheless, the settings for which the novel devices do not provide benefit correspond to settings for F&S0 for which the physical constraints are violated (i.e. $J_2 > 3.5\,[\mathrm{cm}]$, and J_3 is elevated with respect to the typical value of $10\,[\mathrm{kN}]$).

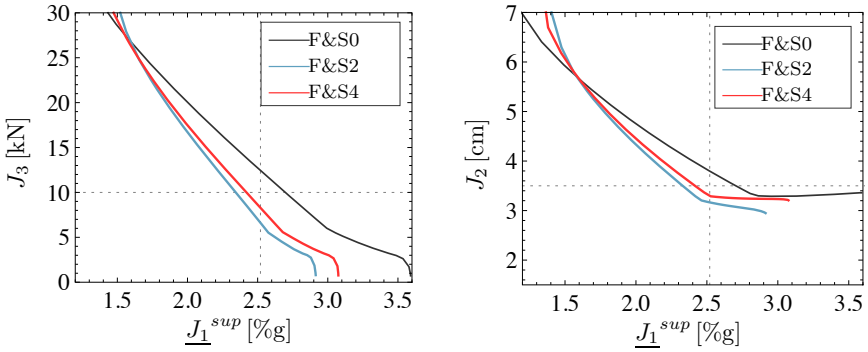

FIGURE 6.32: Comparison of the design trade-off curves for the vehicle with active suspensions and the candidate layouts S0, S2 and S4 from Figure 5.12.

6.6.2 Analysis Phase II: Potential of the integration using LQG-HPF Output Regulator

Results for Criteria I–III are presented in Table 6.15; the settings of the regulator, and hence the estimator, are the same for Criteria II and III. For Criterion I, it was obtained that for producing 30% of improvement in the ride quality $\underline{J_1}^{sup}$, the force index J_3 exceeds the typical maximum value of 10 [kN], and also slightly exceeds the space constraint of 3.5 [cm]. Combining the active control configuration with inerter-based devices eases the problem; a vehicle with secondary suspensions as F&S2 (F&S4) would achieve 30% of improvement in the ride quality with 47% (34%) of reduction in the active forces index respecting the suspension clearance constraint. Therefore, the ride quality that could be achieved with the available suspension clearance and with average size actuators is better when either S2′ or S4′ is integrated to the active suspension. Indeed, these enable up to 33–35% of performance enhancement, contrasted with 25% of benefit provided by the active suspensions only, following Criteria II and III. Plots for the p.s.d. of the vehicle body accelerations at the leading and trailing position, $\ddot{z}_{vL}$ and $\ddot{z}_{vT}$, respectively, and for the ideal control forces applied at the leading and trailing suspensions, $F_{\text{act}L} = F_{cL}$ and $F_{\text{act}T} = F_{cT}$, also respectively, are provided in Figures 6.33–6.34 for the three criteria. The p.s.d. plots for the vehicle body accelerations are very similar to those presented in Sections 6.3–6.4, which validates what has been discussed before. As a particularity, for the active forces, $F_{\text{act}L}$ and $F_{\text{act}T}$, it is remarkable the more pronounced, attenuated component of the p.s.d. plots for the configuration F&S2 around the frequency of the vehicle body bounce mode (0.99 [Hz]).

Besides the need of examining the potential of inerter-based devices for the suspension system performance, for example, or their effects to compensate for real actuat-

ors dynamic, obtaining the optimal values of the parameters of the novel devices may produce even better results than those presented here. Nevertheless, the validation objective was accomplished with the assumed fixed settings.

Table 6.15: Optimisation results for Criteria I–III

Config.	**Ride quality** [%g]			**Other Indices**	
	J_{1L}	J_{1M}	J_{1T}	J_2[cm]	J_3[kN]
Criterion I: $\underline{J_1}^{sup} = (2.52 \pm 0.1)$ [%g]					
F&S0	2.21	1.14	**2.52**	3.8	12.4
F&S2	2.32	1.28	**2.53**	3.2	6.5 (47%)[b]
F&S4	2.20	1.17	**2.53**	3.3	8.2 (34%)[b]
Criteria II and III: $J_2 = (3.5 \pm 0.1)$ [cm] and $J_3 = (10 \pm 0.2)$ [kN]					
F&S0	2.35	1.17	2.70 (25%)[a]	3.5	10.0
F&S2	2.17	1.23	2.34 (35%)[a]	3.5	10.2
F&S4	2.12	1.15	2.42 (33%)[a]	3.5	10.0

[a] Percentage of improvement in the ride quality index, $\underline{J_1}^{sup}$, with respect to the passive conventional suspension: $\underline{J_1}^{sup} = 3.60$[%g].
[b] Percentage of variation in the active force index, J_3, with respect to ${J_3}^{S0} = 12.4$[kN].

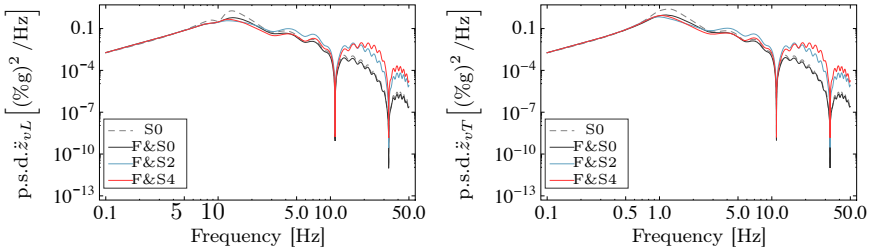

(a) Vehicle body acceleration at the leading position

(b) Vehicle body acceleration at the trailing position

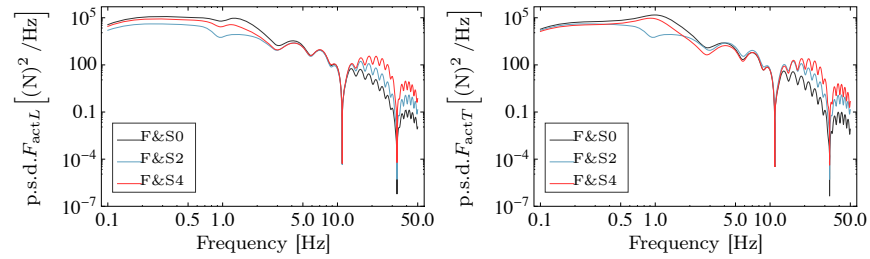

(c) Active forces applied at the leading suspensions, $F_{\text{act}L} = F_{cL}$

(d) Active forces applied at the trailing suspensions, $F_{\text{act}T} = F_{cT}$

Figure 6.33: p.s.d. plots of the vehicle body accelerations and the ideal active forces applied at the leading and the trailing suspensions for settings according to Criterion I (30% of improvement). Comparison for passive and active conventional suspensions (S0 and F&S0, respectively), with the combinations F&S2 and F&S4.

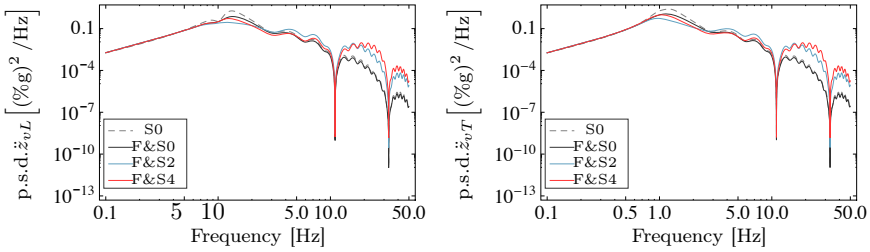

(a) Vehicle body acceleration at the leading position

(b) Vehicle body acceleration at the trailing position

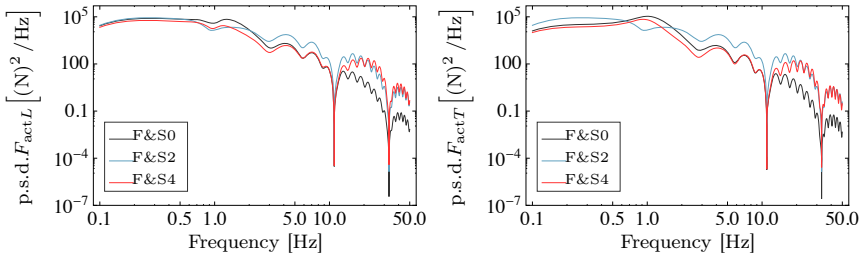

(c) Active forces applied at the leading suspensions, $F_{\text{act}L} = F_{\text{c}L}$

(d) Active forces applied at the trailing suspensions, $F_{\text{act}T} = F_{\text{c}T}$

Figure 6.34: p.s.d. plots of the vehicle body accelerations and the ideal active forces applied at the leading and the trailing suspensions for settings according to Criterion II (3.5 [cm] for the suspension deflection index, J_2). Comparison for conventional (passive and active, S0 and F&S0, respectively) suspensions, with the combinations F&S2 and F&S4.

6.7 Comparison Among Control Strategies

The integration of inerter-based suspensions with each control strategy showed similar characteristics in the trade-off curves for the least ride quality index, $\underline{J_1}^{sup}$, versus the active forces index, J_3, and similarly for the trade-off curves for the least ride quality index, $\underline{J_1}^{sup}$, versus the suspension deflection index, J_2. When comparing the corresponding tables of results for Criteria I–III further conclusions can be extracted. Tables 6.16–6.18 summarise the results for Criteria I–III, respectively, for the configurations: F&S0, F&S2, and F&S4, according to each active control structure.

Table 6.16: Result comparison for each active strategy according to Criterion I (30% of improvement on $\underline{J_1}^{sup}$ w.r.t. the ride quality of the vehicle with conventional passive suspensions, S0.)

	Improvement on J_3	
Control strategy / *Configuration:*	F&S2	F&S4
Modal HPF skyhook damping (J_3 =5.44 [kN])[a]	38%	41%
Local skyhook damping with complementary filtering (J_3 =10.71 [kN])[a]	35%	36%
Local HPF skyhook damping with adaptive stiffness (J_3 =5.65 [kN])[a]	50%	47%
LQG-HPF output feedback regulator (J_3 =12.4 [kN])[a]	35%	36%

[a] J_3 value attained for the conventional active configuration F&S0

Table 6.17: Result comparison for each active strategy according to Criterion II ($J_2 = 3.5$ [cm])

	Improvement[a] on $\underline{J_1}^{sup}$		
Control strategy / *Configuration:*	F&S0	F&S2	F&S4
Modal HPF skyhook damping	41%	45%	44%
Local skyhook damping with complementary filtering	35%	37%	39%
Local HPF skyhook damping with adaptive stiffness	54%	53%	54%
LQG-HPF output feedback regulator	25%	35%	33%

[a] w.r.t. $\underline{J_1}^{sup}$ for the conventional passive configuration, S0.

Following results for Criterion I, Table 6.16 shows that:

1. The index J_3 assessing the magnitude of the active forces required to achieve 30% of improvement in the least ride quality index of the vehicle (as compared to the vehicle with conventional passive suspensions) is lower for Modal HPF skyhook damping and Local HPF skyhook damping with adaptive stiffness strategies.

2. Introducing inerter-based suspensions as S2′ and S4′ in parallel to the airsprings integrated with active suspensions (i.e. implementing F&S2 or F&S4 with ideal actuators), with any of the four control strategies, helps to reduce the active forces index J_3 as compared to the J_3-value obtained for the respective conventional active configuration F&S0. In fact, J_3 can be reduced by 35% and more, according to the control strategy.

3. The configuration with Local HPF skyhook damping with adaptive stiffness

Table 6.18: Result comparison for each active strategy according to Criterion III ($J_3 = 10\,[\text{kN}]$)

	Improvement[a] **on** $\underline{J_1}^{sup}$		
Control strategy / *Configuration:*	F&S0	F&S2	F&S4
Modal HPF skyhook damping	43%	47%	46%
Local skyhook damping with complementary filtering	29%	34%	35%
Local HPF skyhook damping with adaptive stiffness	53%	50%	54%
LQG-HPF output feedback regulator	25%	35%	33%

[a] w.r.t. $\underline{J_1}^{sup}$ for the conventional passive configuration, S0.

strategy was more effected by the insertion of the inerter-based suspensions S2′ and S4′ towards the reduction of the active forces index J_3. In fact, J_3 was reduced by a half for the configuration F&S2.

On the other hand, according to Criterion II, Table 6.17 shows that:

1. The configurations with Local HPF skyhook damping with adaptive stiffness strategy, with and without inerter-based devices, provide better improvements in the least ride quality index $\underline{J_1}^{sup}$ (as compared to the vehicle with conventional passive suspensions) than the other control strategies, followed by Modal HPF skyhook damping; up to 54% of reduction in $\underline{J_1}^{sup}$ is attained with the former.

2. For all the control strategies, excepting Local HPF skyhook damping with adaptive stiffness, implementing F&S2 or F&S4 with ideal actuators helps to enhance the improvements provided by the active configuration. For Local HPF skyhook damping with adaptive stiffness strategy, the improvements on $\underline{J_1}^{sup}$ are about the same for F&S0, F&S2, and F&S4.

3. The lower the improvement on $\underline{J_1}^{sup}$ given by the active suspensions alone with the airsprings (i.e. F&S0), the higher the enhancement given by the insertion of either S2′ or S4′ (i.e. F&S2 or F&S4, respectively).

Similar observations to these for Criterion II apply for the data contained in Table 6.18 for Criterion III.

Analyses extracted Tables 6.16–6.18 clearly reveal a potential of the inerter-based suspensions S2′ and S4′ for enhancing the ride quality of a railway vehicle equipped with active suspensions, and to reduce the levels of demanded forces to achieve certain levels of improvement. Moreover, the outcomes indicate that the benefits

on ride quality enhancement and active forces reduction provided by inerter-based suspensions do not depend strictly on the control strategy but on the degree of improvement in $\underline{J_1}^{sup}$ with respect to the default passive configuration, or equivalently, on the levels of relative effort demanded to the —ideal— actuators. The term 'relative' is adopted to indicate: with respect to each control strategy average active force. This remark is reinforced by the trade-off curves shown in Figures 6.4, 6.15, 6.25, and6.32.

6.8 Final Comments

The benefits of the inerter-based suspensions for the implementation of active suspensions, as studied in this chapter, can be naturally associated to an advantageous modification of the total energy function of the system, as addressed in Section **??**. Particularly, an inerter-based device with a zero of the admittance function located in the origin (e.g. S1', S2' and S3') such that its frequency-characteristic is: inerter-like for low frequencies, damper-like for intermediate frequencies, and spring-like for high frequencies (see Figure 6.5 for example) accepts a direct relation with the ideal inerter for low frequencies. Hence, the results associated with reducing the active forces index J_3 can be clearly associated to what was envisaged from the —more abstract— analyses performed for the potential of an ideal inerter based on the vehicle body kinetic energy function in Subsection 4.3, and on the stochastic mean power dissipated in the passive suspensions in Subsection 4.4. This excludes the structure S5' as it does not develop an inerter-like behaviour in the frequency domain (Figure 5.12). Moreover, the fact that some structures provide further benefit (or degradation as in some cases with S6') than others, depends on the degree of freedom of the corresponding admittance function to change with the frequency, i.e. on the number of poles and zeros and their location in the complex plane. The potential of the inerter-based devices proposed in Figure 5.12 for performing mechanical control tasks was evidenced. Furthermore, a cooperative work between inerter-based novel devices and active suspensions designed for ride quality is feasible.

6.9 Summary of the Chapter

Results and discussions presented in this chapter demonstrated potentials of inerter-based suspensions integrated with ideal active suspensions driven by four different control configurations with low to intermediate feedback gains, in general, for:

- Enhancing the ride quality for configurations with the same active force index, J_3.

- Reducing the active forces while producing the same ride quality.
- Regulating the suspension deflection without deteriorating the ride quality.

An extended study with the implementation of well established skyhook damping configurations, also showed:

- Enhancement of the passive suspensions stochastic mean power dissipation.
- Reduction of the active suspensions stochastic mean power extracted, and thus required by perfect actuators.

Furthermore, the inerter-based suspensions in ideal configurations as tested for Criteria II and III (i.e. with higher feedback gains) produce ride quality and active forces indices similar to those for active suspensions alone with airsprings. However, it was found that the integration benefits the dissipation in the passive suspensions and therefore reduces the power demand which may become an advantage for real implementations, i.e. when the actuators efficiency is not ideal. For further improvements, the active forces index increases for the integrated suspensions and thus, effects on power demand may be reverted.

In addition, a short study on effects on the system with real actuators suggested the inerter-based devices potential for compensating the deteriorating effects of the actuators dynamic even with high feedback gains, together with a reduction of the magnitude of the required active forces. From the ideal configurations, the candidate layouts S2, S3 and S4 were found to be more beneficial.

The following few pages summarise the main achievements through plots obtained from time domain simulations for the vehicle with the four active configurations discussed in this chapter and the effects of inerter-based devices for vehicle body acceleration, and stochastic and deterministic active forces, all assessed at the trailing position as an illustrative example. These suspensions are with settings focused upon the 30% of improvement in the ride quality criterion.

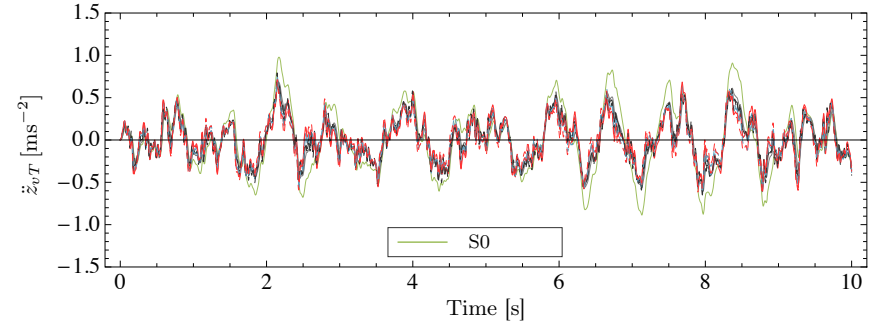

(a) Vehicle body acceleration.

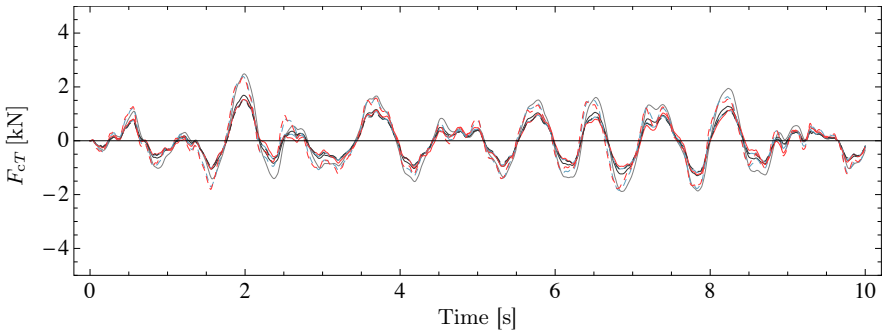

(b) Stochastic (ideal) active force.

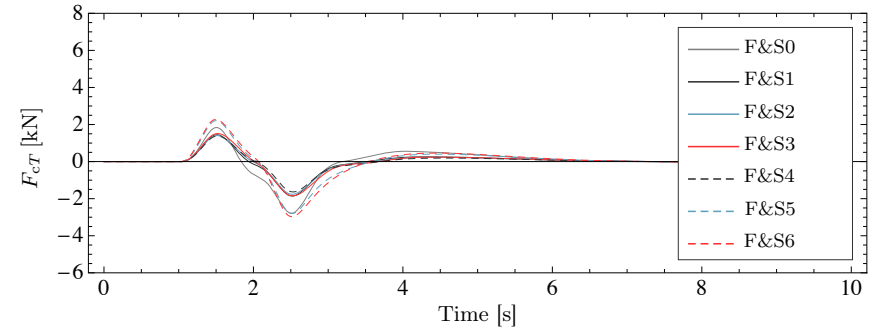

(c) Deterministic active force.

Figure 6.35: Time response for performance variables assessed at the trailing position of the vehicle for the integration with modal skyhook damping in the secondary suspensions.

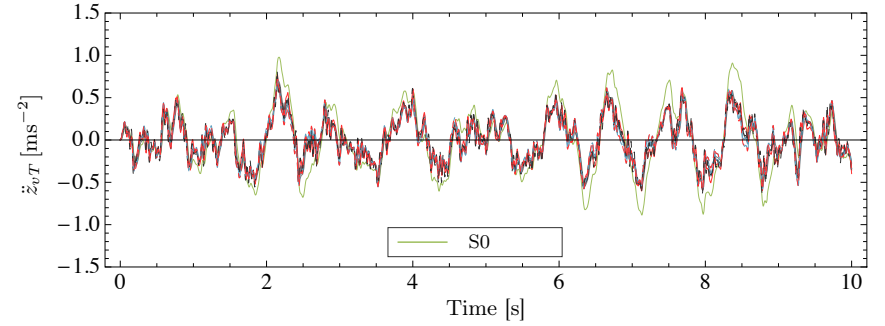

(a) Vehicle body acceleration.

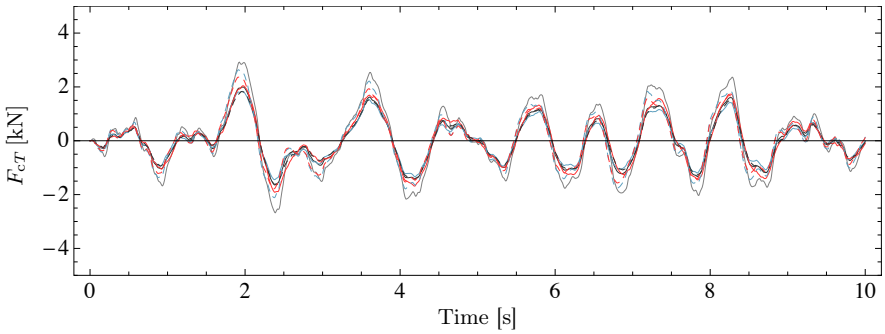

(b) Stochastic (ideal) active force.

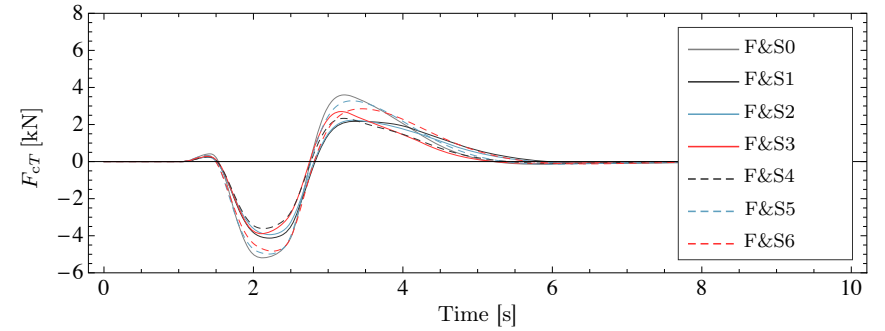

(c) Deterministic active force.

Figure 6.36: Time response for performance variables assessed at the trailing position of the vehicle for the integration with local skyhook damping and complementary filtering.

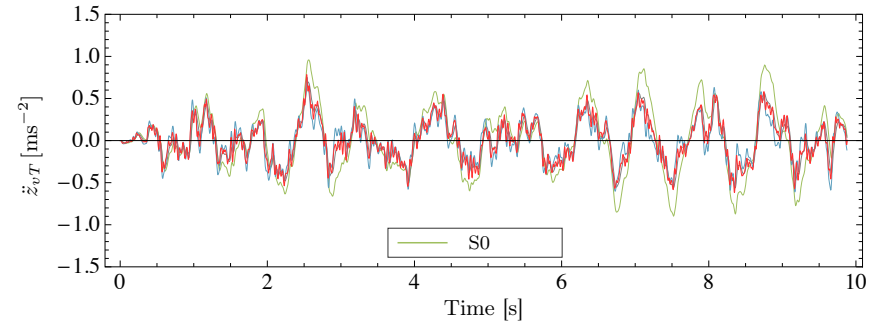

(a) Vehicle body acceleration.

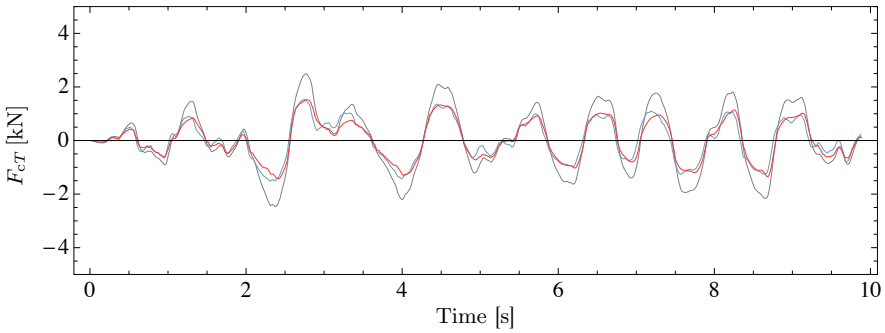

(b) Stochastic (ideal) active force.

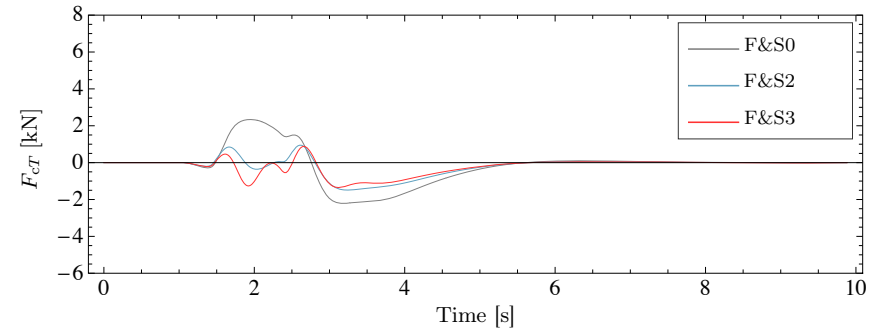

(c) Deterministic active force.

Figure 6.37: Time response for performance variables assessed at the trailing position of the vehicle for the integration with HPF local skyhook damping regulated by adaptive stiffness.

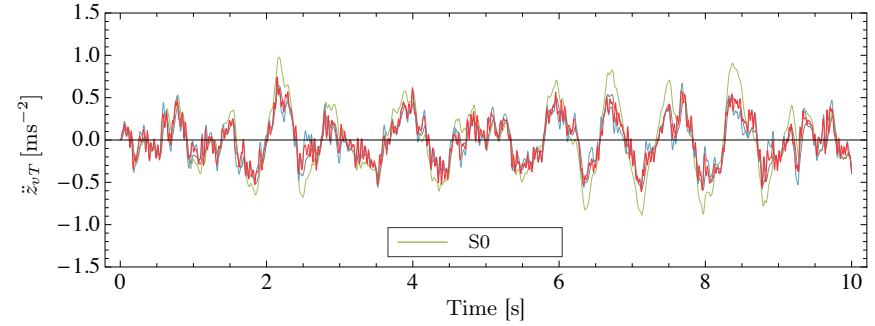

(a) Vehicle body acceleration.

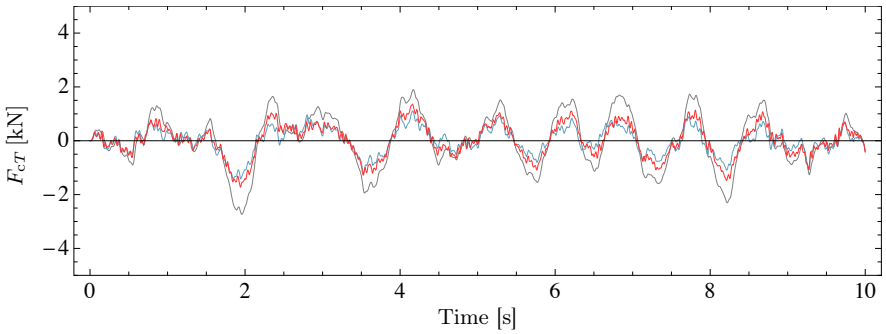

(b) Stochastic (ideal) active force.

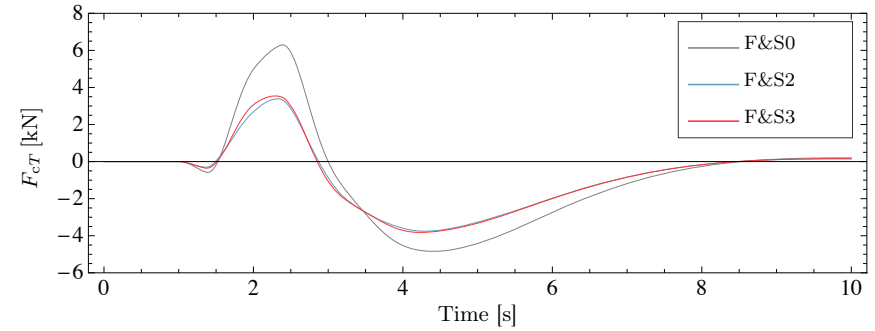

(c) Deterministic active force.

Figure 6.38: Time response for performance variables assessed at the trailing position of the vehicle for the integration with Linear-Quadratic Gaussian (LQG) HPF-output feedback regulator.

7

Integration Test in Advanced Simulation

This chapter reports results attained using a more complex model of a railway vehicle developed by SIMPACK®, a multi-body simulation (MBS) software with dedicated functionalities for railway dynamics simulation. The aim is to ensure that the general trends regarding application of the inerter that have been identified in Chapter 6 using simplified models, are still relevant with a more complex model. A simple control test was performed in the MBS software by integrating modal control with an inerter-based configuration to the conventional secondary suspensions of the vehicle model.

7.1 Advanced Modelling of a Railway Vehicle

To examine the effects of integrating inerters to the active secondary suspensions of a more complex model of a railway vehicle, the simplified example model from the Manchester Benchmark [27, 28] available for the rail add-on module of SIMPACK, SIMPACK Wheel/Rail, was used. However, the type of vehicle considered for the Manchester Benchmark differs from that modelled for the studies presented earlier in this thesis, particularly in the type of secondary suspensions that each model includes. The former includes secondary suspensions comprising a parallel arrangement (shear) spring and damper, instead of airsprings. Nevertheless, the model is still useful to provide some validation of the outcomes from some of the results presented in Chapter 6.

SIMPACK is a Multi-body simulation (MBS) software dedicated to the simulation of mechanical and mechatronic systems [156]. It enables the creation of a model by using either SIMPACK-code or a graphical interface to build up the system by

interconnecting elements (e.g. rigid bodies, force elements, joints, contacts, substructures) with geometry and characteristics defined as required. User-elements with geometry and specifications imported from CAD models are also supported. The building-up process is based on a tree structure so that the inertia frame sets the global reference and the bodies reference frame and their interconnections are generated from there, outwards. The definition of markers easily allows the setting of the interconnection points and the placement of sensors and actuators, for example. From this type of definition, SIMPACK can generate the equations that characterise the system's kinematics and dynamics; specifically, it generates one equation for each degree-of-freedom defined in the model. It comprises linear and nonlinear solvers and a post-processing interface from which a range of specialised analyses can be performed, including animation of the dynamics and the eigenmodes of the system. It also features model and data exporting, and co-simulation with other computational tools. As for adding control capabilities to the model, SIMPACK has control elements which integrate the basic elements of a feedback system: measurements, filtering, control structure, and actuators dynamic. That allows to import control elements created in other dedicated software either as an embedded element or for co-simulation (e.g. with MATLAB/Simulink). Nevertheless, as SIMPACK also enables the creation of user-functions, control schemes with simple structure can be easily created within the MBS software.

7.1.1 Specifications of the base model

It corresponds to a bogied vehicle comprising seven rigid bodies: vehicle body (passengers cabin), two bogie rigid frames, and two solid-axle wheelsets per bogie. Force elements provide the linkages between the bodies. In particular, the secondary suspensions are defined as a shear spring placed in parallel with a damper with variable friction coefficient (in the range of 5×10^3 [Nsm^{-1}]) and finite rod stiffness (6×10^6 [Nm^{-1}]). It imports data for modelling the rail/wheel contact, and a curved track is defined by default. The base model results in a model with 158 states, which includes the 3D dynamics of the vehicle bodies, suspensions, linkages, and track. The system has 44 vibration eigenmodes; the body and bogies pitch and bounce modes are shown in Table 7.1. Figure 7.1 shows a 3D view of the model on a straight track.

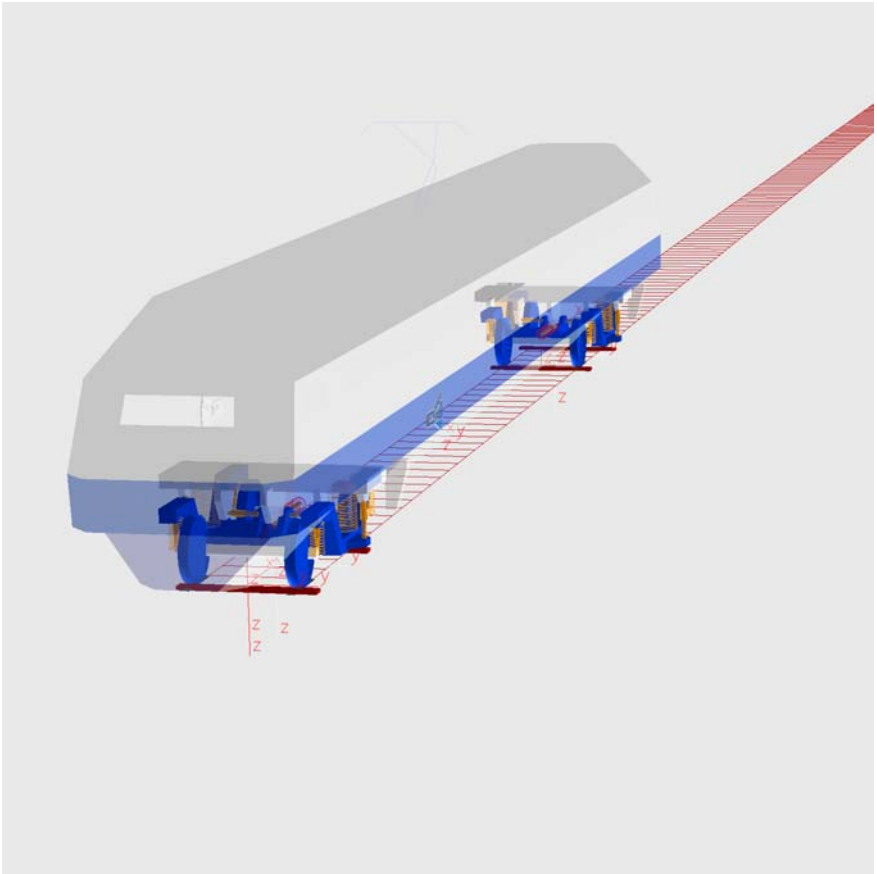

Figure 7.1: SIMPACK railway vehicle example model on a straight track.

Table 7.1: Vibration eigenmodes of the vehicle body and bogies –SIMPACK Model

Mode	Frequency [Hz]	Damping [%]
Vehicle body bounce	1.28	25.7
Vehicle body pitch	1.56	29.8
Leading bogie bounce	11.67	36.2
Trailing bogie bounce	11.89	36.5
Leading bogie pitch	10.07	6.1
Trailing bogie pitch	10.08	6.1

7.1.2 Modifications to the base model

In order to carry-out the required analysis for assessing the vehicle vertical ride quality, the following modifications to the default model were performed:

- The curved track was replaced by a straight track with stochastic irregularities (Track/Road Related Excitation with a shape filter polynomial) .
- Quasi-linear contact geometry (harmonic linearisation) was used instead of the pre-defined nonlinear (Hertzian).
- Sensors and control elements were placed accordingly.
- The travelling speed was set to $55\,[\mathrm{ms}^{-1}]$.
- The value of the parameters in Table 7.2 were changed in order to make a better approximation to the characteristics of the mathematical model used along this thesis.

Table 7.2: Modification of parameter values for the railway vehicle example by SIMPACK

Parameter	Default model	Change
Secondary spring stiffness	$0.43\,[\mathrm{MNm}^{-1}]$	$0.75\,[\mathrm{MNm}^{-1}]^a$
Vehicle body mass	$32000\,[\mathrm{kg}]$	$38000\,[\mathrm{kg}]$
Vehicle body inertia in the pitch direction	$1.97\,[\mathrm{MNm}^2]$	$2.31\,[\mathrm{MNm}^2]$
Bogies mass	$2615\,[\mathrm{kg}]$	$2500\,[\mathrm{kg}]$
Bogies inertia in the pitch direction	$1476\,[\mathrm{kgm}^2]$	$2000\,[\mathrm{kgm}^2]$

[a] This approximates the high-frequency static stiffness of the airspring

7.2 Implementation of the Integrated Suspension

For this test, modal skyhook damping with high-pass filtering strategy was chosen to be integrated with the most simple inerter-based structure from those presented in Chapter 5, i.e. S1' in Figure 5.12. Recall here that the candidate structure S1' corresponds to an inerter in series with fixed-value stiffness and damping elements (approximating a mechanical inerter stiffness and internal friction). Thus, the purpose of this study was to examine the effects of varying the inertance value, as well as the control parameters, to the vertical ride quality index $\underline{J_1}$ and to the stochastic suspensions' deflection and active forces. This exercise considered only the stochastic irregularities of the track, i.e. no analysis was performed with deterministic features. The following describes the implementation of the integration in SIMPACK.

7.2.1 Inerter-based device implementation

The implementation of the inerter-based device was performed by using a control element, as its linear dynamic is approximated by a transfer function characterising its mechanical complex admittance. For this, measurement of the relative velocity of the vertical motion of each secondary suspension, no filtering and ideal actuation were required. An alternative to this, would have been to use SIMPACK force elements, but a new element to model the inerter element would have been required.

7.2.2 HPF modal skyhook damping implementation

For implementation of active suspensions with modal skyhook damping control, accelerometers for measuring pitching and bouncing accelerations at the vehicle body centre of gravity were incorporated, as well as an actuator with perfect dynamic in parallel to each suspension. The acceleration measurements were integrated and filtered by second-order filters as described in Section 5.3.1.1, with corner frequencies of $f_{cb} = 0.225\,[\text{Hz}]$ and $f_{c\rho} = 0.179\,[\text{Hz}]$ for the bounce and pitch measurements, respectively, which were the settings used in Chapter 6 for the same configuration (Section 6.3).

7.2.3 Parameter tuning

Manual tuning for vertical ride quality improvement was performed on the three parameters considered, K_b and K_ρ, from the control structure described in Section 5.3.1.1 (Figure 5.8), and b_1 for the inerter-based structure S1' in Figure 5.12.With this manual procedure, no value for the damping coefficient K_b, for a fixed value of

the corner frequency f_{cb} , was found to benefit the ride quality. Thus, K_b was set to zero and K_ρ and b_1 were adjusted to the best possible values to obtain different sets of parameters, enabling the aimed comparisons.

7.3 Simulation Results and Analysis

Due to the difficulty of performing manual tuning, only three meaningful sets of parameters $K_\rho - b_1$ were obtained for the integration active-plus-novel-passive after a trial-error procedure. In the same way, a good setting for the gain K_ρ of the only active configuration was attained. In order to validate the effect of the implemented configurations, the bar plots in Figure 7.2 illustrate the modification of the damping ratio of the relevant modes with respect to those for the conventional model, for the 'best value' of K_ρ for the only-active configuration, and for the settings $K_\rho - b_1$ for the integration. These relevant modes are specifically: the body bounce and pitch vibrational modes, and the bounce mode of the leading and trailing bogies. It is easily observed that the active configuration in fact improves the damping coefficient for the body pitch mode only, due to the nature of the feedback control law. The pitch mode is further enhanced by the insertion of the inerter-based devices (S1') which compensates for the relative dynamic at the location of every suspension. Therefore, also the bounce mode of the vehicle body and the two bogies are modified. A lower value of inertance b_1 (6000 [kg]) enhances the damping ratio of the vehicle body bounce mode by more than 50% as compared with the mode for the conventional suspension, and the suspensions with only active configuration. For the bounce mode of the bogies, the increased damping given by a passive novel structure with low inertance value is attained for the trailing bogie, whilst the converse is attained for the leading bogie (i.e. increased inertance values improves the bounce mode of the leading bogie, instead). By comparing Figure 7.2(d) to Figure 7.2(c), it can be extracted that the best improvement is attained for $b_1 = 6000$ [kg], which is an important result for reducing the transmission of the vibrations to the vehicle pitch mode as this normally effects more the ride quality at the rear end of the vehicle body. As for the vibrational modes for the other DoF of the system –not associated with the side-view dynamics, these remain mostly unaltered. As expected, that includes also the wheelsets and track vertical modes which are rather constrained.

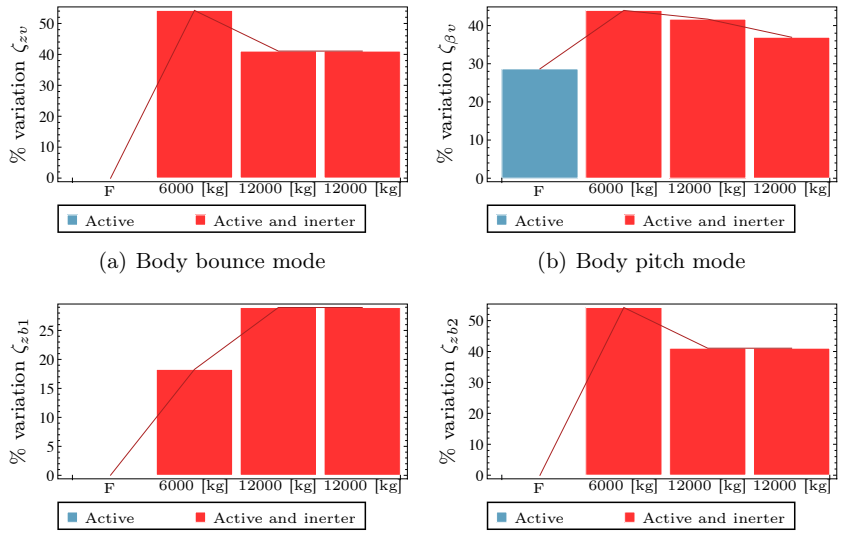

(a) Body bounce mode

(b) Body pitch mode

(c) Leading bogie bounce mode

(d) Trailing bogie bounce mode

Figure 7.2: Damping ratio variation of relevant dynamic modes with different parameter settings.

Results including the trend of the plots for the values of K_ρ and b_1, together with the resultant trade-off plot for the stochastic *active* force applied at the right-leading suspension (F_{FR}) are illustrated in Figure 7.3, against the least vertical ride quality index, $\underline{J_1}^{sup}$. Although very few points could be attained to produce the plots, it can be checked that the trend of the parameters tuning is consistent with the results obtained for the planar side-view model presented in Chapter 6 for different strategies and inerter-based structures. That is, increasing the control gain would require a decreasing inertance value in order to cause further improvements in the least ride quality of the vehicle. Table 7.3 summarises the ride quality indices $\underline{J_1}$ and the maximum r.m.s. values of the active forces applied at the leading and trailing suspensions (i.e. F_{FR}: active force applied at the leading-right suspension, and F_{RL}: active force applied at the trailing-left suspension), for the corresponding time-domain responses.

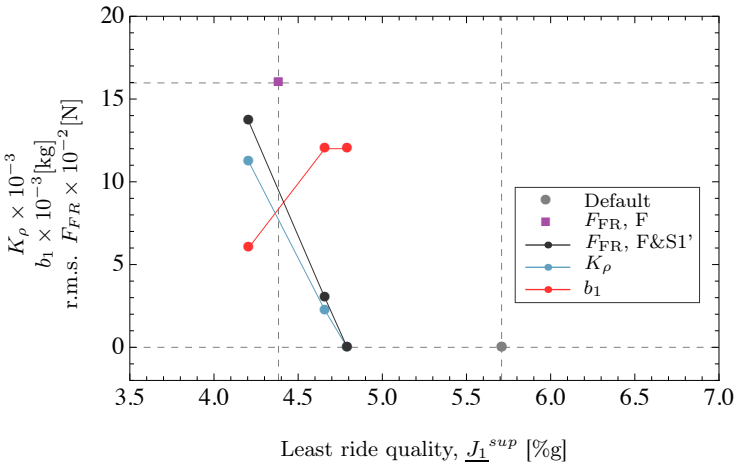

Figure 7.3: Trend of the integrated suspension parameter tuning and the maximum r.m.s. force related to the least ride quality index. A contrast with the ride quality for the conventional passive and for the conventional active suspension with the 'best' manual setting can be readily done.

Table 7.3: Data obtained for the controlled SIMPACK model performance indices with different settings

Configuration	**Ride quality [%g]**			**Force [kN] (r.m.s.)**	
Setting	J_{1L}	J_{1M}	J_{1T}	F_{FR}	F_{RL}
Conventional	3.98	2.24	5.71	0	0
Only active:					
$K_\rho = 12925$	4.20	2.45	4.38	1.6	1.6
Integration 1:					
$K_\rho = 11244$,					
$b_1 = 6000$ [kg]	4.17	2.19	4.20	1.4	1.3
Integration 2:					
$K_\rho = 2249$,					
$b_1 = 12000$ [kg]	4.38	2.38	4.66	0.3	0.3
Integration 3:					
$K_\rho = 0$,					
$b_1 = 12000$ [kg]	4.14	2.14	4.79	0	0

As for a comparison between the force requirements of the configuration with only modal skyhook damping and the integrated configuration with inerters, it can be extracted from the plot in Figure 7.3 that for achieving a ride quality $\underline{J_1}^{sup}$ of 4.38 [%g]

(23% of improvement with respect to the ride quality of the conventional vehicle, 5.7 [%g]), the r.m.s. value of the maximum stochastic force required by the active suspensions is of 1.6 [kN] (F_{FR} as it resulted for the front-right suspension) for the normal active configuration. When the active suspensions are integrated with inerter-based structures, the plot suggests that this value may lower to 0.97 [kN] , i.e. a reduction of 39% to achieve the same least ride quality value, $\underline{J_1}^{sup} = 4.38$ [%g]. Similarly, the the following results were obtained from optimal settings of the same control configuration for the model used for Chapter 6. To achieve 23% of ride quality improvement with the configuration F&S0 (i.e. without inerters), a maximum r.m.s. of active force of 727 [N] is required, whilst for F&S1 (i.e. with inerters), the maximum r.m.s. of active force is of 392 [N]. This means a reduction of the maximum r.m.s. active force by 46%, which agrees with the 39% of reduction for the test performed in SIMPACK. The same correspondence between outcomes from the two models is expected for the response to deterministic track profiles, as well as with other integrated suspension configurations. Further relevant tests were left for a more dedicated work on complex simulations in a future project.

Finally, an example of the time-domain responses obtained by simulation in SIMPACK is shown in Figure 7.4. The plots are for the integrated suspensions with settings as in the row 'Integration 1' from Table 7.3.

Figure 7.4: Time-domain simulations in SIMPACK for the vehicle with active-plus-novel passive suspensions according to the 'integration 1' (Table 7.3).

7.4 Summary of the Chapter

This chapter has reported results attained from SIMPACK® modelling and simulation for a simple validation of the effectiveness of integrating active suspensions dedicated to provide absolute damping to the vehicle body with inerter-based suspensions. Although no exhaustive study using this complex model was done, results achieved from manual tuning of the configurations parameters give a good suggestion on the validity of the achievements for the lower-degree of complexity planar side-view model of the vehicle. In fact, the test performed here showed that for enhancing the vehicle ride quality for the Manchester Benchmark by 23%, inserting a mechanical inerter in parallel to the actuator for each suspension and using the Modal Skyhook Damping strategy, a can reduce the r.m.s. value of the active force by 39%. Similarly, for the model in Chapter 6, a reduction of 46% was attained.

8

Potential of the Inerter for Lateral Stability with Active Solutions

8.1 Introduction

Besides the complete study developed in this thesis for the design of secondary suspensions for ride quality, this chapter presents an investigation on the potential of active-plus-novel-passive solutions using the inerter concept for problems associated to the lateral and yaw vehicle dynamic characteristics. The content of this chapter is only an initial assessment for those problems with this type of synergetic solutions. It concerns wheelset stability control and examines the effects of the proposed solutions on the wheelsets' curving performance. This is an approach that is different to the ones arising from current literature on inerters for railway vehicles [18, 19, 22, 16, 20]. In particular, it investigates the performance merits of introducing the inerter together with the concept of active stability control of wheelsets via the absolute stiffness approach [1].

8.2 Lateral Dynamics Control

Lateral and yaw motions of the bogies are usually controlled by primary suspensions, with the main concern being the vehicle running behaviour at the wheel-rail interface, for which a design conflict between kinematic stability and curving performance exists. A detailed description of previously reported control strategies for active primary suspensions appeared in [10, 157].

The essential kinematic instability of the solid axle wheelsets in the lateral plane of the vehicle is explained in the literature, where the sustained oscillations of the wheelsets are normally referred as *hunting*. Active solutions for the wheelsets' hunting problem re-locate the unstable poles of the wheelsets to the stable semi-plane by employing either lateral or yaw actuation controlled by feedback of yaw angles or lateral velocities, for example. Yaw damping, both relative and absolute yaw stiffness, and lateral damping are some of the previously studied and widely known stabilising solutions in this field. The current study considers the application of frequency dependent relative yaw stiffness through the use of novel mechanical devices. It aims to complement the active control strategy based on absolute yaw stiffness to reduce the required active torques.

Beyond stability, the forces emerging from the wheel-rail interface when wheelsets negotiate curved tracks impose additional requirements to the design. Although the synergetic approach studied here does not directly address the curving problem, analysis on the effects on the creep forces, the bodies' dynamic characteristics, and the control torques is also provided here.

As a background note, steering control is the type of active solution dedicated to solve the curving problem, and is normally separated from stability control solutions. This is dedicated to the 'perfect curving' [157], and in a simplified manner for curves with constant radius, it targets:

- equal lateral creep forces on all the wheelsets to minimise track shifting forces (some lateral creep is required in order to provide the necessary force to counterbalance the centrifugal force on curves [55]), and
- zero quasi-steady state longitudinal creep forces on all wheelsets (longitudinal creep forces are associated to wear and noise and thus the requirement design is to significantly reduce them).

8.3 Mathematical Modelling of the Plan-View

The mathematical model approximating the lateral and inherent dynamics of a railway vehicle with respect to the natural equilibrium condition can be described by linear differential equations [40, 158]. The modelling is based upon the plan-view schematic representation in Figure 8.1. The use of linearised models is a normal practice in the design of active controllers. This is justified by the fact that active solutions reasonably overcome the effects of non-linearities associated with the rail-wheel contact effects and other sources of non-linear behaviour [120], in particular

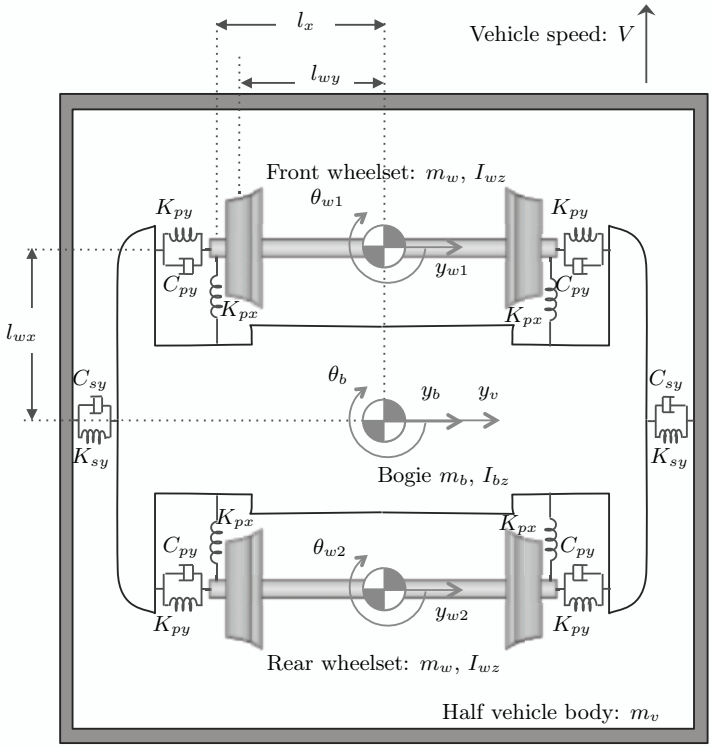

Figure 8.1: Plan-view model of a half-vehicle system.

avoiding significant contact between the wheel flange and the rail. The mathematical description employed here for the assessment of a railway vehicle stability control corresponds to half of the vehicle comprising a two-axle bogie and half-vehicle body. Primary and secondary suspensions in the vehicle provide the vertical linkages between the solid-axle wheelsets and the bogie frame, and the bogie frame and the vehicle body, respectively. In the model, the lateral and longitudinal stiffness of the primary suspension were considered. As for damping, only the lateral primary damping was modelled (i.e. the longitudinal damping of the primary suspensions was neglected). Likewise, the lateral stiffness and damping of the secondary suspension were included.

The wheelsets consist of two wheels with conical profile rigidly joined together through a common solid axle, for which a nominal conicity coefficient, λ, and radius, r_0, are assumed. For linear models describing the facts of the dynamic necessary for stability control design, rail/wheels interaction is typically described by the creep forces arising at the contact points as consequence of the difference in creepages of the wheels and the track (Figure 8.2). Longitudinal and lateral creep forces with ideally constant creep coefficients, f_{11}, and f_{22} are considered [47, 30], which are

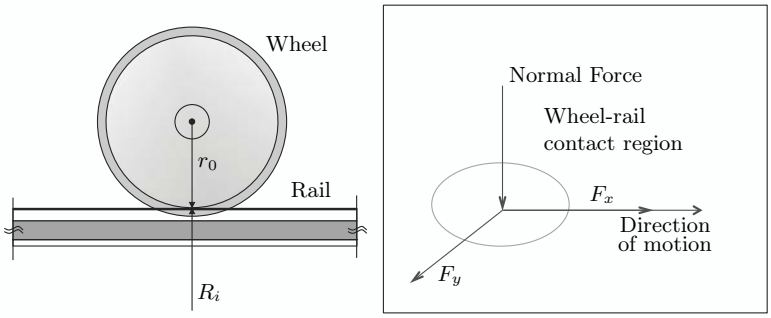

Figure 8.2: Wheel/rail contact diagrams. Left: principal wheel and rail radii of curvatures. Right: Longitudinal and lateral creep forces.

given for every wheelset by:

$$F_x = -2f_{11}l_{wy}\left(\frac{1}{V}\dot{\theta}_w - \frac{1}{R}\right) - \frac{2f_{11}\lambda}{r_0}\left(y_w - y_t\right) \tag{8.1}$$

$$F_y = -2f_{22}\left(\frac{\dot{y}_w}{V} - \theta_w\right) \tag{8.2}$$

respectively.

Table 8.1 lists the parameters and the corresponding numerical values for the schematic diagram in Figure 8.1. The differential equations (8.3)–(8.8) represent the dynamics of the seven degrees-of-freedom of the vehicle, namely: the lateral displacement and yaw angle of the wheelsets, respectively y_{wi} and θ_{wi} for i=1, 2 (1: front, 2: rear), and the bogie, respectively y_b and θ_b, and also the vehicle body lateral motion y_v. This model for stability and curving assessment (including the parameters assumed for the default setting) combines the models in [159, 20], except for the disregarded longitudinal primary damping and that the steering linkage is not included. Instead, passive suspensions replacing the conventional stabilising yaw stiffness were placed in the longitudinal direction on each side of the wheelsets.

$$\begin{aligned} m_w\ddot{y}_{w,i} =& 2k_{py}\left(y_b + (-1)^{i-1}\,l_{wx}\theta_b - y_{w,i}\right) + F_{y,i} \\ &+ 2c_{py}\left(\dot{y}_b + (-1)^{i-1}\,l_{wx}\dot{\theta}_b - \dot{y}_{w,i}\right) \end{aligned} \tag{8.3}$$

$$\begin{aligned} I_{wz}\ddot{\theta}_{w,i} =& 2k_{px}l_x^2\left(\theta_b - \theta_{w,i} - (-1)^i\,\frac{l_{wx}}{R_i}\right) + l_{wy}F_{x,i} \\ &+ \tau_{pn,i} + \tau_{u,i} \end{aligned} \tag{8.4}$$

$$
\begin{aligned}
m_b\ddot{y}_b =& 2k_{py}\left(y_{w1}+y_{w2}-2y_b\right)+2k_{sy}\left(y_v-y_b\right)\\
&+2c_{py}\left(\dot{y}_{w1}+\dot{y}_{w2}-2\dot{y}_b\right)+2c_{sy}\left(\dot{y}_v-\dot{y}_b\right)\\
&+\frac{m_bV^2}{2}\left(\frac{1}{R_1}+\frac{1}{R_2}\right)-m_bg\left(\frac{\theta_{c1}+\theta_{c2}}{2}\right) \qquad (8.5)\\
I_{bz}\ddot{\theta}_b =& 2k_{py}l_{wx}\left(y_{w1}-y_{w2}-2l_{wx}\theta_b\right)\\
&+2k_{px}l_x^2\left(\theta_{w1}+\theta_{w2}-2\theta_b-\frac{l_{wx}}{R_1}+\frac{l_{wx}}{R_2}\right) \qquad (8.6)\\
&+2c_{py}l_{wx}\left(\dot{y}_{w1}-\dot{y}_{w2}-2l_{wx}\dot{\theta}_b\right)\\
&-\left(\tau_{pn1}+\tau_{pn2}\right)-\tau_{u1}-\tau_{u2} \qquad (8.7)
\end{aligned}
$$

$$
\begin{aligned}
m_v\ddot{y}_v =& 2k_{sy}\left(y_b-y_v\right)+2c_{sy}\left(\dot{y}_v-\dot{y}_v\right)\\
&+\frac{m_vV^2}{2}\left(\frac{1}{R_1}+\frac{1}{R_2}\right)-\frac{m_vg}{2}\left(\theta_{c1}+\theta_{c2}\right) \qquad (8.8)
\end{aligned}
$$

It is noticeable from the model above that the suspensions in the longitudinal direction affect the wheelsets and bogie frame yaw mode only, through the developed passive torques $\tau_{pn,i}$. This is explained by the symmetric allocation of those suspensions in the plane with respect to the centre of gravity of the bogie and every wheelset. That partly justifies the nature of the absolute stiffness feedback configuration employed for active steering control (τ_{u1} and τ_{u2} in the model), as discussed later. It is also worth noticing that assessing the wheelsets (and hence vehicle) stability requires only the zero input dynamic model, i.e. all the input terms associated to the track geometry: curve radius, cant, and irregularities, are removed from Equations 8.3–8.8.

For simulations and optimisation purposes, the state-space representation of this open-loop model was derived as

$$\dot{x}=A\,x+B\,u+B_\eta\,\eta \qquad (8.9)$$

$$y_o=C_o x \qquad (8.10)$$

$$y_m=C_m x \qquad (8.11)$$

Table 8.1: Parameter values for the (half-vehicle) Plan-View model

Sym.	Parameter	Value
V	Vehicle speed [ms^{-1}]	55
m_w	Wheelset mass [kg]	1376
I_{wz}	Wheelset yaw inertia [kgm^2]	766
m_g	Bogie frame mass [kg]	3477
I_{gz}	Bogie frame yaw inertia [kgm^2]	3200
m_v	Half vehicle body mass [kg]	17230
r_0	Wheel radius [m]	0.445
λ	Wheel conicity	0.3
f_{11}	Longitudinal creepage coefficient [N]	10^7
f_{22}	Lateral creepage coefficient [N]	10^7
l_{wx}	Semi-longitudinal spacing of wheelsets [m]	1.225
l_{wy}	Half gauge of wheelset [m]	0.75
l_x	Semi-lateral spacing of steering linkages and primary longitudinal suspension [m]	1.2
k_{px}	Primary longitudinal stiffness per axle box [Nm^{-1}]	10^6
k_{py}	Primary lateral stiffness per axle box [Nm^{-1}]	4.71×10^6
c_{py}	Primary lateral damping per axle box [Nsm^{-1}]	1.2×10^4
k_{sy}	Secondary lateral stiffness per axle box [Nm^{-1}]	2.45×10^5
c_{sy}	Secondary lateral damping per axle box [Nsm^{-1}]	2×10^4
R	Radius of the curved track [m]	1500
$\theta_{c,i}$	Cant angle of the curved track [rad]	$6 \times \pi/180$
g	Gravity [ms^{-2}]	9.81

with

$$x=[\dot{y}_{w1},\, y_{w1},\, \dot{\theta}_{w1},\, \theta_{w1},\, \dot{y}_{w2},\, y_{w2},\, \dot{\theta}_{w2},\, \theta_{w2},\, ... \tag{8.12}$$

$$\dot{y}_b,\, y_b,\, \dot{\theta}_b,\, \theta_b,\, \dot{y}_v,\, y_v,\, {}^1/_{R_1},\, {}^1/_{R_2}]^T \tag{8.13}$$

$$u=[\tau_{u1},\, \tau_{u2},\, \tau_{pn1},\, \tau_{pn2})^T \tag{8.14}$$

$$\eta=[{}^1/_{\dot{R}_1},\, \theta_{c1},\, y_{t1},\, {}^1/_{\dot{R}_2},\, \theta_{c2},\, y_{t2}]^T \tag{8.15}$$

$$y_o=[F_{x1},\, F_{x2},\, F_{y1},\, F_{y2}]^T \tag{8.16}$$

$$y_m=[\theta_{w1},\, \theta_{w2},\, \dot{\theta}_b - \dot{\theta}_{w1},\, \dot{\theta}_b - \dot{\theta}_{w2}]^T \tag{8.17}$$

where u is the vector of the active and passive control inputs applied to the system, η are the exogenous inputs from the railway track as required by the model, y_o are the outputs related to the performance of the excited system, and y_m are the variables/measurements to be fed back through the passive and active control configurations described in this paper.

8.4 Absolute Stiffness Stability Control [1]

Highly stiff passive connections in the longitudinal direction between every axle and the bogie frame of a railway vehicle are known to provide the required levels of wheelset stability at high speeds on straight tracks [7, 1, 72, 73]. However, since the bogie is relatively light, the two wheelsets and bogie become strongly coupled. The consequence is that an even higher longitudinal stiffness is necessary to achieve satisfactory stability levels, but because this stiffness also affects curving performance there is an increase in wheel and rail wear.

A practical approach using passive suspensions for a *track-friendly* bogie was developed for the Swedish Green Train research and development programme [72, 73]. Dampers allocated between the bogies and the vehicle body in the longitudinal direction were proven to stabilise the yaw motion of the bogie and the lateral oscillations above certain travelling speed. In particular, the authors in [72, 73] showed that adding yaw damping this way would compensate for lower guiding stiffness.

Also, a range of active solutions to the conflicting problems has been proposed. In particular, Mei and Goodall in [1] presented an effective implementation for stiffness-based stabilisation in contrast with the conventional passive stiffness, the absolute stiffness –*skyhook stiffness* approach. This is an active configuration in which a longitudinal/yaw force/torque proportional to the high-pass filtered absolute wheelset yaw angle is applied between every wheelset and the bogie frame. The strategy decouples the wheelset dynamics, preventing their stability being affected by the bogie dynamic and hence overcoming the complexity of the wheelsets stabilisation due to the wheelsets and bogie interaction. As pointed out by Mei and Goodall [1] the use of pure absolute yaw stiffness would cause problems for curving, so the high-pass filtering is necessary. In this manner absolute stiffness is an appealing solution to the stability problem.

The implementation of the strategy in this approach consists of the measurement of the wheelsets' yaw angles, which are filtered using individual second order high-pass filters of the same cut-off frequency, and are fed-back through a proportional controller to the respective actuators mounted between the wheelsets axles and the bogie frame applying the control torques, as represented in Figure 8.3 and Equation (8.18):

$$\hat{\tau}_{u,i} = -K_u \left(\frac{s^2/(2\pi f_c)^2}{s^2/(2\pi f_c)^2 + 1.414\, s/2\pi f_c + 1} \right) \hat{\theta}_{w,i} \tag{8.18}$$

The controllable realisation of (8.18) is obtained in A_τ, B_τ, C_τ, D_τ for a definition of the individual sub-systems (i.e. front—$i = 1$ and rear—$i = 2$ controllers) in the

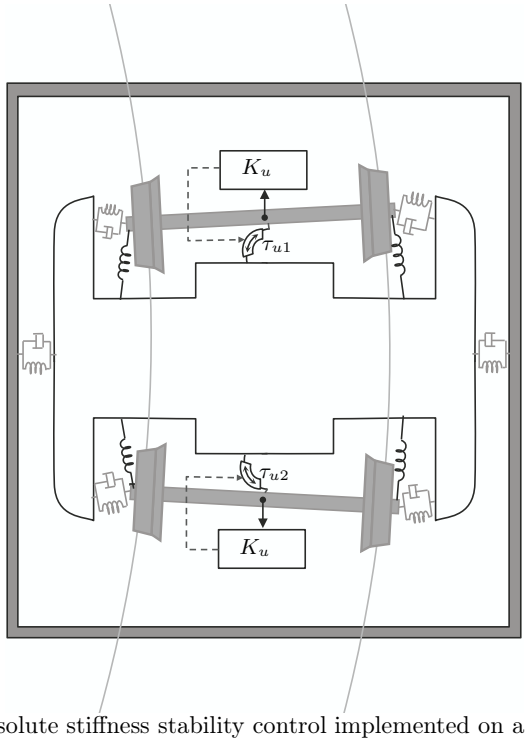

Figure 8.3: Absolute stiffness stability control implemented on a half-vehicle model.

state-space as

$$\dot{x}_{\tau,i}{=}A_\tau\, x_{\tau,i} + B_\tau\, \theta_{w,i} \tag{8.19}$$

$$\tau_{u,i}{=}C_\tau\, x_{\tau,i} + D_\tau\, \theta_{w,i} \tag{8.20}$$

Variants of the implementation would be the estimation of the wheelsets' yaw angle if the physical measurements are difficult to obtain, and/or to use linear actuators in the longitudinal direction instead of rotational ones. Here, the availability of the measurements and ideal actuators were supposed. Note, however, that Mei and Goodall [1] explain how a robust yaw gyro might effectively be used to derive the high-pass filtered yaw angle. Also in [1] Mei and Goodall point out the analogy between absolute stiffness and a "skyhook spring", i.e. a spring virtually connected between the wheelset and the "sky" —in a similar manner that absolute damping is often referred as skyhook damping, as in active secondary suspensions. As the authors noted in their paper [1], the analogy is not exact since in any practical implementation through a linear or rotational actuator there must be an equal and opposite reaction/force between the wheelset and bogie. The true reaction forces/torques are illustrated in Figure 8.3 and implemented in the dynamic equations (8.3)–(8.8).

8.5 Integration of Passive Suspensions with Absolute Stiffness Stability Control

Absolute stiffness configurations mounted for each wheelset were integrated with different passive suspensions allocated in the longitudinal direction between each wheelset and the bogie frame. The objective was to investigate the possibility of creating a cooperation between the passive and active schemes to increase the wheelset stability with minimal effects on curving (i.e. minimal wheelsets-bogie interaction forces while curving), whilst reducing the control gains.

In the previous section, a description of two solutions for the bogie stability problem was provided, based on the use of passive (relative) and active (absolute) stiffness. After having exposed that one of the major difficulties of applying either yaw or longitudinal stiffness alone between the wheelsets and the bogie is the response during curving, a frequency-based focus is provided in this section to introduce the role of more extensive passive suspensions.

In general, rail geometry characteristics in the lateral direction can be separated into high frequency for stochastic irregularities (predominant in straight tracks), and low frequency for curves. In fact, for the application of absolute stiffness it was already mentioned that high-pass filtering would alleviate the issues arising on curving. From the control perspective, the frequency response of mechanical suspensions is clearly a distinctive fact. For instance, a linear spring has a flat frequency response to relative displacements between its terminals; this has a counterpart for the vehicle's behaviour which was described in the previous section. To ease this, a range of passive networks can be designed using springs and dampers to 'relax' the longitudinal stiffness at certain frequencies, or either implement active yaw relaxation together with the longitudinal stiff rod providing the wheelset stability [56, 160]. In the case of passive relaxation, the possibilities of designing convenient passive configurations considering only (linear) springs and dampers is, however, limited. This resulted in an interesting opportunity case for investigating the potential of the inerter concept, which enables to some extent freedom in the design of the frequency response of passive suspensions [3].

The candidate suspensions tested for this initial assessment are fairly simple, as shown in Figure 8.4. These basically consider the introduction of an inerter-based device in the longitudinal plane defining different dynamical stiffness characteristic. This augments the longitudinal stiffness already provided by the primary suspensions, k_{px}. Schematically, the devices in Figure 8.4 are placed in parallel to the springs k_{px} illustrated in Figure 8.3. Those are represented in Figure 8.4, for which the parameter b_1 is the inertance property of the inerter, and c_1 and k_1 stand for normal damping

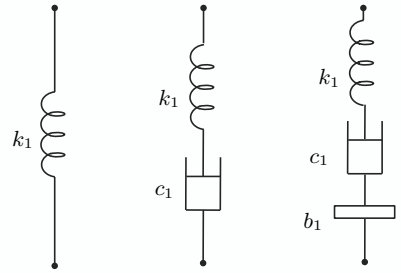

Figure 8.4: Candidate suspension layouts .

and stiffness design parameters.

The passive forces applied on the wheelsets and the bogie are characterised by the candidate layouts complex mechanical admittance Y_{pn} (see [3]) as

$$\hat{F}_{pn} = \mathrm{Y}_{pn}(s)\, s\, \hat{x}_r \tag{8.21}$$

for x_r the length variation of the corresponding suspension with respect to the equilibrium condition. Thus, the resultant torque applied on each wheelset i and reacting on the bogie frame, is expressed as

$$\begin{aligned}
\hat{\tau}_{pn,i} &= l_x\, \hat{F}_{pn}\Big|_{\mathrm{Left},\,i} - l_x\, \hat{F}_{pn,i}\Big|_{\mathrm{Right},\,i} && (8.22)\\
&= \hat{\tau}_{pn}|_{\mathrm{Left},\,i} - \hat{\tau}_{pn}|_{\mathrm{Right},\,i} && (8.23)\\
&= 2l_x^2 \mathrm{Y}_{pn}(s)\, s \left(\hat{\theta}_b - \hat{\theta}_{w,i} - (-1)^i \frac{l_{wx}}{R} \hat{h}_R\, e^{-\tau_i s}\right) && (8.24)
\end{aligned}$$

under consideration of small yaw angles, i.e. $\mathrm{Sin}\,(\theta_*) \approx \theta_*$. In Equations 8.22–8.23, $F_{pn}|_{\mathrm{Left},\,i}$ ($F_{pn}|_{\mathrm{Right},\,i}$) and $\tau_{pn}|_{\mathrm{Left},\,i}$ ($\tau_{pn}|_{\mathrm{Right},\,i}$), are respectively, the force and torque developed by the left (right) side suspension acting on the wheelset i. In Equation 8.24, $h_R(t)$ defines the transition of the curve, normally $\tau_1 = 0$, and τ_2 is the time delay associated to the wheelsets separation and the travelling speed. Hence, for the model of the system, Equations 8.3–8.8 and thereafter, $R_1^{-1}(t) = R^{-1}h_R(t)$ and $R_2(t) = R_1\,(t - \tau_2)$.

The complex admittance of every layout in Figure 8.4 is given in Table 8.2. For every passive layout, the controllable canonical form was obtained in $\mathbf{A}_{pn}$, $\mathbf{B}_{pn}$, $\mathbf{C}_{pn}$, $\mathbf{D}_{pn}$, which is common to the two subsystems with, respectively: state vectors $\underline{x_{pn1}}$ and $\underline{x_{pn2}}$, output passive torques τ_{pn1} and τ_{pn2}, and inputs $\dot{\theta}_b - \dot{\theta}_{w1} - l_{wx}R^{-1}\dot{h}_R(t)$ and $\dot{\theta}_b - \dot{\theta}_{w2} + l_{wx}R^{-1}\dot{h}_R(t - \tau_2)$.

It is recognised that this reduced selection of passive structures does not enable

Table 8.2: Complex Admittance Function of the Mechanical Networks in Figure 8.4

PN	Complex Admittance	Coefficients
L1	$k_1 \frac{1}{s+\beta_0}$	$\beta_0 = {}^{k_1}/_{c_1}$
L2	$k_1 \frac{s}{s^2+\beta_1 s+\beta_0}$	$\beta_1 = {}^{k_1}/_{c_1}$, $\beta_0 = {}^{k_1}/_{b_1}$

a comprehensive assessment of the inerter effects on the performance of a vehicle equipped with stability control, but has been defined to identify the potential of inerter-based suspensions to create a synergy with stability solutions and to lead future research work.

8.6 Optimisation Problem and Performance Assessment

Once the structure of the controllers has been established, both active and passive, a multi-objective optimisation problem was formulated on the closed-loop system represented in the state-space as

$$\underline{\dot{x}_{cl}} = \mathcal{A}\,\underline{x_{cl}} + \mathcal{B}_\eta \underline{\eta} \tag{8.25}$$

$$\underline{y_{cl}} = \mathcal{C}\,\underline{x_{cl}} \tag{8.26}$$

for the augmented state vector

$$\underline{x_{cl}} = \left[\underline{x}^T \middle| \underline{x_{\tau 1}}^T \middle| \underline{x_{\tau 2}}^T \middle| \underline{x_{pn1}}^T \middle| \underline{x_{pn2}}^T\right]^T \tag{8.27}$$

the output vector $\underline{y_{cl}} = \underline{y_o}$ re-written accordingly, and the closed-loop system's matrices defined as

$$\mathcal{A} = \left[\begin{array}{c|c} \mathbf{A} + \mathbf{B}\,\mathbf{\Lambda}_D^u \mathbf{C}_m & \mathbf{B}\,\mathbf{\Lambda}_C^u \\ \hline \mathcal{A}_{21} & \mathbf{\Lambda}_A^u \end{array}\right] \tag{8.28}$$

$$\mathcal{B} = \left[\mathbf{B}_\eta^T \middle| \mathbf{0} \middle| \mathbf{0} \middle| \mathbf{0}\right]^T \text{ and} \tag{8.29}$$

$$\mathcal{C} = \left[\mathbf{C}_o \middle| \mathbf{0} \middle| \mathbf{0} \middle| \mathbf{0}\right] \tag{8.30}$$

with

$$\mathbf{\Lambda}_A^u = \text{diag}\,(\mathbf{A}_\tau,\, \mathbf{A}_\tau,\, \mathbf{A}_{pn},\, \mathbf{A}_{pn}) \tag{8.31}$$

$$\mathbf{\Lambda}_C^u = \text{diag}\,(\mathbf{C}_\tau,\, \mathbf{C}_\tau,\, \mathbf{C}_{pn},\, \mathbf{C}_{pn}) \tag{8.32}$$

$$\mathbf{\Lambda}_D^u = \text{diag}\,(\mathbf{D}_\tau,\, \mathbf{D}_\tau,\, \mathbf{D}_{pn},\, \mathbf{D}_{pn}) \tag{8.33}$$

and

$$\mathcal{A}_{21}=\Big[\ \mathbf{C}^T_{m(1,*)}\mathbf{B}^T_\tau\Big|\mathbf{C}^T_{m(2,*)}\mathbf{B}^T_\tau\Big|\mathbf{C}^T_{m(3,*)}\mathbf{B}^T_{pn}\Big|\mathbf{C}^T_{m(4,*)}\mathbf{B}^T_{pn}\Big]^T \tag{8.34}$$

The "zero" entries in the matrices definition are zero vectors/matrices of appropriate dimension, and $\mathbf{C}^T_{m(i,*)}$ corresponds to the i-th row of the matrix $\mathbf{C}_m$ in (8.11).

The design objectives described in the preceding sections were therefore reunited in the formulation of a multi-objective optimisation problem as

$$obj:\ min\left(J_{\zeta w},\, K_u\right) \tag{8.35}$$

with

$$J_{\zeta w} = -min\left(\underline{\zeta_w}\right) = -\zeta_{cw}$$

equivalent to the maximisation of the least damping ratio ζ_{wc} among the wheelsets' kinematic modes $\underline{\zeta_w}$. The other design objective compromises the achievement of optimum stability but, as stated before, the minimisation of the active control gain is also of interest of the active control design. The problem was formulated for the closed-loop system of the vehicle travelling at the nominal speed ($V = 55\,[\mathrm{ms}^{-1}]$).

8.6.1 Optimisation solution

As it was done in Chapter 6, a genetic algorithm from the *Global Optimization Toolbox* from MATLAB®, `gamultiobj`, was utilised to obtain the trade-off curve emerging from this multiobjective formulation. All the active and passive control parameters were tuned by optimisation, i.e. the control gain, K_u, the cut-off frequency of the high-pass filter, f_c, and the stiffness, damping and inertance parameters according to each candidate layout in Figure 8.4. Reasonable values for the physical constraints on the parameters were supplied to the algorithm. This way, the maximum stiffness allowed for k_1 considered the non-infinite stiffness quality of the damper and the inerter, and the limiting stiffness imposed by the attachments of the device to the bodies, for example. Nevertheless, proper modelling of the bushes was not included.

Thus, numerical optimisation was performed over each configuration to improve the most critical kinematic mode of the conventional passive bogie, ζ_{cw}. Figure 8.5 shows the trade-off plot of $J_{\zeta w}$ versus optimal control gain values, K_u, for the active-plus-passive configurations (i.e. active torque together with yaw dynamical stiffness —layouts L1 and L2 from Figure 8.4). It is noticeable that incorporating yaw relative

dynamic passive stiffness enhances the stability provided by the absolute yaw stiffness only (default active). This occurs, however, for high active gain values (i.e. over 23×10^6).

According to Figure 8.5, the inerter-based suspension from layout L2 provides the best benefits to the integration active-plus-passive for the wheelset stability problem. Table 8.3 summarises the best values attained by the optimisation algorithm with a tolerance of 10^{-3} for such —originally critical— mode. With these results, the stability of the wheelsets of an active bogie, either default or combined with L1/L2, clearly contrasts with that of the passive bogie's, which has 6.51 [%] of least damping ratio given by passive *static* yaw stiffness (L0), with $K_x = 37.7[\text{MNm}^{-1}]$. Furthermore, incorporating an inerter in the suspension provides 26 % of wheelset stability improvement over that provided by the default active configuration. On the other hand, as shown in Figure 8.5, the integration enables also the reduction of the active torque control gain required to achieve the maximum kinematic stability of the default configuration. That is, the default configuration requires $K_u = 31.5{\times}10^6$, whilst integrating active with L1 needs $K_u = 26.32 \times 10^6$, and with L2, $K_u = 25.87 \times 10^6$. Later, a discussion on the amplitude of the control torque applied on the wheelsets and bogie whilst curving is provided.

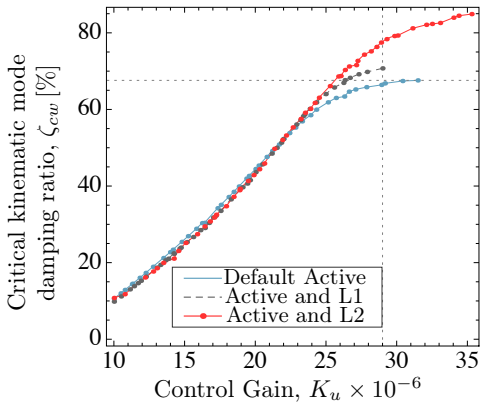

Figure 8.5: Trade-off plots for the active configuration combined with the passive structures L1 and L2 from Figure 8.4.

8.6.2 Results for stability of the kinematic modes

The plots for the least damping ratio of the kinematic mode, ζ_{wc}, versus travelling speed, V, for the optimal tuning presented in Table 8.3 (attained for each configuration and with a nominal speed $V = 55\,[\text{ms}^{-1}]$) are shown in Figure 8.6. Comparison

Table 8.3: Optimisation results for the system with absolute stiffness and the candidate layouts L1 and L2 in Figure 8.4

Configuration	ζ_{wc}[%]	$K_u \times 10^6$	Other design parameters
Default Active	67.59	31.5×10^6	$f = 0.50$
$\mathcal{T}_u$&L1	70.73	29.0×10^6	$f = 0.50$, $k_1 = 1.09 \times 10^6$, $c_1 = 7.38 \times 10^3$
$\mathcal{T}_u$&L2	84.90	35.3×10^6	$f = 0.52$, $k_1 = 1.98 \times 10^6$, $c_1 = 3.23 \times 10^4$, $b_1 = 2.83 \times 10^6$

[a] f [Hz], k_1 [Nm^{-1}], c_1 [Nsm^{-1}], b_1 [kg]

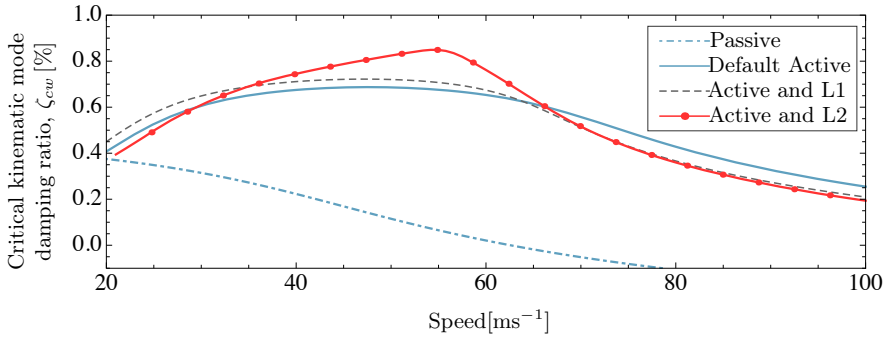

Figure 8.6: Damping ratio for the critical kinematic mode versus speed.

with the stability curve for the passive conventional system and the default active control is provided.

Improved stability was achieved with the inerter-based suspension L2 for a speed range of $28 - 67$ [ms^{-1}], as contrasted with the response for the default active configuration. The characteristic of the speed versus kinematic mode damping ratio curve for the configuration with L1 is closer to that for the active configuration alone, although still with some enhancement. For any of the configurations including active torque, a higher critical speed is evidenced in comparison with that for the conventional passive vehicle. However, a slight reduction of the critical speed may be caused when relative yaw suspensions are incorporated. This, however, should not pose a problem as the design nominal speed is well below these speed values.

8.6.3 Results for curving

To complete the formulated study on the potential of integrating an inerter-based yaw suspension to the selected active stability control solution, curving behaviour in the time domain was also assessed. For this, two criteria diferring in the configuration parameter settings were used: Criterion A and B.

- *Criterion A*: the parameter settings correspond to these providing 67.6 [%] (approx.) of kinematic mode damping ratio (as referred in Subsection 8.6.2), and
- *Criterion B*: the parameter settings correspond to these providing optimal damping of the kinematic modes according to each configuration (Table 8.3).

For this end, a curved track of 1500 [m] radius and cant angle of 6° were assumed; both characteristics with a transition time of 3 seconds for a nominal travelling speed of $V = 55\,[\mathrm{ms}^{-1}]$ as in [20]. Note that in the plots from Figures 8.7–8.13 bold curves correspond to responses associated to the leading wheelset, while normal curves are for the trailing wheelset (i.e. dynamic states, and forces and torques actuating on the wheelsets).

Criterion A: Equal kinematic stability for all the configurations

The first observation from the curving responses for this criterion is that the insertion of passive suspensions —with dynamic stiffness characteristic— in the longitudinal direction do not affect the quasi-static responses of the bodies (see Figures 8.7–8.11). In fact, this slightly improves the transient behaviours, although it is very difficult to check by simple inspection of the corresponding plots. Hence, for instance, the rear wheelset quasi-static state lateral displacement of $y_{w2} = 0.71\,[\mathrm{mm}]$ is a common fact for the configurations with active control (Figure 8.7). This is very close to the lateral displacement required for pure rolling, $y = 0.74\,[\mathrm{mm}]$ calculated as $y = {}^{l_{wy}r_o}/_{\lambda\,R}$ [161] for nominal conditions. The leading wheelset, however, showed a higher displacement. Therefore, non-zero longitudinal creep forces F_x evidently arise from the wheel/rail interface at the front wheelset, with very small quasi-static force for the trailing wheelset F_{x2} for any of the configurations including active control, as depicted in Figure 8.8.

The lateral creep forces F_y required for the vehicle cant deficiency are shown in the top plot of Figure 8.8. Negative quasi-static yaw angles symmetric to $-0.59\,[\mathrm{mrad}]$ were obtained, again commonly, for the configurations including active control. The difference between the quasi-static lateral creep forces developed with the leading and trailing wheelsets, $|F_{y1} - F_{y2}|$, resulted smaller for all these configurations; that is without distinction in the passive yaw suspension employed (Default —none, L1 or L2). Thus, the track shifting forces are not affected by the suspensions L1/L2 allocated in the longitudinal direction. This means that the non-flat stiffness characteristic of the suspensions L1 and L2 prevents affecting the vehicle curving quasi-static response.

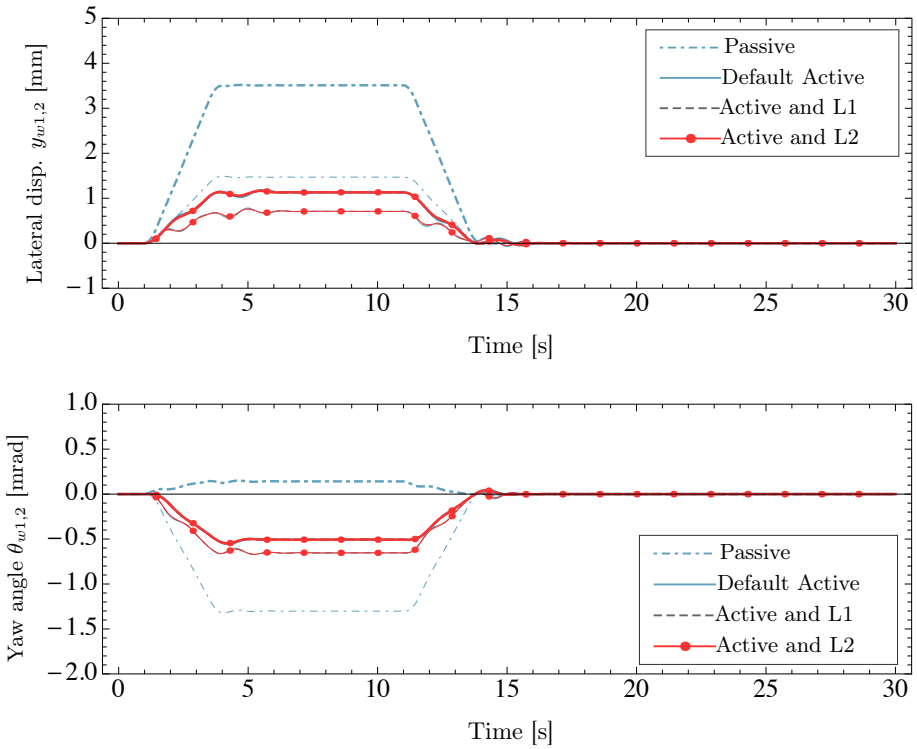

Figure 8.7: Time-response for the wheelsets' dynamic characteristics: Top- Lateral displacement, Bottom- Yaw angle, Criterion A.

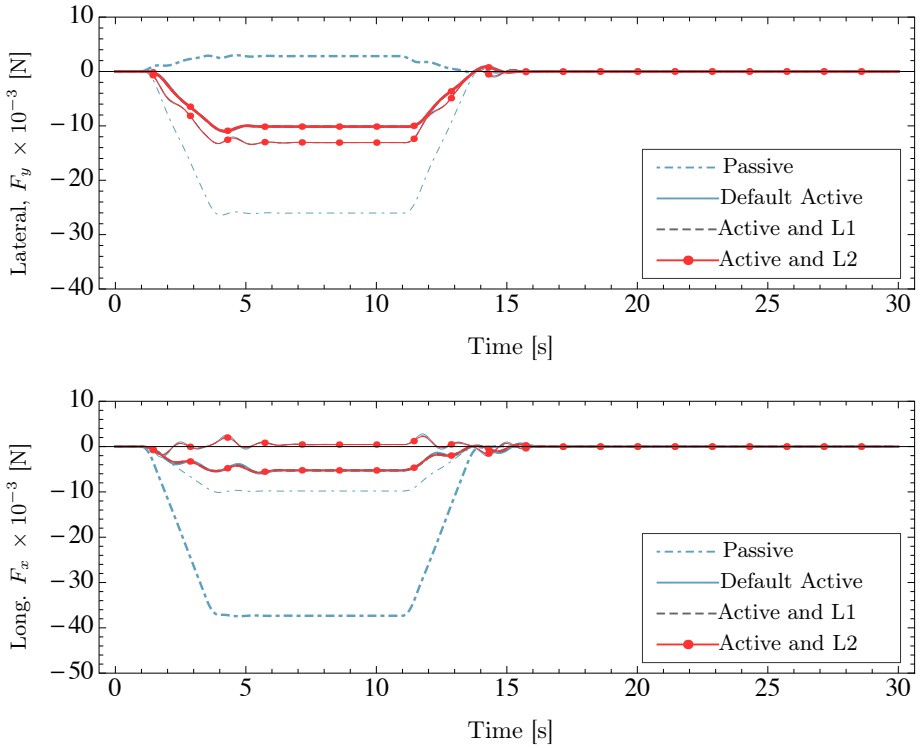

Figure 8.8: Time-response for the creep forces: Top- Lateral, Bottom- Longitudinal, Criterion A.

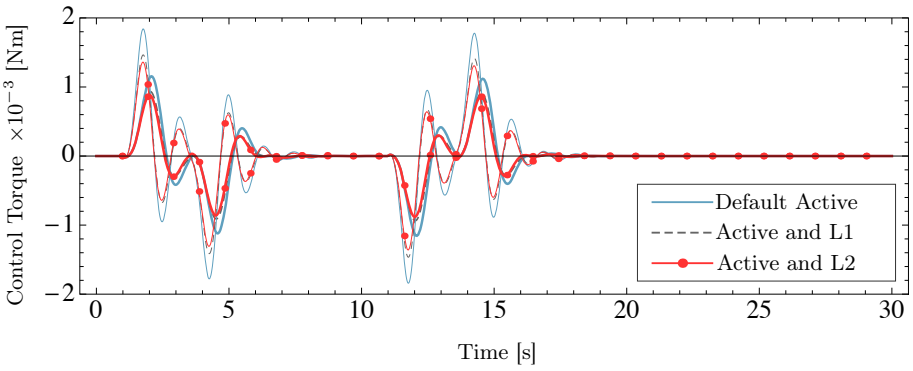

Figure 8.9: Time-response for the applied control torque, Criterion A.

The active control torques required to produce the dynamics described above for each configuration are shown in Figure 8.9. For the default implementation of absolute stiffness, the amplitude of the active control torque maximum peaks is higher than that of the configurations including passive dynamical stiffness. Moreover, integrating the inerter-based suspension (L2) reduces the active torque requirements over the use of the simply relaxed suspension (L1).

Furthermore, a bogie with any of the tested configurations including active control has reduced lateral displacement and rotation in the curving process quasi-static state, compared to a pure passive bogie (see Figures 8.10). Finally, it is also observed that these configurations slightly reduce the amplitude of the quasi-static state of the vehicle body in the lateral direction (Figure 8.11), whilst maintaining 'similar' transient characteristic. An examination of the lateral ride quality should be performed in the future to complete the latter statement.

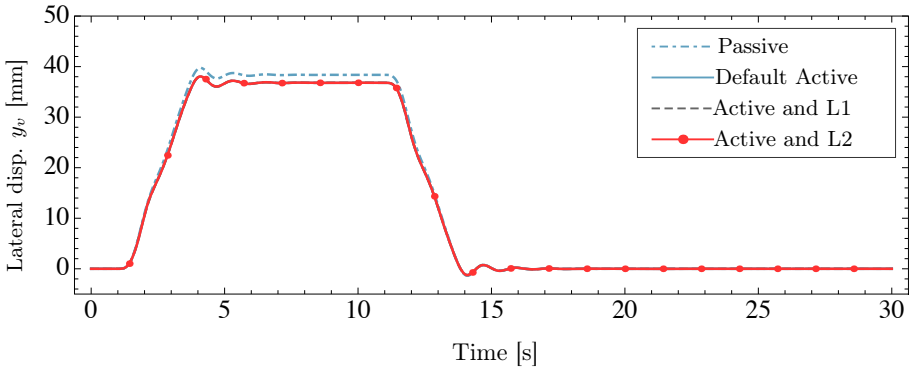

Figure 8.11: Time-response for the half-body lateral displacement, Criterion A.

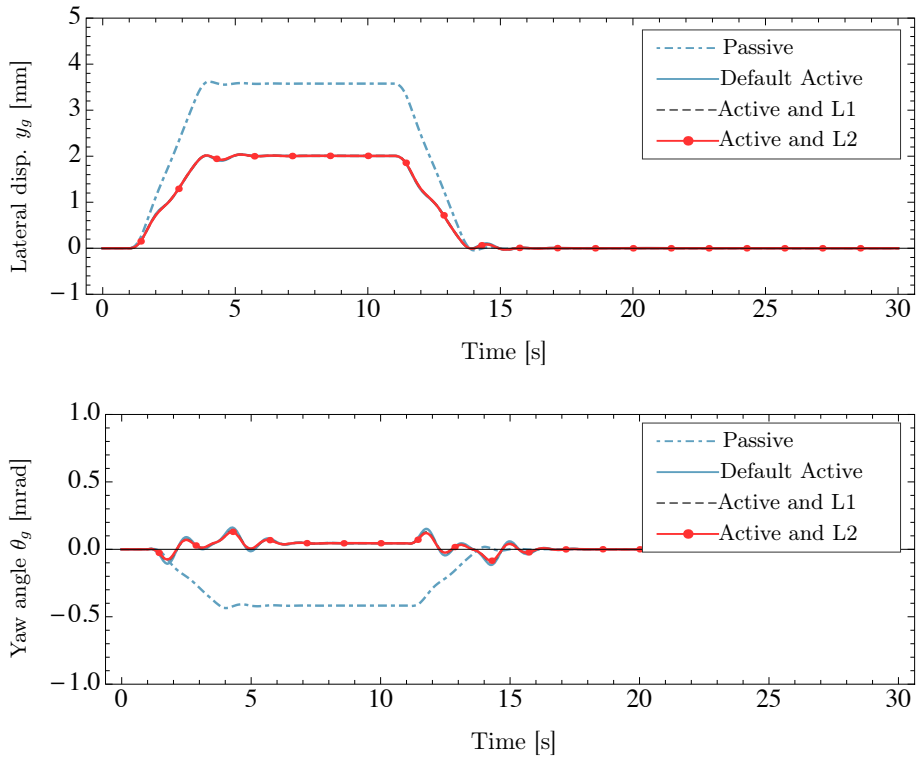

Figure 8.10: Time-response for the bogie dynamic characteristics: Top- Lateral displacement, Bottom- Yaw angle, Criterion A.

Criterion B: Optimal kinematic stability for every configuration

While assessing the curving performance of the vehicle with the different configurations and their corresponding optimal settings for maximum kinematic stability, it was found again that neither L1 nor L2 affect the curving characteristics, regardless the improved stability these produce. This is shown in Figure 8.12 for the creep forces time-response. However, and as expected according to the active control gain K_u values in Table 8.3, higher control torques are required by the configurations including passive control. This is depicted in Figure 8.13.

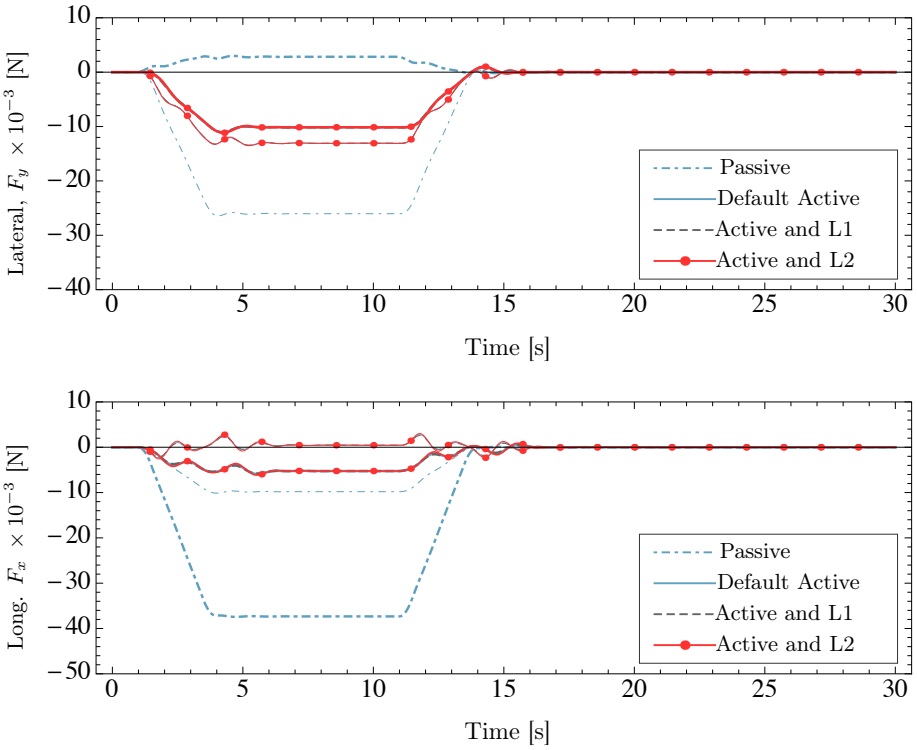

Figure 8.12: Time-response for the creep forces: Top- Lateral, Bottom- Longitudinal, Criterion B.

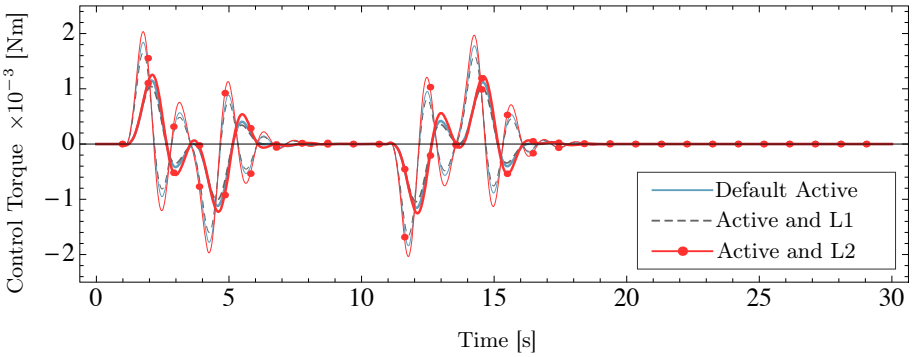

FIGURE 8.13: Time-response for the applied control torque, Criterion B.

Results from optimisation disclose that the active control technique based on the feedback of absolute position of the wheelsets can be further improved by feeding back the relative position of the wheelsets with adequate compensation. By introducing the inerter concept to the passive suspensions for the yaw kinematic modes of the wheelsets, the following benefits were obtained:

- lower active torque while curving for the same kinematic stability and curving response as in the conventional implementation of active torques, and
- higher kinematic stability for configurations with high active control gains without affecting the curving response.

8.7 Summary of the Chapter

This chapter presented results attained for integrated configurations active-plus-passive for the wheelset lateral stability problem; these included an inerter-based suspension. Simple candidate layouts were proposed for an initial assessment in a railway vehicle plan-view associated dynamic problems. After performing numerical optimisation of the parameters for each configuration, the settings were used to investigate the dynamic characteristics of the vehicle bodies and the creep forces produced while curving. It also assessed the active forces required for producing the transient and quasi-static behaviour of the half-vehicle showed in the analyses. A better compromise was achieved with the inerter-based suspension for the design objectives formulated via GA optimisation: maximum kinematic stability for the

nominal travelling speed and reduction of the control gain. Time domain simulation results illustrated the usefulness of adding the inerter to the active control solution, i.e. improvement in the kinematic mode stability was attained without affecting either the longitudinal or the lateral creep quasi-static forces.

Outcomes from this initial study opens the field for researching with a wider range of mechanical compensation schemes for the yaw modes of the wheelsets to enhance the performance of active solutions for the wheelset hunting problem. The findings in this chapter complement the results obtained for enhancing the performance of active secondary suspensions for the vehicle vertical ride quality studied in the previous chapters. For the ride quality problem it was found that inerter-based suspensions benefit more the active suspensions with low to intermediate levels of 'active dissipation'. Results in this chapter induce the hypothesis of inerter-based suspensions having potential for the design of active stability control configurations with high control gain. This is a theme for future study.

9

Conclusions and Future Work

9.1 Research Summary and Contributions

This thesis was devoted to study the potential use of novel mechanical devices for simplifying the design of active solutions for railway vehicle dynamics. These types of design are normally subject to conflicting objectives extensively known in the railway dynamics field. The research work was focused especially on the enhancement of the vertical ride quality of a bogied railway vehicle by integration of inerter-based devices (in general) and active configurations in parallel to the conventional secondary suspensions. For this aim, analytical and simulation studies were accomplished on a planar and linear incremental model of the vehicle.

The simplicity of the ride quality problem, as compared to other more complex issues arising in the dynamics of a railway vehicle, enabled a better understanding of the potential of the inerter and inerter-based suspension configurations. This prevented the risk of hiding the dynamic attributes of the novel suspensions with the effects of complex dynamical factors. Having focused on a simpler problem also enabled new perspectives for the methodology of study. Moreover, it facilitated the identification of other potential applications of the inerter technology. In fact, a later piece of work within this research considered the lateral stability problem and the inherent trade-off with the requirements of quasi-static curving as a more complex application.

The inerter, as a concept, was widely considered throughout this thesis. Given its significance to mechanical networks modelling using springs, dampers and inerters only, it facilitated the assessment of inertial effects appearing in the airsprings and electromechanical actuators. The frequency response of the thermodynamical model of an

airspring provided with an external reservoir was approximated by using mechanical networks synthesis. The airspring inerter-based model added a series inerter-damper to the well known Nishimura model to introduce the oscillatory dynamic of the air-mass and friction losses occurring inside the connecting pipe. It was found, however, that the referred oscillatory effects of the air-mass could be obviated by provision of high airspring's damping. Under the assumption of having a well-damped airspring, a more conventional model of the airspring as Nishimura's was preferred to carry out the study. Nevertheless, a preliminary study —not included in this thesis— on optimisation of the parameters of the inerter-based airspring model revealed a potential of the airspring's inertial effects to offer a better ride quality. On the other hand, the inertial effects of the rotor of the electro-mechanical actuators placed in parallel to the conventional suspensions were confirmed to degrade the application of the control forces.

For the analytical study presented in Chapter 4, an ideal inerter was assumed; the implications of this were recognised. It followed a non-standard methodology, including analysis of the influence of the system's parameters on optimal ride quality, a rather qualitative study of the kinetic energy functions of the system's components, and an evaluation of the effects of the ideal inerter on the stochastic mean power dissipated in the passive suspensions of the vehicle. The main outcome of this analytical approach envisaged a confirmation of the research hypothesis for the ride quality problem. Briefly, it was found that an inerter, with optimal inertance designed for ride quality, could reorganise the total energy stored by the passive system so that it was advantageous for passive dissipation and for implementation of control strategies dedicated to energy extraction —virtual dissipation as defined in the chapter. Dissipative active suspensions are effective in the improvement of ride quality, which is essentially a vibration problem. Absolute velocity feedback, better known in the literature as 'sky-hook damping', is in fact a virtually dissipative active suspension and was the basis of most of the control configurations studied in this thesis for the ride quality objective. In addition, some of the analyses suggested that the insertion of an inerter in parallel to the airspring and an ideal actuator would barely affect the application of the —virtually dissipative— active control forces. This analytical confirmation of the research hypothesis was comprehensively supported later by numerical results in Chapter 6.

For the simulation study in Chapter 6, a more realistic mechanical inerter was considered. Also, different inerter-based devices were proposed by definition of a range of mechanical networks comprising inerters, springs and dampers. Two of these structures found correspondence with the approximated model of inerter-based hydraulic devices currently in existence.

The possibility of attaining synergy from the integration of the aforementioned novel

devices with active suspensions was appraised for several control configurations. Output-based and model-based linear control strategies for improving ride quality, accounting also for suspension deflection regulation, were considered.

Inspired by the passivity of the system, and motivated by the constraint described by the invariant equations about influencing suspension deflection and vehicle body accelerations together, an appealing, nonlinear, output-based control strategy was proposed. It was called 'adaptive stiffness', despite the fact that its current implementation possibilities are merely through active suspensions. It generates an additive command force for suspension deflection regulation. 'Adaptive stiffness' was conceived specifically to complement dissipative control laws for ride quality improvement. The integration with this nonlinear strategy completed the set of relevant control strategies considered as sufficient to study the proposed integration for ride quality problems. Namely, the control strategies studied for the integration were: 'modal sky-hook damping with high-pass filtering', 'local sky-hook damping with complementary filtering', 'local sky-hook damping with high-pass filtering and adaptive stiffness', and 'Linear-Quadratic Gaussian-output regulator with high-pass filtering'. The latter included feedback of the suspension deflection time-integral.

In most of the cases, the outcomes from the integration were obtained after performing multi-objective numerical optimisation over all the parameters, i.e. the free parameters of the passive and active part of the suspensions configurations. The exception was the implementation of the optimal control configuration, the LQG-output regulator. The primary optimisation objective was the minimisation of the 'least ride quality index' of the vehicle. The setting of the optimal problem was complemented by the definition of typical conditions relevant to the design of active suspensions: minimisation of the active forces and suspension deflection, as well as realistic constraints which would also guarantee the passivity of the novel devices and the stability of the system.

The overall result for ride quality was that inerter-based devices (with inerter-like behaviour at low frequencies) in fact could benefit the design of —ideal— active suspensions, under certain conditions. The potential was demonstrated for specific inerter-based structures. The outcomes indicate main benefits for active force reduction and ride quality enhancement. These advantageous effects did not depend strictly on the control strategy. For the reduction of the active forces, that was related to the levels of ride quality expected from the design. Similarly, for enhanced ride quality, these effects were rather connected to the 'relative' magnitude of the design forces. The "relative magnitude" of the design forces is quoted here in reference to the average magnitude of the forces required to cause a change in the ride quality, which does depend on the control strategy. Notwithstanding, the effectiveness of the cooperation between the inerter-based devices and the actuators changed from

one strategy to another. In fact, the integration with 'local sky-hook damping with high-pass filtering and adaptive stiffness' revealed better results for active forces reduction (up to 50%), as compared to the other strategies, in the achievement of 30% of improvement in the ride quality. These results confirm a potential of inerter-based suspensions for reducing the size of the actuators in the implementation of secondary active suspensions for enhancing the ride quality of railway vehicles, within certain limits for the design objectives.

A brief test on the foregoing conclusion was performed in a more sophisticated model using multi-body simulation in SIMPACK®. The model included all the degrees-of-freedom of the rigid bodies and the wheel/rail interaction; the results agreed with the outcomes attained for the planar model of the vehicle. Nevertheless, this sophisticated model did not consider airsprings for the secondary suspensions nor the real dynamic of the actuators. Introducing the inertial effects associated with these elements of the suspensions are believed necessary to complete the validation.

Other important facts were also assessed from the integration *active-plus-novel-passive* suspensions: the average stochastic power dissipated in the passive suspensions and the average stochastic power virtually dissipated by perfect actuators. From this, an advantage owed to the insertion of passive damping and inertance to the system was found: a reduction in the mean power required to drive the actuators. That was anticipated in Chapter 4 as a reduction in the levels of mean power that ideal actuators would have to remove from the system.

Furthermore, a review of results obtained after including the model of an electro-mechanical actuator for a more realistic assessment of the integrated suspensions performance, revealed a potential of inerter-based suspensions to compensate for undesirable effects caused by the actuators dynamics. This, however, deserves a more extended study.

Finally, a short assessment was performed on the integration of an inerter-based suspension to a particular active solution of the 'hunting problem' arising in railway vehicles with solid-axle wheelsets. This is fundamentally a stability problem whose solutions normally conflict with the natural curving ability of the vehicle. To investigate the potentiality of the inerter concept for this trade-off, very simple passive suspensions were considered for implementing frequency-dependent stiffness in the primary yaw suspensions. The integration considered the 'absolute stiffness' strategy extracted from the literature. From the synergy with passive suspensions, a better compromise was achieved for the design objectives formulated: maximum wheelset stability for the nominal travelling speed and reduction of the active control gain. In particular, including an inerter in the suspension resulted better than integrating active control with yaw relaxed suspensions (i.e. series spring-damper, without inert-

ers). Further, improving the kinematic stability control design by using passive yaw suspensions with dynamic stiffness characteristic did not affect the longitudinal and lateral creep forces developed while curving. The integration with the tested suspensions showed that a reduction in the magnitude of the active torques is also possible, and was more evident for the suspension layout including the inerter. These achievements provide the railway dynamics field with the first evidences on the potential of inerter-based suspensions to simplify problems in the design of active suspensions for the wheelset hunting problem.

9.2 Conclusions

It was found that integrating inerter-based devices to the implementation of active suspension systems for enhancing the vertical ride quality of a railway vehicle, simplifies the design problem for configurations with low to intermediate feedback active gains. Moreover, from the integration with the novel active control strategy for regulating suspension deflection, *adaptive stiffness*, it was found that control strategies inspired by the passivity and dissipativity properties of the system can provide further benefits to the suspension design. A promising synergy between inerter-based devices and the aforementioned strategy implemented with a practical configuration of 'skyhook damping' was observed by a modification of the design trade-off curves in a wider range of feedback gains and thus, enabling further improvements in the vehicle's vertical ride quality. As a highlight, it is worth mentioning that the active forces required for achieving 30% of improvement in the vertical ride quality could be reduced by up to 50% when inerter-based devices are inserted. Moreover, integrating adaptive stiffness and inerter-based suspensions to skyhook damping can provide up to 54% of improvement in the ride quality with active forces of less than 10 [kN], and within the suspension clearance. These results are justified by the modification of the patterns of the kinetic energy storage function of the vehicle body given by insertion of novel means of kinetic energy storage such as inerters in the suspensions, apart from the extra passive damping provided by the novel mechanical devices. This assertion comes from the analytical study developed in Chapter 4, which anticipated the potential of the inerter as a kinetic energy storage device for the performance of the vehicle equipped with conventional mechatronic suspensions.

On the other hand, for the stability of the vehicle's kinematic modes for which 'absolute stiffness' was employed as active stabilising strategy, the integration of a simple inerter-based suspension in the yaw direction showed relevant benefits. The inerter-based suspension increased the least kinematic mode damping by 26% over the default active configuration, without effecting the curving response. This enables the reduction of the required active torques for achieving wheelset stability

levels corresponding to these for the default active configuration. Furthermore, the results suggested the potential of yaw mechanical suspensions with dynamic stiffness characteristic being for high active control gains only. This is a theme of study for the future.

9.3 Future work

A range of appealing research possibilities derives from the outcomes of this thesis for distinct branches of Control and Railway Engineering. Some of them have been already identified and are mentioned in the following, together with further work on what was developed in this time-limited research.

- Extend the study on the ride quality considering aspects such as:
  - the inertial effects of the airspring dynamics, which in a preliminary analysis were found beneficial for the vehicle's ride quality by parameter optimisation using the inerter-based model developed in this thesis. In fact, about 20% of improvement in the ride quality, as compared with the nominal airspring used in this research, can be achieved using conventional suspensions only,
  - the main flexible modes of the vehicle body.
- Further investigate the effects of integrating inerter-based devices to active suspensions implemented by electro-mechanical actuators and other technologies. For this, two particular aspects are suggested for deeper research: 1) on the compensation for the undesirable dynamics of the actuators, and 2) on the potential reduction of the actuator power requirements with possible benefits to actuator efficiency.
- Perform experimental work to further validate the outcomes of this thesis with real airsprings, inerter-based devices and actuators.
- Continue the work on the potential of the inerter for the lateral stability problem and associated conflicting issues:
  - Extend the analyses of the results presented in Chapter 8 including the assessment of the track wear number and ride quality indices, as well as a robustness study on the outcomes to variation in the equivalent conicity of the wheels, curve radii, cant deficiency, and running speed.

  - Consider a possible change in the optimisation methodology including directly the track wear number instead of the yaw stiffness parameter may return better results to the trade-off between stability and curving problems.
  - Complete the study with different stability control strategies and more inerter-based structures.

- Validate the outcomes from the analytical work for enhancement of the lateral ride quality.
- Identify potential uses of inerter-based devices integrated to tilting solutions.
- Consider including integrated suspensions on other models of railway vehicles, such as the two-axle vehicle for which some collaborative work with the University of Cambridge on the use of the inerter has been undertaken [21] . Investigate other type of systems whose performance could be also enhanced by inerter-based mechatronic suspensions.
- Extend the studies on the control strategy formulated in this thesis for regulating suspension deflection without affecting the dissipative parallel forces, the so-called in this work 'adaptive stiffness'. Develop complete stability and robustness analyses, and investigate the possibilities of devising a semi-active device with these dynamic characteristics.
- Consider the use of energy-based concepts for the design of dissipative and passivity-based suspension systems for railway vehicles. The dynamics of a railway vehicle can be clearly characterised by either Euler-Lagrange or Hamilton's equations, thus, it is natural to see a potential for investigating solutions to the railway vehicles' dynamical problems within this control research area. Evidences for the potentialities of conducting research work in the field are found in this thesis. Clear examples of this are: the analytical treatment given to the research problem formulated in this thesis (Chapter 4), and the effectiveness of the integrated solution using the 'adaptive stiffness' concept, together with the dissipative characteristic of the 'sky-hook damping' concept, and the potential of using passive mechanical controllers using inerters (Chapter 6).
- Continue the analytical work towards a theoretical formulation of the relation between the geometry defined by the kinetic energy function of the sprung mass of a vibrational system and its first time-derivative, and the optimal parameters of the system with either passive or active suspensions.

Other control strategies, apart from these fully developed in the content of this thesis, were investigated in the course of this research. However, the adequate selection of

the control laws actually required to test the research hypothesis, constrained the continuity of that work. Nevertheless, it is expected to continue studies on these strategies applied to railway vehicle dynamics. Such work included:

- A flatness-based control strategy using generalised-proportional-integral (GPI) observers, whose numerical complexity (very determined by the order of the system), unfeasibility of the required measurements, and dependency on a preview control scheme, left the strategy out from the selection. This is, even though, a very robust technique which should be explored deeply for a potential application in railway vehicle dynamics, such as steering control and actuators' force/torque tracking control. The outcomes of this strategy based on GPI-observers, applied to a quarter-vehicle with simple suspensions for the ride quality problem, were published in [162] and [163].

- Relative acceleration feedback, derived from the concept of 'positive acceleration feedback' [164], which finds similarity with the use of the inerter-based suspensions. Further work should study to what extent passive implementation of control strategies including acceleration feedback is preferred to active, or vice versa, when combined with sky-hook damping-based strategies, for example. Preliminary work showed that not much cooperation between relative acceleration feedback and passive networks using inerters is achieved.

- Design of $\mathcal{H}_2/\mathcal{H}_\infty$ passive and active compensators using Youla parametrisation and LMI to study the limitations in the design of low-order passive compensators synthesised by mechanical networks comprising springs, dampers and inerters. Initial work developed the Youla parameterisation and carried out initial compensators design using BMI (Bilinear Matrix Inequalities) solvers with YALMIP.

- A Passivity-Based Control (PBC) strategy [138] which deserved further development to be considered in the techniques selected for this thesis.

References

[1] T. X. Mei and R. M. Goodall, "Stability control of railway bogies using absolute stiffness: Sky-hook spring approach," *Vehicle System Dynamics*, vol. 44, no. sup1, pp. 83–92, 2006.

[2] A. O. Gilchrist, *A history of engineering research on British railways*. Institute of Railway Studies and Transport History, 2009, vol. 10.

[3] M. C. Smith, "Synthesis of mechanical networks: The inerter," *IEEE Transactions on Automatic Control*, vol. 47, no. 10, pp. 1648–1662, 2002.

[4] R. M. Goodall and T. X. Mei, *Active Suspensions*, ser. Handbook of railway vehicle dynamics. United States of America: CRC Press, 2006, p. 327.

[5] I. Pratt, "Active suspension applied to railway trains," Ph.D. dissertation, Loughborough University, 1996.

[6] J. Evans and M. Berg, "Challenges in simulation of rail vehicle dynamics," *Vehicle System Dynamics*, vol. 47, no. 8, pp. 1023–1048, 2009.

[7] S. Iwnicki, *Handbook of railway vehicle dynamics*, S. Iwnicki, Ed. United States of America: CRC Press, 2006.

[8] A. C. Zolotas and R. M. Goodall, *Modelling and control of railway vehicle suspensions*, ser. Mathematical Methods for Robust and Nonlinear Control. Lecture Notes in Control and Information Sciences. Springer, 2007, vol. 367, pp. 373–411.

[9] J. R. Evans, "Rail vehicle dynamic simulations using vampire," *Vehicle System Dynamics supl.*, vol. 31, p. 135, 1999.

[10] S. Bruni, R. Goodall, T. X. Mei, and H. Tsunashima, "Control and monitoring for railway vehicle dynamics," *Vehicle System Dynamics*, vol. 45, no. 7-8, pp. 743–779, 2007.

[11] P. E. Wellstead, *Introduction to Physical Systems Modelling*. Control Systems Principles, 2000. [Online]. Available: http://www.control-systems-principles.co.uk

[12] M. Z. Q. Chen, C. Papageorgiou, F. Scheibe, F. C. Wang, and M. C. Smith, "The missing mechanical circuit element," *Circuits and Systems Magazine, IEEE*, vol. 9; 9, no. 1, pp. 10–26, 2009.

[13] S. Evangelou, D. J. N. Limebeer, R. S. Sharp, and M. C. Smith, "Mechanical steering compensators for high-performance motorcycles," *Journal of Applied Mechanics- Transactions of the ASME*, vol. 74, no. 2, pp. 332–346, 2007.

[14] ——, *An H-inf Loop-Shaping Approach to Steering Control for High-Performance Motorcycles*, ser. Control of Uncertain Systems (LNCIS). Germany: Springer-Verlag, 2006, vol. 329, p. 257.

[15] F.-C. Wang, C.-W. Chen, M.-K. Liao, and M.-F. Hong, "Performance analyses of building suspension control with inerters," in *Proceedings of the 46th IEEE Conference on Decision and Control*, 2007, pp. 3786–3791.

[16] F. C. Wang, "The performance improvements of train suspension systems with inerters," *Proceedings of the 45th IEEE Conference on Decision and Control*, vol. 1, no. 14, pp. 1110–1115, 2006.

[17] F. C. Wang, M. K. Liao, B. H. Liao, W. J. Su, and H. A. Chan, "The performance improvements of train suspension systems with mechanical networks employing inerters," *Vehicle System Dynamics*, vol. 47, no. 7, pp. 805–830, 2009.

[18] F. C. Wang and M. K. Liao, "The lateral stability of train suspension systems employing inerters," *Vehicle System Dynamics*, 2009.

[19] ——, "The lateral stability of train suspension systems employing inerters," *Vehicle System Dynamics*, vol. 48, no. 5, pp. 619–643, 2009.

[20] J. Z. Jiang, A. Z. Matamoros-Sanchez, R. M. Goodall, and M. C. Smith, "Passive suspensions incorporating inerters for railway vehicles," *Vehicle System Dynamics*, vol. 50, no. sup1, pp. 263–276, 2012.

[21] ——, *Performance Benefits in Two-Axle Railway Vehicle Suspensions Employing Inerters*, ser. Developments in Control Theory towards Glocal Control. Institute of Engineering and Technology (IET), 2012, ch. 11.

[22] F.-C. Wang, M.-R. Hsieh, and H.-J. Chen, "A full-train with inerters: stability and performance," in *Proceedings of the 22nd International Symposium on Dynamics of Vehicles on Roads and Tracks*, 2011.

[23] O. Polach, M. Berg, and S. Iwnicki, *Simulation*, ser. Handbook of railway vehicle dynamics. United States of America: CRC Press, 2006, p. 359.

[24] H. Rahnejat and R. Whalley, *Multi-body dynamics : : monitoring and simulation techniques*. London: Mechanical Engineering Publications, 1997.

[25] B. M. Eickhoff, J. R. Evans, and A. J. Minnis, "A review of modelling methods for railway vehicle suspension components," *Vehicle System Dynamics*, vol. 24, no. 6-7, pp. 469–496, 1995.

[26] J. Evans and M. Berg, "Challenges in simulation of rail vehicle dynamics," *Vehicle System Dynamics*, vol. 47, no. 8, pp. 1023–1048, 2009.

[27] S. Iwnicki, "The Manchester Benchmarks for rail simulators - an introduction," *Vehicle System Dynamics*, vol. 29, no. sup1, pp. 717–722, 1998.

[28] S. Iwnick, "Manchester Benchmarks for rail vehicle simulation," *Vehicle System Dynamics*, vol. 30, no. 3-4, pp. 295–313, 1998.

[29] N. J. Mansfield, *Human Response to Vibration*. United States of America: CRC Press LLC, 2005.

[30] A. H. Wickens, *Fundamentals of Rail Vehicle Dynamics: Guidance and Stability*. Lisse, Netherlands: Swets & Zeitlinger, 2003.

[31] W. Zhai and X. Sun, "A detailed model for investigating vertical interaction between railway vehicle and track," *Vehicle System Dynamics*, vol. 23, pp. 603–615, 1994.

[32] J. A. Elkins, "Prediction of wheel/rail interaction:: the state-of-the-art," *Vehicle System Dynamics*, vol. 20, pp. 1–27, 1992.

[33] T. Dahlberg, *Track Issues*, ser. Handbook of railway vehicle dynamics. United States of America: CRC Press, 2006, p. 143.

[34] J. R. Evans, *Multi-body techniques in railway applications*, ser. Multi-Body Dynamics: Monitoring and Simulation Techniques. Bradford, UK: University of Bradford, 1997, vol. 31, p. 281.

[35] S. Bruni, J. Vinolas, M. Berg, O. Polach, and S. Stichel, "Modelling of suspension components in a rail vehicle dynamics context," *Vehicle System Dynamics*, vol. 49, no. 7, pp. 1021–1072, 2011.

[36] A. Facchinetti, L. Mazzola, S. Alfi, and S. Bruni, "Mathematical modelling of the secondary airspring suspension in railway vehicles and its effect on safety and ride comfort," *Vehicle System Dynamics supl.*, vol. 48, p. 429, 2010.

[37] M. Presthus, "*Derivation of Air Spring Model Parameters for Train Simulation*," Lulea, Sweden, M.Phil thesis, Lulea University of Technology, 2002.

[38] A. C. Mellado, C. Casanueva, J. Vinolas, and J. G. Gimenez, "A lateral active suspension for conventional railway bogies," *Vehicle System Dynamics*, vol. 47, no. 1, p. 1, 2009.

[39] S. Bruni, J. Vinolas, M. Berg, O. Polach, and S. Stichel, "Modelling of suspension components in a rail vehicle dynamics context," *Vehicle System Dynamics*, vol. 49, no. 7, p. 1021, 2011.

[40] A. C. Zolotas, J. T. Pearson, and R. M. Goodall, "Modelling requirements for the design of active stability control strategies for a high speed bogie," *Multibody System Dynamics*, vol. 15, no. 1, pp. 51–66, 2006.

[41] X. Zheng, "Active vibration control of flexible bodied railway vehicles via smart structures," Ph.D. dissertation, Loughborough University, Loughborough, United Kingdom, 2011.

[42] H. Md Yusof, "Technologies and control for active railway suspension actuators," Ph.D. dissertation, Loughborough University, Loughborough, United Kingdom, 2013.

[43] M. Arnold, B. Burgermeister, C. Führer, G. Hippmann, and G. Rill, "Numerical methods in vehicle system dynamics: state of the art and current developments," *Vehicle System Dynamics*, vol. 49, no. 7, pp. 1159–1207, 2011.

[44] E. Foo and R. Goodall, "Active suspension control strategies for flexible-bodied railway vehicles," in *Proceedings of Control '98. UKACC International Conference on (Conf. Publ. No. 455)*, vol. 2, 1998, pp. 1300–1305.

[45] A. Orvnäs, "On Active Secondary Suspension in Rail Vehicles to Improve Ride comfort," Ph.D. dissertation, KTH Engineering Sciences, Stockholm, Sweden, 2011.

[46] International Organization for Standardization, "ISO 2631-1. Mechanical Vibration and Shock. Evaluation of Human Exposure to Whole Body Vibration. Part 1: General Requirements," Geneva, 1997.

[47] V. K. Garg and R. V. Dukkipati, *Dynamics of Railway Vehicle Systems*. United Kingdom: Accademic Press, 1984.

[48] CEN, "ENV 12299: Railway applications — Ride comfort for passengers — Measurement and evaluation," Brussels, 1999.

[49] A. Orvnäs, "Methods for reducing vertical carbody vibrations of a rail vehicle," KTH Engineering Sciences, Tech. Rep., 2010.

[50] N. J. Mansfield, "Literature review on low frequency vibration comfort," Tech. Rep., 2006, Asia Link Program.

[51] R. Narayanamoorthy, V. H. Saran, V. K. Goel, S. P. Harsha, S. Khan, and M. Berg, "Determination of activity comfort in swedish passenger trains," in *Proceedings of the 8th World Congress on Railway Research*. COEX, 2008.

[52] M. K. Bhiwapurkar, V. H. Saran, S. P. Harsha, V. K. Goel, and M. Berg, "Effect of magnitudes and directions (mono-axis and multi-axis) of whole body-vibration exposures and subjects postures on the sketching performance," *Proceedings of the Institution of Mechanical Engineers, Part F: Journal of Rail and Rapid Transit*, vol. 225, no. 1, pp. 71–83, 2011.

[53] J. T. Pearson and R. M. Goodall, "An active stability system for a high speed railway vehicle," in *Electronic Systems and Control Division Research*. United Kingdom: Loughborough University, 2003.

[54] J. T. Pearson, R. M. Goodall, T. X. Mei, and G. Himmelstein, "Active stability control strategies for a high speed bogie," *Control Engineering Practice*, vol. 12, no. 11, pp. 1381–1391, 2004.

[55] S. Shen, T. X. Mei, R. M. Goodall, and J. T. Pearson, "A novel control strategy for active steering of railway bogies," in *Proceedings of the UKACC Conference Control 2004*, UK, 2004.

[56] G. Shen and R. Goodall, "Active yaw relaxation for improved bogie performance," *Vehicle System Dynamics*, vol. 28, no. 4, p. 273, 1997.

[57] E. K., B. J.H., and N. S.P., "Energy requirements of a passive and an electromechanical active suspension system," *Vehicle System Dynamics*, vol. 34, no. 6, pp. 437–458,, 2000.

[58] G. Corriga, S. Sanna, and G. Usai, "An optimal tandem active-passive suspension system for road vehicles with minimum power consumption," *Industrial Electronics, IEEE Transactions on*, vol. 38, no. 3, pp. 210–216, 1991.

[59] A. Giua, C. Seatzu, and G. Usai, "A mixed suspension system for a half-car vehicle model," *Dyn.Control*, vol. 10, no. 4, pp. 375–397, 2000.

[60] M. C. Smith and S. J. Swift, "Power dissipation in automotive suspensions," *Vehicle System Dynamics*, vol. 49, no. 1-2, pp. 59–74, 2010.

[61] A. Casavola and F. D. Iorio, "Increasing energy harvesting in regenerative suspension systems via multiobjective H_∞ control robust control design." IFAC online, 2012.

[62] S. B. David and B. Z. Bobrovsky, "Actively controlled vehicle suspension with energy regeneration capabilities," *Vehicle System Dynamics*, vol. 49, no. 6, pp. 833–854, 2011.

[63] L. Zuo and P.-S. Zhang, "Energy harvesting, ride comfort, and road handling of regenerative vehicle suspensions," *ASME Conference Proceedings*, vol. 2011, no. 54761, pp. 295–302, 2011.

[64] F. D. Iorio and A. Casavola, "A multiobjective H_∞ control strategy for energy harvesting while damping for regenerative vehicle suspension systems," in *Proceedings of 2012 American Control Conference*, Montréal, Canada, 2012, pp. 491–496.

[65] M. N. Ichchou, T. Loukil, O. Bareille, and J. G Chamberland and, "A reduced energy supply strategy in active vibration control," *Smart Materials and Structures*, vol. 20, no. 12, p. 125008, 2011.

[66] H. Frahm, "Device for damping vibrations of bodies," Patent 989 958, 1911.

[67] K. Liu and G. Coppola, "Optimal design of damped dynamic vibration absorber for damped primary systems," *Transactions of the Canadian Society for Mechanical Engineering*, vol. 34, no. 1, p. 119, 2010.

[68] M. Zilletti, S. J. Elliott, and E. Rustighi, "Optimisation of dynamic vibration absorbers to minimise kinetic energy and maximise internal power dissipation," *Journal of Sound and Vibration*, vol. 331, no. 18, pp. 4093–4100, 2012.

[69] R. M. Goodall, "Control for railways - active suspensions and other opportunities," in *Proceedings of the 19th Mediterranean Conference on Control & Automation (MED)*, 2011, pp. 639–643.

[70] A. Orlova and Y. Boronenko, *The Anatomy of Railway Vehicle Running Gear*, ser. Handbook of Railway Vehicle Dynamics. United States of America: CRC Press, 2006, p. 39.

[71] H. Sayyaadi and N. Shokouhi, "New dynamics model for rail vehicles and optimizing air suspension parameters using ga," *Scientia Iranica. Transaction B: Mechanical Engineering*, vol. 16, no. 6, p. 496, 2009.

[72] A. Orvnäs, E. Andersson, and R. Persson, "Development of track-friendly bogies for high speed," Division of Rail Vehicles, Department of Aeronautical and Vehicle Engineering, KTH, Tech. Rep., 2007.

[73] E. Andersson, A. Orvnäs, and R. Persson, "On the optimization of a track-friendly bogie for high speed," in *Proceedings of the 21st International Symposium on Dynamics of Vehicles on Roads and Tracks, IAVSD'09*, 2009.

[74] B. Peikari, *Fundamentals of network analysis and synthesis.* Englewood Cliffs, NJ: Prentice Hall, 1974.

[75] M. C. Smith, "Force-controlling mechanical device," Patent US 7 316 303 B2, 2008.

[76] M. C. Smith, N. E. Houghton, P. J. G. Long, and R. A. Glover, "Force-controlling hydraulic device," Patent US 2012/0 199 428 A1, 2012.

[77] B. Gartner and M. Smith, "Damping and inertial hydraulic device," Patent W0 2011/095 787 A1, 2011.

[78] R. Tuluie, "Fluid Inerter," Patent WO 2011/089 373 A1, 2011.

[79] F.-C. Wang, M.-S. Hsu, W.-J. Su, and T.-C. Lin, "Screw type inerter mechanism," Patent US 2009/0 108 510 A1, 2009.

[80] F.-C. Wang and H.-a. Chan, "Mechatronic suspension system and method for shock absorbing thereof," Patent US 2010/0 148 463 A1, 2010.

[81] C. Li, M. Liang, Y. Wang, and Y. Dong, "Vibration suppression using two-terminal flywheel. part i: Modeling and characterization," *Journal of Vibration and Control*, 2011.

[82] ——, "Vibration suppression using two-terminal flywheel. part ii: application to vehicle passive suspension," *Journal of Vibration and Control*, 2011.

[83] L. Lagiewka, S. Gumula, and G. Piontek, "Project EPAR," http://www.epar.pl/en/, 2011, [Accessed date: December 2012].

[84] F. C. Wang, "Impact of inerter nonlinearities on vehicle suspension control," *Vehicle System Dynamics*, vol. 46, no. 7, pp. 575–595, 2008.

[85] ——, "Inerter nonlinearities and the impact on suspension control," in *Proceedings of the American Control Conference 2008*, W. Su, Ed., vol. 1–12. IEEE Xplore, 2008, pp. 3245–3250.

[86] C. Papageorgiou, N. E. Houghton, and M. C. Smith, "Experimental testing and analysis of inerter devices," *Journal of Dynamic Systems, Measurement, and Control*, vol. 131, no. January 2009, 2009.

[87] J. Z. Jiang, M. C. Smith, and N. E. Houghton, "Experimental testing and modelling of a mechanical steering compensator," Cambridge University, Department of Engineering, Tech. Rep., 2007.

[88] M. C. Smith and F. C. Wang, "Performance benefits in passive vehicle suspensions employing inerters," *Vehicle System Dynamics*, vol. 42, no. 4, pp. 235–257, 2004.

[89] F. Scheibe and M. Smith, "Analytical solutions for optimal ride comfort and tyre grip for passive vehicle suspensions," *Vehicle System Dynamics*, pp. 1, ifirst, 2009.

[90] F. C. Wang and H. A. Chan, "Mechatronic suspension design and its applications to vehicle suspension control," *Proceedings of the 47th IEEE Conference on Decision and Control*, 2008.

[91] S. Evangelou, "Steering compensation for high-performance motorcycles," *43rd IEEE Conference on Decision and Control (CDC), vols. 1-5*, pp. 749–754, 2004.

[92] C. Papageorgiou, "Positive real synthesis using matrix inequalities for mechanical networks: Application to vehicle suspension," *IEEE Transactions on Control Systems Technology*, vol. 14, no. 3, pp. 423–435, 2006.

[93] J. Lofberg, "YALMIP : a toolbox for modeling and optimization in MATLAB," in *Proceedings of the IEEE International Symposium on Computer Aided Control Systems Design*, 2004, pp. 284–289.

[94] J. Jiang and M. Smith, "Regular positive-real functions and the classification of transformerless series-parallel networks," vol. 398, pp. 15–25, 2010.

[95] J. Z. Jiang and M. C. Smith, "Synthesis of positive-real functions with low-complexity series-parallel networks," in *Proceedings of the 48th IEEE Conference on Decision and Control held jointly with the 28th Chinese Control Conference. CDC/CCC*, 2009, pp. 7086–7091.

[96] E. Guglielmino, T. Sireteanu, C. W. Stammers, G. Ghita, and M. Giuclea, *Semi-active Suspension Control: Improved Vehicle Ride and Road Friendliness*. London: Springer, 2010.

[97] K. Tanifuji, S. Koizumi, and R. hei Shimamune, "Mechatronics in japanese rail vehicles: active and semi-active suspensions," *Control Engineering Practice*, vol. 10, no. 9, pp. 999–1004, 2002.

[98] D. H. Wang and W. H. Liao, "Semi-active suspension systems for railway vehicles using magnetorheological dampers. part i: system integration and modelling," *Vehicle System Dynamics*, vol. 47, no. 11, pp. 1305–1325, 2009.

[99] D. Fischer and R. Isermann, "Mechatronic semi-active and active vehicle suspensions," *Control Engineering Practice; Mechatronic Systems*, vol. 12, no. 11, pp. 1353–1367, 2004.

[100] L. Tian-ye, W. Zhong-dong, T. Ming-xiang, and Z. Wan-ling, "Study on semi-active secondary suspension of railway vehicle," in *Proceedings of the International Conference on Transportation, Mechanical, and Electrical Engineering (TMEE 2011)*, 2011, pp. 1269–1272.

[101] C. Li and Q. Zhao, "Fuzzy control of vehicle semi-active suspension with MR damper," in *Proceedings of WASE International Conference on Information Engineering (ICIE)*, vol. 3, 2010, pp. 426–429.

[102] S. H. Zareh, A. Sarrafan, M. Abbasi, and A. Khayyat, *Intelligent neuro-fuzzy application in semi-active suspension system*, ser. Fuzzy logic -Controls, concepts, theories and applications. Online: Intech, 2012, p. 237.

[103] H. Du, K. Y. Sze, and J. Lam, "Semi-active control of vehicle suspension with magneto-rheological dampers," *Journal of Sound and Vibration*, vol. 283, no. 3, pp. 981–996, 2005.

[104] K. Hudha, M. H. Harun, M. H. Harun, and H. Jamaluddin, "Lateral suspension control of railway vehicle using semi-active magnetorheological damper," in *Intelligent Vehicles Symposium (IV), 2011 IEEE*, 2011, pp. 728–733.

[105] H. A. E. Gamal, S. F. Rezeka, I. M. E. Faham, and M. M. Abd El Kader, "Sliding control of magneto-rheological dampers in trains," *American Journal of Scientific Research*, no. 44, p. 139, 2012.

[106] L. Mei, L. Zhongxing, S. Xufeng, and G. Jiwei, "Study on PID control for semi-active air suspension for riding comfort," in *Proceedings of the Second WRI Global Congress on Intelligent Systems (GCIS)*, vol. 2, 2010, pp. 47–50.

[107] S. Iwnicki, "Future trends in railway engineering," *Proceedings of the Institution of Mechanical Engineers, Part C: Journal of Mechanical Engineering Science*, vol. 223, no. 12, p. 2743, 2009.

[108] D. Karnopp, *Active and passive isolation of random vibration*, ser. Isolation of Mechanical Vibration Impact and Noise. ASME Monograph, American Society of Mechanical Engineers, 1973, p. 64.

[109] H. Li and R. M. Goodall, "Linear and non-linear skyhook damping control laws for active railway suspensions," *Control Engineering Practice*, vol. 7, no. 7, pp. 843–850, 1999.

[110] H. Li, "*Non-linear control approaches for active railway suspensions*," Loughborough, United Kingdom, M.Phil thesis, Loughborough University, 1997.

[111] S. Alfi, S. Bruni, E. D. Gialleonardo, and A. Facchinetti, "Active control of airspring secondary suspension for improving ride comfort in presence of random track irregularities," *Journal of Mechanical Systems for Transportation and Logistics*, vol. 3, no. 1, 2010.

[112] T. X. Mei and R. G. M, "Use of multiobjective genetic algorithms to optimize inter-vehicle active suspensions," *Proceedings of The Institution of Mechanical Engineers Part F-journal of Rail and Rapid Transit*, vol. 216, no. 1, pp. 53–63, 2002.

[113] N. Hohenbichler, K. Six, and D. Abel, "The benefit of skyhook control in high speed railway vehicles." IFAC-PapersOnline, 2006, p. 890.

[114] D. Hrovat, "Optimal active suspension structures for quarter-car vehicle models," *Automatica*, vol. 26, no. 5, pp. 845–860, 1990.

[115] T. X. Mei, H. Li, and R. M. Goodall, "Kalman filters applied to actively controlled railway vehicle suspensions," *Transactions of the Institute of Measurement and Control*, vol. 23, no. 3, pp. 163–181, 2001.

[116] H. Selamat, A. J. Alimin, and M. A. Zawawi, "Optimal control of railway vehicle system," in *Proceedings of the IEEE International Congress on Industrial Technology, 2009. ICIT*, 2009, pp. 1–6.

[117] T. Yoshimura, "Construction of an active suspension system of a quarter car model using the concept of sliding mode control," *Journal of Sound and Vibration*, vol. 239, no. 2, p. 187, 2001.

[118] Y. M. Sam, J. H. S. Osman, and M. R. A. Ghani, "A class of proportional-integral sliding mode control with application to active suspension system," *Systems and Control Letters*, vol. 51, no. 3-4, pp. 217–223, 2004.

[119] A. Alleyne and J. K. Hedrick, "Nonlinear adaptive control of active suspensions," *Control Systems Technology, IEEE Transactions on*, vol. 3, no. 1, pp. 94–101, 1995.

[120] T. X. Mei and R. M. Goodall, "Recent development in active steering of railway vehicles," *Vehicle System Dynamics*, vol. 39, no. 6, pp. 415–436, 2003.

[121] P. E. Orukpe, X. Zheng, I. M. Jaimoukha, A. C. Zolotas, and R. M. Goodall, "Model predictive control based on mixed h-2/h-infinity control approach for active vibration control of railway vehicles," *Vehicle System Dynamics*, vol. 46, pp. 151–160, 2008.

[122] M. V. C. Rao and V. Prahlad, "A tunable fuzzy logic controller for vehicle-active suspension systems," *Fuzzy Sets Systems*, vol. 85, no. 1, pp. 11–21, 1997.

[123] S. Sezer and A. E. Atalay, "Dynamic modeling and fuzzy logic control of vibrations of a railway vehicle for different track irregularities," *Simulation Modelling Practice and Theory*, vol. 19, no. 9, pp. 1873–1894, 2011.

[124] I. J. Fialho and G. J. Balas, "Design of nonlinear controllers for active vehicle suspensions using parameter-varying control synthesis," *Vehicle System Dynamics*, vol. 33, no. 5, pp. 351–370, 2000.

[125] B. T. Fijalkowski, *Automotive mechatronics: operational and practical issues. Volume II.* London: Springer, 2011, vol. 52, no. II.

[126] M. J. Smith, K. M. Grigoriadis, and R. E. Skelton, "The optimal mix of passive and active control in structures," in *Proceedings of the American Control Conference 1991*, 1991, pp. 1459–1464.

[127] F.-C. Wang and H. an Chan, "Network optimization and synthesis using a combined mechanical and electrical system: Application to vehicle suspension control," in *Proceedings of the 19th International Symposium on Mathematical Theory of Networks and Systems*, 2010.

[128] A. Pacchioni, R. M. Goodall, and S. Bruni, "Active suspension for a two-axle railway vehicle," *Vehicle System Dynamics*, vol. 48, no. sup1, pp. 105–120, 2010.

[129] P. J. Remington, *Wheel and rail excitation from roughness*, ser. Noise and Vibration from High-Speed Trains. London: Thomas Telford Publishing, 2001, p. 29.

[130] G. A. Hunt, "Dynamic analysis of railway vehicle/track interaction forces," Ph.D. dissertation, Loughborough University, Loughborough, United Kingdom, 1986.

[131] J. C. O. Nielsen, R. Lundèn, A. Johansson, and T. Vernersson, "Train-track interaction and mechanisms of irregular wear on wheel and rail surfaces," *Vehicle System Dynamics*, vol. 40, no. 1-3, pp. 3–54, 2003.

[132] A. C. Zolotas, "Advanced control strategies for tilting trains," Ph.D. dissertation, Loughborough University, Loughborough, United Kingdom, 2002.

[133] A. Alonso, J. G. Gimenez, J. Nieto, and J. Vinolas, "Air suspension characterisation and effectiveness of a variable area orifice," *Vehicle System Dynamics*, vol. 48, pp. 271–286, 2010.

[134] A. Z. Matamoros-Sanchez and R. M. Goodall, "The optimisation problem in the enhancement of railway vehicles performance using novel suspension systems," in *Proceedings of the XI International Congress on Numerical Methods in Engineering and Applied Sciences*, 2012.

[135] J. E. Paddison, "Advanced control strategies for maglev suspension systems," Ph.D. dissertation, Loughborough University, 1995.

[136] S. H. Crandall and W. D. Mark, *Random Vibration in Mechanical Systems*. London: Academic Press, 1963.

[137] J. A. Sokolowski and C. M. Banks, *Handbook of Real-World Applications of Modeling and Simulation*. Canada: John Wiley & Sons, 2012.

[138] R. Ortega, A. Loria, P. J. Nicklasson, and H. Sira-Ramirez, *Passivity-based Control of Euler-Lagrange Systems*. Great Britain: Springer, 1998.

[139] D. A. Dirksz and J. M. A. Scherpen, "Passivity-based tracking control of port-Hamiltonian mechanical systems with only position measurements," in *Proceedings of the European Control Conference 2009*. ECC2009, 2009, p. 4689.

[140] R. Ortega, A. J. V. D. Schaft, I. Mareels, and B. Maschke, "Putting energy back in control," *Control Systems Magazine, IEEE*, vol. 21, no. 2, pp. 18–33, 2001.

[141] A. M. Bloch, N. E. Leonard, and J. E. Marsden, "Controlled lagrangians and the stabilization of mechanical systems i: The first matching theorem," *Automatic Control, IEEE Transactions on*, vol. 45, no. 12, pp. 2253–2270, 2000.

[142] ——, "Stabilization of mechanical systems using controlled Lagrangians," in *Proceedings of the 36th IEEE Conference on Decision and Control*, vol. 3. IEEE Xplore, 1997, pp. 2356–2361.

[143] A. M. Bloch, D. E. Chang, N. E. Leonard, and J. E. Marsden, "Controlled lagrangians and the stabilization of mechanical systems. ii. potential shaping," *Automatic Control, IEEE Transactions on*, vol. 46, no. 10, pp. 1556–1571, 2001.

[144] A. M. Bloch, N. E. Leonard, and J. E. Marsden, "Potential shaping and the method of controlled Lagrangians," in *Proceedings of the 38th IEEE Conference on Decision and Control*, vol. 2, 1999, pp. 1652–1657.

[145] A. D. Lewis, "Notes on energy shaping," in *Proceedings of the 43rd IEEE Conference on Decision and Control, 2004. CDC*, vol. 5, 2004, pp. 4818–4823.

[146] B. Brogliato, R. Lozano, B. Maschke, and O. Egeland, *Dissipative Systems Analysis and Control. Theory and Applications*. Great Britain: Springer, 2000.

[147] J. S. Moon, "Stability analysis and control for bipedal locomotion using energy methods," Ph.D. dissertation, University of Illinois, Urbana, United States, 2011.

[148] A. Cesur, "*A numerical study of fluid-structure interaction of non-deformable cylinders*," Lund, Sweden, 2011, Licenciate of Engineering thesis, Lund University.

[149] J. Zhou, R. Goodall, L. Ren, and H. Zhang, "Influences of car body vertical flexibility on ride quality of passenger railway vehicles," *Proceedings of the Institution of Mechanical Engineers, Part F: Journal of Rail and Rapid Transit*, vol. 223, no. 5, pp. 461–471, 2009.

[150] M. C. Smith and F. C. Wang, "Controller parameterization for disturbance response decoupling: application to vehicle active suspension control," *Control Systems Technology, IEEE Transactions on*, vol. 10, no. 3, pp. 393–407, 2002.

[151] J. K. Hedrick and T. Butsuen, "Invariant properties of automotive suspensions," *Proceedings of the Institution of Mechanical Engineers, Part D: Journal of Automobile Engineering*, vol. 204, no. 1, pp. 21–27, 1990.

[152] P. Dorato, C. Abdallah, and V. Cerone, *Linear-Quadratic Control: An Introduction*. USA: Prentice Hall, 1995.

[153] MathWorks, "Optimization toolbox. matlab r2012b." *Matlab Users Guide*, 2012.

[154] P. Albertos-Pérez and A. Sala, *Multivariable Control Systems: An Engineering Approach*. London: Springer, 2004.

[155] G. F. Franklin, J. D. Powell, and A. Emami-Naeini, *Feedback Control of Dynamic Systems*, 4th ed. Upper Saddle River, NJ: Prentice Hall, 2002.

[156] SIMPACK, "SIMPACK MBS Software," http://www.simpack.com, 2013, [Accessed date: January 2013].

[157] R. M. Goodall, "Concepts and prospects for actively controlled railway running gear," *Vehicle System Dynamics*, vol. 44, pp. 60–70, 2006.

[158] T. X. Mei, Z. Nagy, and R. M. Goodall, "Modelling comparison of actively-steered railway vehicles using simpack and matlab," in *Proceedings of the 5th European Control Conference*, 1999.

[159] T. X. Mei, S. Shen, R. M. Goodall, and J. T. Pearson, "Active steering control for railway bogies based on displacement measurements," in *Proceedings of the 16th IFAC World Congress*. Elsevier IFAC Publications, 2005, p. 586.

[160] A. H. Wickens, R. M. Goodall, and J. Li, "Re-evaluation of the limitations of the railway wheelset: passive and active," *Vehicle System Dynamics*, vol. 44, no. 1 supp 1, p. 14, 2006.

[161] J. Perez, J. M. Busturia, and R. M. Goodall, "Control strategies for active steering of bogie-based railway vehicles," *Control Engineering Practice*, vol. 10, p. 1005, 2002.

[162] H. Sira-Ramirez, A. Z. Matamoros-Sanchez, and R. M. Goodall, "Flatness based control of a suspension system: a GPI observer approach," in *Proceedings of the 18th IFAC World Congress*, 2011.

[163] A. Z. Matamoros-Sanchez, H. Sira-Ramírez, and R. M. Goodall, *Estimación y control por realimentación de los estados de la salida plana de un vehículo utilizando un observador GPI*, ser. Aplicaciones de Control, Automatización, Robótica y Visión Artificial. Venezuela: Universidad de Los Andes, 2012.

[164] A. Cabrera-Amado and G. Silva-Navarro, "Positive position and acceleration feedback control for the unbalance response in a rotor-bearing system," in *6th International Conference on Electrical Engineering, Computing Science and Automatic Control, CCE*, 2009.

[165] M. T. Ltd., "Motor Technology," http://www.controlinmotion.com, 2012, [Accessed date: September 2012].

[166] J. Hedrick and H. Firouztash, "The covariance propagation equation including time-delayed inputs," *IEEE Transactions on Automatic Control*, vol. 19, no. 5, pp. 587 – 589, 1974.

A

'Shaping' the Dynamic of an Actual Airspring

Table A.1: Parameters of the biquadratic real-rational functions approximating the experimental response of an actual airspring

Model	Block	$f_{1,i}$ [Hz]	$\zeta_{1,i}$	$f_{2,i}$ [Hz]	$\zeta_{2,i}$
One-block	1	4.58	0.27	7	0.3
Two-block	1	4.58	0.22	6.21	0.27
	2	7.8	0.3	8.28	0.3
Three-block (A)	1	4.58	0.22	6.21	0.27
	2	7.8	0.3	8.28	0.3
	3	13.53	0.22	13.21	0.22
Three-block (B)	1	4.58	0.22	6.21	0.27
	2	7.8	0.3	8.28	0.3
	3	14.163	0.14	13.85	0.13

[a] $J_m^\flat$ and $c_m^\flat$ are for analysis of motor inertia and friction purposes, only.

The plots in Figure A.2 allow to associate variations in the inertance value b_g and the damping value c_g in the inerter-based model in Figure 3.4 to the connecting pipe length variation . By qualitative comparison with results reported by Sayyaadi and Shokouhi [71], the longer the pipe, the higher the inertance and the series damping which can be associated to frictions in the pipe. Similarly, the plots in Figure

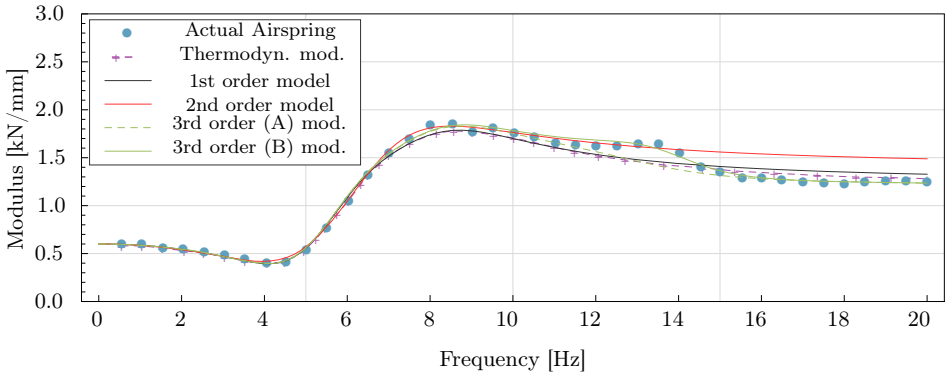

(a) Airspring dynamic stiffness gain

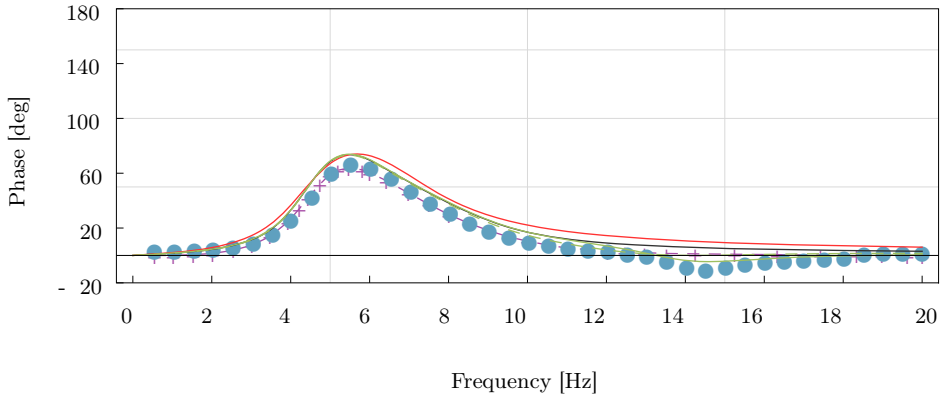

(b) Airspring dynamic stiffness phase

Figure A.1: Frequency response of linear approximations of an actual airspring vertical dynamic

A.3 depicts that variations in the inertance value b_g and the damping value c_r can be associated to diameter variation of the connecting pipe; the smaller the pipe's cross-sectional area, the higher the inertance and the parallel damping which can be associated also to losses in the pipework. Finally, Figure A.4 shows that variations in c_r only are related to damping design; the smaller the orifice of a restriction in the connecting pipe, the higher the parallel damping value which this time is an actual damping parameter and not to friction losses.

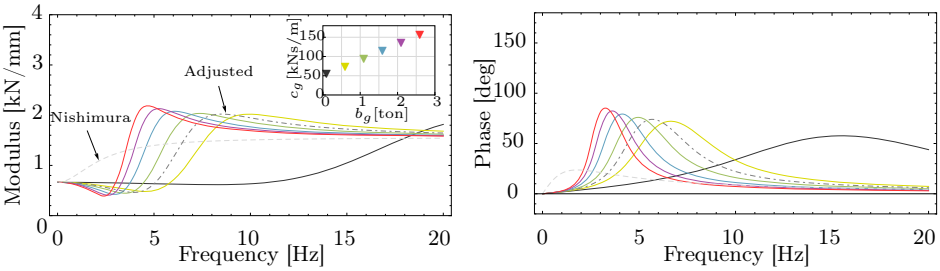

(a) Airspring dynamic stiffness gain (b) Airspring dynamic stiffness phase

FIGURE A.2: b_g and c_g variation, equivalent to the airspring connecting pipe's length variation.

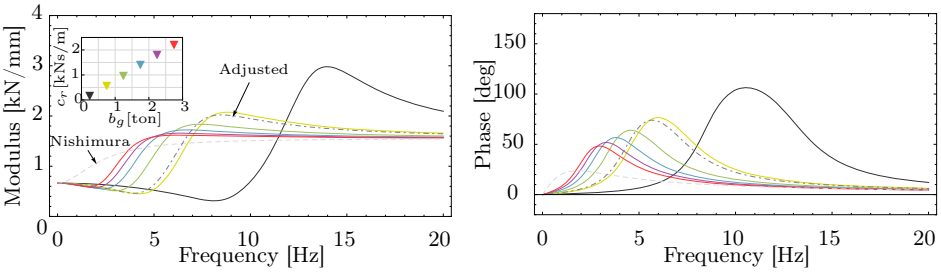

(a) Airspring dynamic stiffness gain (b) Airspring dynamic stiffness phase

FIGURE A.3: b_g and c_r variation, equivalent to the airspring connecting pipe's diameter variation.

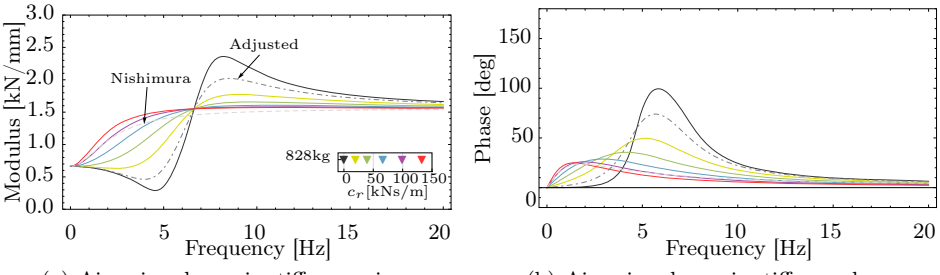

(a) Airspring dynamic stiffness gain (b) Airspring dynamic stiffness phase

FIGURE A.4: c_r variation, equivalent to orifice damping variation.

B

System Matrices

$$\mathbf{M} = \begin{pmatrix} m_v & 0 & 0 & 0 & 0 & 0 & 0 & 0 & 0 & 0 \\ 0 & I_{vy} & 0 & 0 & 0 & 0 & 0 & 0 & 0 & 0 \\ 0 & 0 & m_b + b_g & 0 & 0 & -b_g & 0 & 0 & 0 & 0 \\ 0 & 0 & 0 & I_{by} & 0 & 0 & 0 & 0 & 0 & 0 \\ 0 & 0 & 0 & 0 & m_p & 0 & 0 & 0 & 0 & 0 \\ 0 & 0 & -b_g & 0 & 0 & m_p + b_g & 0 & 0 & 0 & 0 \\ 0 & 0 & 0 & 0 & 0 & 0 & m_b + b_g & 0 & 0 & -b_g \\ 0 & 0 & 0 & 0 & 0 & 0 & 0 & I_{by} & 0 & 0 \\ 0 & 0 & 0 & 0 & 0 & 0 & 0 & 0 & m_p & 0 \\ 0 & 0 & 0 & 0 & 0 & 0 & -b_g & 0 & 0 & m_p + b_g \end{pmatrix}$$

$$\mathbf{C} = \begin{pmatrix} 0 & 0 & 0 & 0 & 0 & 0 & 0 & 0 & 0 & 0 \\ 0 & 0 & 0 & 0 & 0 & 0 & 0 & 0 & 0 & 0 \\ 0 & 0 & 2\,c_p + c_r & 0 & -c_r & 0 & 0 & 0 & 0 & 0 \\ 0 & 0 & 0 & 2\,c_p l_b^2 & 0 & 0 & 0 & 0 & 0 & 0 \\ 0 & 0 & -c_r & 0 & c_r + c_g & -c_g & 0 & 0 & 0 & 0 \\ 0 & 0 & 0 & 0 & -c_g & c_g & 0 & 0 & 0 & 0 \\ 0 & 0 & 0 & 0 & 0 & 0 & 2\,c_p + c_r & 0 & -c_r & 0 \\ 0 & 0 & 0 & 0 & 0 & 0 & 0 & 2\,c_p l_b^2 & 0 & 0 \\ 0 & 0 & 0 & 0 & 0 & 0 & -c_r & 0 & c_r + c_g & -c_g \\ 0 & 0 & 0 & 0 & 0 & 0 & 0 & 0 & -c_g & c_g \end{pmatrix}$$

$$
\mathrm{K} = \begin{pmatrix}
\kappa_v & 0 & -k_a & 0 & -k_s & 0 & -k_a & 0 & -k_s & 0 \\
0 & \kappa_v l_v^2 & -k_a l_v & 0 & -k_s l_v & 0 & k_a l_v & 0 & k_s l_v & 0 \\
-k_a & -k_a l_v & \kappa_b & 0 & -k_r & 0 & 0 & 0 & 0 & 0 \\
0 & 0 & 0 & 2\,k_p l_b^2 & 0 & 0 & 0 & 0 & 0 & 0 \\
-k_s & -k_s l_v & -k_r & 0 & k_s + k_r & 0 & 0 & 0 & 0 & 0 \\
0 & 0 & 0 & 0 & 0 & 0 & 0 & 0 & 0 & 0 \\
-k_a & k_a l_v & 0 & 0 & 0 & 0 & \kappa_b & 0 & -k_r & 0 \\
0 & 0 & 0 & 0 & 0 & 0 & 0 & 2\,k_p l_b^2 & 0 & 0 \\
-k_s & k_s l_v & 0 & 0 & 0 & 0 & -k_r & 0 & k_s + k_r & 0 \\
0 & 0 & 0 & 0 & 0 & 0 & 0 & 0 & 0 & 0
\end{pmatrix}
$$

$\kappa_v = 2\ (k_s + k_a)$

$\kappa_b = k_r + k_a + 2\,k_p$

$$
\mathbf{Q}_m = \begin{pmatrix}
0 & 0 & 0 & 0 \\
0 & 0 & 0 & 0 \\
k_p & k_p & 0 & 0 \\
k_p l_b & -k_p l_b & 0 & 0 \\
0 & 0 & 0 & 0 \\
0 & 0 & 0 & 0 \\
0 & 0 & k_p & k_p \\
0 & 0 & k_p l_b & -k_p l_b \\
0 & 0 & 0 & 0 \\
0 & 0 & 0 & 0
\end{pmatrix}, \text{ and } \dot{\mathbf{Q}}_m = \begin{pmatrix}
0 & 0 & 0 & 0 \\
0 & 0 & 0 & 0 \\
c_p & c_p & 0 & 0 \\
c_p l_b & -c_p l_b & 0 & 0 \\
0 & 0 & 0 & 0 \\
0 & 0 & 0 & 0 \\
0 & 0 & c_p & c_p \\
0 & 0 & c_p l_b & -c_p l_b \\
0 & 0 & 0 & 0 \\
0 & 0 & 0 & 0
\end{pmatrix}
$$

C

Electromechanical Actuator

The electromechanical actuator was sized following the procedure described by Pratt in [5], for the following specifications:

1. Actuator peak load: $F^{\text{act}}_{\text{max}} = 10\,\text{kN}$
2. Actuator rms load: $F^{\text{act}}_{\text{rms}} = 1\,\text{kN}$
3. Actuator maximum velocity: $\dot{z}^{\text{act}}_{max} = \text{rms}\,(\dot{z}_{act}) \times 3 = 132\,\text{mms}^{-1}$
4. Maximum motor speed: it was assumed $\omega^{\text{m}}_{max} = 3000\,\text{r.p.m.} = 314.16\,\text{rads}^{-1}$

From which: the screw pitch parameter is calculated as $n_{sc} = \frac{\dot{z}^{\text{act}}_{max}}{\omega^{\text{m}}_{max}}$, the motor rating as $\omega^{\text{m}}_{\text{rms}} = \frac{1}{3}\omega^{\text{m}}_{max} = 104.7\,\text{rads}^{-1}$, the rated motor power as $P^{m}_{rms} = \text{rms}\,(\dot{z}_{act}) \times F^{\text{act}}_{\text{rms}} = 44\,\text{W}$, the peak torque as $\tau_{\text{peak}} = \frac{n_{sc}F^{\text{act}}_{\text{max}}}{0.8} = 5.25\,\text{Nm}$ (according to a ball screw efficiency index of 0.8), and the rms torque as $\tau_{\text{rms}} = \frac{n_{sc}F^{\text{act}}_{\text{rms}}}{0.8} = 0.525\,\text{Nm}$. By following a commercial catalogue [165] for a LSH motor (with compressed winding technology and low inertia), the values in the Table C.1 for the motor parts of the electromechanical actuator were obtained.

Also, the values for the remaining mechanical elements of the electromechanical actuator were obtained following Pratt [5]. The referred values are typical to produce up to 1 kW of power, and a 100% damped dynamic with a high natural frequency of 1000 Hz, and are found in Table C.2.

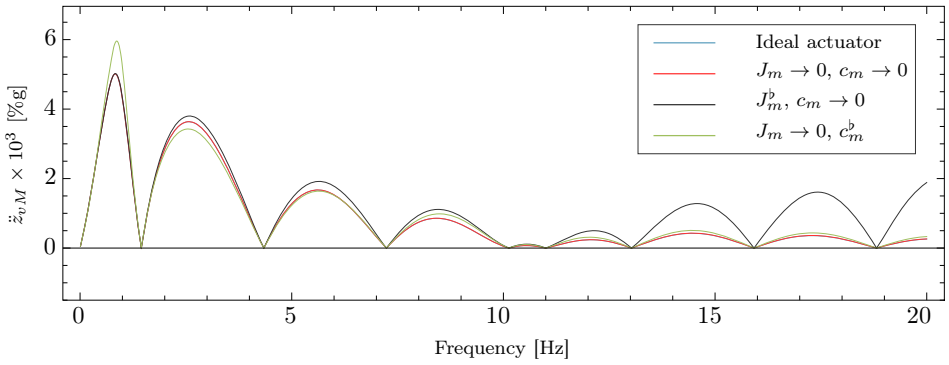

(a) Effects of motor inertia and friction, individually.

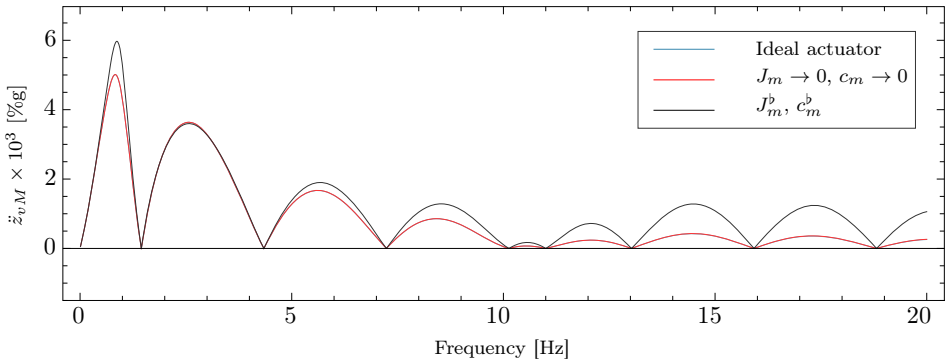

(b) Motor with inertia and friction

Figure C.1: Comparison of the power spectrum density for the vehicle body acceleration (middle, $\ddot{z}_{vM}$) with and without actuator model, with and without motor inertia and/or friction.

Table C.1: Electromechanical actuator motor parameters values

Symbol	Parameter	Unit	Value
K_t	Motor torque constant	$^{\mathrm{Nm}}/_{\mathrm{A}}$	0.69
L_{arm}	Winding inductance	H	15.4×10^{-3}
J_m	Rotor inertia	kgm^2	7×10^{-5}
K_e	Motor back–emf gain	$^{\mathrm{V}}/_{\mathrm{rads}^{-1}}$	41.5×10^{-3}
R_{arm}	Winding resistance	Ohm	4
c_m	Motor friction	$^{Nms}/_{rad}$	2.3×10^{-2}

Table C.2: Electromechanical actuator parameters mechanical-subsystem

Sym.	Parameter	Value	
k_c	Coupling stiffness	$^{\mathrm{N}}/_{\mathrm{m}}$	1×10^7
m_{sc}	Screw mass	kg	2
c_{sc}	Screw friction	$^{\mathrm{Ns}}/_{\mathrm{m}}$	25.13×10^3
n_{sc}	Screw pitch	$^{\mathrm{m}}/_{\mathrm{rad}}$	0.42×10^{-3}
k_{sc}	Screw stiffness	$^{\mathrm{N}}/_{\mathrm{m}}$	12.57×10^6
$J_m^{\flat}$	Rotor inertia	kgm^2	3.53×10^{-5}
$c_m^{\flat}$	Motor friction	$^{\mathrm{Nms}}/_{\mathrm{rad}}$	3.53×10^{-3}

[a] $J_m^{\flat}$ and $c_m^{\flat}$ are for analysis of motor inertia and friction purposes, only.

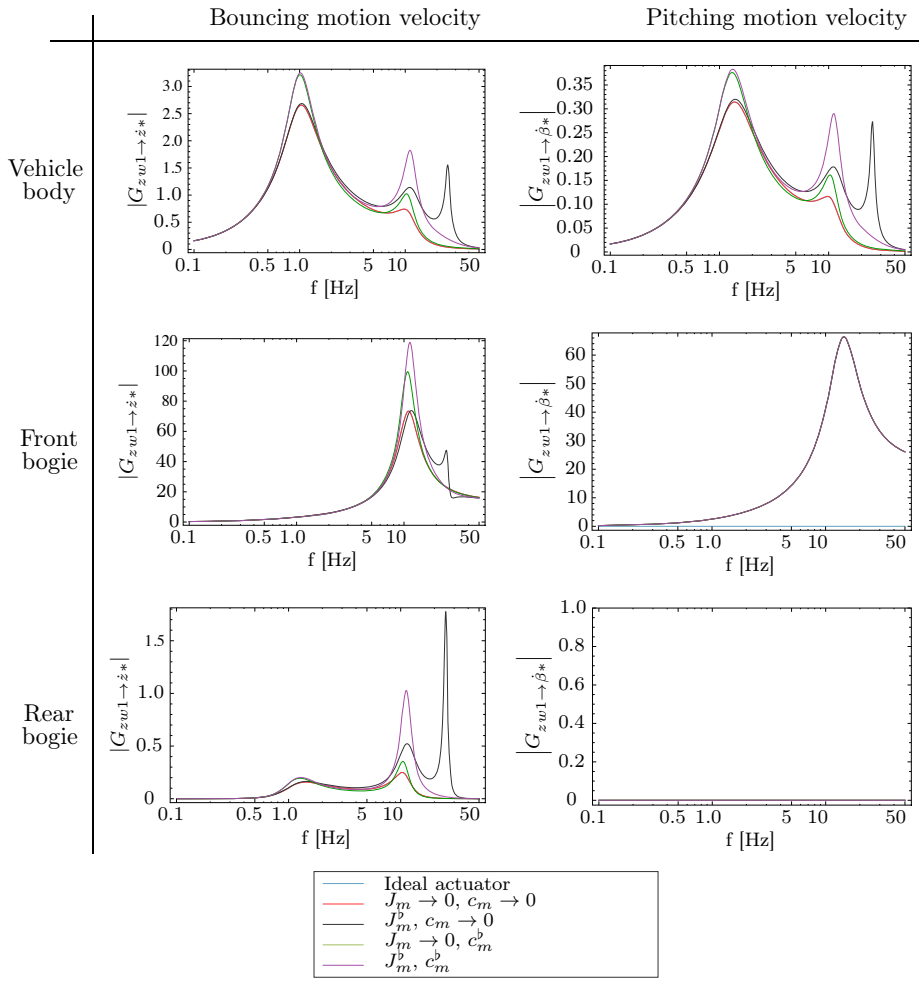

Figure C.2: Gain frequency response for the vehicle's bodies dynamics when excited through the leading wheelset for a vehicle with active suspension (skyhook damping with filtering strategy) and electromechanical actuator. Variation of motor friction and inertia parameters.

D

Theory Supplement

This Appendix includes a theoretical background for the content of this thesis.

D.1 Derivation of the Temporal Spectral Density Function

The spatial spectral density $S_s^{\delta_z}(f_s)$ for a random stationary process of zero mean (i.e. $\bar{\delta}_z = 0$), with f_s the spatial linear frequency, given by

$$S_s^{\delta_z}(f_s) = \frac{\Omega_z}{f_s^2} \quad \left[\mathrm{m}^2\,(^{cycle}/_{\mathrm{m}})^{-1}\right] \tag{D.1}$$

has the equivalent $S_s^{\delta_z}(\omega_s)$ in the circular spatial frequency ω_s derived as

$$\begin{aligned} S_s^{\delta_z}(f_s) &= \frac{\Omega_z}{f_s^2} \quad \left[m^2 \times \frac{m}{cycle} \times \frac{1\,cycle}{2\pi\,rad}\right] \\ &= \frac{\Omega_z}{2\pi f_s^2} \quad \left[m^2\,(^{rad}/_{m})^{-1}\right] \end{aligned} \tag{D.2}$$

$$S_s^{\delta_z}(\omega_s) = \frac{2\pi\,\Omega_z}{\omega_s^2} \quad \left[\mathrm{m}^2\,(^{rad}/_{\mathrm{m}})^{-1}\right] \tag{D.3}$$

The Wiener-Khintchine relations for the Fourier transform pairs given in Equations (D.4)–(D.5) conduct the derivation of the expression for the temporal spectral density, $S_t^{\delta_z}(\omega_t)$,

$$S_t^{\delta_z}(\omega_t) = \frac{1}{2\pi}\int_{-\infty}^{\infty} R_t^{\delta_z}(\tau)\,e^{-j\,\omega_t\tau}d\tau \tag{D.4}$$

where ω_t is the temporal circular frequency, and where

$$R_{\omega}^{\delta_z}(\tau) = \int_{-\infty}^{\infty} S_t^{\delta_z}(\omega_t)\, e^{j\,\omega_t \tau}\, d\omega_t \tag{D.5}$$

includes both positive and negative frequencies and is the non-normalised autocorrelation function of $\delta_z(t)$, i.e. $R_t^{\delta_z}(\tau) = \mathrm{E}[\delta_z(t_2)\,\delta_z(t_1)]$, which has a physical meaning only for the limiting case in which $\tau = t_2 - t_1 = 0$. Thus,

$$R_{\omega}^{\delta_z}(0) = \int_{-\infty}^{\infty} S_t^{\delta_z}(\omega_t)\, d\omega_t \tag{D.6}$$

which is equivalent to the mean-square value of $\delta_z(t)$, i.e.

$$\sigma_{\delta_z}^2 = \mathrm{E}[\delta_z^2(t)] = R_{\omega}^{\delta_z}(0). \tag{D.7}$$

Assuming a constant speed v for the change of $\delta_z(z)$ in the horizontal direction, $\delta_z(z)$ can be converted to a time-function by using the equation of motion: $z = v\,t$. Also the spatial frequency, $\omega_s\,[\mathrm{rad\,m^{-1}}]$, is converted to a temporal frequency, $\omega_t\,[\mathrm{rad\,s^{-1}}]$, by doing $\omega_s = \omega_t / v$. As consequence for Equation (D.6) and using the spatial spectral density described in Equation (D.3), the term $S_t^{\delta z}(\omega_t)\, d\omega_t$ results in

$$S_t^{\delta_z}(\omega_t)\, d\omega_t = \frac{2\pi\,\Omega_z\, v^2}{\omega_t^2}\frac{d\omega_t}{v} \tag{D.8}$$

giving

$$S_t^{\delta_z}(\omega_t) = \frac{2\pi\,\Omega_z\, v}{\omega_t^2} \quad \left[\mathrm{m^2\,(rad/s)^{-1}}\right] \tag{D.9}$$

for the spectral density function in the temporal domain.

D.2 Derivation of the Statistically Stationary Covariance Matrix

The solution for the states of a system with n inputs grouped in the inputs vector $\underline{\dot{\delta}}_m\,(\tau)$,

$$\underline{\dot{x}}^{\flat}(t) = \mathbf{A}^{\flat}\,\underline{x}^{\flat}(t) + \mathbf{B}_{\dot{\delta}}^{\flat}\,(t)\,\underline{\dot{\delta}_m}(t), \tag{D.10}$$

$$\underline{x}^{\flat}(t_0) = \underline{0},\ t_0 = 0 \tag{D.11}$$

is written as

$$\underline{x}^{\flat}(t) = \int_0^t \mathbf{\Phi}(\tau)\,\mathbf{B}_{\dot{\delta}}^{\flat}\underline{\dot{\delta}}_m(\tau)\, d\tau \tag{D.12}$$

by using the state transition matrix $\mathbf{\Phi}(\tau) = e^{\mathbf{A}^{\flat}\,(t-\tau)}$.

If all the system's inputs correspond to a "white" random stationary process with a Gaussian distribution with power p, and are applied to the system at a different time,

$t-\tau_i$ ($i=1,\,2,\,\ldots,n$), one has statistically that they are related through time-delays between every pair of inputs as in the $\mathbf{R}_{\dot{\delta}}(t,\,\tau)$ matrix:

$$
\begin{aligned}
\mathbf{R}_{\dot{\delta}}(t,\,\tau)=&\mathrm{E}\left[\underline{\dot{\delta}}_m(t)\,\underline{\dot{\delta}}_m^T(\tau)\right]\\
=&\mathrm{E}\begin{bmatrix}
\dot{\delta}_z(t-\tau_1)\dot{\delta}_z(\tau-\tau_1) & \cdots & \dot{\delta}_z(t-\tau_1)\dot{\delta}_z(\tau-\tau_n)\\
\dot{\delta}_z(t-\tau_2)\dot{\delta}_z(\tau-\tau_1) & \cdots & \dot{\delta}_z(t-\tau_2)\dot{\delta}_z(\tau-\tau_n)\\
\vdots & \ddots & \vdots\\
\dot{\delta}_z(t-\tau_{n-1})\dot{\delta}_z(\tau-\tau_1) & \cdots & \dot{\delta}_z(t-\tau_{n-1})\dot{\delta}_z(\tau-\tau_n)\\
\dot{\delta}_z(t-\tau_n)\dot{\delta}_z(\tau-\tau_1) & \cdots & \dot{\delta}_z(t-\tau_n)\dot{\delta}_z(\tau-\tau_n)
\end{bmatrix}\\
=&p\begin{bmatrix}
\delta(t-\tau) & 0 & 0 & \cdots & 0\\
0 & \delta(t-\tau) & 0 & \cdots & 0\\
0 & 0 & \delta(t-\tau) & \cdots & 0\\
\vdots & \vdots & \vdots & \ddots & \vdots\\
0 & 0 & 0 & \cdots & \delta(t-\tau)
\end{bmatrix}\\
&+p\begin{bmatrix}
0 & 0 & \cdots & 0 & 0\\
\delta(\tau_{2,\,1}) & 0 & \cdots & 0 & 0\\
\vdots & \vdots & \ddots & \vdots & \vdots\\
\delta(\tau_{n-1,\,1})\delta(\tau_{n-1,\,2}) & \cdots & & 0 & 0\\
\delta(\tau_{n,\,1}) & \delta(\tau_{n,\,2}) & \cdots & \delta(\tau_{n,\,n-1}) & 0
\end{bmatrix}\\
&+p\begin{bmatrix}
0 & \delta(\tau_{1,\,2}) & \cdots & \delta(\tau_{1,\,n-1}) & \delta(\tau_{1,\,n})\\
0 & 0 & \cdots & \delta(\tau_{2,\,n-1}) & \delta(\tau_{2,\,n})\\
\vdots & \vdots & \ddots & \vdots & \vdots\\
0 & 0 & \cdots & 0 & \delta(\tau_{n-1,\,n})\\
0 & 0 & \cdots & 0 & 0
\end{bmatrix}
\end{aligned}
\tag{D.13}
$$

with $\tau_{j,\,i}=t-\tau-(\tau_j-\tau_i)$ for all $i=1,\,2,\,3,\,4$, and $j=1,\,2,\,3,\,4$, where every τ_i/τ_j is the time of application of the i-th/j-th input.

For the mean value of the states associated to the bodies equilibrium, i.e. $\bar{\underline{x}}^{\flat}(t)=\underline{0}$, one has that the covariance matrix for the states of the system is $\mathbf{P}(t)=\mathrm{E}\left[\underline{x}^{\flat}(t)\,\underline{x}^{\flat}(t)^T\right]$ with its first derivative, $\dot{\mathbf{P}}(t)$, a covariance propagation differential equation [166], following Equations (3.96) and (D.12),

$$
\begin{aligned}
\dot{\mathbf{P}}(t)=&\mathrm{E}\left[\dot{\underline{x}}^{\flat}(t)\,\underline{x}^{\flat}(t)^T+\underline{x}^{\flat}(t)\,\dot{\underline{x}}^{\flat}(t)^T\right]\\
=&\mathbf{A}^{\flat}\,\mathbf{P}(t)+P(t)\,\mathbf{A}^{\flat T}+\mathbf{B}_{\dot{\delta}}^{\flat}\int_0^t\mathrm{E}\left[\underline{\dot{\delta}}_m(t)\,\underline{\dot{\delta}}_m(\tau)^T\right]\,\mathbf{B}_{\dot{\delta}}^{\flat T}\,\mathbf{\Phi}(\tau)^T\,d\tau\\
&+\left(\mathbf{B}_{\dot{\delta}}^{\flat}\int_0^t\mathrm{E}\left[\underline{\dot{\delta}}_m(t)\,\underline{\dot{\delta}}_m(\tau)^T\right]\,\mathbf{B}_{\dot{\delta}}^{\flat T}\,\mathbf{\Phi}(\tau)^T\,d\tau\right)^T
\end{aligned}
\tag{D.14}
$$

which for the statistically stationary covariance matrix $\mathbf{P}(t) = \mathbf{P}$ (i.e. $\dot{\mathbf{P}}(t) = \mathbf{0}$) results in the Lyapunov-type equation

$$\mathbf{A}^{\flat}\,\mathbf{P} + \mathbf{P}\,\mathbf{A}^{\flat T} = -p\,\mathbf{B}_{\dot{\delta}}^{\flat}\mathbf{B}_{\dot{\delta}}^{\flat T} - p\sum_{\substack{j=1\\ j>i}}^{4}\sum_{i=1}^{4}\underline{B}_{\dot{\delta}j}^{\flat}\,\underline{B}_{\dot{\delta}i}^{T}\mathbf{\Phi}(\tau_j - \tau_i)^T - \left(p\sum_{\substack{j=1\\ j>i}}^{4}\sum_{i=1}^{4}\underline{B}_{\dot{\delta}j}^{\flat}\,\underline{B}_{\dot{\delta}i}^{T}\mathbf{\Phi}(\tau_j - \tau_i)^T\right)^T \tag{D.15}$$

given $\mathrm{E}\left[\underline{\dot{\delta}}_m(t)\,\underline{\dot{\delta}}_m^T(\tau)\right] = \mathbf{R}_{\dot{\delta}}(t,\,\tau)$, and after evaluation of the convolution integrals arising from decomposition in sums of matrices of the first and second terms of $\mathbf{R}_{\dot{\delta}}(t,\,\tau)$ and with substitution in Equation (D.14); all the convolution integrals related to the third term of $\mathbf{R}_{\dot{\delta}}(t,\,\tau)$ decomposition are zero.

D.3 Derivation of the Side-View Decoupled Model by 'Simplicity'

The transformation matrix L_h in [150] is used here to decouple the system dynamics in two stages: the model of the individual bogies and then a side-view model with only two external excitations. For this, L_h is here a function of the distance between the c.o.g. of the rotating body (bogie or vehicle body), and the force application symmetric points (attachment point of the primary or secondary suspensions), i.e. $L_h(l)$ in general, with:

$$L_h\,(l) = \frac{1}{2\,l}\begin{bmatrix} l & l \\ 1 & -1 \end{bmatrix} \tag{D.16}$$

Therefore, l will take l_b for the first decoupling stage, and l_v for the second one. By defining,

$$\begin{bmatrix} (\hat{z}_{w\,i,\,j})_b \\ (\hat{z}_{w\,i,\,j})_\rho \end{bmatrix} = L_h\,(l_b)\begin{bmatrix} \hat{z}_{w,\,i} \\ \hat{z}_{w,\,j} \end{bmatrix} \tag{D.17}$$

it is not difficult to see that the bouncing components of the wheelsets linked to the front and rear bogies, respectively, can be expressed as:

$$(\hat{z}_{w12})_b = \frac{\hat{z}_{w1} + \hat{z}_{w2}}{2} \tag{D.18}$$

$$(\hat{z}_{w34})_b = \frac{\hat{z}_{w3} + \hat{z}_{w4}}{2} \tag{D.19}$$

where the subindex 'b' is used to denote bouncing components, and the subindex 'ρ'

for pitching components. Also with the same transformation matrix, now $L_h\left(l_v\right)$, the definition

$$\begin{bmatrix}(\hat{x})_b\\(\hat{x})_\rho\end{bmatrix} = L_h\left(l_v\right)\underline{\hat{x}} = L_h\left(l_v\right)\begin{bmatrix}\hat{x}_1\\\hat{z}_2\end{bmatrix} \tag{D.20}$$

for $\hat{x}$ taking the variables: $\hat{z}_b$, $\hat{z}_{wij}$, and $\hat{F}_{\text{act}}$, with:

$$\underline{\hat{z}_b} = \left[\hat{z}_{b1}\hat{z}_{b2}\right]^T \tag{D.21}$$

$$\underline{\hat{z}_{wij}} = \left[\hat{z}_{w12}\hat{z}_{w34}\right]^T \tag{D.22}$$

$$\underline{\hat{F}_{\text{act}}} = \left[\hat{F}_{\text{act}1}\hat{F}_{\text{act}2}\right]^T \tag{D.23}$$

allows to rewrite the model of the system in Equations 3.64–3.67 for examining the dynamics of the vehicle body and the secondary suspensions. That is,

$$\frac{1}{2}m_v s^2\hat{z}_v = -\mathrm{Y}_s(s)s\left(\hat{z}_v - (\hat{z}_b)_b\right) - \left(\hat{F}_{\text{act}}\right)_b \tag{D.24}$$

$$\frac{1}{2}I_{vy}s^2\hat{\beta}_v = l_v^2\left(-\mathrm{Y}_s(s)s\left(\hat{\beta}_v - (\hat{z}_b)_\rho\right) - \left(\hat{F}_{\text{act}}\right)_\rho\right) \tag{D.25}$$

$$\begin{aligned} m_b s^2\left(\hat{z}_b\right)_b = {} & \mathrm{Y}_s(s)s\left(\hat{z}_v - (\hat{z}_b)_b\right) + \left(\hat{F}_{\text{act}}\right)_b \\ & - 2\mathrm{Y}_p(s)s\left((\hat{z}_b)_b - (\hat{z}_{wij})_b\right) \end{aligned} \tag{D.26}$$

$$\begin{aligned} l_v^2 m_b s^2\left(\hat{z}_b\right)_\rho = {} & l_v^2\Bigg(\mathrm{Y}_s(s)s\left(\hat{\beta}_v - (\hat{z}_b)_\rho\right) + \left(\hat{F}_{\text{act}}\right)_\rho \\ & -2\mathrm{Y}_p(s)s\left((\hat{z}_b)_\rho - (\hat{z}_{wij})_\rho\right)\Bigg) \end{aligned} \tag{D.27}$$

where: $\mathrm{Y}_s(s) = \mathrm{Y}_a(s) + \mathrm{Y}_{pn}(s)$.

If one derives the equations for the 'generic' quarter-vehicle represented in Figure 5.2:

$$m_2 s^2\hat{z}_2 = -\mathrm{Y}_s(s)s\left(\hat{z}_2 - \hat{z}_1\right) - F_{\text{act}} \tag{D.28}$$

$$m_1 s^2\hat{z}_1 = \mathrm{Y}_s(s)s\left(\hat{z}_2 - \hat{z}_1\right) + F_{\text{act}} - \mathrm{Y}_p(s)s\left(\hat{z}_1 - \hat{z}_0\right) \tag{D.29}$$

one can directly extract that Equations D.24 and D.26 indeed define a 'bounce quarter-vehicle model', and that Equations D.25 and D.27 define a 'pitch quarter-vehicle model' due to the decoupling of the bounce and pitch modes.

E

Data and Results Supplement

E.1 Preliminar Considerations

The data provided here for the tuning of the different configurations is based on the planar model of the side-view of the vehicle. For the 3D vehicle, in case of either left and right parallel actuators, left and right parallel novel devices, or both, the coefficients should be divided, accordingly, by a factor of 2.

E.2 Parameters for the Integration with Modal Skyhook Damping

Table E.1: Parameters for the results in Table 6.1 (passive suspensions)

Layout	Parameters values
F&S1	$b_1 = 4280$
F&S2	$c_1 = 4.2452 \times 10^4$, $b_1 = 5411$
F&S3	$c_1 = 3.3607 \times 10^4$, $b_1 = 3773$, $k_2 = 4.9161 \times 10^5$
F&S4	$c_1 = 2.6455 \times 10^4$, $b_1 = 1870$, $b_2 = 243$
F&S5	$c_1 = 1.863 \times 10^4$, $b_1 = 6.1898 \times 10^4$, $k_2 = 1.8303 \times 10^6$, $c_2 = 1.3366 \times 10^4$
F&S6	$c_1 = 1.6944 \times 10^4$, $b_1 = 3.513 \times 10^4$, $c_2 = 2.6302 \times 10^4$, $b_2 = 5851$

[a] $b_{1,2}\,[\mathrm{kg}]$, $k_2\,[\mathrm{Nm}^{-1}]$, $c_{1,2}\,[\mathrm{Nsm}^{-1}]$

Table E.2: Parameters for the results in Table 6.2 (Criterion I: 30% of improvement in the ride quality)

Layout	Parameters values
F&S0	$K_b = 6 \times 10^3$, $K_\rho = 3.7085 \times 10^4$
F&S1	$K_b = 1.679 \times 10^3$, $K_\rho = 2.5849 \times 10^4$, $b_1 = 2636$
F&S2	$K_b = 1.079 \times 10^3$, $K_\rho = 2.5198 \times 10^4$, $c_1 = 3.9252 \times 10^4$, $b_1 = 3926$
F&S3	$K_b = 762$, $K_\rho = 2.7101 \times 10^4$, $c_1 = 3.6334 \times 10^4$, $b_1 = 2704$, $k_2 = 3.6434 \times 10^5$
F&S4	$K_b = 311$, $K_\rho = 2.3344 \times 10^4$, $c_1 = 2.6278 \times 10^4$, $b_1 = 3068$, $b_2 = 238$
F&S5	$K_b = 1.791 \times 10^3$, $K_\rho = 4.1227 \times 10^4$, $c_1 = 1.3189 \times 10^4$, $b_1 = 6.147 \times 10^4$, $k_2 = 2.8404 \times 10^6$, $c_2 = 1.3655 \times 10^4$
F&S6	$K_b = 2.148 \times 10^3$, $K_\rho = 4.4998 \times 10^4$, $c_1 = 1.6944 \times 10^4$, $b_1 = 3.513 \times 10^4$, $c_2 = 2.6302 \times 10^4$, $b_2 = 5851$

[a] $b_{1,2}$ [kg], k_2 $\left[\mathrm{Nm}^{-1}\right]$, $c_{1,2}\left[\mathrm{Nsm}^{-1}\right]$

Table E.3: Parameters for the results in Table 6.3 (Criterion II: $J_2 = 3.5$[cm])

Layout	Parameters values
F&S0	$K_b = 1.0836 \times 10^4$, $K_\rho = 7.4333 \times 10^4$
F&S1	$K_b = 8.1773 \times 10^3$, $K_\rho = 7.8796 \times 10^4$, $b_1 = 1895$
F&S2	$K_b = 8.9560 \times 10^3$, $K_\rho = 7.6103 \times 10^4$, $c_1 = 3.5362 \times 10^4$, $b_1 = 1192$
F&S3	$K_b = 1.1818 \times 10^4$, $K_\rho = 7.4061 \times 10^4$, $c_1 = 4.2504 \times 10^4$, $b_1 = 1349$, $k_2 = 3.4030 \times 10^5$
F&S4	$K_b = 9.6582 \times 10^3$, $K_\rho = 7.7454 \times 10^4$, $c_1 = 2.4575 \times 10^4$, $b_1 = 1907$, $b_2 = 190$
F&S5	$K_b = 8.6906 \times 10^3$, $K_\rho = 1.1310 \times 10^5$, $c_1 = 1.0383 \times 10^4$, $b_1 = 5.7672 \times 10^4$, $k_2 = 2.3433 \times 10^6$, $c_2 = 1.3037 \times 10^4$
F&S6	$K_b = 6.3179 \times 10^3$, $K_\rho = 1.1402 \times 10^5$, $c_1 = 1.6944 \times 10^4, b_1 = 3.5133 \times 10^4$, $c_2 = 2.6302 \times 10^4$, $b_2 = 5851$

[a] $b_{1,2}$ [kg], k_2 $[\mathrm{Nm}^{-1}]$, $c_{1,2}$ $[\mathrm{Nsm}^{-1}]$

Table E.4: Parameters for the results in Table 6.4 (Criterion III: $J_3 = 10$[kN])

Layout	Parameters values
F&S0	$K_b = 1.2147 \times 10^4$, $K_\rho = 8.7981 \times 10^4$
F&S1	$K_b = 9.8471 \times 10^3$, $K_\rho = 9.5873 \times 10^4$, $b_1 = 1841$
F&S2	$K_b = 1.1338 \times 10^4$, $K_\rho = 9.4583 \times 10^4$, $c_1 = 3.4761 \times 10^4$, $b_1 = 1154$
F&S3	$K_b = 1.3409 \times 10^4$, $K_\rho = 9.1709 \times 10^4$, $c_1 = 4.2580 \times 10^4$, $b_1 = 1330$, $k_2 = 3.3652 \times 10^5$
F&S4	$K_b = 1.1265 \times 10^4$, $K_\rho = 9.7826 \times 10^4$, $c_1 = 2.4567 \times 10^4$, $b_1 = 1923$, $b_2 = 182$
F&S5	$K_b = 5.9671 \times 10^3$, $K_\rho = 9.4839 \times 10^4$, $c_1 = 1.0645 \times 10^4$, $b_1 = 5.6549 \times 10^4$, $k_2 = 2.2914 \times 10^6$, $c_2 = 1.3070 \times 10^4$
F&S6	$K_b = 5.8867 \times 10^3$, $K_\rho = 1.0243 \times 10^5$, $c_1 = 1.6944 \times 10^4$, $b_1 = 3.5133 \times 10^4$, $c_2 = 2.6302 \times 10^4$, $b_2 = 5851$

[a] $b_{1,2}$ [kg], k_2 $\left[\mathrm{Nm}^{-1}\right]$, $c_{1,2}\left[\mathrm{Nsm}^{-1}\right]$

E.3 Parameters for the Integration with Local Skyhook Damping and Complementary Filtering

Table E.5: Parameters for the results in Table 6.7 (Criterion I: 30% of improvement in the ride quality)

Layout	Parameters values
F&S0	$K_l = 4.684 \times 10^4$, $f_c = 0.2797$
F&S1	$K_l = 2.9033 \times 10^4$, $f_c = 0.2243$, $b_1 = 2285$
F&S2	$K_l = 2.8635 \times 10^4$, $f_c = 0.2332$, $c_1 = 3.3497 \times 10^4$, $b_1 = 4083$
F&S3	$K_l = 3.3093 \times 10^4$, $f_c = 0.2770$, $c_1 = 4.0556 \times 10^4$, $b_1 = 1314$, $k_2 = 5.3981 \times 10^5$
F&S4	$K_l = 2.8834 \times 10^4$, $f_c = 0.2598$, $c_1 = 2.7956 \times 10^4$, $b_1 = 1955$, $b_2 = 253$
F&S5	$K_l = 4.4223 \times 10^4$, $f_c = 0.2664$, $c_1 = 9.0421 \times 10^3$, $b_1 = 6.3351 \times 10^4$, $k_2 = 2.3840 \times 10^6$, $c_2 = 1.4251 \times 10^4$
F&S6	$K_l = 3.7789 \times 10^4$, $f_c = 0.2395$, $c_1 = 1.1648 \times 10^4$, $b_1 = 3.9587 \times 10^4$, $c_2 = 1.5208 \times 10^4$, $b_2 = 8059$

[a] f_c [Hz], $b_{1,2}$ [kg], k_2 $\left[\mathrm{Nm}^{-1}\right]$, $c_{1,2}\left[\mathrm{Nsm}^{-1}\right]$

Table E.6: Parameters for the results in Table 6.8 ((Criterion II: $J_2 = 3.5$[cm])

Layout	Parameters values
F&S0	$K_l = 6.1017 \times 10^4$, $f_c = 0.2568$
F&S1	$K_l = 6.1521 \times 10^4$, $f_c = 0.2553$, $b_1 = 2080$
F&S2	$K_l = 5.7120 \times 10^4$, $f_c = 0.2285$, $c_1 = 3.2839 \times 10^4$, $b_1 = 3922$
F&S3	$K_l = 5.4491 \times 10^4$, $f_c = 0.2254$, $c_1 = 4.0088 \times 10^4$, $b_1 = 1030$, $k_2 = 5.7073 \times 10^5$
F&S4	$K_l = 6.2259 \times 10^4$, $f_c = 0.2628$, $c_1 = 2.6716 \times 10^4$, $b_1 = 2036$, $b_2 = 193$
F&S5	$K_l = 6.6144 \times 10^4$, $f_c = 0.2327$, $c_1 = 8.7835 \times 10^3$, $b_1 = 6.4108 \times 10^4$, $k_2 = 2.2672 \times 10^6$, $c_2 = 1.3838 \times 10^4$
F&S6	$K_l = 6.2789 \times 10^4$, $f_c = 0.2309$, $c_1 = 1.1141 \times 10^4$,$b_1 = 3.9580 \times 10^4$, $c_2 = 1.5295 \times 10^4$, $b_2 = 8176$

[a] f_c [Hz], $b_{1,2}$ [kg], k_2 $\left[\mathrm{Nm}^{-1}\right]$, $c_{1,2}\left[\mathrm{Nsm}^{-1}\right]$

Table E.7: Parameters for the results in Table 6.9 (Criterion III: $J_3 = 10$[kN])

Layout	Parameters values
F&S0	$K_l = 4.3741 \times 10^4$, $f_c = 0.2823$
F&S1	$K_l = 4.1137 \times 10^4$, $f_c = 0.2358$, $b_1 = 2211$
F&S2	$K_l = 4.2207 \times 10^4$, $f_c = 0.2335$, $c_1 = 3.3023 \times 10^4$, $b_1 = 4031$
F&S3	$K_l = 4.3110 \times 10^4$, $f_c = 0.2680$, $c_1 = 4.0539 \times 10^4$, $b_1 = 1127$, $k_2 = 5.5956 \times 10^5$
F&S4	$K_l = 4.4127 \times 10^4$, $f_c = 0.2612$, $c_1 = 2.6857 \times 10^4$, $b_1 = 1993$, $b_2 = 215$
F&S5	$K_l = 4.5408 \times 10^4$, $f_c = 0.2661$, $c_1 = 8.9718 \times 10^3$, $b_1 = 6.3398 \times 10^4$, $k_2 = 2.3792 \times 10^6$, $c_2 = 1.4227 \times 10^4$
F&S6	$K_l = 4.3784 \times 10^4$, $f_c = 0.2415$, $c_1 = 1.1440 \times 10^4$, $b_1 = 3.9582 \times 10^4$, $c_2 = 1.5078 \times 10^4$, $b_2 = 8085$

[a] f_c [Hz], $b_{1,2}$ [kg], k_2 $\left[\mathrm{Nm}^{-1}\right]$, $c_{1,2}\left[\mathrm{Nsm}^{-1}\right]$

E.4 Parameters for the Integration with HPF Local Skyhook Damping and Adaptive Stiffness

Table E.8: Parameters for the results in Table 6.12 (Criterion I: 30% of improvement in the ride quality)

Layout	Parameters values
F*&S0	$K_l = 30 \times 10^3$
F&S0	$K_l = 38.26 \times 10^3$, $\kappa = 82.19 \times 10^4$
F&S2	$K_l = 30.66 \times 10^3$, $\kappa = 123.75 \times 10^4$, $c_1 = 4 \times 10^4$, $b_1 = 8354$
F&S4	$K_l = 27.93 \times 10^3$, $\kappa = 149.36 \times 10^4$, $c_1 = 2.403 \times 10^4$, $b_1 = 2256$, $b_2 = 206$

[a] $b_{1,2}$ [kg], k_2 $\left[\mathrm{Nm}^{-1}\right]$, $c_{1,2}\left[\mathrm{Nsm}^{-1}\right]$

Table E.9: Parameters for the results in Table 6.13 (Criterion II: $J_2 = 3.5$[cm])

Layout	Parameters values
F*&S0	$K_l = 40 \times 10^3$
F&S0	$K_l = 142.21 \times 10^3$, $\kappa = 490.64 \times 10^4$
F&S2	$K_l = 228.68 \times 10^3$, $\kappa = 11.09 \times 10^6$, $c_1 = 4 \times 10^4$, $b_1 = 3403$
F&S4	$K_l = 150.21 \times 10^3$, $\kappa = 563.38 \times 10^4$, $c_1 = 2.22 \times 10^4$, $b_1 = 3015$, $b_2 = 213$

[a] $b_{1,2}$ [kg], k_2 $\left[\mathrm{Nm}^{-1}\right]$, $c_{1,2}\left[\mathrm{Nsm}^{-1}\right]$

Table E.10: Parameters for the results in Table 6.14 (Criterion III: $J_3 = 10$[kN])

Layout	Parameters values
F*&S0	$K_l = 40 \times 10^3$
F&S0	$K_l = 135.90 \times 10^3$, $\kappa = 462.26 \times 10^4$
F&S2	$K_l = 171.41 \times 10^3$, $\kappa = 780.39 \times 10^4$, $c_1 = 4 \times 10^4$, $b_1 = 4296$
F&S4	$K_l = 150.21 \times 10^3$, $\kappa = 563.38 \times 10^4$, $c_1 = 2.22 \times 10^4$, $b_1 = 3015$, $b_2 = 213$

[a] $b_{1,2}$ [kg], k_2 $\left[\mathrm{Nm}^{-1}\right]$, $c_{1,2}$ $\left[\mathrm{Nsm}^{-1}\right]$

E.5 Feedback Gains for the Linear-Quadratic Gaussian (LQG) HPF-Output Feedback Regulator

Configuration F&S0**:**

States vector:

$$\underline{x}' = [z_v\, \beta_v\, z_{p11}\, z_{p12}\, z_{b1}\, \beta_{b1}\, z_{b2}\, \beta_{b2}\, \dot{z}_v\, \dot{\beta}_v\, \dot{z}_{p11} \ldots \dot{z}_{p12}\, \dot{z}_{b1}\, \dot{\beta}_{b1}\, \dot{z}_{b2}\, \dot{\beta}_{b2}\, x_{iD1}\, x_{iD2}]^T$$

Optimal feedback gain matrices according to Criterion I:

$$\mathbf{K}_u^{\mathrm{CI}} = \begin{pmatrix} 110. \times 10^3 & 47. \times 10^3 \\ -600. \times 10^3 & 650. \times 10^3 \\ 410. \times 10^3 & -40. \times 10^3 \\ -43. \times 10^3 & 340. \times 10^3 \\ -190. \times 10^3 & -23. \times 10^3 \\ 0 & 0 \\ -20. \times 10^3 & -170. \times 10^3 \\ 0 & 0 \\ 94. \times 10^3 & 76. \times 10^3 \\ 690. \times 10^3 & -570. \times 10^3 \\ 12. & 0 \\ 0 & 10. \\ -61. & 54. \\ 0 & 0 \\ 46. & -18. \\ 0 & 0 \\ -2.4 \times 10^6 & -14. \times 10^3 \\ -78. \times 10^3 & -1.9 \times 10^6 \end{pmatrix}^T$$

Optimal feedback gain matrices according to Criteria II and III:

$$\mathbf{K}_u^{\mathrm{CII/III}} = \begin{pmatrix} 81.\times 10^3 & 31.\times 10^3 \\ -530.\times 10^3 & 550.\times 10^3 \\ 350.\times 10^3 & -32.\times 10^3 \\ -35.\times 10^3 & 290.\times 10^3 \\ -180.\times 10^3 & -18.\times 10^3 \\ 0 & 0 \\ -14.\times 10^3 & -160.\times 10^3 \\ 0 & 0 \\ 81.\times 10^3 & 65.\times 10^3 \\ 590.\times 10^3 & -480.\times 10^3 \\ 11. & 0 \\ 0 & 9.3 \\ -17. & 42. \\ 0 & 0 \\ 37. & 7.6 \\ 0 & 0 \\ -2.1\times 10^6 & -3.7\times 10^3 \\ -56.\times 10^3 & -1.7\times 10^6 \end{pmatrix}^T$$

Configuration F&S2**:**

States vector:

$$\begin{aligned}\underline{x}' =&[z_v\,\beta_v\,z_{p11}\,z_{p12}\,z_{b1}\,\beta_{b1}\,z_{b2}\,\beta_{b2}\,\dot{z}_v\,\dot{\beta}_v\,\dot{z}_{p11}\\ &\ldots\dot{z}_{p12}\,\dot{z}_{b1}\,\dot{\beta}_{b1}\,\dot{z}_{b2}\,\dot{\beta}_{b2}\,x_{iD1}\,x_{iD2}\Big|^{\mathrm{S2}'}\underline{x}^T_{pf1}(t)\ \Big|^{\mathrm{S2}'}\underline{x}^T_{pf2}(t)\Big]^T\end{aligned}$$

Optimal feedback gain matrices according to Criterion I:

$$\mathbf{K}_u^{\mathrm{CI}} = \begin{pmatrix} 90.\times10^3 & 48.\times10^3 \\ -230.\times10^3 & 360.\times10^3 \\ 300.\times10^3 & -25.\times10^3 \\ -27.\times10^3 & 260.\times10^3 \\ -210.\times10^3 & -16.\times10^3 \\ 0 & 0 \\ -15.\times10^3 & -170.\times10^3 \\ 0 & 0 \\ 70.\times10^3 & 59.\times10^3 \\ 490.\times10^3 & -420.\times10^3 \\ 7.7 & 0 \\ 0 & 6.7 \\ -790. & 280. \\ 0 & 0 \\ 280. & -690. \\ 0 & 0 \\ -1.9\times10^6 & -13.\times10^3 \\ -41.\times10^3 & -1.6\times10^6 \\ -15.\times10^6 & -1.\times10^6 \\ 670.\times10^3 & -210.\times10^3 \\ -810.\times10^3 & -13.\times10^6 \\ -210.\times10^3 & 580.\times10^3 \end{pmatrix}^T$$

Optimal feedback gain matrices according to Criteria II and III:

$$\mathbf{K}_u^{\mathrm{CII/III}} = \begin{pmatrix} 140.\times10^3 & 83.\times10^3 \\ -310.\times10^3 & 540.\times10^3 \\ 400.\times10^3 & -40.\times10^3 \\ -42.\times10^3 & 360.\times10^3 \\ -240.\times10^3 & -26.\times10^3 \\ 0 & 0 \\ -25.\times10^3 & -210.\times10^3 \\ 0 & 0 \\ 92.\times10^3 & 79.\times10^3 \\ 660.\times10^3 & -570.\times10^3 \\ 8.1 & 0 \\ 0 & 7.2 \\ -1.3\times10^3 & 400. \\ 0 & 0 \\ 400. & -1.1\times10^3 \\ 0 & 0 \\ -2.5\times10^6 & -40.\times10^3 \\ -81.\times10^3 & -2.1\times10^6 \\ -17.\times10^6 & -1.6\times10^6 \\ 1.1\times10^6 & -330.\times10^3 \\ -1.3\times10^6 & -15.\times10^6 \\ -330.\times10^3 & 970.\times10^3 \end{pmatrix}^T$$

Configuration F&S4**:**

States vector:

$$\begin{aligned}\underline{x}' =&[z_v\,\beta_v\,z_{p11}\,z_{p12}\,z_{b1}\beta_{b1}\,z_{b2}\beta_{b2}\,\dot{z}_v\dot{\beta}_v\dot{z}_{p11}\\ &\ldots\dot{z}_{p12}\dot{z}_{b1}\dot{\beta}_{b1}\dot{z}_{b2}\dot{\beta}_{b2}x_{iD1}x_{iD2}\Big|^{\mathrm{S4'}}\underline{x^T_{pf1}}(t)\ \Big|^{\mathrm{S4'}}\underline{x^T_{pf2}}(t)\Big]^T\end{aligned}$$

Optimal feedback gain matrices according to Criterion I:

$$\mathbf{K}_u^{\mathrm{CI}} = \begin{pmatrix} 70.\times10^3 & 28.\times10^3 \\ -510.\times10^3 & 520.\times10^3 \\ 320.\times10^3 & -28.\times10^3 \\ -31.\times10^3 & 260.\times10^3 \\ -190.\times10^3 & -15.\times10^3 \\ 0 & 0 \\ -13.\times10^3 & -160.\times10^3 \\ 0 & 0 \\ 74.\times10^3 & 59.\times10^3 \\ 530.\times10^3 & -430.\times10^3 \\ 7.8 & 0 \\ 0 & 6.7 \\ -910. & 310. \\ 0 & 0 \\ 310. & -710. \\ 0 & 0 \\ -1.9\times10^6 & -6.6\times10^3 \\ -47.\times10^3 & -1.5\times10^6 \\ -2.1\times10^9 & -180.\times10^6 \\ 78.\times10^6 & -31.\times10^6 \\ 710.\times10^3 & -220.\times10^3 \\ -140.\times10^6 & -1.8\times10^9 \\ -31.\times10^6 & 60.\times10^6 \\ -220.\times10^3 & 560.\times10^3 \end{pmatrix}^T$$

Optimal feedback gain matrices according to Criteria II and III:

$$\mathbf{K}_u^{\mathrm{CII/III}} = \begin{pmatrix} 88.\times10^3 & 38.\times10^3 \\ -590.\times10^3 & 620.\times10^3 \\ 370.\times10^3 & -34.\times10^3 \\ -38.\times10^3 & 300.\times10^3 \\ -200.\times10^3 & -19.\times10^3 \\ 0 & 0 \\ -17.\times10^3 & -170.\times10^3 \\ 0 & 0 \\ 83.\times10^3 & 68.\times10^3 \\ 600.\times10^3 & -490.\times10^3 \\ 8. & 0 \\ 0 & 7.1 \\ -1.1\times10^3 & 370. \\ 0 & 0 \\ 360. & -900. \\ 0 & 0 \\ -2.2\times10^6 & -14.\times10^3 \\ -63.\times10^3 & -1.7\times10^6 \\ -2.3\times10^9 & -220.\times10^6 \\ 100.\times10^6 & -38.\times10^6 \\ 900.\times10^3 & -270.\times10^3 \\ -170.\times10^6 & -2.\times10^9 \\ -38.\times10^6 & 78.\times10^6 \\ -270.\times10^3 & 700.\times10^3 \end{pmatrix}^T$$

F

Plots supplement

F.1 Parameters for the Integration with Modal Skyhook Damping

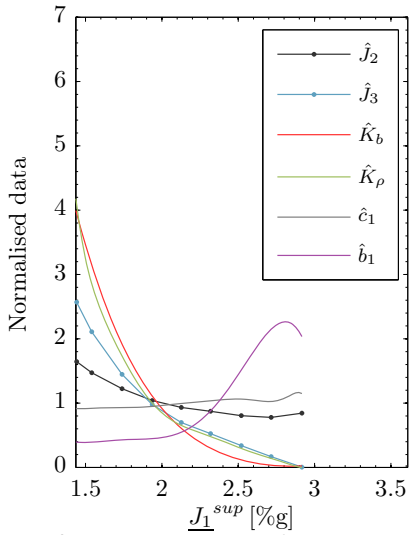

Figure F.1: Optimisation results for the integration F&S2 [1].

[1] with $\hat{J}_2 = J_2/3.5\,[\text{cm}]$, $\hat{J}_3 = J_3/10\,[\text{kN}]$, $\hat{K}_b = K_b/\overline{K}_b$, $\hat{K}_\rho = K_\rho/\overline{K}_\rho$, $\hat{c}_1 = c_1/\overline{c}_1$, $\hat{b}_1 = b_1/\overline{b}_1$, for the mean parameters values: $\overline{K}_b = 9.10 \times 10^3$, $\overline{K}_\rho = 8.46 \times 10^4$, $\overline{c}_1 = 3.694 \times 10^4\,[\text{Nsm}^{-1}]$ and $\overline{b}_1 = 2613[\text{kg}]$.

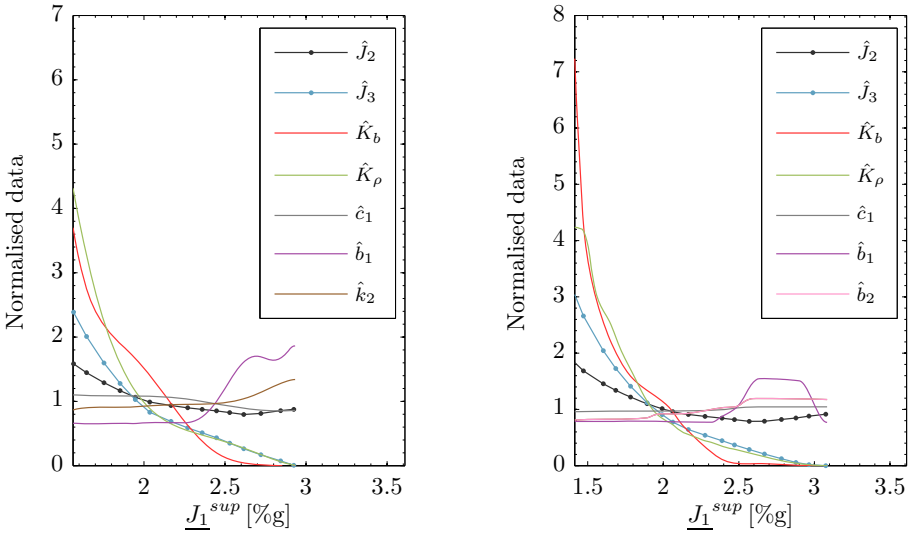

(a) F&S3 [2] (b) F&S4 [3]

Figure F.2: Optimisation results for the integration F&S3 and F&S4.

[2] with $\hat{J}_2 = J_2/3.5\,[\text{cm}]$, $\hat{J}_3 = J_3/10\,[\text{kN}]$, $\hat{K}_b = K_b/\overline{K}_b$, $\hat{K}_\rho = K_\rho/\overline{K}_\rho$, $\hat{c}_1 = c_1/\overline{c}_1$, $\hat{b}_1 = b_1/\overline{b}_1$, $\hat{k}_2 = k_2/\overline{k}_2$, for the mean parameters values: $\overline{K}_b = 7.99 \times 10^3$, $\overline{K}_\rho = 7.80 \times 10^4$, $\overline{c}_1 = 3.931 \times 10^4\,[\text{Nsm}^{-1}]$, $\overline{b}_1 = 2028[\text{kg}]$, and $\overline{k}_2 = 3.670 \times 10^5\,[\text{Nm}^{-1}]$.

[3] with $\hat{J}_2 = J_2/3.5\,[\text{cm}]$, $\hat{J}_3 = J_3/10\,[\text{kN}]$, $\hat{K}_b = K_b/\overline{K}_b$, $\hat{K}_\rho = K_\rho/\overline{K}_\rho$, $\hat{c}_1 = c_1/\overline{c}_1$, $\hat{b}_1 = b_1/\overline{b}_1$, $\hat{b}_2 = b_2/\overline{b}_2$, for the mean parameters values: $\overline{K}_b = 8.80 \times 10^3$, $\overline{K}_\rho = 9.57 \times 10^4$, $\overline{c}_1 = 2.530 \times 10^4\,[\text{Nsm}^{-1}]$, $\overline{b}_1 = 2433[\text{kg}]$, and $\overline{b}_2 = 207[\text{kg}]$.

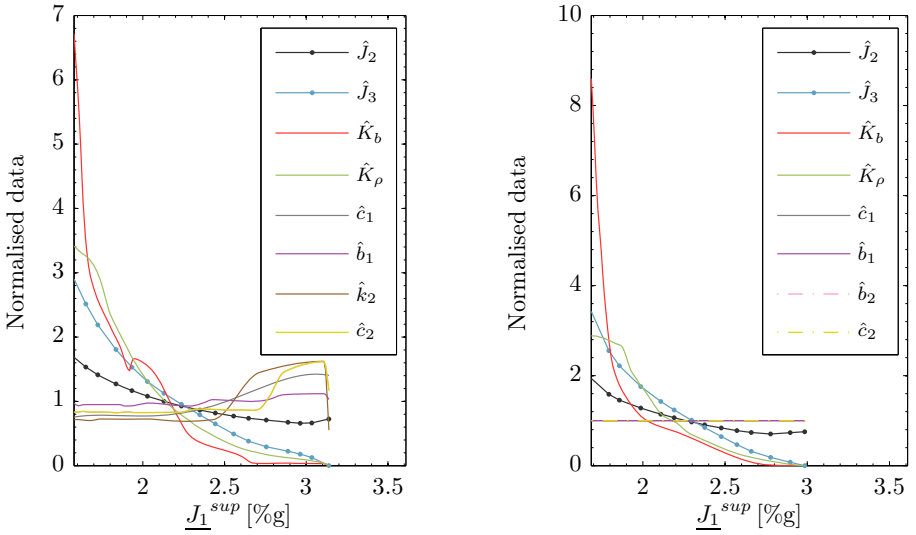

(a) F&S5 [4] (b) F&S6 [5]

Figure F.3: Optimisation results for the integration F&S5 and F&S6.

[4] with $\hat{J}_2 = J_2/3.5\,[\text{cm}]$, $\hat{J}_3 = J_3/10\,[\text{kN}]$, $\hat{K}_b = K_b/\overline{K}_b$, $\hat{K}_\rho = K_\rho/\overline{K}_\rho$, $\hat{c}_1 = c_1/\overline{c}_1$, $\hat{b}_1 = b_1/\overline{b}_1$, $\hat{k}_2 = k_2/\overline{k}_2$, $\hat{c}_2 = c_2/\overline{c}_2$, for the mean parameters values: $\overline{K}_b = 7.64 \times 10^3$, $\overline{K}_\rho = 1.13 \times 10^5$, $\overline{c}_1 = 1.319 \times 10^4\,[\text{Nsm}^{-1}]$, $\overline{b}_1 = 6.047 \times 10^4[\text{kg}]$, $\overline{k}_2 = 3.315 \times 10^6\,[\text{Nm}^{-1}]$, and $\overline{b}_2 = 1.577 \times 10^4[\text{kg}]$.

[5] with $\hat{J}_2 = J_2/3.5\,[\text{cm}]$, $\hat{J}_3 = J_3/10\,[\text{kN}]$, $\hat{K}_b = K_b/\overline{K}_b$, $\hat{K}_\rho = K_\rho/\overline{K}_\rho$, $\hat{c}_1 = c_1/\overline{c}_1$, $\hat{b}_1 = b_1/\overline{b}_1$, $\hat{c}_2 = c_2/\overline{c}_2$, $\hat{b}_2 = b_2/\overline{b}_2$, for the mean parameters values: $\overline{K}_b = 9.38 \times 10^3$, $\overline{K}_\rho = 1.44 \times 10^5$, $\overline{c}_1 = 1.694 \times 10^4\,[\text{Nsm}^{-1}]$, $\overline{b}_1 = 3513[\text{kg}]$, $\overline{c}_2 = 2.630 \times 10^4\,[\text{Nsm}^{-1}]$, and $\overline{b}_2 = 5851[\text{kg}]$.

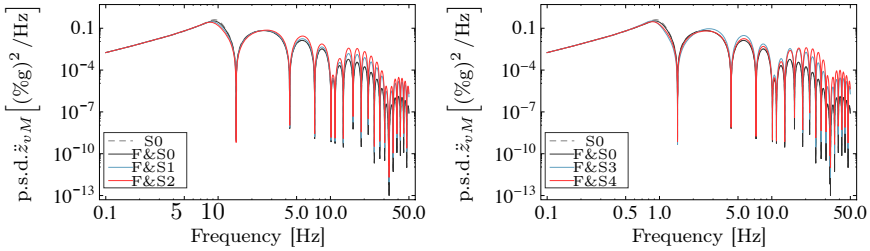

(a) S1–S2

(b) S3–S4

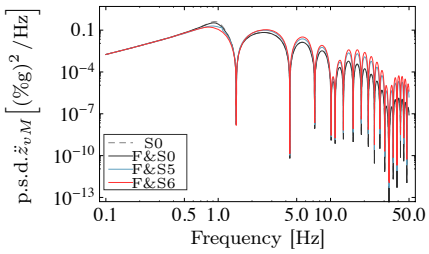

(c) S5–S6

Figure F.4: Plots of the p.s.d. for the vehicle body accelerations at the middle position ($\ddot{z}_{vM}$) for suspensions settings according to Criterion I, with ideal actuators.

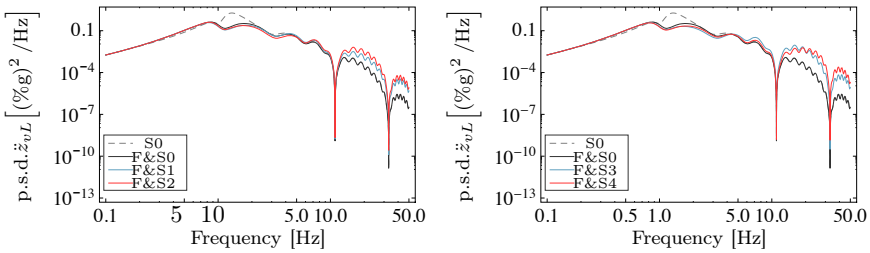

(a) S1–S2 (b) S3–S4

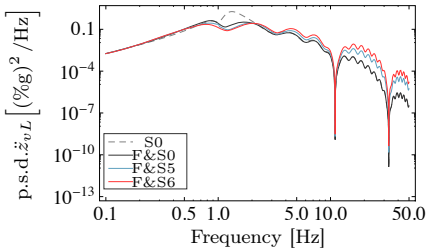

(c) S5–S6

Figure F.5: Plots of the p.s.d. for the vehicle body accelerations at the leading position ($\ddot{z}_{vL}$) for suspensions settings according to Criterion II, with ideal actuators.

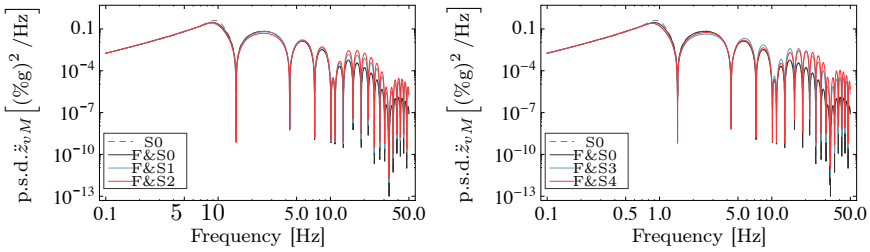

(a) S1–S2 (b) S3–S4

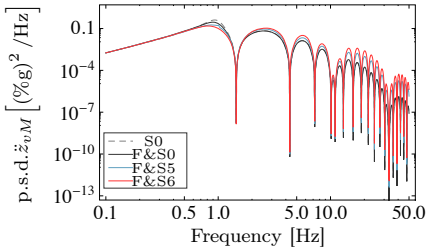

(c) S5–S6

Figure F.6: Plots of the p.s.d. for the vehicle body accelerations at the middle position ($\ddot{z}_{vM}$) for suspensions settings according to Criterion II, with ideal actuators.

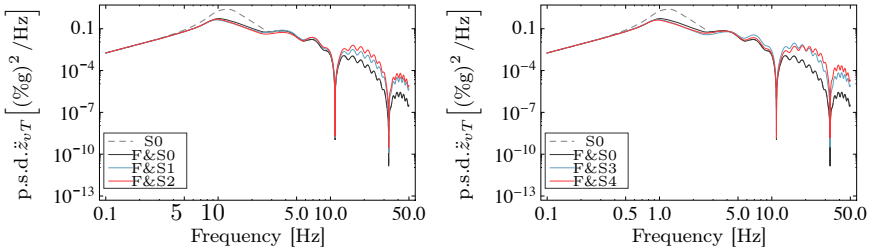

(a) S1–S2 (b) S3–S4

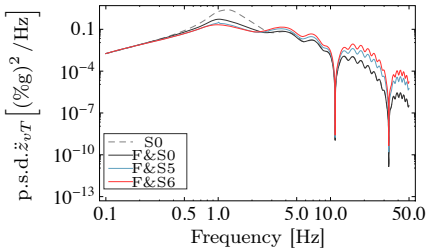

(c) S5–S6

Figure F.7: Plots of the p.s.d. for the vehicle body accelerations at the trailing position ($\ddot{z}_{vT}$) for suspensions settings according to Criterion II, with ideal actuators.

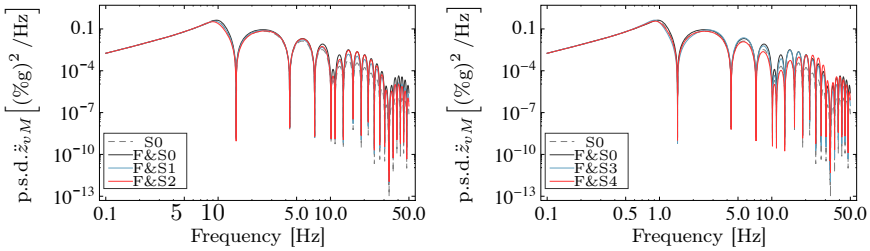

(a) S1–S2 (b) S3–S4

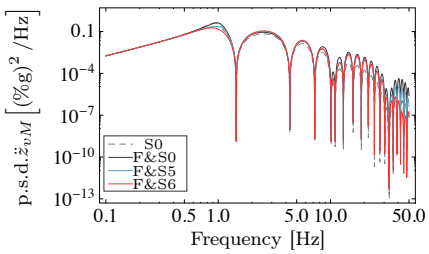

(c) S5–S6

Figure F.8: Plots of the p.s.d. for the vehicle body accelerations at the middle position ($\ddot{z}_{vM}$) for suspensions settings according to Criterion I, with real actuators.

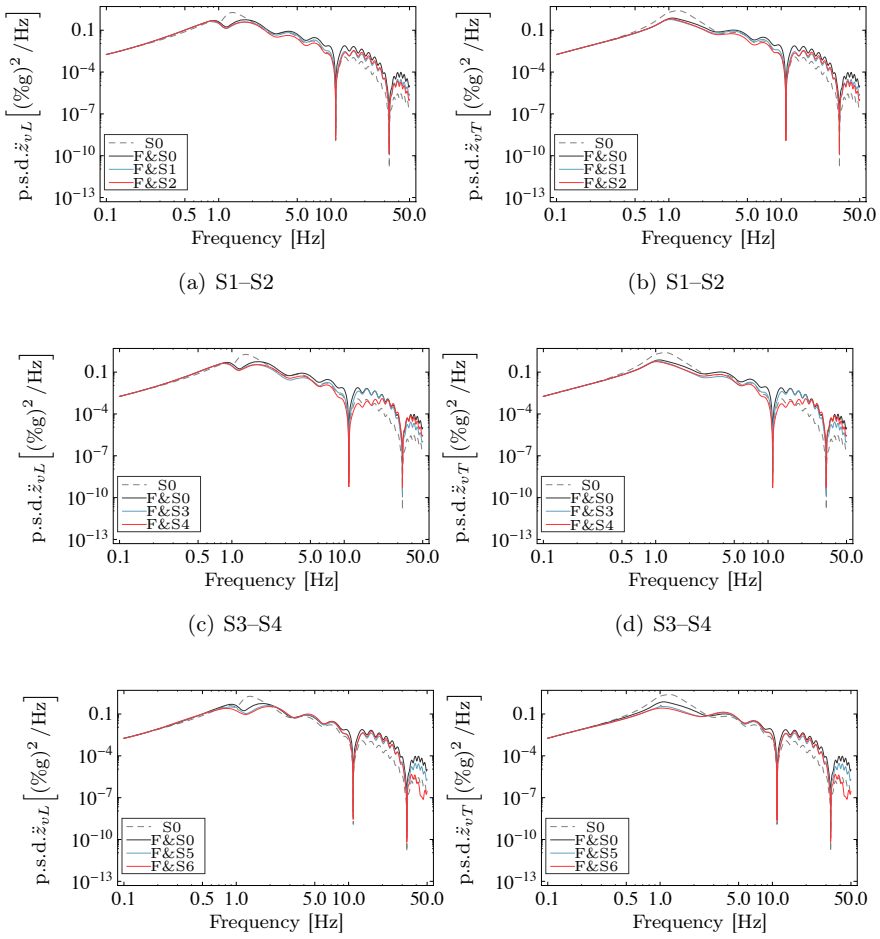

(a) S1–S2 (b) S1–S2

(c) S3–S4 (d) S3–S4

(e) S5–S6 (f) S5–S6

Figure F.9: Plots of the p.s.d. for the vehicle body accelerations at the leading position ($\ddot{z}_{vL}$) for suspensions settings according to Criterion II, with real actuators.

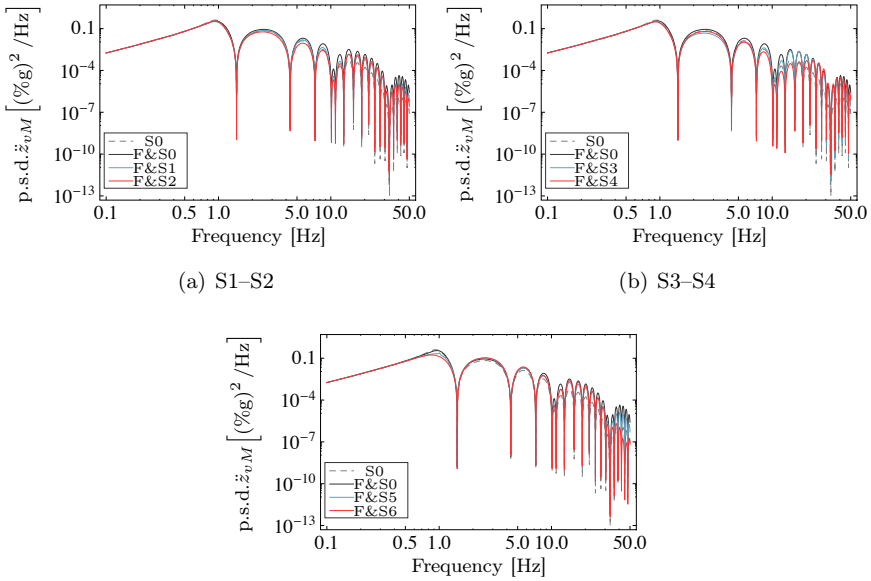

(a) S1–S2

(b) S3–S4

(c) S5–S6

Figure F.10: Plots of the p.s.d. for the vehicle body accelerations at the middle position ($\ddot{z}_{vM}$) for suspensions settings according to Criterion II, with real actuators.

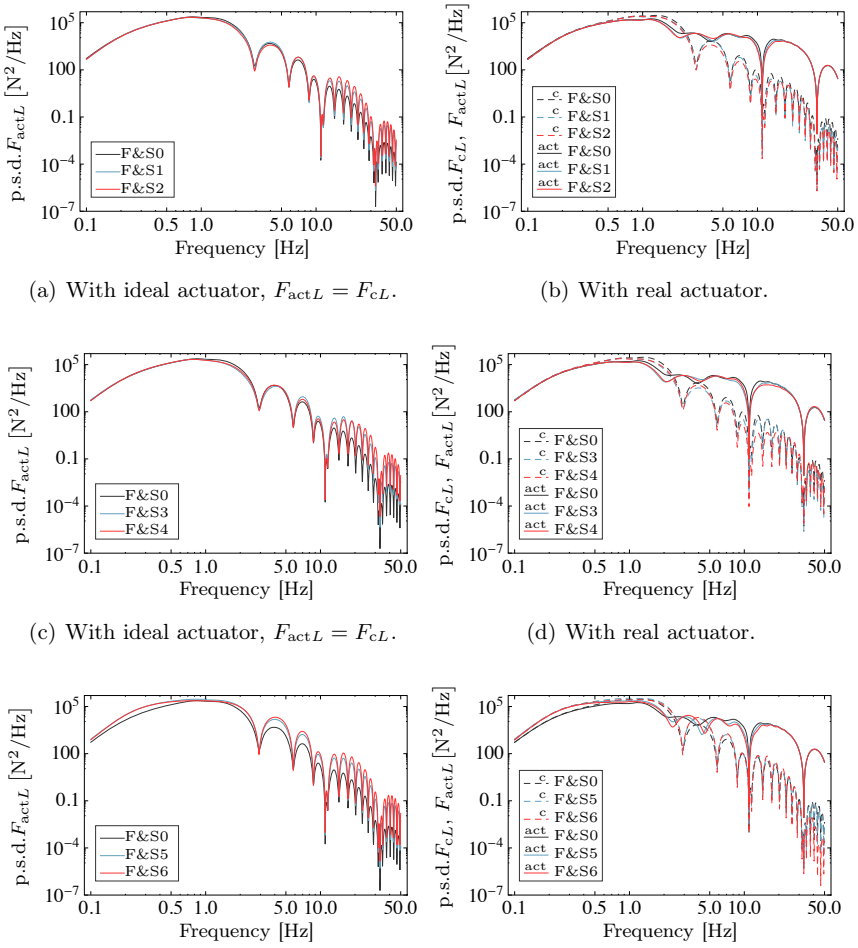

(a) With ideal actuator, $F_{\mathrm{act}L} = F_{\mathrm{c}L}$.

(b) With real actuator.

(c) With ideal actuator, $F_{\mathrm{act}L} = F_{\mathrm{c}L}$.

(d) With real actuator.

(e) With ideal actuator, $F_{\mathrm{act}L} = F_{\mathrm{c}L}$.

(f) With real actuator.

Figure F.11: Plots of the p.s.d. for the applied forces at the front suspensions; comparison of ideal versus real for suspensions settings according to Criterion II.

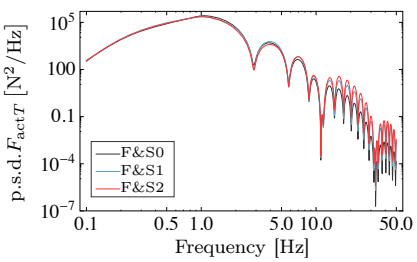

(a) With ideal actuator, $F_{\mathrm{act}T} = F_{cT}$.

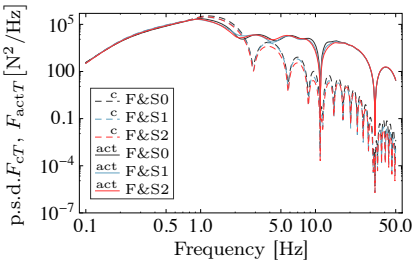

(b) With real actuator.

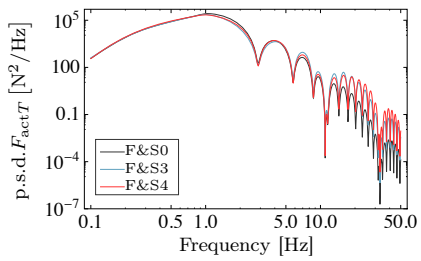

(c) With ideal actuator, $F_{\mathrm{act}T} = F_{cT}$.

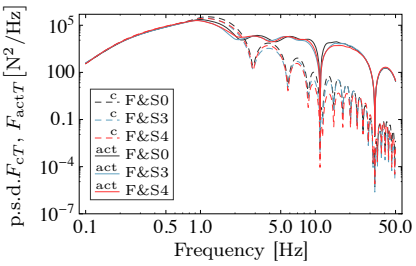

(d) With real actuator.

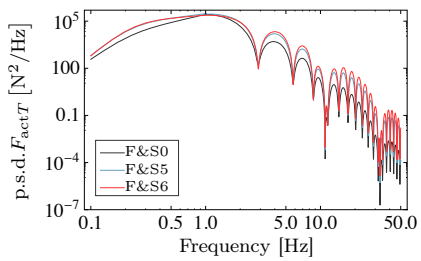

(e) With ideal actuator, $F_{\mathrm{act}T} = F_{cT}$.

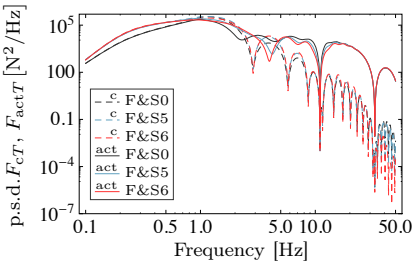

(f) With real actuator.

Figure F.12: Plots of the p.s.d. for the applied forces at the rear suspensions; comparison of ideal versus real for suspensions settings according to Criterion II.

F.2 Parameters for the Integration with Local Skyhook Damping and Complementary Filtering

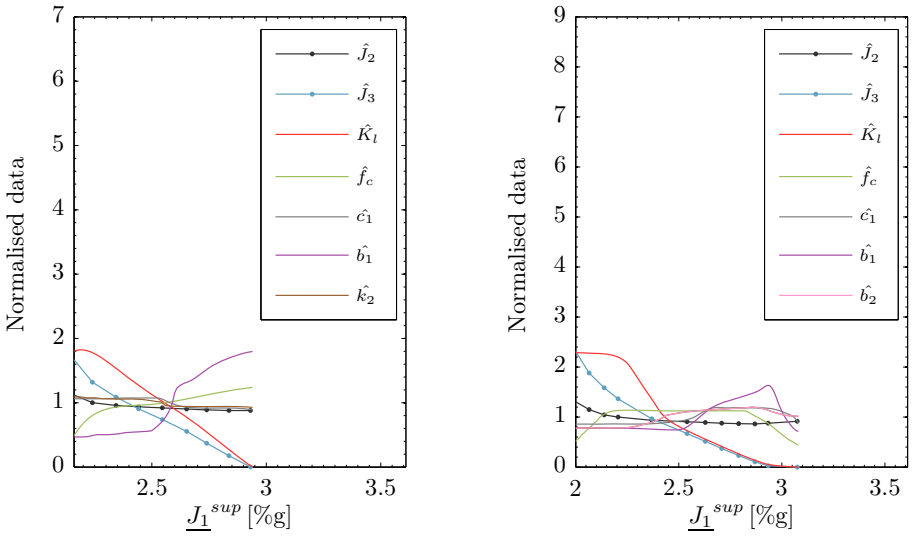

(a) F&S3 [6] (b) F&S4 [7]

Figure F.13: Optimisation results for the integration F&S3 and F&S4.

[6] with $\hat{J}_2 = J_2/3.5\,[\text{cm}]$, $\hat{J}_3 = J_3/10\,[\text{kN}]$, $\hat{K}_l = K_l/\overline{K}_l$, $\hat{f}_c = f_c/\overline{f}_c$, $\hat{c}_1 = c_1/\overline{c}_1$, $\hat{b}_1 = b_1/\overline{b}_1$, $\hat{k}_2 = k_2/\overline{k}_2$, for the mean parameters values: $\overline{K}_l = 3.06\times10^4$, $\overline{f}_c = 0.2816[\text{Hz}]$, $\overline{c}_1 = 3.7745\times10^4\,[\text{Nsm}^{-1}]$, $\overline{b}_1 = 2100[\text{kg}]$, and $\overline{k}_2 = 5.2981\times10^5\,[\text{Nm}^{-1}]$.

[7] with $\hat{J}_2 = J_2/3.5\,[\text{cm}]$, $\hat{J}_3 = J_3/10\,[\text{kN}]$, $\hat{K}_l = K_l/\overline{K}_l$, $\hat{f}_c = f_c/\overline{f}_c$, $\hat{c}_1 = c_1/\overline{c}_1$, $\hat{b}_1 = b_1/\overline{b}_1$, $\hat{b}_2 = b_2/\overline{b}_2$, for the mean parameters values: $\overline{K}_l = 3.26\times10^4$, $\overline{f}_c = 0.2313[\text{Hz}]$, $\overline{c}_1 = 3.1022\times10^4\,[\text{Nsm}^{-1}]$, $\overline{b}_1 = 2629[\text{kg}]$, and $\overline{b}_2 = 239[\text{kg}]$.

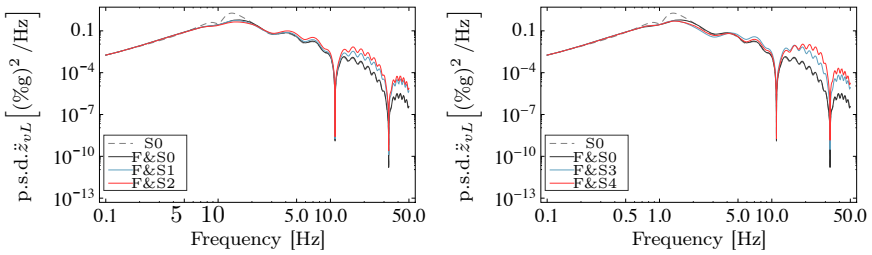

(a) S1–S2

(b) S3–S4

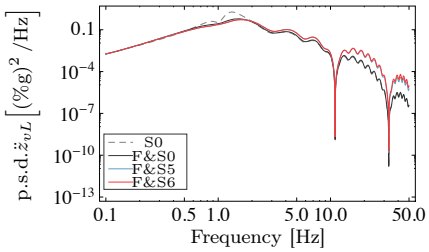

(c) S5–S6

Figure F.14: Plots of the p.s.d. for the vehicle body accelerations at the leading position ($\ddot{z}_{vL}$) for suspensions settings according to Criterion I, with ideal actuators. Local skyhook damping with complementary filtering configuration.

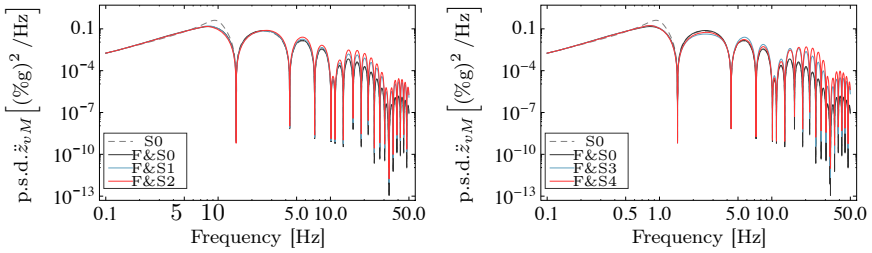

(a) S1–S2

(b) S3–S4

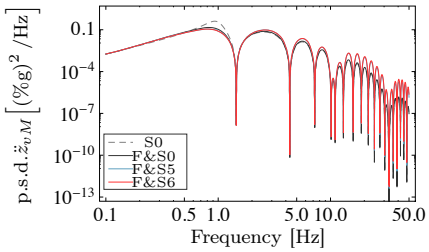

(c) S5–S6

Figure F.15: Plots of the p.s.d. for the vehicle body accelerations at the middle position ($\ddot{z}_{vM}$) for suspensions settings according to Criterion I, with ideal actuators. Local skyhook damping with complementary filtering configuration.

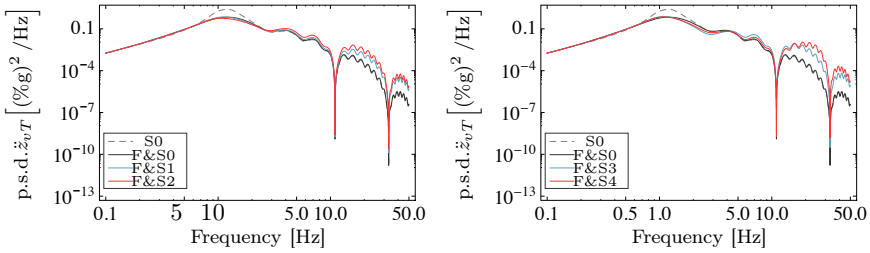

(a) S1–S2

(b) S3–S4

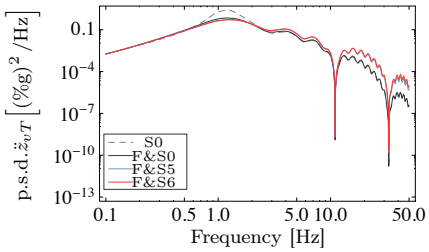

(c) S5–S6

Figure F.16: Plots of the p.s.d. for the vehicle body accelerations at the trailing position ($\ddot{z}_{vT}$) for suspensions settings according to Criterion I, with ideal actuators. Local skyhook damping with complementary filtering configuration.